NASA/CR-2004-213014

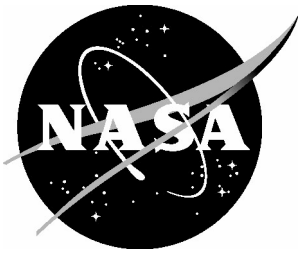

High Speed Research Noise Prediction Code (HSRNOISE) User's and Theoretical Manual

John W. Rawls, Jr. and Jessie C. Yeager
Lockheed Martin Engineering and Sciences Company, Hampton, Virginia

November 2004

The NASA STI Program Office . . . in Profile

Since its founding, NASA has been dedicated to the advancement of aeronautics and space science. The NASA Scientific and Technical Information (STI) Program Office plays a key part in helping NASA maintain this important role.

The NASA STI Program Office is operated by Langley Research Center, the lead center for NASA's scientific and technical information. The NASA STI Program Office provides access to the NASA STI Database, the largest collection of aeronautical and space science STI in the world. The Program Office is also NASA's institutional mechanism for disseminating the results of its research and development activities. These results are published by NASA in the NASA STI Report Series, which includes the following report types:

- TECHNICAL PUBLICATION. Reports of completed research or a major significant phase of research that present the results of NASA programs and include extensive data or theoretical analysis. Includes compilations of significant scientific and technical data and information deemed to be of continuing reference value. NASA counterpart of peer-reviewed formal professional papers, but having less stringent limitations on manuscript length and extent of graphic presentations.

- TECHNICAL MEMORANDUM. Scientific and technical findings that are preliminary or of specialized interest, e.g., quick release reports, working papers, and bibliographies that contain minimal annotation. Does not contain extensive analysis.

- CONTRACTOR REPORT. Scientific and technical findings by NASA-sponsored contractors and grantees.

- CONFERENCE PUBLICATION. Collected papers from scientific and technical conferences, symposia, seminars, or other meetings sponsored or co-sponsored by NASA.

- SPECIAL PUBLICATION. Scientific, technical, or historical information from NASA programs, projects, and missions, often concerned with subjects having substantial public interest.

- TECHNICAL TRANSLATION. English-language translations of foreign scientific and technical material pertinent to NASA's mission.

Specialized services that complement the STI Program Office's diverse offerings include creating custom thesauri, building customized databases, organizing and publishing research results ... even providing videos.

For more information about the NASA STI Program Office, see the following:

- Access the NASA STI Program Home Page at ***http://www.sti.nasa.gov***

- E-mail your question via the Internet to help@sti.nasa.gov

- Fax your question to the NASA STI Help Desk at (301) 621-0134

- Phone the NASA STI Help Desk at (301) 621-0390

- Write to:
  NASA STI Help Desk
  NASA Center for AeroSpace Information
  7121 Standard Drive
  Hanover, MD 21076-1320

NASA/CR-2004-213014

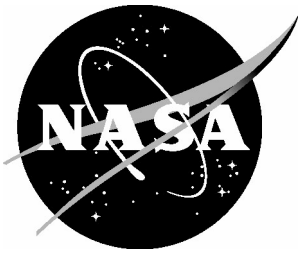

High Speed Research Noise Prediction Code (HSRNOISE) User's and Theoretical Manual

John W. Rawls, Jr. and Jessie C. Yeager
Lockheed Martin Engineering and Sciences Company, Hampton, Virginia

National Aeronautics and
Space Administration

Langley Research Center
Hampton, Virginia 23681-2199

Prepared for Langley Research Center
under Contract NAS1-00135

November 2004

Available from:

NASA Center for AeroSpace Information (CASI)
7121 Standard Drive
Hanover, MD 21076-1320
(301) 621-0390

National Technical Information Service (NTIS)
5285 Port Royal Road
Springfield, VA 22161-2171
(703) 605-6000

Table of Contents

1.0 Introduction

From 1989 to 1999, NASA and US industry partners conducted the High Speed Research (HSR) program to advance technology toward the development of a supersonic commercial transport. One element of the program was to ensure that the aircraft could be certified according to FAA FAR 36 Noise Certification regulations. During the HSR program, system noise studies were made using the NASA Langley Aircraft Noise Prediction Program (ANOPP) and the Boeing Multiple Component Predictor (MCP) program. Since the source for both of these codes is proprietary to their respective agencies, neither was suitable to be archived at the end of the HSR program. The HSRNOISE computer code, described in this report, was developed to document the noise prediction effort of the HSR program and to provide a code for continued research on a supersonic commercial transport.

Research was conducted on several engine concepts during Phase I of the HSR program. Among them were the turbine bypass engine, the variable cycle engine, and the mixed flow turbofan. The mixed flow turbofan was ultimately chosen as the primary engine for the Phase II studies. For this engine, jet noise was acknowledged as a noise source that would require substantial suppression. Suppressors were designed to promote rapid mixing of the supersonic jet with aspirated ambient flow by a multilobe mixer inside an ejector. The new propulsion concepts warranted the development of new prediction methods to study the noise impact of the High Speed Civil Transport (HSCT). Fan and jet noise algorithms were developed specifically for the mixed flow turbofan and mixer ejector nozzle. Combustor, turbine, and airframe noise prediction algorithms were obtained from published methods and correlated with model and/or full-scale data.

This report provides instruction on executing the HSRNOISE code, documents the noise prediction algorithms, and provides comparisons of predicted noise levels from the MCP and HSRNOISE codes for the Technology Concept (TC) aircraft. A flow chart of the HSRNOISE code is provided in figure 1.0. Whenever possible, algorithms provided by Boeing from the MCP system were incorporated into the HSRNOISE code. Algorithms obtained from the MCP system include subroutines in the Aircraft Flight Definition section, the jet noise subroutines (JN8C4), and the atmospheric attenuation subroutines. Modern Technologies Corporation developed an alternative mixer ejector noise prediction method for General Electric Aircraft Engines, which has also been incorporated into the HSRNOISE code. The remainder of the HSRNOISE code was developed at NASA Langley.

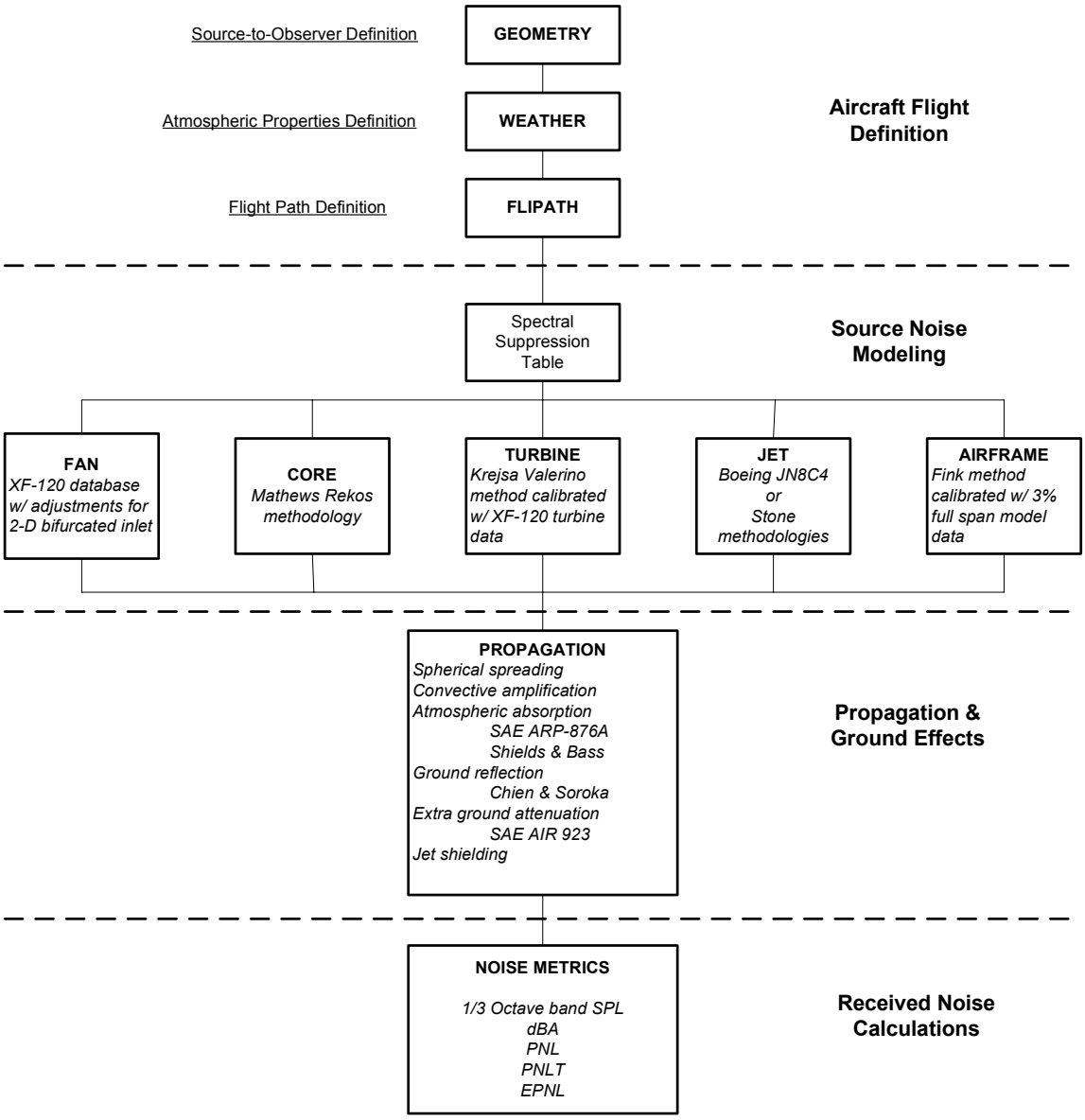

Figure 1.0 Flow Chart of the HSRNOISE code

2.0 User's Manual

This section provides instructions on creating input files, and executing the HSRNOISE code. The HSRNOISE code was developed at NASA Langley on a DEC Alpha workstation using the UNIX OAS1 version 4.0 operating system. The code was compiled with the Digital FORTRAN F77/90 compiler.

2.1 Creating the Executable

All subroutines required to create an executable are provided in a tar file. Once the FORTRAN files have been extracted, the executable `hsrnoise` is created by entering the following command:

```
> make -f makefile.hsrnoise
```

HSRNOISE prompts the user for the names of the input and output files. To execute the program with an input file named `sample.input` enter:

```
> hsrnoise (return)
     ENTER INPUT FILENAME:    sample.input   (return)
     ENTER OUTPUT FILENAME:   sample.output  (return)
```

An output file named `sample.output` will be created which contains flight path information, ambient weather conditions as a function of altitude, and noise levels for each noise source. The name of the output file is arbitrary.

2.2 Creating an Input File

Input to the HSRNOISE code is provided through NAMELIST statements. The following 11 NAMELIST groups have been established and must be input in the order specified:

GEOM	Defines the geometric relationship between the aircraft and the observer
WEATHER	Defines ambient weather conditions at ground level
FLIPATH	Defines the flight path parameters
SOURCE	Defines noise source and propagation adjustment for atmospheric attenuation, ground reflections, and EGA
DELTAS	Defines spectral adjustment (Required if IDELTA = TRUE)
FANIN	Defines fan noise parameters (Required if IFAN = TRUE)
COREIN	Defines combustor noise parameters (Required if ICORE = TRUE)
TURIN	Defines turbine noise parameters (Required if ITUR = TRUE)
JET1IN	Defines jet noise parameters (Required if IJET = TRUE, JETMETHOD = 1)
JET2IN	Defines jet noise parameters (Required if IJET = TRUE, JETMETHOD = 2)
AIRFIN	Defines airframe noise parameters (Required if IAFRAM = TRUE)

The parameters defined within each namelist are described in the following sections. Care should be taken to ensure that the parameters are in the proper units.

2.2.1 NAMELIST GEOM

Variable	Units	Default	Definition
ANGLE	degrees	10,20,…,170	Emission angle measured from engine inlet axis
HMIC	ft	4.	Height of microphone above ground level
NANG		17	Number of elements in array ANGLE
SL	ft	0.	Sideline distance

2.2.2 NAMELIST WEATHER

Variable	Units	Default	Definition
PSIAMB	lb/in^2	14.7	Ambient pressure at ground level
RH	%	70	Relative humidity at ground level
SIGMA	$lbm/sec\text{-}ft^3$	9.4E3	Ground flow resistance
TFAMB	^oF	77	Ambient temperature at ground level

2.2.3 NAMELIST FLIPATH

Variable	Units	Default	Definition
ALTEVO	ft	700.	Aircraft altitude at overhead
FPA	degrees	0.	Flight Path Angle. Angle between airplane instantaneous flight path and the horizontal direction. Positive for Climb.
PAE	degrees	0.	Angle between engine axis and horizontal direction. Equals the sum of the airplane flight path angle (FPA), the airplane body angle-of-attack, and the angle between the airplane reference axis and the engine axis. Positive for inlet up.
VAIR	ft/sec	0.	Aircraft velocity

2.2.4 NAMELIST SOURCE

Variable	Default	Definition
IAFRAM	TRUE	Airframe source flag, (TRUE / FALSE)
IATM	1	Atmospheric absorption flag
		= 0 ; no atmospheric absorption
		= 1 ; SAE ARP866A
		= 2 ; Shields & Bass
ICORE	TRUE	Core source flag, (TRUE / FALSE)
IDELTA	FALSE	User supplied suppression flag, (TRUE / FALSE)
IEGA	TRUE	Extra ground attenuation flag, (TRUE / FALSE)
IFAN	TRUE	Fan source flag, (TRUE / FALSE)
IGRND	TRUE	Ground reflection flag, (TRUE / FALSE)
IJET	TRUE	Jet source flag, (TRUE / FALSE)
IJETSHLD	TRUE	Jet shielding flag, (TRUE / FALSE)
ITUR	TRUE	Turbine source flag, (TRUE / FALSE)
JETMETHOD	1	Jet method flag
		= 1, Boeing JN8C4 Method
		= 2, Stone's Method
NENG	1	Number of engines

2.2.5 NAMELIST DELTAS

Variable	Units	Default	Definition
FANDIBB	dB	17*0.0	Fan broadband directivity delta array
FANSPBB	dB	24*0.0	Fan broadband spectrum delta array
FANBPF	dB	0.0	Fan first harmonic delta
FAN2BPF	dB	0.0	Fan second harmonic delta
FAN3BPF	dB	0.0	Fan third harmonic delta
FAN4BPF	dB	0.0	Fan fourth harmonic delta
CORDIBB	dB	17*0.0	Combustor broadband directivity delta
CORSPBB	dB	24*0.0	Combustor broadband spectrum delta
TURDIBB	dB	17*0.0	Turbine broadband directivity delta
TURSPBB	dB	24*0.0	Turbine broadband spectrum delta
TURDITN	dB	17*0.0	Turbine tone directivity delta
TURSPTN	dB	24*0.0	Turbine tone spectrum delta
AIRFDICW	dB	17*0.0	Airframe directivity delta (Clean Wing)
AIRFDILE	dB	17*0.0	Airframe directivity delta (Leading Edge Slat)
AIRFDITEI	dB	17*0.0	Airframe directivity delta (Trailing Edge Inboard Slat)
AIRFDITEO	dB	17*0.0	Airframe directivity delta (Trailing Edge Outboard Slat)
AIRFDIHT	dB	17*0.0	Airframe directivity delta (Horizontal Tail)
AIRFDIVT	dB	17*0.0	Airframe directivity delta (Vertical Tail)
AIRFDIMG	dB	17*0.0	Airframe directivity delta (Main Gear)
AIRFDING	dB	17*0.0	Airframe directivity delta (Nose Gear)
AIRFSPCW	dB	24*0.0	Airframe spectrum delta (Clean Wing)
AIRFSPLE	dB	24*0.0	Airframe spectrum delta (Leading Edge Slat)
AIRFSPTEI	dB	24*0.0	Airframe spectrum delta (Trailing Edge Inboard Slat)
AIRFSPTEO	dB	24*0.0	Airframe spectrum delta (Trailing Edge Outboard Slat)
AIRFSPHT	dB	24*0.0	Airframe spectrum delta array (Horizontal Tail)
AIRFSPVT	dB	24*0.0	Airframe spectrum delta array (Vertical Tail)
AIRFSPMG	dB	24*0.0	Airframe spectrum delta array (Main Gear)
AIRFSPNG	dB	24*0.0	Airframe spectrum delta array (Nose Gear)

2.2.6 NAMELIST FANIN

Variable	Units	Default	Definition
AFAN	ft^2	20	Fan inlet annulus area
FANRPM	rev/min	5000	Fan RPM
IDOOR		0	Flag for fan doors open or closed = 0 ; doors closed = 1 ; doors open
ISHAPE		0	Flag for 2D Bifurcated Inlet Shape Correction = 0 ; No correction = 1 ; Correction
NB1		25	Number of fan blades
UT	ft/sec	1000	First stage corrected tip speed (Equation 4 page 21)

2.2.7 NAMELIST COREIN

Variable	Units	Default	Definition
AB	in^2	100.0	Burner cross sectional area
BL	ft	1.0	Burner length
ICR		1	Burner type = 1; Can (JT3D, JT4, JT8D) = 2; Annular (JT9D, JT10D)
NFN		1	Number of fuel nozzles
PLD		1.0	Transmission loss factor
P3	lb/ in^2	111.8	Burner inlet pressure
P4	lb/ in^2	104.2	Burner exit pressure
P7	lb/ in^2	19.4	Low pressure turbine exit total pressure
T3	^oR	1007.5	Burner inlet total temperature
T4	^oR	1883.5	Burner exit total temperature
T7	^oR	1172.3	Low pressure turbine exit total temperature
W3	lbm/sec	450.0	Burner air mass flow rate
WFP4	(lbm/sec)/ (lb/ ft^2)	0.0155	Fuel-flow-rate to burner-exit pressure ratio at takeoff

2.2.8 NAMELIST TURIN

Variable	Units	Default	Definition
CSS	%	100	Stator axial chord to stator rotor spacing ratio
MDOT	lbm/sec	200	Primary mass flow rate at turbine exit
NBLADE		60	Number of turbine blades is last stage
TS	^{o}R	1300	Turbine exit static temperature
TURCAL	dB	10	Turbine calibration constant
TURRPM	rev/min	3600	Last stage turbine rotational speed
VTR	ft/sec	850	Relative tip speed of the last rotor of the turbine. If unknown use 0.7 times the tip speed. (Equation 4 page 36)

2.2.9 NAMELIST JET1IN (Boeing JN8C4 Methodology)

Variable	Units	Default	Definition
APRI	ft^2	8.6562	Primary nozzle exit area
ASEC	ft^2	16.832	Secondary nozzle exit area
ATHP	ft^2	8.5466	Throat area of the primary nozzle
CFG		0.95	Mixer-ejector thrust coefficient
DELMIX	dB	0	Mixed jet suppression
DELPE	dB	0	Primary external jet suppression
DELPI	dB	0	Primary internal jet suppression
DIVANG	degrees	0	Spoke divergence angle. Outer tangent line relative to ejector flow surface at nozzle downstream of mixer exit.
EJASP		1.5	Mixer-ejector aspect ratio major/minor axis
EJD	ft	5.274	Equivalent inner diameter of the ejector at the mixer exit
EJL	ft	13.3	Ejector length
EJLIN	ft	9.0	Length of ejector lining
FLIN	Hz	2000	Liner design center frequency
PEN		0.925	Mixer spoke penetration to nozzle full height ratio
PLUGD	ft	0	Plug diameter at nozzle exit station
PSI0	degrees	0	Rectangular exit plane major axis roll angle relative to wing plane
SPOKE		18.0	Number of spokes or lobes of the mixer
TPRI	^oR	1553.0	Primary jet total temperature
TSEC	^oR	529.0	Secondary jet total temperature
VPRI	ft/sec	2378.0	Primary jet fully expanded velocity
VSEC	ft/sec	449.0	Secondary jet velocity
WPRI	lbm/sec	811.3	Primary jet mass flow rate
WSEC	lbm/sec	566.9	Secondary jet mass flow rate
XMAR		0.97	Ejector exit area to mixing plane area ratio

2.2.10 NAMELIST JET2IN (Stone Methodology)

Variable	Units	Default	Definition
APT	ft^2	8.5466	Throat area of the primary nozzle
AS	ft^2	16.832	Secondary nozzle flow area
CER			Core expansion ratio
DHP	ft	0.5	Hydraulic diameter of primary flow DHP = 4 * Area / Perimeter
DL	dB/ft	0.7	Peak perforate suppression at FPK
DM		0	Degree of mixing (calculated if not supplied)
FPK	Hz	1995	Peak frequency of broad-band suppression
GAMMAC		0.	Specific heat ratio of primary stream. Internally calculated if set to 0.
HEX	ft	4.0	Ejector height at nozzle exit
IEX		0	Mixed jet parameter flag for TEX & VEX =0 calculate internally =1 use input values
ISUPPR		0	Suppression flag =0 negate suppression of internal noise sources =1 suppress internal noise sources
LBE	ft	10.	Length to end of bulk treatment from primary exit
LBS	ft	0.	Length to start of bulk treatment from primary exit
LE	ft	10.	Ejector length
LPE	ft	0.	Length to end of perforate treatment from primary exit For perforate over bulk treatment, add bulk length to perforate
LPS	ft	0.	Length to start of perforate treatment from primary exit
MMC		0.	Molecular mass (weight) of primary stream. Calculated internally if set to zero
MPD		1.2	Design Mach number of primary nozzle
PC	lb/ft^2		Total pressure of primary stream upstream of nozzle
PEN		0.925	Mixer spoke penetration to nozzle full height ratio
SAR			Ratio of total mixing area to primary nozzle throat
SUPPK	dB/ft	1.6628	Peak bulk suppression
TC	^oR		Total temperature of primary stream upstream of nozzle
TEX	^oR		Mixed exit total temperature
VEX	ft/sec		Mixed exit velocity
WEX	ft	6.0	Ejector width at nozzle exit
WSWP			Pumping ratio

2.2.11 NAMELIST AIRFIN

Variable	Units	Defaults	Definition
ICWING		2	Flag for clean wing component = 0 ; Do not compute = 1 ; Clean Wing = 2 ; Super Clean Wing
IVTAIL		1	Flag for vertical tail component = 0 ; Do not compute = 1 ; Compute
IHTAIL		1	Flag for horizontal tail component = 0 ; Do not compute = 1 ; Compute
ILEDGE		1	Flag for leading edge slat component = 0 ; Do not compute = 1 ; Compute
ITEIN		1	Flag for inboard trailing edge flap component = 0 ; Do not compute = 1 ; Compute
ITEOUT		1	Flag for outboard trailing edge flap component = 0 ; Do not compute = 1 ; Compute
INGEAR		1	Flag for nose gear component = 0 ; Do not compute = 1 ; Compute
IMGEAR		1	Flag for main gear component = 0 ; Do not compute = 1 ; Compute
AW	ft^2	8878.0	Wing area
BW	ft	154.3	Wing span
AV	ft^2	435.0	Vertical tail area
BV	ft	16.8	Vertical tail span
AH	ft^2	726.0	Horizontal tail area
BH	ft	71.0	Horizontal tail span
AFIN	ft^2	100.0	Wing inboard trailing edge flap area
BFIN	ft	10.0	Inboard flap span
FLAIN	degrees	10.0	Inboard flap deflection angle

NFSIN		1	Number of inboard trailing edge slots
AFOUT	ft^2	200.0	Wing outboard trailing edge flap area
BFOUT	ft	20.0	Outboard flap span
FLAOUT	degrees	10.0	Outboard flap deflection angle
NFSOUT		1	Number of outboard trailing edge slots
NNG		1	Number of nose landing gear
NWNG		2	Number of wheels per nose landing gear
DNG	ft	3.3	Nose gear wheel diameter
RLNG	ft	13.7	Length of nose landing gear strut
NMG		2	Number of main landing gear
NWMG		8	Number of wheels per main landing gear
DMG	ft	3.7	Main gear wheel diameter
RLMG	ft	16.0	Length of main landing gear strut

3.0 Theoretical Manual

The HSRNOISE program predicts one-third-octave band sound pressure levels for a supersonic commercial transport powered by mixed flow turbofan engines with rectangular mixer-ejectors. Total aircraft noise is modeled as a combination of fan, core, turbine, jet, and airframe noise sources. This section provides a description of the noise prediction methods used in the HSRNOISE program. A brief description of the methods used to determine the geometry, weather, and flight path is also provided.

3.1 Geometry (GEOM)

The relationship between the aircraft and the observer is established by the parameters defined in the GEOM namelist. Points on the flight path where noise predictions are to be made and subsequently propagated to the observer are defined by an array of emission angles. The variable ANGLE contains the array of desired emission angles. Each angle is checked to determine if it corresponds to a point that is above ground. Any angle not passing the test is removed from the array and a revised emission angle array is defined for subsequent noise calculation. The observer location and height are defined by the parameters SL and HMIC.

3.2 Atmospheric Properties (WEATHER)

Ambient weather conditions are required for the calculation of atmospheric absorption. The ambient pressure, ambient temperature, relative humidity, and ground flow resistance are input at ground level. Changes in atmospheric properties as a function of altitude are computed from the conditions at ground level and a temperature lapse rate of 3.566 degrees per 1000 feet. The relative humidity does not change with altitude.

Ambient sound speed: $$c_a(z) = 49.01\sqrt{(T_a + 459.7) - .003566z} \qquad (1)$$

Ambient pressure: $$P_a(z) = P_a(z=0)\left[\frac{(T_a + 459.7) - .003566z}{T_a + 459.7}\right]^{5.26} \qquad (2)$$

Ambient density: $$\rho_a(z) = \frac{144P_a(z)}{R(T_a + 459.7 - .003566z)} \qquad (3)$$

The ground flow resistivity is an important parameter in the calculation of the ground reflection attenuation. Table 3.2.1 provides a range of values for ground flow resistivity typical of aeroacoustic predictions.

Table 3.2.1 Range of Flow Resistivity for Various Ground Surfaces

Surface Type	Pa-sec/m^2	lbm/sec-ft^3
Grass	1.5 - 3 x 10^5	9.4 - 19.0 x 10^3
Asphalt	1.5 - 3 x 10^7	9.4 - 19.0 x 10^6
Concrete	3 - 10 x 10^7	1.9 - 6.2 x 10^8

from NASA RP 1258 vol. 2 Table 1 page 66

3.3 Flight Path (FLIPATH)

When predicting noise for a single observer, a complete description of the flight path is not necessary. Only the portion of the flight path that is significant to that observer is required. The flight path is defined as a straight line with the flight path angle, pitch angle, and aircraft velocity remaining constant. The altitude is established by defining the altitude when the aircraft is directly above the observer.

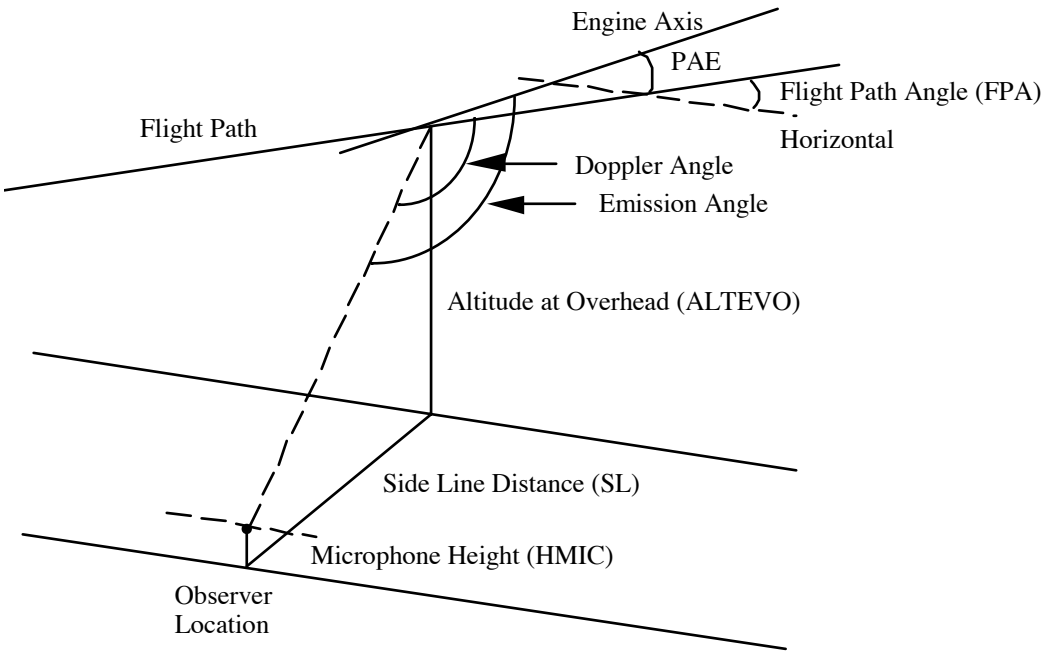

Figure 3.1 Flight path geometry

3.4 Aircraft Noise Sources (SOURCES)

The parameters in the SOURCE namelist allow the user to select the noise sources that will model the total aircraft noise. Noise is computed for the fan, core, turbine, jet, and airframe when the appropriate source noise flag is set to TRUE. The input also allows the user to control certain propagation effects, such as atmospheric attenuation, ground reflection attenuation, and extra ground attenuation. These propagation effects are computed when the proper parameters are set to TRUE. Atmospheric attenuation is controlled by the IATM parameter, which has the following options:

- no atmospheric attenuation
- atmospheric attenuation determined using the SAE ARP866A method
- atmospheric attenuation determined using the Shields & Bass method

Two criteria are used to determine the attenuation frequency for the one-third-octave band analysis. For the SAE ARP866A method, the attenuation coefficient is determined using the following criteria:

- one-third-octave band center frequency for frequencies below 4000 Hz.
- one-third-octave band lower band edge frequency for frequencies 5000 Hz. and above

When the Shields & Bass method is selected, the atmospheric attenuation coefficients are determined using the one-third-octave band center frequency.

3.5 Suppression (DELTAS)

The DELTAS namelist allows the spectra of a noise source to be altered by a suppression function. Suppression is applied as

$$SPL_{\text{suppressed}} = SPL_{\text{unsuppressed}} + \Delta(f,\theta) \tag{1}$$

where Δ is a function of frequency and emission angle . The suppression function is calculated as a product as indicated by equation 2.

$$\Delta = A(\theta)B(f) \tag{2}$$

The function A is a multiplier and is usually positive. The function B provides the spectral suppression and is usually negative. Note that the sign of the suppression function can be positive or negative depending on whether noise is to be added or subtracted from the original spectra.

There are several important points to note concerning the suppression function.

- The default values for the fan harmonics (see parameters FANBPF, FAN2BPF, FAN3BPF, and FAN4BPF in section 2.2.5) are not arrays but single valued parameters. Instead of the suppression function, each fan harmonic is suppressed by a constant value that is not a function of the emission angle.

- Jet noise suppression has been incorporated into the jet noise methods. See JET1IN and JET2IN for details.

- Airframe noise is comprised of eight subcomponents. A unique suppression function can be applied to each subcomponent. When predicting airframe noise for a high speed civil transport other than the TC aircraft, an adjustment to the subsonic airframe prediction method will be required. The suppression function derived for the TC aircraft is defined in section 3.11.

3.6 Fan Noise

The fan noise prediction method is based on the empirical formulation of XF-120 fan data derived by Gliebe [1]. The method assumes that inlet fan noise radiates from the first stage only and that noise from the 2nd and 3rd stages do not contribute. The method employs empirical functions to define the broadband and discrete tone noise components. The broadband and tone noise peak sound pressure levels are correlated as a function of fan corrected tip speed and polar directivity angle. The broadband spectral function is predicted using the spectral shape function from the Heidmann fan noise prediction method [2]. The total noise is obtained by summing the broadband and tone noise mean-square acoustic pressures for each frequency and polar directivity angle.

Symbols

a	broadband coefficient for 2-D inlet correction
A_{fan}	first stage rotor inlet annulus area, (ft^2) (***input parameter*** - `AFAN`)
A_{ij}	broadband correlation coefficients
c	tone coefficient for 2-D inlet correction
C_{ij}	tone correlation coefficients
d	fan rotor diameter, ft
f	frequency, Hz
f_b	blade passing frequency, Hz
n	harmonic number
N_b	number of first stage fan blades (***input parameter*** – `NB1`)
N_2	fan rotational speed, (rpm) (***input parameter*** – `FANRPM`)
p_{ref}	reference pressure, ($4.177x10^{-7} lb/ ft^2$)
r_s	distance from source to observer, (ft)
SI	spectrum index function, dB
T_a	ambient temperature, ^oR
U^*	nondimensional corrected tip speed, re U_{ref}
U_{ref}	reference tip speed, (1000 ft/sec)
U_t	first stage corrected tip speed, (ft/sec) (***input parameter*** – `UT`)
η	frequency parameter
θ	polar directivity angle, degrees
σ	spectral shape function constant ($\sigma = 2.2$)

Superscript:

*	dimensionless quantity

Subscript:

a	ambient
bb	broad band
i	tip speed index
j	directivity angle index
l	one-third-octave band lower limit
n	harmonic index
ref	reference
tone	discrete tone
u	one-third-octave band upper limit

Inlet Broadband Noise

The prediction of inlet broadband noise is based on the correlation of fan data from the GE XF-120 engine. The sound pressure level (SPL) at the observer is

$$SPL_{bb}(r_s,\theta) = SPL_{peak} + 10Log_{10}\left(A_{fan}/5.584\right) + SI(\eta) \tag{1}$$

The broadband peak sound pressure level is determined by the following polynomial function of polar angle and corrected tip speed

$$SPL_{peak} = \sum_{i=1}^{4}\left[\sum_{j=1}^{3} A_{ij}\left(\theta/90\right)^{j-1}\right]\left(U^*\right)^{i-1} \tag{2}$$

The broadband correlation coefficients A_{ij} are given in table 3.6.1, and the normalized corrected tip speed is defined as

$$U^* = \frac{U_t}{U_{ref}} \tag{3}$$

The corrected tip speed is calculated by

$$U_t = \frac{\pi d N_2 / 60}{\sqrt{T_a / 518.67}} \tag{4}$$

Table 3.6.1 - Broadband Noise Correlation Coefficients A_{ij}

	Polar Angle Index (j)		
Tip Speed Index (i)	1	2	3
1	61.85	-183.92	143.42
2	21.667	705.25	-653.16
3	2.0071	-790.26	731.70
4	-6.2733	272.17	-242.45

Figure 3.6.1 shows a contour plot of the peak SPL function defined by equation 2. Figure 3.6.2 shows the peak SPL as a function of directivity angle for corrected tip speeds of 0.5, 1.0, and 1.5.

Scaling for airflow was not possible due to the classified nature of the XF-120 noise data. However, the broadband noise level is scaled for size based on rotor inlet area by the expression $10Log_{10}\left(A_{fan}/5.584\right)$.

Broadband Spectrum Index Function

The broadband noise spectrum is computed by a modified version of the Heidmann spectral shape function [2]. The spectrum function $S(\eta)$ (figure 3.6.3) is given by

$$SI(\eta) = 10Log_{10}\left[\exp\left\{-\frac{1}{2}\left[\frac{\ln(\eta)}{\ln(\sigma)}\right]^2\right\}\right] \tag{5}$$

where the nondimensional frequency parameter η is

$$\eta = (1 - M_a \cos\theta)\frac{f}{f_{peak}} \tag{6}$$

The peak frequency is Doppler shifted to account for the effect of source motion. The peak frequency is correlated as a function of tip speed and blade passing frequency. The equation for the peak frequency is

$$f_{peak} = \left[2.265 + 0.07298\left(U^*\right) - 0.2039\left(U^*\right)^2\right] f_b \tag{7}$$

where the blade passing frequency is

$$f_b = N_b \frac{N_2}{60} \tag{8}$$

The constant σ is given the value 2.2 as in the Heidmann method. The XF-120 data showed no significant dependence of the spectral shape function on polar angle. A plot of the peak frequency function is provided in figure 3.6.4.

Inlet Tone Noise

The correlation of the discrete tone noise levels is similar to the correlation of the broadband levels defined earlier. The fundamental tone and 2nd, 3rd, and 4th harmonics are computed as a function of polar angle and tip speed by

$$SPL_n = \sum_{i=1}^{4}\left[\sum_{j=1}^{3} C_{ij}(\theta/90)^{j-1}\right](U^*)^{i-1} \qquad n = 1, 2, 3, 4 \qquad (9)$$

where n represents the harmonic number. The coefficients C_{ij} for the first four harmonics are defined in tables 3.6.2 through 3.6.5.

Table 3.6.2 - Fundamental Tone Correlation Coefficients C_{ij} $(n = 1)$

	Polar Angle Index (j)		
Tip Speed Index (i)	1	2	3
1	125.00	-112.91	14.02
2	-245.82	688.66	-392.05
3	330.86	-883.86	534.18
4	-117.90	315.53	-187.56

Table 3.6.3 - 2nd Harmonic Correlation Coefficients C_{ij} $(n = 2)$

	Polar Angle Index (j)		
Tip Speed Index (i)	1	2	3
1	92.291	-59.79	38.335
2	-127.82	601.89	-576.26
3	195.66	-821.53	751.96
4	-74.199	298.90	-258.03

Table 3.6.4 - 3rd Harmonic Correlation Coefficients C_{ij} $(n = 3)$

	Polar Angle Index (j)		
Tip Speed Index (i)	1	2	3
1	135.93	-247.51	102.80
2	-185.54	856.79	-501.16
3	210.26	-942.98	597.45
4	-74.01	322.24	-208.53

Table 3.6.5 - 4th Harmonic Correlation Coefficients C_{ij} $(n = 4)$

	Polar Angle Index (j)		
Tip Speed Index (i)	1	2	3
1	232.20	-793.54	742.31
2	-571.51	2836.35	-2612.96
3	621.24	-3001.07	2627.40
4	-205.75	962.39	-797.31

Equation 9 is plotted in figure 3.6.5 for the first four harmonics. Note that the 4th harmonic is not calculated when the tip speed is greater than 1300 ft/sec and the emission angle is greater than 90 degrees. The discrete tone noise levels are corrected for engine size, distance from source to observer, and source motion in the same manner as the broadband noise level.

$$SPL_{tone}(r_s, \theta) = SPL_n(U^*, \theta) + 10Log_{10}\left(A_{fan} / 5.584\right) \tag{10}$$

The frequency associated with each harmonic is obtained by Doppler shifting the blade passing frequency and multiplying by the appropriate harmonic number.

$$f_n = \frac{nf_b}{1 - M_a \cos\theta} \qquad n = 1, 2, 3, 4 \tag{11}$$

2D Bifurcated Inlet Correction

Inlet shape effects are applied using correlation equations based on HSCT inlet data taken in Boeing's low speed aeroacoustic facility (LSAF) in 1995. These equations detail suppression differences between the 2D bifurcated inlet and typical subsonic inlets. Deltas from these correlations are applied spectrally and include directivity effects. The broadband correction is expressed as a polynomial function of frequency and emission angle.

$$\Delta SPL_{bb} = a_0 + a_1 f + a_2 f^2 + a_3 \theta + a_4 \theta^2 + a_5 f\theta \tag{12}$$

Table 3.6.6 defines the coefficients for approach, sideline, and centerline microphone positions.

Table 3.6.6 Broadband Coefficients for 2D Bifurcated Inlet Correction

	a_0	a_1	a_2	a_3	a_4	a_5
Sideline	4.26E+00	3.86E-04	-1.10E-07	-7.46E-02	2.30E-04	1.57E-05
Approach	1.99E+00	-5.60E-04	-6.65E-08	7.63E-02	-9.76E-04	-4.99E-06
Centerline (Doors Closed)	7.34E+00	-5.35E-04	4.75E-08	-1.05E-01	1.50E-04	-7.25E-06
Centerline (Doors Open)	3.76E+00	1.28E-03	-1.44E-07	-1.08E-01	5.49E-04	1.67E-06

The tone correction is expressed as a polynomial function of the emission angle.

$$\Delta SPL_{tone} = c_0 + c_1 \theta + c_2 \theta^2 \tag{13}$$

Tables 3.6.7 through 3.6.10 define the coefficients for the first four fan harmonics.

Table 3.6.7 1st Harmonic Coefficient for 2D Bifurcated Inlet Correction

	c_0	c_1	c_2
Sideline	-5.34E+00	1.52E-01	-6.06E-04
Approach	-1.40E+01	4.25E-01	-2.82E-03
Centerline (Doors Closed)	0.0	0.0	0.0
Centerline (Doors Open)	0.0	0.0	0.0

Table 3.6.8 2nd Harmonic Coefficient for 2D Bifurcated Inlet Correction

	c_0	c_1	c_2
Sideline	-8.56E+00	3.48E-01	-3.36E-03
Approach	-3.90E+01	1.21E+00	-1.01E-02
Centerline (Doors Closed)	0.0	0.0	0.0
Centerline (Doors Open)	0.0	0.0	0.0

Table 3.6.9 3rd Harmonic Coefficient for 2D Bifurcated Inlet Correction

	c_0	c_1	c_2
Sideline	6.17E+00	-1.26E-01	1.06E-05
Approach	-5.40E-01	-1.89E-01	0.0
Centerline (Doors Closed)	0.0	0.0	0.0
Centerline (Doors Open)	0.0	0.0	0.0

Table 3.6.10 4th Harmonic Coefficient for 2D Bifurcated Inlet Correction

	c_0	c_1	c_2
Sideline	6.09E+00	-1.31E-01	9.11E-04
Approach	1.61E+00	-8.57E-02	6.25E-04
Centerline (Doors Closed)	0.0	0.0	0.0
Centerline (Doors Open)	0.0	0.0	0.0

Total Noise

The total mean-square acoustic pressure is the sum of the broadband component and the discrete tones

$$\left\langle p^2 \right\rangle_{total} = \left\langle p^2 \right\rangle_{bb} + \left\langle p^2 \right\rangle_{tone} \tag{14}$$

where

$$\left\langle p^2 \right\rangle_{bb} = p_{ref}^2 10^{(SPL_{bb} + \Delta SPL_{bb})/10} \tag{15}$$

and

$$\left\langle p^2 \right\rangle_{tone} = p_{ref}^2 10^{(SPL_{tone}+\Delta SPL_{tone})/10} \tag{16}$$

Since broadband noise is computed at the one-third-octave band center frequency and tone noise occurs at discrete frequencies, it is necessary to identify the one-third-octave band which contains the tone. For a given center frequency, f, the lower limit of the band is

$$f_l = 2^{-1/6} f \tag{17}$$

and the upper limit is

$$f_u = 2^{-1/6} f . \tag{18}$$

The tone mean-square acoustic pressure at each harmonic number, n, is then added to the band in which the relation $f_l \le f < f_u$ is true.

The free-field lossless total inlet radiated fan sound pressure level is

$$SPL_{total}(r_s, \theta) = 10 Log_{10} \left\langle p^2 \right\rangle_{total} \tag{19}$$

Propagation effects are defined in section 3.13.

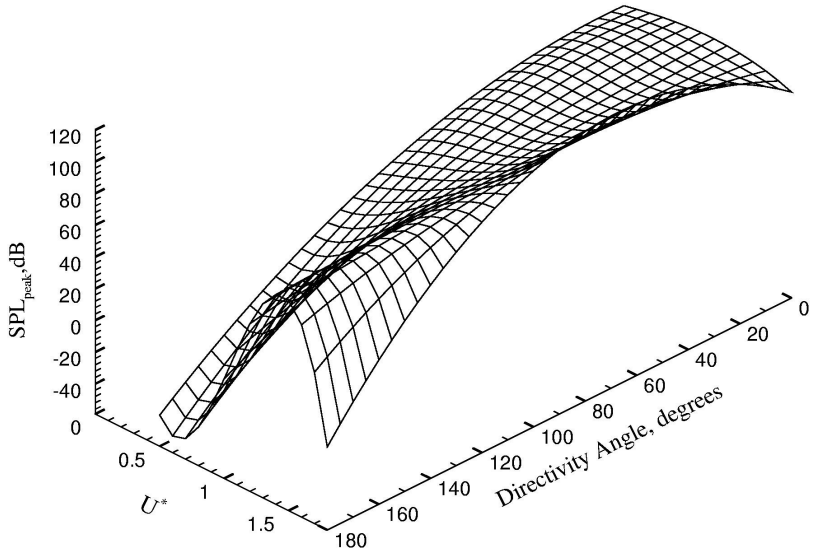

Figure 3.6.1 Contour plot of the XF120 broadband SPL_{peak} function

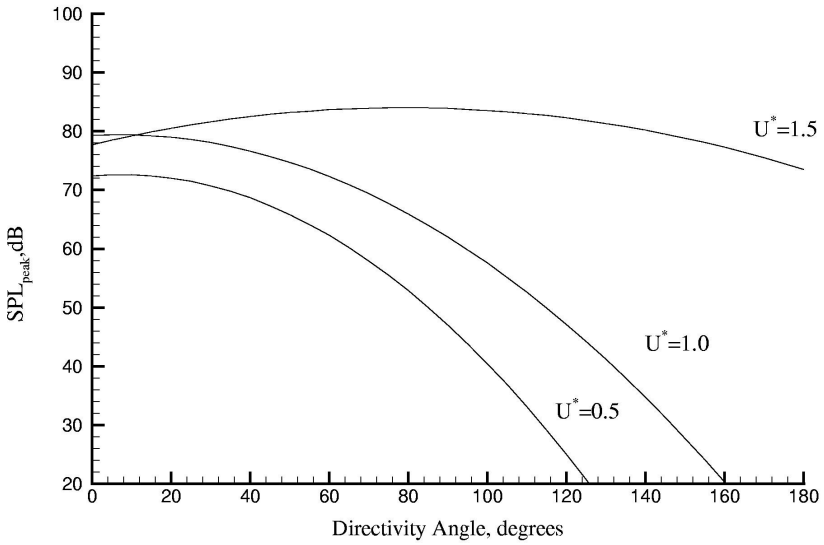

Figure 3.6.2 XF120 broadband directivity levels

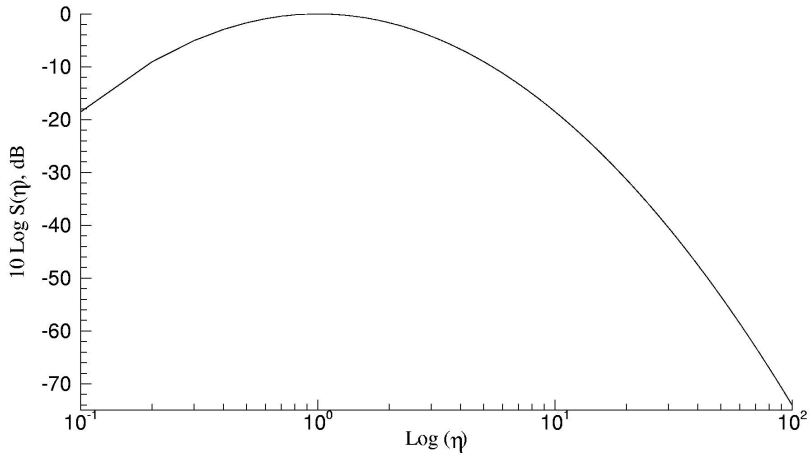

Figure 3.6.3 XF120 fan broadband spectrum function

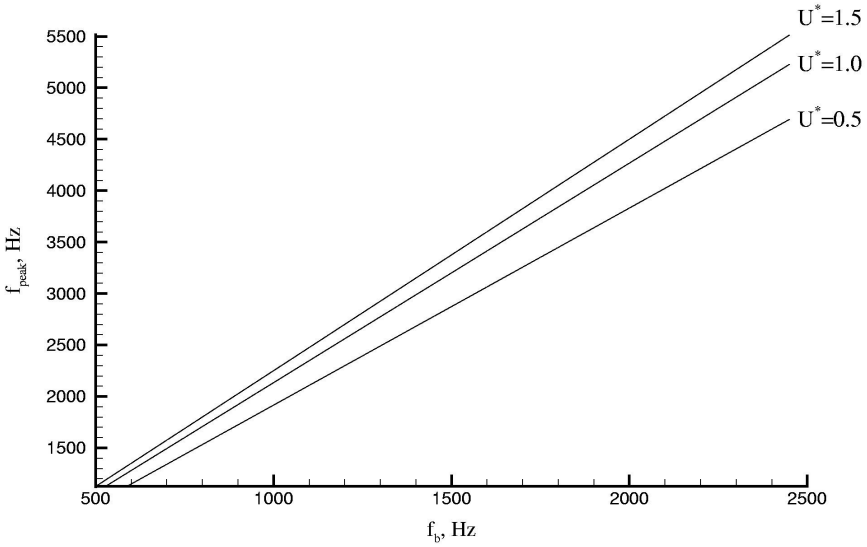

Figure 3.6.4 XF120 broadband peak frequency as a function of blade passing frequency

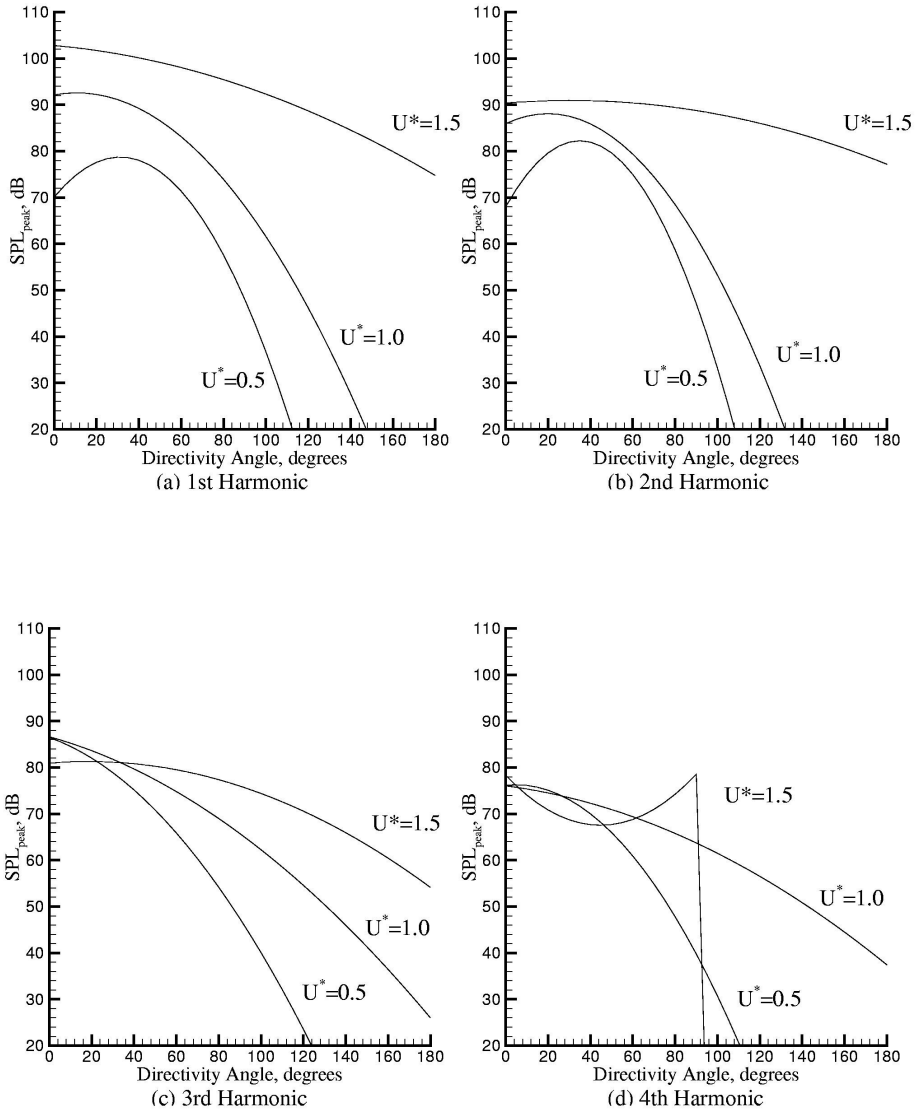

Figure 3.6.5 XF120 fan tone directivity levels

3.7 Combustor Noise

The combustion noise prediction method adopted for the HSR program is based on the method developed by Mathews and Rekos [3]. This method was developed from several JT8D burner configurations and full-scale turbofan engine data. The full-scale engines included the JT8D-109, JT9D-7A, JT9D-70, and the JT10D. Comparisons of predictions with data from both the turbine rigs and the full-scale engines showed that the equation for the OAPWL fits the data with a standard deviation of 1.7 dB. Reference 3 provided no comparisons with flight data.

Symbols

A_b	burner cross-sectional area, (ft^2) (***input parameter*** **–** `AB`)
B_l	burner length, (ft) (***input parameter*** - `BL`)
c_p	specific heat at constant pressure = 0.28 BTU/lbm ^oR
$DI(\theta)$	directivity index function
f	frequency, Hz
F	ratio of acoustic impedances across turbine
F_b	burner fuel to air ratio (***input parameter*** – `FB`)
f_{peak}	combustion noise peak frequency, Hz
F_{st}	Stochiometric fuel to air ratio = 0.068
H_f	fuel heating value 18,500 BTU/lbm
ICR	burner type (***input parameter*** – `ICR`)
K_f	coefficient in peak frequency equation
$(L/\pi D)$	transmission loss through burner exit duct (***input parameter*** – `PLD`)
N_f	number of fuel nozzles (***input parameter*** - `NFN`)
$OAPWL$	overall power level, dB
p_{ref}	reference pressure, 4.177 x 10^{-7} (lb/ft^2)
$< p^2 >$	mean-square acoustic pressure, $(lb/ft^2)^2$
P_{t3}	burner inlet total pressure, (lb/ft^2) (***input parameter*** – `P3`)
P_{t4}	burner exit total pressure, (lb/ft^2) (***input parameter*** – `P4`)
P_{t7}	low "pressure" turbine exit total pressure, (lb/ft^2) (***input parameter*** – `P7`)
r_s	distance from source to observer, (ft)
R	gas constant = 53.35 ft-lbf/ lbm °R
$SI(\eta)$	spectrum function
SPL	sound pressure level, dB
TL	combustion noise transmission loss, dB
T_{t3}	burner inlet total temperature, (°R) (***input parameter*** – `T3`)
T_{t4}	burner exit total temperature, (°R) (***input parameter*** – `T4`)
T_{t7}	low "pressure" turbine exit total temperature, (°R) (***input parameter*** – `T7`)
w_3	burner mass air flow rate, (lbm/sec) (***input parameter*** – `W3`)

$\left(w_f / P_{t4}\right)_{ref}$ fuel-flow-rate to burner-exit-pressure ratio at takeoff, (lbm/sec / lb/ft^2) (***input parameter*** – `WFP4`)

η nondimensional frequency parameter

θ polar directivity angle, degrees

Method

The combustion noise prediction method adopted for the HSR program is based on the method developed by Mathews and Rekos [3]. The free-field lossless sound pressure level is

$$SPL(r_s,\theta) = OAPWL - TL + DI(\theta) + SI(\eta) \tag{1}$$

where the overall acoustic power is

$$OAPWL = 10Log_{10}\left[\frac{1}{N_f}\ A_b^2\ {P_{t3}}^2\left(\frac{w_3\sqrt{T_{t4}}}{P_{t3}A_b}\right)^4\left(1+\frac{H_f F_{st}}{c_p T_{t3}}\right)^2 F_b^2\right] + 131.3 \tag{2}$$

Propagation effects are defined in section 3.13.

Equation 2 was derived from Strahle's equation for sound produced by open flames in terms of burner geometry and performance parameters. The acoustic power is directly proportional to the burner air flow rate, the fuel-to-air ratio, and the total temperature at the burner exit. Increasing either the air flow rate or the fuel to air ratio will increase the acoustic power. The acoustic power is inversely proportional to the number of fuel nozzles, the cross sectional area, and the burner inlet total pressure and temperature. Increasing either the number of fuel nozzles or the burner cross sectional area will reduce the acoustic power.

Transmission Losses

Transmission losses are caused by the loss of energy through the duct leading into the turbine and across the turbine rotor and stator blades. The transmission loss factor is defined by two expressions. The equation for the total transmission loss is

$$TL = 10Log_{10}\left[(1+F)^2 / 4F(L/\pi D)\right] \tag{3}$$

The transmission loss associated with the turbomachinery is given by

$$F = (P_{t4}/P_{t7})\sqrt{T_{t7}/T_{t4}} \tag{4}$$

Equation 4 was derived by modeling the turbine as a discontinuity in characteristic impedance. The ratio of the characteristic impedance across the turbine is a function of

the total pressures and total temperatures at the combustor and turbine exit locations. An increase in combustor exit total pressure or turbine exit total temperature increases the transmission losses and reduces the combustor noise. An increase in combustor exit total temperature or turbine exit total pressure reduces the transmission losses and increases the combustor noise. The expression $L/\pi D$ is associated with losses in the duct and has a value of 0.15 for the mixed flow turbofan. Note that the transmission loss through the duct can be ignored by setting $L/\pi D = 1$.

Directivity Function

The directivity function, defined in table 3.7.1, was established for observers located at a distance of 150 feet from the source. The directivity function is plotted in figure 3.7.1.

Table 3.7.1 - Directivity Function

θ	$DI(\theta)$	θ	$DI(\theta)$
0.0	-60.0	95.0	-42.9
10.0	-58.3	100.0	-42.0
20.0	-56.5	105.0	-41.2
30.0	-54.8	110.0	-40.4
40.0	-53.0	115.0	-39.8
50.0	-51.1	120.0	-39.2
60.0	-49.3	130.0	-40.9
70.0	-47.5	135.0	-42.6
80.0	-45.7	140.0	-44.3
90.0	-43.8	150.0	-48.0
		180.0	-59.0

Spectrum Function

The spectrum function was derived from a combination of combustor rig and full scale engine data. The peak frequency is a function of the burner geometry and burner type. The expression for the peak frequency is

$$f_{peak} = K_f \frac{RH_f}{c_p}\left(\frac{w_f}{P_{t3}}\right)_{ref} \frac{1}{A_b B_l} \tag{5}$$

where $K_f = 8$ for can type burners and $K_f = 3$ for annular type burners. Equation 5 indicates that can type burners have higher peak frequencies than annular burners of comparable size. The spectrum function in table 3.7.2 is tabulated as a function of the nondimensional parameter

$$\eta = 10Log_{10}\left(\frac{f}{f_{peak}}\right) \tag{6}$$

The spectrum function is plotted in figure 3.7.2. Note that the spectrum is not Doppler shifted.

Table 3.7.2 - Spectrum Function

η	$SI(\eta)$
$\eta < -7$	$SI(\eta) = -24.7 + 2.5(\eta + 7)$
-7	-24.7
-6	-22.3
-5	-19.5
-4	-16.8
-3	-14.1
-2	-11.4
-1	-8.8
0	-6.8
1	-8.1
2	-9.9
3	-11.5
4	-13.3
5	-15.0
6	-16.8
7	-18.6
8	-20.5
9	-22.4
10	-24.3
11	-26.3
$\eta > 11$	$SI(\eta) = -26.3 - 2.0(\eta - 11)$

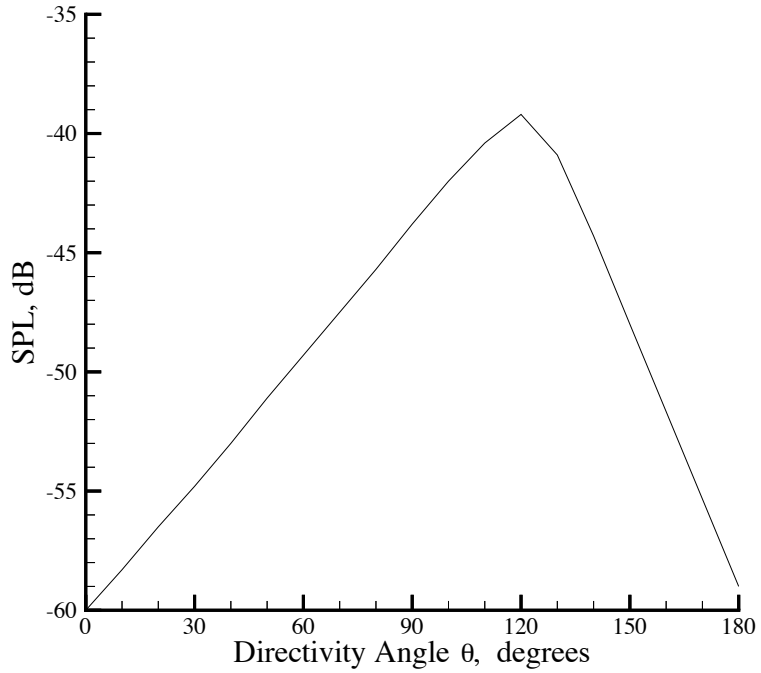

Figure 3.7.1 Mathews Rekos combustion noise directivity function (150 foot radius)

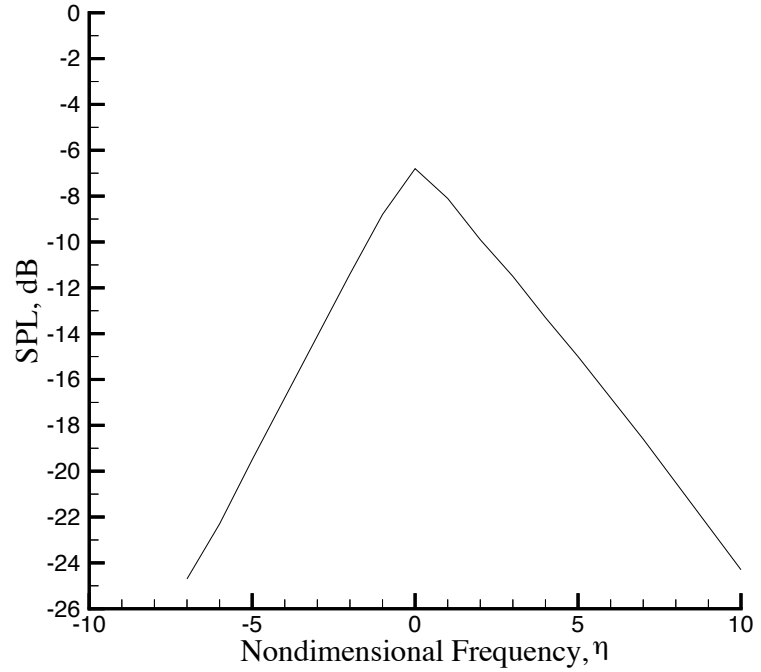

Figure 3.7.2 Mathews Rekos combustion noise spectrum function

3.8 Turbine Noise

The turbine noise prediction method adopted for the HSR program is based on the method recommended by Krejsa and Valerino [4]. The empirical correlation was developed from turbine rig and full scale engine data. The uncertainty in predicted levels can be as high as +/- 5 dB for the fundamental tone and +/- 9 dB for the broadband noise when compared against data from commercial turbofan engines. The large prediction uncertainty is due to the wide range in turbine designs, geometry, and the complex interaction with noise from upstream turbine stages. An evaluation of this method was made with data from the GE XF120 engine [5]. These comparisons indicated that the trend with increasing turbine speed was not well predicted and that the model would over predict HSCT turbine noise by as much as 10 dB. Consequently, it is suggested that the turbine calibration constant *TURCAL* be set to -10 dB.

Symbols

c_{ref}	reference sound speed, c_{ref} = 1116.45 ft/ sec
c_{tex}	sound speed at the turbine exit, ft/sec
C / S	stator axial chord / stator rotor spacing (***input parameter*** – `CSS`)
d	last stage turbine rotor diameter, ft
DI	directivity index, dB
f	one-third-octave band center frequencies, Hz
f_{bpf}	blade passing frequency, Hz
g_c	gravitational constant, 32.174ft/sec^2
$\dot{m}$	primary mass flow rate at turbine exit, lbm/sec (***input parameter*** – `MDOT`)
$\dot{m}_{ref}$	reference mass flow rate at the turbine exit, $\dot{m}_{ref}$ = lbm/sec
N_b	number of turbine blades in the last stage (***input parameter*** – `NBLADE`)
N_2	rotational speed, rpm (***input parameter*** - `TURRPM`)
r_s	distance from source to observer, r_s = 150 ft
R	gas constant, 53.35 ft-lbf / lbm ^oR
SI	spectrum index, dB
T_s	turbine exit static temperature, ^oR (***input parameter*** – `TS`)
$TURCAL$	turbine calibration constant, dB (***input parameter*** – `TURCAL`)
V_{ref}	reference tip speed, V_{ref} = ft/sec
V_t	tip wheel speed, ft/sec
V_{tr}	relative tip speed, ft/sec (***input parameter*** – `VTR`)
γ_{tex}	ratio of specific heats at the turbine exit
η	nondimensional frequency parameter
θ	emission angle, degrees

Method

The free-field sound pressure levels for the broadband and discrete tone noise at a radius of 150 feet are given by equations 1 and 2.

$$SPL_{bb}\left(r_s = 150, f, \theta\right) = 10Log_{10}\left[\left(\frac{V_{tr}c_{ref}}{V_{ref}c_{tex}}\right)^3\left(\frac{\dot{m}}{\dot{m}_{ref}}\right)\right] + DI_{bb}\left(\theta\right) + SI_{bb}\left(\eta\right) - 10 \qquad (1)$$

$$SPL_{tone}\left(r_s = 150, f_{bpf}, \theta\right) = 10Log_{10}\left[\left(\frac{V_{tr}}{V_{ref}}\right)^{0.6}\left(\frac{c_{ref}}{c_{tex}}\right)^3\left(\frac{\dot{m}}{\dot{m}_{ref}}\right)\left(\frac{C}{S}\right)\right] + DI_{tone}\left(\theta\right) + SI_{tone}\left(f_{bpf}\right) + 56 \qquad (2)$$

The free-field lossless total turbine noise is obtained by combining the broadband and discrete tone noise components and removing the atmospheric absorption effects.

$$SPL_{total}(r_s, f, \theta) = 10Log_{10}\left(10^{0.1SPL_{bb}} + 10^{0.1SPL_{tone}}\right) + F_{abs}\left(f\right) - TURCAL \qquad (3)$$

The function F_{abs} is corrects the total noise to a lossless condition by the removal of the standard day (i.e. 59 ^{o}F, 70% relative humidity) atmospheric attenuation at a distance of 150 feet as defined in reference 6. Note that turbine calibration constant *TURCAL* allows the user to choose the amount of noise reduction to be applied to the total turbine noise. *TURCAL* was determined to be -10 dB for the HSR program based on data from the GE XF120 engine. Propagation effects are defined in section 3.13.

It is assumed that the design of the HSR turbine rotor blades will remove most or all of the swirl. To the accuracy of the method, this allows the relative tip flow velocity to be calculated (by the user) as

$$V_{tr}^2 = V_t^2 + V_x^2 \qquad (4)$$

where the tip speed of the last stage rotor is

$$V_t = \frac{\pi d N_2}{60} \qquad (5)$$

The axial flow velocity is given by

$$V_x^2 = \left[\frac{2}{\gamma_{tex} - 1}\left(\frac{T_t}{T_s} - 1\right)\right] c_{tex}^2 \tag{6}$$

where the ratio of specific heat is

$$\gamma_{tex} = 1 + \frac{0.4}{1 + 0.4\left[\frac{\tau^2 e^\tau}{\left(e^\tau - 1\right)^2}\right]} \tag{7}$$

and τ represents the temperature ratio defined by

$$\tau = 5000/T_S \tag{8}$$

The speed of sound at the turbine exit is

$$c_{tex} = \sqrt{\gamma_{tex} g_c R T_S} \tag{9}$$

Stator Rotor Spacing

The stator rotor spacing is defined in figure 3.8.1 and usually has a value greater than 1.

Directivity Function

The broadband and discrete tone directivity functions are tabulated in table 3.8.1.

Table 3.8.1. Broadband and Discrete Tone Directivity Functions

θ	$DI_{bb}(\theta)$, dB	$DI_{tone}(\theta)$, dB
0	-37.0	-56.0
40	-21.0	-27.5
60	-12.9	-18.0
80	-7.0	-10.0
100	-1.3	-2.4
110	0.0	0.0
120	-1.3	-2.2
140	-8.8	-14.0
160	-19.0	-26.0
180	-31.5	-40.0

Spectrum Index Function

The variation in broadband noise as a function of frequency is given by the spectrum index function. The broadband spectra peaks at the blade passing frequency as indicated by equation 10. The discrete tone spectrum decays 10 dB for each harmonic greater than the blade passing frequency.

$$SI_{bb}(\eta) = \begin{cases} 10Log_{10}\eta & \eta \le 1 \\ -20.176Log_{10}\eta & \eta > 1 \end{cases} \tag{10}$$

$$SI_{tone} = -10(\eta - 1) \quad \eta = 1,2,3... \tag{11}$$

The spectrum index function is defined in terms of the nondimensional frequency parameter η where η is the ratio of the observed one-third-octave band center frequency to the Doppler shifted blade passing frequency.

$$\eta = \frac{f}{f_{bpf}} \tag{12}$$

$$f_{bpf} = N_b \frac{N_2}{60(1 - M_a \cos\theta)} \tag{13}$$

Table 3.8.2 defines the atmospheric absorption in decibels that must be added to correct the predicted levels to a lossless condition. The atmospheric absorption levels are calculated for a distance of 150 feet using reference 6 for standard day conditions defined as 59 ^{o}F and 70% relative humidity.

Table 3.8.2 Standard Day Atmospheric Absorption

One-third-octave Band Center Frequency, Hz	$F_{abs}(f)$, dB
50	0.02
63	0.02
80	0.02
100	0.02
125	0.03
160	0.03
200	0.05
250	0.06
315	0.08
400	0.09
500	0.11
630	0.14
800	0.18
1000	0.23
1250	0.29
1600	0.36
2000	0.45
2500	0.60
3150	0.81
4000	1.14
5000	1.37
6300	1.91
8000	2.78
10000	4.11

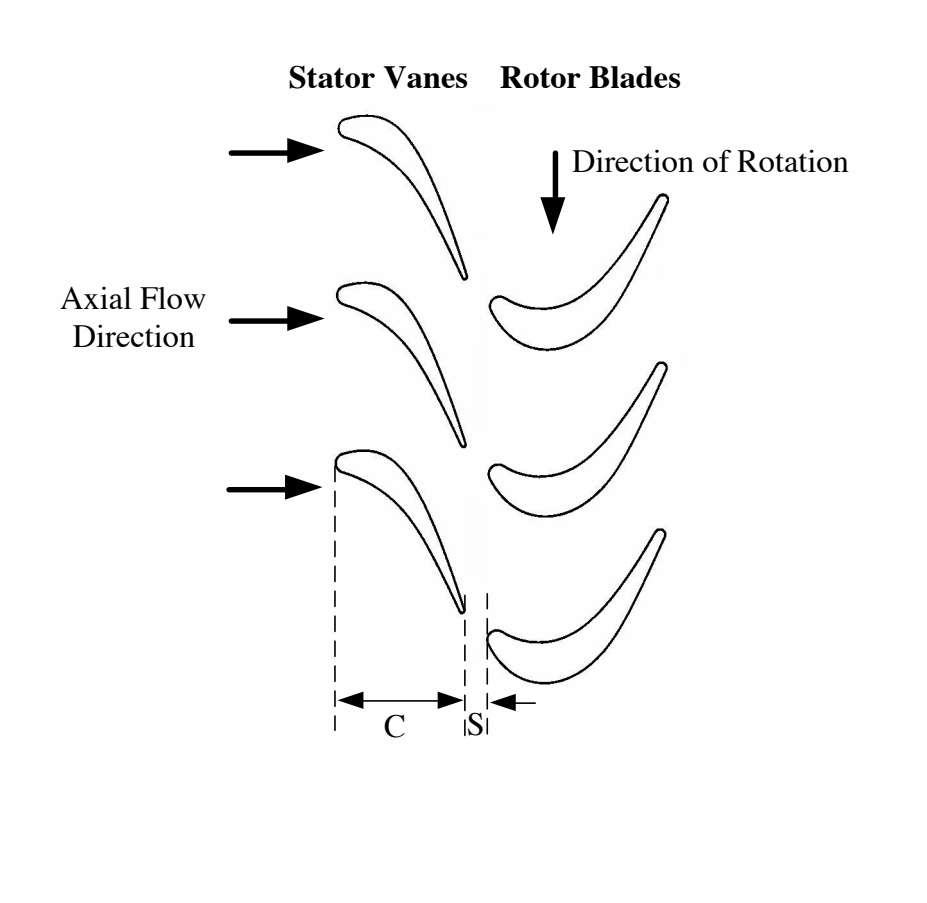

$$CSS = \frac{C}{S} \equiv \frac{\text{Stator Axial Chord}}{\text{Stator Rotor Spacing}}$$

Figure 3.8.1 Definition of stator chord to stator rotor spacing ratio

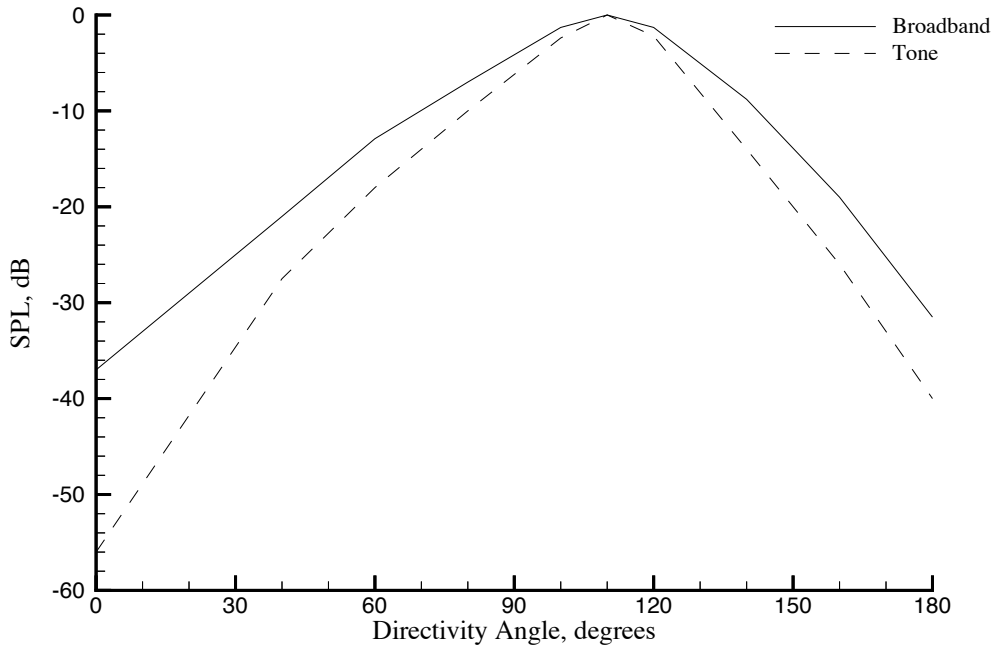

Figure 3.8.2 Turbine broadband and discrete tone directivity functions

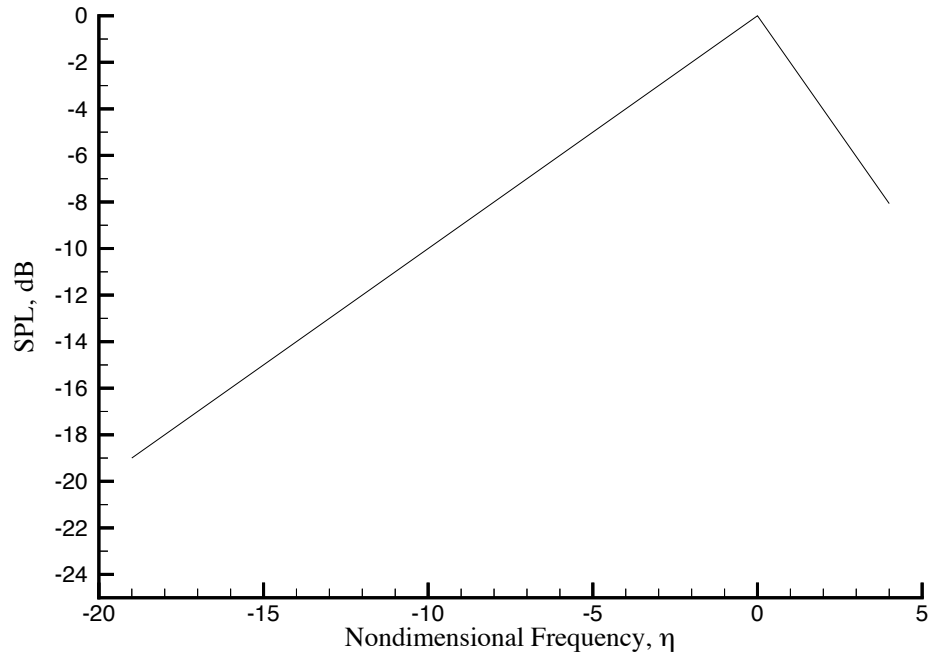

Figure 3.8.3 Turbine broadband spectrum function

3.9 Jet Noise (Boeing JN8C4 Methodology)

Adoption of the mixer-ejector as a means of reducing jet noise necessitated the development of new jet noise prediction methods. Research was conducted on a number of mixer-ejector configurations during the HSR program for both circular and rectangular configuration. As data became available, empirical jet noise prediction methods were developed at Boeing with the designation JN8. The method described in this section is the JN8C4 version developed by Lu and Viswanathan [7,8,9] for a supersonic jet issuing from a multilobe mixer into a rectangular ejector.

The jet is conceptually divided into three regions, the primary internal jet, the primary external jet, and the mixed jet. High frequency noise, termed "primary internal noise", is generated by the turbulent mixing of the supersonic primary flow with the entrained air. Shocks may be present in this region as a result of non-ideal expansion of the supersonic primary flow. Mid-frequency noise, termed "primary external or pre-merged noise", is produced by a combination of two mechanisms; (a) the continued mixing of the primary and the entrained flows inside the ejector and immediately downstream of the ejector exit, and (b) the initial mixing of the engine flow with the freestream. If the mixed jet is supersonic, the shock-associated noise of the mixed jet will also appear in the mid-frequency region. Low frequency noise, termed "mixed or merged noise", is generated by the mixing of the "mixed" jet (the initially rectangular jet having decayed to a near circular shape) with the freestream. The peak noise source is several equivalent diameters downstream of the ejector exit, where the length scale is quite large, usually on the order of the ejector equivalent diameter. Figure 3.9.1 shows a graphical representation of the three mixing noise components in the physical and spectral domains. The procedure predicts the one-third-octave band sound pressure level (SPL) for each component. The total jet noise SPL is the logarithmic sum of the five components:

1. primary internal noise
2. primary external or pre-merged noise
3. mixed or merged noise
4. broadband shock noise from the primary jet
5. broadband shock noise from the mixed jet

For certain operating conditions, the contribution of broadband shock noise to the total noise produced by the mixed ejector could be significant. The shock noise prediction procedure incorporated into this module is based on the instability wave/shock cell interaction source model developed by Tam [10,11]. The prediction of broadband shock noise in the internal jet region follows Tam's model for circular jets. Empirical adjustment is made for the rectangular geometry, liner effects, and frequency. Shocks in the primary external jet are predicted by Tam model for rectangular nozzles [12]. Empirical adjustments are made for flight effects.

Symbols

A_{abs}	atmospheric attenuation coefficient, dB/ft
A_p	primary nozzle exit area, ft^2 ***(input parameter*** – APRI***)***
A_s	secondary nozzle exit area, ft^2 ***(input parameter*** – ASEC***)***
A_T	throat area of the primary nozzle, ft^2 ***(input parameter***– ATHP***)***
A_2	area of a single lobe, ft^2
$\overline{A}$	shock cell strength function
b	source length, ft
b_{ej}	width of nozzle at exit plane, ft
c_a	ambient speed of sound, ft/sec
c_m	wave number parameter
c_s	speed of sound in secondary jet, ft/sec
$\overline{c}$	broadband shock constant
C_{fg}	mixer-ejector thrust coefficient (default =0.95) ***(input parameter*** – CFG***)***
D_{ej}	equivalent inner diameter of the ejector at the mixer exit, ft ***(input parameter*** – EJD***)***
D_i	Mixed jet nozzle exit diameter, ft
D_{plug}	primary nozzle exit diameter, ft ***(input parameter*** – PLUGD***)***
D_2	diameter of a single lobe, ft
d_ψ	$d_\psi = (\psi - \psi_0) / (0.5\pi)$
E_{asp}	mixer-ejector aspect ratio major/minor axis ***(input parameter*** – EJASP***)***
E_{asp1}	mixer-ejector aspect ratio minus one (E_{asp} – 1)
F	spectral distribution function
FV_i	Source strength function
f	one-third-octave band center frequency, Hz
f_{lin}	liner design center frequency, Hz ***(input parameter*** – FLIN***)***
f_m	Doppler shifted one-third-octave band center frequency, Hz
f_p	$f_p = \dfrac{f}{1 - M_a \cos\theta_p}$
G	ground effects, dB
h_{ej}	height of nozzle at exit plane, ft
h_j	fully expanded nozzle height, ft
J_1	first order Bessel function
k_m	wave number
L	shock cell spacing
L_{ej}	ejector length, ft ***(input parameter*** - EJL***)***
L_{lin}	length of ejector lining, ft ***(input parameter*** – EJLIN***)***
l_{div}	exit divergence angle, degrees ***(input parameter*** – DIVANG***)***
M_a	aircraft Mach number ***(input parameter*** – MA***)***
M'_a	special flight effect aircraft Mach number

M_c	convection Mach number
M_d	design Mach number
M_j	fully expanded jet Mach number
N_{eng}	number of engines
N_l	number of spokes or lobes of the mixer ***(input parameter*** – `SPOKE`***)***
n_i	velocity exponent
P_a	ambient pressure, lb/ft^2 ***(input parameter*** – `PAMB`***)***
P_{en}	mixer spoke penetration to nozzle full height ratio, ***(input parameter*** – `PEN`***)***
P_{std}	standard day pressure, lb/ft^2
$\langle p^2 \rangle$	mean-square pressure, (lb/ft^2)^2
r_m	distance from apparent source (in the mixed jet) to observer, ft
r_p	distance from apparent source (in the primary jet) to observer, ft
r_s	distance from nozzle exit to observer at the time of emission, ft
rh	relative humidity, %
R_{ej}	ratio of ejector length to minimum inner diameter of the ejector
R_{lin}	ratio of ejector lining length to minimum inner diameter of the ejector
S_i	Strouhal number
S_{lin}	liner Strouhal number
T_a	ambient temperature at microphone location, (^{o}R) ***(input parameter*** – `TAMB`***)***
T_p	primary jet total temperature, (^{o}R) ***(input parameter*** – `TPRI`***)***
T_s	secondary jet total temperature, (^{o}R) ***(input parameter*** – `TSEC`***)***
V_a	aircraft velocity, ft/sec ***(input parameter*** – `VAIR`***)***
V_c	convection velocity, ft/sec
V_m	mixed jet velocity, ft/sec
V_p	primary jet fully expanded velocity, ft/sec ***(input parameter*** – `VPRI`***)***
V_{pe}	external velocity, ft/sec
V_s	secondary jet velocity, ft/sec ***(input parameter*** – `VSEC`***)***
W_p	primary jet mass flow rate, lbm/sec ***(input parameter*** – `WPRI`***)***
W_s	secondary jet mass flow rate, lbm/sec ***(input parameter*** – `WSEC`***)***
X_i	noise source location down stream of the primary of common exit, ft
y_{obs}	observer sideline distance from flight path, ft ***(input parameter*** – `YOBS`***)***
z_o	observer altitude, ft
z_s	source altitude, ft
β_j	pressure ratio parameter
χ	Mach number ratio
ϕ	azimuth angle, degrees
ρ_a	ambient density, lbm/ft^3
ρ_j	jet density, lbm/ft^3

Γ	modal summation parameter
γ	ratio of specific heats
ψ	azimuth angle measured from the ejector major axis, radians
ψ_0	rectangular exit plan major axis roll angle relative to wing plane, degrees ***(input parameter*** – `PSI0`***)***
Π	acoustic power
θ_{obs}	observer angle measured from inlet, degrees
θ_i	wave normal angle measured from inlet, radians
σ_m	zeros of the zero-order Bessel function
ξ	$1 - M_a^2 \sin(\psi)$

Subscripts

i	general index ($i = p, pi, pe, \text{or } m$)
p	primary
pe	primary external
pi	primary internal
m	mixed
s	secondary

Component SPL Formulation

The general formula for calculating the one-third-octave band SPL for each jet mixing noise component is given by

$$SPL_i(f,\theta) = \left[(Z1_i)Log(FV_i) + (Z2_i)\right]\left[LogS_i - (Z3_i)Log(FV_i) - (Z4_i)\right]^2 + (Z5_i)Log(FV_i) + (Z6_i) \quad (1)$$

Formulas for the source strength FV_i, the Strouhal number S_i, and the coefficients $Z1_i$ through $Z6_i$ are provided in following sections. The subscript i is a general index, which indicates the jet component. Here $i = pi, pe,$ or m to indicate the primary internal, primary external, or the mixed jet component. When the primary internal and the primary external components share calculations, the index $i = p$ is used.

The source strength function FV_i is correlated as a function of nondimensional shear layer velocity difference, eddy convection velocity, and for the primary jet, the Mach number and the ambient flow effects. The velocity exponent provides the scaling of SPL_i with the jet and ambient flow acoustic Mach numbers (nondimensional velocities). The velocity exponent has a strong directivity dependence and a weak Strouhal number dependence. The Strouhal number is defined for each component, using the shear layer velocity difference, the component jet diameter and source frequency.

Figure 3.9.2 shows graphically how each coefficient affects the SPL. Coefficients $Z1_i$ and $Z2_i$ determine the spectrum distribution. Coefficients $Z3_i$ and $Z4_i$ determine the location of the peak frequency. Coefficients $Z5_i$ and $Z6_i$ determine the SPL amplitude. All the coefficients are more directivity dependent than Strouhal number dependent.

Coefficients $Z1_i$ through $Z6_i$ are functions of the source radiation angle and other parameters. The mixing noise components are modeled as a distribution of point sources. Each source has a unique radiation angle. Calculation of the radiation angle from the distributed source location is explained in the following sections.

Jet Noise Source Distributions

Noise sources are distributed over a wide range of the jet mixing region, which extends from the nozzle exit to a distance of 15 mixed jet diameters downstream. Each source has a radiation angle that differs from the geometric angle associated with the position of the aircraft. The location of the source within the mixing region, the radiation distance, the source radiation angle, and the source frequency are uniquely determined for each source and observer position. This section describes the procedure for locating the sources in the primary internal jet, the primary external jet, and the mixed jet.

Source Distribution for the Primary Internal and Primary External Jets

The source distribution for the primary internal and external jets is given by

$$X_p = \left[4 + 4\tan^{-1}\left(\frac{18\theta_p}{\pi} - 9 \right) + \frac{A_s}{A_p} \right] \frac{D_p}{\sqrt{1 + N_l P_{en}}} \tag{2}$$

Sources radiating in the forward arc are located close to the nozzle exit, while sources radiating in the aft arc are located further downstream of the nozzle exit. Note that the source distribution formula for the primary jets is independent of frequency. Frequency dependent forms were tested but did not improve agreement with measured data.

Source Distribution for the Mixed Jets

The mixed (merged) jet source location normalized by mixed jet diameter is given empirically by

$$X_m = \left\{ 3 + \exp(-S_m) + \left[2 + 1.1\tan^{-1}\left(\frac{18.\theta_m}{\pi} - 13 \right) \right] \left(1 + 0.5 S_m^{-1/2} \right) \right\} \tag{3}$$
$$\times \left(0.5 + 0.5 \frac{V_m}{c_a} \right)^{1/2} \left(\frac{V_m}{V_m - V_a} \right) \frac{D_m}{\sqrt{1 + Log_{10}(1 + N_l)}}$$

Although the mixed jet does not have a potential core, the characteristics of source distributions are similar to that of the primary internal and primary external jets. The source distribution function for the mixed jet is a function of frequency.

Determination of Radiation Angle and Source Frequency

Since noise sources are distributed over a wide range of the jet mixing region, the geometric angle, which identifies the observer location with respect to the nozzle exit, differs from the source radiation angle. The source location and radiation angle associated with a given observer is determined by an iterative procedure described below.

<u>Static or Wind Tunnel Coordinates</u>

When there is no relative motion between the observer and the nozzle, (figure 3.9.3a) the source for a given component is located at X_i and radiates sound at an angle θ_i (wave normal angle). The subscript $i = p$ or m and the angles θ_i are in radians. The observer (microphone) angle is θ_{obs} at sideline distance y_{obs} as shown in figure 3.9.3b. The source location and radiation angle are determined by the following iterative procedure.

Step 1. For a given one-third-octave band frequency (Strouhal number S_i), initialize $\theta_i = \pi/2$ and compute the source location X_i (dimensional) for the desired region from equations 2 or 3.

Step 2. Compute a new radiation angle $\theta_{i,new}$ using

$$\theta_{i,new} = \sin^{-1}\left[\frac{-M_a B + \sqrt{B^2 - M_a^2 + 1}}{B^2 + 1}\right] \qquad M_a < 1$$

where

$$B = \left(X_i / SL\right) + \cot\theta_{obs}$$

X_i is the source location from step 1, SL is the sideline distance, and θ_{obs} is the angle for the nozzle exit to the observer measured from the inlet axis. Compute a new source location X_i using $\theta_i = \theta_{i,new}$.

Step 3a. Let $\theta_1 = \theta_{i,new}$.
Step 3b. Compute a new radiation angle $\theta_{i,new}$ using X_i.
Step 3c. Let $\theta_2 = \theta_{i,new}$ obtained from step 3b.
Step 4a. Let $\theta_i = \left(\theta_1 + \theta_2\right)/2$.
Step 4b. Compute a new source location X_i using $\theta_i = \left(\theta_1 + \theta_2\right)/2$.
Step 4c. Let $X_{i,new} = X_i$.
Step 5. Repeat steps (3) and (4) until $\left|X_i - X_{i,new}\right| \le 0.05 D_i$.

<u>Transformation from Wind Tunnel to Ground-Fixed Coordinates</u>

The iteration procedure for ground-fixed coordinates is the same as the wind tunnel case except, the source radiation angle (wave normal) is given by

$$\theta_i = \sin^{-1}\left[\frac{1}{B^2 + 1}\right] \qquad (4)$$

Calculation of the Mixed Jet Parameters for the Aspirated Mixer-Ejector

Calculation of the mixed jet noise component level requires mixed jet parameters as well as some primary, secondary, and the ambient flow parameters. The mixed jet parameters are not independent parameters, since they are calculated from the primary and the secondary jet parameters under the fully-mixed assumption. For most mixer-ejectors, the "secondary" jet is the aspirated (induced or entrained) ambient flow. To calculate the mixed jet velocity, it is assumed that the total momentum of the primary stream and the aspirated stream, before and after mixing, is conserved (i.e., the net thrust is independent

of aspiration). Since the aspirated flow has the ambient stream momentum, calculation of the mixed jet velocity V_m for the aspirated mixer-ejector is given by:

$$V_m = \frac{V_p W_p + V_a W_s}{W_p + W_s} \tag{5}$$

where the ambient (wind tunnel or airplane) velocity V_a is used. Other conditions of the mixed jet are calculated by using conservation of mass flow and total enthalpy.

$$T_m = T_{t,m} = \frac{T_p W_p + T_s W_s}{W_p + W_s} \tag{6}$$

$$A_m = \frac{W_p + W_s}{\rho_m V_m} \tag{7}$$

$$D_m = \sqrt{\frac{4A_m}{\pi}} \tag{8}$$

The mixed jet density in addition to other jet parameters is determined by a two step procedure. The ratios of specific heats for the primary, secondary, and mixed jets are calculated initially using the total temperatures as follows

$$\gamma_p = 1.357 + 0.058 \tan^{-1}\left(\frac{1200 - T_{t,s}}{870}\right) \tag{9}$$

$$\gamma_s = 1.368 + 0.050 \tan^{-1}\left(\frac{1200 - T_{t,s}}{870}\right) \tag{10}$$

$$\gamma_m = 1.363 + 0.054 \tan^{-1}\left(\frac{1200 - T_{t,m}}{830}\right) \tag{11}$$

The static temperature are computed by

$$T_{s,p} = T_{t,p} - \frac{\gamma_p - 1}{2}\left(\frac{V_p^2}{\gamma_p R}\right) \tag{12}$$

$$T_{s,s} = T_{t,s} - \frac{\gamma_s - 1}{2}\left(\frac{V_s^2}{\gamma_s R}\right) \tag{13}$$

$$T_{s,m} = T_{t,m} - \frac{\gamma_m - 1}{2}\left(\frac{V_m^2}{\gamma_m R}\right) \tag{14}$$

The ratios of specific heats are recalculated using

$$\gamma_p = 1.357 + 0.058 \tan^{-1}\left(\frac{1200 - T_{p,avg}}{870}\right) \tag{15}$$

$$\gamma_s = 1.368 + 0.050 \tan^{-1}\left(\frac{1200 - T_{s,avg}}{800}\right) \tag{16}$$

$$\gamma_m = 1.363 + 0.054 \tan^{-1}\left(\frac{1200 - T_{m,avg}}{830}\right) \tag{17}$$

where the average between the total and static temperatures is

$$T_{p,avg} = \frac{T_{t,p} + T_{s,p}}{2} \tag{18}$$

$$T_{s,avg} = \frac{T_{t,s} + T_{s,p}}{2} \tag{19}$$

$$T_{m,avg} = \frac{T_{t,m} + T_{s,m}}{2} \tag{20}$$

Finally, the static temperature for the primary, secondary, and mixed jets is determined by

$$T_{s,p} = T_{t,p} - \frac{\gamma_p - 1}{2}\left(\frac{V_p^2}{\gamma_p R}\right) \tag{21}$$

$$T_{s,s} = T_{t,s} - \frac{\gamma_s - 1}{2}\left(\frac{V_s^2}{\gamma_s R}\right) \tag{22}$$

$$T_{s,m} = T_{t,m} - \frac{\gamma_m - 1}{2}\left(\frac{V_m^2}{\gamma_m R}\right) \tag{23}$$

From the quantities computed above, the fully expanded jet Mach number, jet densities, and pressure ratio parameters can be computed.

Fully expanded jet Mach number parameters

$$M_{j,p} = \left[\frac{2}{\gamma_p - 1} \left(\frac{T_{t,p}}{T_{s,p}} - 1 \right) \right]^{\frac{1}{2}} \tag{24}$$

$$M_{j,s} = \left[\frac{2}{\gamma_s - 1} \left(\frac{T_{t,s}}{T_{s,s}} - 1 \right) \right]^{\frac{1}{2}} \tag{25}$$

$$M_{j,m} = \left[\frac{2}{\gamma_m - 1} \left(\frac{T_{t,m}}{T_{s,m}} - 1 \right) \right]^{\frac{1}{2}} \tag{26}$$

Jet density parameters

$$\rho_p = \frac{P_a}{RT_{s,p}} \tag{27}$$

$$\rho_s = \frac{P_a}{RT_{s,s}} \tag{28}$$

$$\rho_m = \frac{P_a}{RT_{s,m}} \tag{29}$$

Pressure ratio parameters

$$\beta_p = \sqrt{M_{j,p}^2 - 1} \tag{30}$$

$$\beta_s = \sqrt{M_{j,s}^2 - 1} \tag{31}$$

$$\beta_m = \sqrt{M_{j,m}^2 - 1} \tag{32}$$

Primary Internal Component of Jet Mixing Noise

The high frequency noise, termed "primary internal noise", is generated by the turbulent mixing of the supersonic primary flow with the entrained air. The length scales in this regime are small with the macro scales being on the order of the lobe width. The sound pressure level for the primary internal jet mixing noise is

$$SPL_{pi}(f,\theta,\phi,r_s) = \left[(Z1_{pi})Log_{10}(FV_{pi}) + (Z2_{pi})\right]\left[Log_{10}S_{pi} - (Z3_{pi})Log_{10}(FV_{pi}) - (Z4_{pi})\right]^2 + (Z5_{pi})Log_{10}(FV_{pi}) + (Z6_{pi}) + \Delta SPL_{pi} \quad (33)$$

The last term in the equation above represents propagation effects which are discussed later in this section. Formulas for the source strength FV_{pi}, the Strouhal number S_{pi}, and the coefficients $Z1_{pi}$ through $Z6_{pi}$ are provided below.

Source Strength Function	***Primary Internal Jet***

$$FV_{pi} = \left(\frac{V_p - V_s}{c_a}\right)^{0.6}\left(\frac{V_p + V_s}{c_a}\right)^{0.4} \quad (34)$$

Strouhal Number	***Primary Internal Jet***

$$S_{pi} = \frac{fD_p}{(V_p - V_s)} \quad (35)$$

$$D_p = \sqrt{\frac{4A_p}{\pi}} \quad (36)$$

Coefficient Z1	***Primary Internal Jet***

$$Z1_{pi} = -18\left(\frac{1.8\theta_p}{\pi} - 0.6\right)^2 \quad (37)$$

Coefficient Z2	***Primary Internal Jet***

$$Z2_{pi} = -23 - 20\left(\frac{1.8\theta_p}{\pi} - 0.6\right)^2 + 5\left(1 + Log_{10}S_{pi}\right)\left\{1 + \left(\frac{1.8\theta_p}{\pi} - 0.6\right)\right\} + C21(R_{ej},\theta_p) \quad (38)$$

Adjustment for ejector length to inner diameter ratio

$$C21 = +15\left[1 - \exp\left(-R_{ej}\right)\right]\left(\frac{1.8\theta_p}{\pi} - 0.6\right)^2 \tag{39}$$

$$R_{ej} = \frac{L_{ej}}{D_{ej}} \tag{40}$$

Coefficient Z3 **Primary Internal Jet**

$$Z3_{pi} = 0 \tag{41}$$

Coefficient Z4 **Primary Internal Jet**

$$\begin{aligned} Z4_{pi} = {} & 0.6 Log_{10}\left(1 + N_l\right)\left\{1 - 0.2\exp\left[-5\left(\theta_p - 1.8\right)^2\right]\right\} - 0.6\frac{V_p - V_s}{c_a}\left(\frac{1.8\theta_p}{\pi} - 0.6\right)^2 \\ & - 0.2\frac{W_s}{W_p} + 0.1\left(\beta_p + 1\right)\left(\frac{1.8\theta_p}{\pi} - 0.6\right) + 0.5 \\ & + C41(P_{en}) + C42(E_{asp}, \theta_p) + C43(R_{ej}, \theta_p) \end{aligned} \tag{42}$$

Adjustment for lobe penetration

$$C41 = 0.2P_{en} \tag{43}$$

Adjustment for aspect ratio

$$C42 = +0.1E_{asp}\left[1 - \left(\frac{1.8\theta_p}{\pi} - 0.6\right)\right] \tag{44}$$

Adjustment for ejector length to inner diameter ratio

$$C43 = -0.4 Log_{10}\left(1 + R_{ej}\right)\left[1 - \left(\frac{1.8\theta_p}{\pi} - 0.6\right)^4\right] \tag{45}$$

$$E_{asp1} = \begin{cases} E_{asp} \Big/ X_{mar} - 1 & \text{for } E_{asp1} > 0 \\ 0 & \text{for } E_{asp1} \le 0 \end{cases} \tag{46}$$

$$\beta_p = \sqrt{M_p^2 - 1} \tag{47}$$

Coefficient Z5 **Primary Internal Jet**

$$Z5_{pi} = 50 + 20\exp\left[-\left(\theta_p - 2.6\right)^2\right] \tag{48}$$

Coefficient Z6 **Primary Internal Jet**

$$\begin{aligned} Z6_{pi} &= 142 - 56\left(\frac{1.8\theta_p}{\pi} - 0.6\right) + 46\exp\left[-\left(\theta_p - 2.5\right)^2\right] - 8\,Log_{10}\left(1 + N_l\right) - 5\frac{W_s}{W_p} \\ &+ 2\exp\left[-10\left(\theta_p - 2.5\right)^2\right] + 5\exp\left[-5\left(\theta_p - 1.9\right)^2\right] \\ &+ C61(E_{asp}, E_{asp1}, d_\psi) + C62(C_{fg}) + C63(M'_a, d_\psi) + C64(R_{ej}, R_{lin}, S_p, S_{lin}) \end{aligned} \tag{49}$$

Adjustment for aspect ratio and azimuth angle

$$\begin{aligned} C61 &= E_{asp1}d_\psi^2\left\{1 + 6\exp\left[-10\left(\theta_p - 2.6\right)^2\right]\right\} - 6E_{asp1}\left(\frac{1.8\theta_p}{\pi} - 0.6\right) \\ &+ 5\sqrt{E_{asp1}} - 8E_{asp1}\left(1 - 0.4d_\psi^2\right)\left(\frac{1.8\theta_p}{\pi} - 0.6\right) \\ &+ 2E_{asp}\exp\left[-10\left(\theta_p - 2.5\right)^2\right] + 5\sqrt{E_{asp1}}\exp\left[-5\left(\theta_p - 1.4\right)^2\right]\left(1 - 0.5d_\psi^2\right) \end{aligned} \tag{50}$$

Adjustment for thrust loss

$$C62 = -40\left(1 - C_{fg}\right) \tag{51}$$

Adjustment for flight effects and azimuth angle

$$\begin{aligned} C63 &= +3\sqrt{M'_a}\left\{\exp\left[-10\left(\theta_p - 1\right)^2\right] - \exp\left[-10\left(\theta_p - 2.4\right)^2\right]\right\} \\ &+ 15\sqrt{M'_a}d_\psi^2\exp\left(-5\beta_p\right)\left\{\exp\left[-10\left(\theta_p - 2.3\right)^2\right] - 0.8\exp\left[-20\left(\theta_p - 1.5\right)^2\right]\right\} \end{aligned} \tag{52}$$

Adjustment for ejector length to inner diameter ratio, ejector liner, and Strouhal number

$$
\begin{aligned}
C64 = {} & -10\left[1-\exp\left(-R_{ej}\right)\right]\left\{1-0.5\exp\left[-5\left(\theta_p-1.6\right)^2\right]+0.4\exp\left[-5\left(\theta_p-2.2\right)^2\right]\right\} \\
& -0.3R_{ej}^2\exp\left[-5\left(\theta_p-1\right)^2\right] \\
& -\left[2.5-\left(\frac{1.8\theta_p}{\pi}-0.6\right)\right]R_{lin}\left[2-\exp\left(R_{lin}-R_{ej}\right)\right]\exp\left[-0.5\left(Log_{10}S_{pi}-Log_{10}S_{lin}\right)^2\right] \\
& -1.3\left\{1+0.4\exp\left[-5\left(\theta_p-1.6\right)^2\right]\right\}R_{lin}\left[2-\exp\left(R_{lin}-R_{ej}\right)\right]\exp\left[-0.5\left(Log_{10}S_{pi}-Log_{10}S_{lin}\right)^2\right]
\end{aligned}
\tag{53}
$$

$$
d_\psi = \frac{\psi-\psi_0}{0.5\pi} \tag{54}
$$

$$
M_a' = \begin{cases} M_a & \text{for } M_a < 0.3 \\ 0.3 & \text{for } M_a \geq 0.3 \end{cases} \tag{55}
$$

$$
R_{lin} = \frac{L_{lin}}{D_{ej}} \tag{56}
$$

$$
S_{lin} = \frac{\left(f_{lin}+0.01\right)D_p}{\left(V_p-V_s\right)} \tag{57}
$$

Primary External Component of Jet Mixing Noise

The mid-frequency noise, termed "primary external or pre-merged noise", is produced by a combination of two mechanisms; (a) the continued mixing of the primary and the entrained flows inside the ejector and immediately downstream of the ejector exit, and (b) the initial mixing of the engine flow with the freestream. The sound pressure level for the primary external jet mixing noise is

$$
\begin{aligned}
SPL_{pe}\left(f,\theta,\phi,r_s\right) = {} & \left[\left(Z1_{pe}\right)\log\left(FV_{pe}\right)+\left(Z2_{pe}\right)\right]\left[\log S_{pe}-\left(Z3_{pe}\right)\log\left(FV_{pe}\right)-\left(Z4_{pe}\right)\right]^2 \\
& +\left(Z5_{pe}\right)\log\left(FV_{pe}\right)+\left(Z6_{pe}\right)+\Delta SPL_{pe}
\end{aligned}
\tag{58}
$$

The last term in the equation above represents propagation effects which are discussed later in this section. Formulas for the source strength FV_{pe}, the Strouhal number S_{pe}, and the coefficients $Z1_{pe}$ through $Z6_{pe}$ are provided below.

Source Strength Function	***Primary External Jet***

$$FV_{pe} = \left(\frac{V_{pe} - V_a}{c_a}\right)^{n_{pc}} \left(\frac{V_{pe} + V_a}{V_p}\right)^{1-n_{pe}} \tag{59}$$

$$n_{pe} = 0.35 + 0.9\exp\left[-1.5\left(\theta_p - 2.4\right)^2\right] \tag{60}$$

$$V_{pe} = 0.7V_p + 0.3V_s \tag{61}$$

Strouhal Number	***Primary External Jet***

$$S_{pe} = \frac{fD_p}{\left(V_p - V_s\right)} \tag{62}$$

Coefficient Z1	***Primary External Jet***

$$Z1_{pe} = -18\left(\frac{1.8\theta_p}{\pi} - 0.6\right)^2 \tag{63}$$

Coefficient Z2	***Primary External Jet***

$$Z2_{pe} = -23 - 20\left(\frac{1.8\theta_p}{\pi} - 0.6\right)^2 + 20\beta_p\left(\frac{1.8\theta_p}{\pi} - 0.6\right)^2 + 6\exp\left[-10\left(\theta_p - 2.8\right)^2\right] \tag{64}$$

Coefficient Z3	***Primary External Jet***

$$Z3_{pe} = 0 \tag{65}$$

Coefficient Z4	***Primary External Jet***

$$\begin{aligned} Z4_{pe} = {} & 0.6Log_{10}\left(1 + N_l\right)\left\{1 - 0.2\exp\left[-5\left(\theta_p - 1.8\right)^2\right]\right\} - 0.6\frac{V_p - V_s}{c_a}\left(\frac{1.8\theta_p}{\pi} - 0.6\right)^2 \\ & - 0.2\frac{W_s}{W_p} + 0.1\beta_p\left(\frac{1.8\theta_p}{\pi} - 0.6\right) - 0.6 + 0.1\left(\frac{1.8\theta_p}{\pi} - 0.6\right) \\ & - 0.2\exp\left[-10\left(\theta_p - 1\right)^2\right] \\ & + C41(P_{en}, l_{div}) + C42(E_{asp1}, E_{asp1}, R_{ej}) + C43(d_\psi, M'_a, \beta_p) \end{aligned} \tag{66}$$

Adjustment for lobe penetration and divergence angle

$$C41 = 0.2P_{en} - 0.01l_{div} \tag{67}$$

Adjustment for aspect ratio and ejector length to inner diameter ratio

$$C42 = -0.3E_{asp1}\left[1-\left(\frac{1.8\theta_p}{\pi}-0.6\right)\right] + 0.1E_{asp}\left[1-\left(\frac{1.8\theta_p}{\pi}-0.6\right)\right] \tag{68}$$

Adjustment for azimuth angle

$$C43 = 0.2\exp\left[5-(\theta_p-1.9)^2-2\left(1-d_\psi^2\right)\right] - 2\sqrt{M'_a}\exp\left(-5\beta_p\right) \tag{69}$$

Coefficient Z5 ***Primary External Jet***

$$Z5_{pe} = 50 + 20\exp\left[-(\theta_p-2.6)^2\right] \tag{70}$$

Coefficient Z6 ***Primary External Jet***

$$Z6_{pe} = 137 - 40\left(\frac{1.8\theta_p}{\pi}-0.6\right) + 46\exp\left[-(\theta_p-2.5)^2\right] - 8Log_{10}(1+N_l) - 5\frac{W_s}{W_p} + 2\exp\left[-10(\theta_p-2.5)^2\right] + (2+3\beta_p)\left(\frac{1.8\theta_p}{\pi}-0.6\right) - 3\exp\left[-10(\theta_p-2.3)^2\right] + 2\exp\left[-10(\theta_p-1.9)^2\right] + C61(l_{div}) + C62(M'_a,\beta_p) + C63(d_\psi,E_{asp1}) + C64(R_{lin},R_{ej}) + C65(C_{fg},M'_a) \tag{71}$$

Adjustment for divergence angle

$$C61 = 0.4l_{div}\left[0.4-\left(\frac{1.8\theta_p}{\pi}\right)-0.6\right] \tag{72}$$

Adjustment for flight effects

$$C62 = 15\sqrt{M'_a}\exp\left(-5\beta_p\right)\exp\left[-10(\theta_p-2.4)^2\right] \tag{73}$$

Adjustment for aspect ratio and azimuth angle

$$C63 = -3\left(1 - d_\psi^2\right)\sqrt{E_{asp1}}\left(\frac{1.8\theta_p}{\pi} - 0.6\right) + E_{asp1}d_\psi^2\left\{1 + 6\exp\left[-10\left(\theta_p - 2.6\right)^2\right]\right\} - 6E_{asp1}\left(\frac{1.8\theta_p}{\pi} - 0.6\right) \quad (74)$$

Adjustment for ejector length to inner diameter ratio and liner length to inner diameter

$$C64 = -\left[2.5 - \left(\frac{1.8\theta_p}{\pi} - 0.6\right)\right]R_{lin}^{\left[2-\exp\left(R_{lin}-R_{ej}\right)\right]} \quad (75)$$

Adjustment for thrust loss and flight effects

$$C65 = -40\left(1 - C_{fg}\right)\left(1 - M_a'\right) \quad (76)$$

Mixed Jet Component of Jet Mixing Noise

The low frequency noise, termed "mixed or merged noise", is generated by the mixing of the so-called "mixed" jet (the initially rectangular jet having decayed to a near circular shape) with the freestream. The peak noise source is several equivalent diameters downstream of the ejector exit, where the length scale is quite large, usually on the order of the ejector equivalent diameter. The characteristics of the merged noise are similar to those of subsonic round jets. The sound pressure level for the mixed jet is

$$SPL_m\left(f,\theta,\phi,r_s\right) = \left[\left(Z1_m\right)Log_{10}\left(FV_m\right) + \left(Z2_m\right)\right]\left[Log_{10}S_m - \left(Z3_m\right)Log_{10}\left(FV_m\right) - \left(Z4_m\right)\right]^2 + \left(Z5_m\right)Log_{10}\left(FV_m\right) + \left(Z6_m\right) + \Delta SPL_m \quad (77)$$

The last term in the equation above represents propagation effects which are discussed later in this section. Formulas for the source strength FV_m, the Strouhal number S_m, and the coefficients $Z1_m$ through $Z6_m$ are provided below.

Source Strength Function	***Mixed Jet Component***

$$FV_m = \left(\frac{V_m - V_a}{c_a}\right)^{n_m}\left(\frac{V_m + V_a}{c_a}\right)^{1-n_m} \quad (78)$$

$$n_m = \left(\frac{V_m}{c_a}\right)^{1/2}\left\{0.6 + \frac{0.2}{0.2 + S_m}\exp\left[-0.3\left(\theta_m + \frac{S_m}{1 + S_m} - 2.7\right)^2\right]\right\} \quad (79)$$

Strouhal Number **Mixed Jet Component**

$$S_m = \frac{fD_m}{(V_m - V_a)} \tag{80}$$

Coefficient Z1 **Mixed Jet Component**

$$Z1_m = -30\left(\frac{1.8\theta_m}{\pi} - 0.6\right)^2 \tag{81}$$

Coefficient Z2 **Mixed Jet Component**

$$Z2_m = -9 - 4\left(\frac{V_p - V_s}{c_a}\right) - 38\left(\frac{1.8\theta_m}{\pi} - 0.6\right)^3 - 10(1 + 2\beta_m)\left(\frac{1.8\theta_m}{\pi} - 0.6\right)^2 \tag{82}$$
$$+ 30\left[0.6 - Log_{10}\left(1 + \frac{A_s}{A_p}\right)\right]\left(\frac{1.8\theta_m}{\pi} - 0.6\right)$$
$$+ \left(\frac{V_m - V_a}{c_a}\right)\left(\frac{1.8\theta_m}{\pi} - 0.6\right)\left\{2Log_{10}(1 + N_l) + 6\left[1 + 2\left(\frac{1.8\theta_m}{\pi} - 0.6\right)^2\right]\left[1 - \exp(-R_{ej})\right]\right\}$$

Coefficient Z3 **Mixed Jet Component**

$$Z3_m = 1 - 0.4\left(\frac{1.8\theta_m}{\pi} - 0.6\right)^2 \tag{83}$$

Coefficient Z4 **Mixed Jet Component**

$$Z4_m = 0.44 - 0.5\exp\left[-\left(\frac{4.5\theta_{mj}}{\pi} - 4\right)^2\right] + \frac{0.2V_p - 0.7V_m}{c_a} - 0.2Log_{10}\left(1 + \frac{A_s}{A_p}\right) \tag{84}$$
$$- 0.8\left[1 - \exp(-R_{ej})\right]\frac{Log_{10}(1 + N_l)}{1 + Log_{10}(1 + N_l)}$$
$$+ 0.1\left(\frac{V_m}{c_a} + 5\beta_m\right)\left(\frac{1.8\theta_m}{\pi} - 0.6\right)^2 + C41(E_{asp}, C_{fg})$$

where $\theta_{mj} = \theta_m$ and $\frac{\pi}{3} \le \theta_{mj} \le \frac{8}{9}\pi$

Adjustment for thrust loss

$$C41 = 0.15E_{asp} - \left(1 - C_{fg}\right) \tag{85}$$

Coefficient Z5	***Mixed Jet Component***

$$Z5_m = 34 + \frac{81\theta_{mj}}{\pi} - 20\left(\frac{1.8\theta_m}{\pi} - 0.6\right)^3 \tag{86}$$

Coefficient Z6	***Mixed Jet Component***

$$Z6_m = 123 + 12\left(\frac{1.8\theta_m}{\pi} - 0.6\right) + 7\exp\left[-8\left(\theta_m - 2.4\right)^2\right] + 5\beta_m \exp\left[-15\left(\theta_m - 2.3\right)^2\right] + C61(C_{fg}, M'_a) + C62(E_{asp1}, d_\psi, M'_a) \tag{87}$$

Adjustment for thrust loss and flight effects

$$C61 = -40\left(1 - C_{fg}\right)\left(1 - M'_a\right) \tag{88}$$

Adjustment for aspect ratio, azimuth angle, and flight effects

$$C62 = 2E_{asp1}\exp\left[-10\left(\theta_m - 1.8\right)^2\right]\left(1 + d_\psi^2\right) - \left(2 + 5\sqrt{M'_a}\right)E_{asp1}\left(1 - 0.2d_\psi^2\right)\left(\frac{1.8\theta_m}{\pi} - 0.6\right) \tag{89}$$

Broadband Shock Noise

For a supersonic jet inside an ejector, formation of broadband shocks in the internal flow is unavoidable due to the presence of pressure gradients and non-ideal expansion at off-design operating conditions. For very high nozzle pressure ratios, the mixed jet velocity may be supersonic at the ejector exit, which could lead to shock formations in the primary external plume. For certain operating conditions, the contribution of shock noise to the total noise produced by the mixer-ejector could be significant. The shock noise prediction procedure incorporated into this module is based on the instability wave/shock cell interaction source model developed by Tam [10,11]. The prediction of broadband shock noise in the internal jet region follows Tam's model for circular jets. Empirical adjustment is made for the rectangular geometry, liner effects, and frequency. Shocks in the primary external jet are predicted by Tam's model for rectangular nozzles [12]. Empirical adjustments are made for flight effects.

Primary Internal Broadband Shock Noise

The mean-square acoustic pressure for the broadband shock noise associated with the primary internal jet is

$$\left\langle p^2(r_s,\theta,\phi,f)\right\rangle_{shock,pi} = \frac{\Pi A_2}{R_s^2} F(\psi,\phi,f) \tag{90}$$

where Π is the overall acoustic power, A_2 is the area of a single lobe given by,

$$A_2 = A_p / N_l \tag{91}$$

and F is the spectral distribution function. The right side of equation 90 represents the mean-square pressure for a stationary observer in nozzle fixed coordinates. Figure 3.9.4 shows the relationship between the nozzle fixed coordinate system and the ground based observer coordinate system. Since the noise at the observer is independent of the coordinate system, the mean-square pressure can be transformed from nozzle fixed coordinates to the ground fixed coordinates by the following geometric relations

$$\psi = \tan^{-1}\left[\frac{\sin\theta}{\cos\theta - M_a}\right] \tag{92}$$

and

$$R_s = r_s \frac{\sin\theta}{\sin\psi} \tag{93}$$

Primary Internal Shock Acoustic Power

The broadband shock acoustic power adjusted for the mixer configuration is

$$\Pi = \frac{\bar{c} L^2 \bar{A}^2 \frac{V_p^2}{c_a^2}}{\xi^2} \tag{94}$$

where

$$\bar{c} = 0.0001 \tag{95}$$

and

$$\xi^2 = 1 - M_a^2 \sin^2(\psi) \tag{96}$$

L is the shock cell spacing parameter and is assigned a constant value

$$L = 3.3 \tag{97}$$

The shock cell strength function $\overline{A}$ is defined for over and underexpanded jets as

$$\overline{A}^2 = \begin{cases} \dfrac{\chi^2}{1+3\chi^3}\dfrac{A_2}{A_{j,p}} & M_p > M_d \text{ Underexpanded Jet} \\ \dfrac{\chi^2}{1+6\chi^5} & M_p \le M_d \text{ Overexpanded Jet} \end{cases} \tag{98}$$

where

$$\chi = \frac{\left|M_{j,p}^2 - M_d^2\right|}{1+\left(\frac{\gamma_p - 1}{2}\right)M_d^2} \tag{99}$$

A_2 is the area of a single lobe and $A_{j,p}$ is the fully expanded jet area given by

$$A_{j,p} = A_p\left[\frac{1+\frac{1}{2}\left(\gamma_p - 1\right)M_{j,p}^2}{1+\frac{1}{2}\left(\gamma_p - 1\right)M_d^2}\right]^{\frac{1}{2}\left(\frac{\gamma_p+1}{\gamma_p-1}\right)}\left(\frac{M_d}{M_{j,p}}\right) \tag{100}$$

Spectral Distribution Function

The one-third-octave band spectrum function is obtained by integrating

$$\mathrm{F}(\psi,\phi,f) = \int_{fl}^{fu}\frac{\Gamma_m}{f_{re}\left(f_{re}D_2/V_p\right)}df \tag{101}$$

The upper and lower limits of integration are

$$f_u = 2^{\frac{1}{6}}f \tag{102}$$

and

$$f_l = 2^{-\frac{1}{6}}f \tag{103}$$

where f is the one-third-octave band center frequency. The argument of the integral is evaluated at 20 points within a one-third-octave band and integrated numerically using Simpson's rule. In equation 101, f_{re} is

$$f_{re} = \frac{4D_2}{D_{ej} - D_{plug}} f \tag{104}$$

The parameter Γ_m represents the sum of the modal contributions for a given frequency

$$\Gamma_m = \sum_{m=1}^{35} \frac{1}{\sigma_m^2 J_1^2(\sigma_m)} \exp\left\{ -\left(\frac{f_m}{f_{re}} - 1 \right)^2 \left[1 + M_c \left(\frac{M_a \xi + \cos(\psi)}{\xi(1 - M_a^2)} \right) \right]^2 \left(\frac{V_p}{V_c} \right)^2 \frac{L^2}{2 \ln 2} \right\} \tag{105}$$

Summation takes place over the first 35 modes or until the quantity $(f_{re} D_2 / V_p)$ becomes greater than 5.5, at which point the summation is terminated. The factors σ_m are the zeros of the zero-order Bessel function and $J_1(\sigma_m)$ is the first order Bessel function. Values for σ_m and $J_1(\sigma_m)$ are given in table 3.9.1. The modal frequency parameter f_m is defined in terms of the wave number k_m and the convection velocity V_c by

$$f_m = \frac{k_m V_c}{2\pi} \left\{ 1 + M_c \left[\frac{M_a \xi + \cos(\psi)}{(1 - M_a^2)\xi} \right] \right\}^{-1} \tag{106}$$

The convection velocity is

$$V_c = 0.7 V_p + 0.3 V_a \tag{107}$$

and

$$M_c = V_c / c_a \tag{108}$$

The wave number is given by

$$k_m = \frac{2.2 c_m \sigma_m}{D_j \sqrt{M_p^2 - 1}} \qquad m = 1,2,...35 \tag{109}$$

The parameters c_m are given by

$$c_1 = 1.1596 - 0.1773 M_p \tag{110}$$

$$c_2 = 1.1 \tag{111}$$

and wave numbers 3 through 35 are given by

$$c_m = 1.0 \tag{112}$$

Primary Internal Broadband SPL

The broadband shock noise associated with the primary internal jet is determined by

$$SPL_{shock,pi} = 10Log_{10}\left(\left\langle p^2 \right\rangle / p_{ref}^2\right) + R_{ej}\left(1 + 5M_a\right) - 3\left\{1 + 0.5\exp\left[-5\left(\theta_p - 1.6\right)^2\right]\right\} \times R_{lin}\left[2 - \exp\left(R_{lin} - R_{ej}\right)\right]\exp\left[-0.5\left(Log_{10}S_p - Log_{10}S_{lin}\right)^2\right] + \Delta SPL_{shock} \quad (113)$$

Lu and Viswanathan developed empirical adjustment for geometry, liner effects, and frequency. The last term in the equation above represents propagation effects, which are discussed later in this section.

Table 3.9.1 - Values of σ_m and $J_1(\sigma_m)$

Mode number, m	σ_m	$J_1(\sigma_m)$
1	2.404826	0.519147
2	5.520078	- 0.340265
3	8.653728	0.271452
4	11.791534	- 0.232460
5	14.930918	0.206546
6	18.071064	- 0.187729
7	21.211637	0.173266
8	24.352472	- 0.161702
9	27.493479	0.152181
10	30.634606	- 0.144166
11	33.775820	0.137297
12	36.917100	- 0.131325
13	40.058426	0.126069
14	43.199792	- 0.121399
15	46.341188	0.117211
16	49.482613	- 0.113429
17	52.624054	0.109991
18	55.765514	- 0.106848
19	58.906986	0.103960
20	62.048470	- 0.101293
21	65.189964	0.098823
22	68.331474	- 0.096524
23	71.472984	0.094379
24	74.614510	- 0.092371
25	77.756027	0.090485
26	80.897560	- 0.088711
27	84.039093	0.087037
28	87.180634	- 0.085454
29	90.322174	0.083955
30	93.463722	- 0.082532
31	96.605270	0.081179
32	99.746819	- 0.079890
33	102.888374	0.078661
34	106.029938	- 0.077487
35	109.171494	0.076364

Mixed Jet Broadband Shock Noise

The mean-square acoustic pressure for the broadband shock noise associated with the mixed jet is

$$\left\langle p^2\left(r_s,\theta,\phi,f\right)\right\rangle_{shock,m} = \frac{\Pi A_{j,m}}{R_s^2} F\left(\psi,\phi,f\right) \tag{114}$$

where Π is the acoustic power and $A_{j,m}$ is the fully expanded jet mach number. The acoustic power of a jet with a rectangular nozzle is

$$\Pi^* = \frac{\bar{c}\bar{A}_s^2 M_{j,m}^2}{\xi^2\left(1+\frac{\gamma_m-1}{2}M_{j,m}^2\right)} \tag{115}$$

where

$$\bar{c} = 2.886\times10^{-4} \tag{116}$$

and

$$\xi^2 = 1 - M_a^2\sin^2\left(\psi\right) \tag{117}$$

The shock cell strength function for over and under expanded jet is

$$\bar{A}_s^2 = \begin{cases} \bar{A}^2 & M_{j,m} > M_d \left(\text{Under expanded jet}\right) \\ \bar{A}^2\dfrac{A_{j,m}}{A_p} & M_{j,m} \le M_d \left(\text{Over expanded jet}\right) \end{cases} \tag{118}$$

where $\bar{A}^2$ is

$$\bar{A}^2 = \frac{\left(\dfrac{M_{j,m}^2 - M_d^2}{1+\frac{1}{2}\left(\gamma_m-1\right)M_d^2}\right)^2 \dfrac{E_{asp}{}^2}{1+E_{asp}{}^2}}{1+\left[\left(\dfrac{M_{j,m}^2 - M_d^2}{1+\frac{1}{2}\left(\gamma_m-1\right)M_d^2}\right)^2 \dfrac{E_{asp}{}^2}{1+E_{asp}{}^2}\right]^{\frac{3}{2}}} + \frac{\left(\dfrac{M_{j,m}^2 - 1}{1+\frac{1}{2}\left(\gamma_m-1\right)}\right)^2 \dfrac{1}{1+E_{asp}{}^2}}{1+\left[\left(\dfrac{M_{j,m}^2 - 1}{1+\frac{1}{2}\left(\gamma_m-1\right)}\right)^2 \dfrac{1}{1+E_{asp}{}^2}\right]^{\frac{3}{2}}} \tag{119}$$

The fully expanded jet area is calculated using the following equation

$$A_{j,m} = A_p \left[\frac{1 + \frac{1}{2}(\gamma_m - 1) M_{j,m}^2}{1 + \frac{1}{2}(\gamma_m - 1) M_d^2} \right]^{\frac{1}{2}\left(\frac{\gamma_m + 1}{\gamma_m - 1}\right)} \left(\frac{M_d}{M_{j,m}} \right) \tag{120}$$

where M_d is the design jet Mach number and $M_{j,m}$ is the fully expanded jet Mach number. The rectangular nozzle exit area is

$$A_p = b_{ej} h_{ej} \tag{121}$$

The parameter E_{asp} represents the aspect ratio of the rectangular nozzle defined by

$$E_{asp} = \frac{b_{ej}}{h_{ej}} \tag{122}$$

Rectangular Nozzle Spectrum Function

The one-third-octave band spectrum function in the fly-over plane (i.e. $\phi = 0$) is obtained by integrating

$$\mathrm{F}(\psi, \phi = 0, f) = \int_{fi}^{fu} \frac{F_1 + F_2}{f_{re}} df \tag{123}$$

The argument of the integral is evaluated at 20 points within a one-third-octave band and integrated numerically using Simpson's rule.

The functions F_1 and F_2 are expressions for the odd and even modes, respectively.

The function F_1 is

$$F_1 = \sum_{m=1}^{30} \sum_{n=1}^{30} \frac{\exp\left\{ -\left[\frac{V_c}{L_{mn}(\xi - M_a \cos\psi)\xi f} - 1 - \frac{M_c(\cos\psi + \xi M_a)}{\xi(1 - M_a^2)} \right]^2 \left(\frac{V_j}{V_c} \right)^2 \frac{L^2}{2 \ln 2} \right\}}{(2m-1)^2 (2n-1)[1 + 2(n-1)] \exp\{-(E_{asp} - 1)\}} \tag{124}$$

The convection velocity, V_c, of the large turbulent structure of the jet is given by

$$V_c = \left[0.5 - 0.2\exp\left\{-\left(\frac{E_{asp}-1}{2}\right)\right\} - 0.06\left(\frac{T_{t,m}}{T_a}-1\right)\right]\left(V_m - V_a\right) + V_a \tag{125}$$

and the half-width of the similarity noise source is

$$L = 3.0\frac{x_c}{8.0}\left[1.0 + \left(1.114 - 0.36\frac{T_{t,m}}{T_a}\right)M_a\right] \tag{126}$$

with a core length to jet diameter ratio defined as

$$x_c = \begin{cases} 4.3 + 1.2M_{j,m}^2 & T_{t,m}/T_a > 1.0 \\ 4.3 + 1.2M_{j,m}^2 + 1.2\left(1.0 - \dfrac{T_{t,m}}{T_a}\right)T_{t,m}/T_a & \le 1.0 \end{cases} \tag{127}$$

The spacing of the odd shock cells is defined as

$$L_{mn} = \frac{2\sqrt{M_{j,m}^2 - 1}\left[1.0 + \left(0.812 - 0.254\dfrac{T_{t,m}}{T_a}\right)M_a\right]}{C_m\sqrt{\left(\dfrac{2n-1}{b_{ej}}\right)^2 + \left(\dfrac{2m-1}{h_j}\right)^2}} \quad \begin{matrix} m = 1,2,3,...30 \\ n = 1,2,3,...30 \end{matrix} \tag{128}$$

where C_m is an empirical correction factor, which refines the spacing for the *m*th mode

$$C_m = \begin{cases} \alpha_1 + \left[0.756 - 0.195M_{j,m} - (\alpha_1 - 1)\right]\exp\left\{-\left[0.4\left(E_{asp}-1\right)^2\right]\right\} & m = 1 \\ \alpha_1 + (1.1 - \alpha_1)\exp\left\{-0.4\left(E_{asp}-1\right)^2\right\} & m \ge 2 \end{cases} \tag{129}$$

and where

$$\alpha_1 = 1.0 + 0.578\exp\left\{-\left[4.75\left(M_{j,m}-1\right)^2\right]\right\} \tag{130}$$

The fully expanded jet height, h_j, is defined with respect to the fully expanded jet area as

$$h_j = h_{ej}\frac{A_{j,m}}{b_{ej}} \tag{131}$$

The function F_2 is defined as

$$F_2 = \sum_{m=1}^{3} \frac{\exp\left\{ -\left[\frac{V_c}{\hat{L}_m\left(\xi - M_a \cos\psi\right)\xi f} - 1 - \frac{M_c\left(\cos\psi + \xi M_a\right)}{\xi\left(1 - M_a^2\right)} \right]^2 \left(\frac{V_j}{V_c}\right)^2 \frac{L^2}{2\ln 2} \right\}}{4m^2} \tag{132}$$

with the spacing of the even mode shock cells given by

$$\hat{L}_m = \frac{2\sqrt{M_{j,m}^2 - 1}\left[1.0 + \left(0.812 - 0.254 \frac{T_{t,m}}{T_a} \right) M_a \right]}{C_m \sqrt{\left(\frac{1}{b_{ej}}\right)^2 + \left(\frac{2m}{h_j}\right)^2}} \qquad m = 1,2,3 \tag{133}$$

Mixed Jet Broadband SPL

The broadband shock noise associated with the mixed jet is determined by

$$SPL_{shock,m}(f,\theta,\phi,r_s) = 10Log_{10}\left(\left\langle p^2 \right\rangle / \, p_{ref}^2\right) - \Delta(E_{asp},\phi)$$

$$-10\left\{ \exp\left[-\left(\frac{1.8\theta_m}{\pi} - 0.6 \right) \right] - 1 + 3M_a' \right\} + \Delta SPL_{shock} \tag{134}$$

The prediction is extended to azimuthal angles other than zero, $\Delta(E_{asp},\phi)$ which was developed by Ponton, Manning and Seiner [13]. The azimuthal correction factor is given by

$$\Delta(E_{asp},\phi) = \left[0.3992 - 0.5228 E_{asp} + 0.1192 {E_{asp}}^2 \right] \left(\frac{\phi}{\pi/2} \right) + \left[-1.48 + 1.6764 E_{asp} - 0.192 {E_{asp}}^2 \right] \left(\frac{\phi}{\pi/2} \right)^2 \tag{135}$$

and depends on the aspect ratio of the jet E_{asp} and the azimuthal angle ϕ in radians. The last term in the equation for SPL is an empirical flight effects adjustment developed by Lu and Viswanathan. The last term in the SPL equation above represents propagation effects, which are discussed next.

Propagation Adjustments

For ease of discussion, the term propagation effects will also include flight effects and the number of engines. Propagation effects must be incorporated into the noise predictions as a function of frequency, emission angle, and radiation distance. The adjustments required to predict the noise at the observer are different for each of the five jet noise components. The jet mixing sources for example include geometric near-field and acoustic near- field effects, which are not a part of the shock noise model. This section describes the propagation effects for the five jet noise components.

Geometric Near-Field

The jet mixing noise components include adjustments for acoustic near-field and geometric near-field effects. When the observer (microphone) is close to the jet, the acoustic field is simulated better by a line source than a point source. The transition from the near-field to the far-field is made by the following empirical formula for the mean-square acoustic pressure

$$\left\langle p^2 \right\rangle \propto \left(D/r\right)^2 \left(1 + b/r\right)^{-1} \tag{136}$$

The parameter D is the jet diameter for each component of the jet, r is the distance from the apparent source to the observer, and b is an empirically defined source length. Converting the acoustic pressure to SPL, one finds that $20Log_{10}\left(D/r\right)$ is the far-field spherical divergence and $-10Log_{10}\left(1 + b/r\right)$ is the near-field correction which decreases the extrapolated far-field SPL in the geometric near-field. The source length b is empirically determined and is listed in tables 3.9.2 and 3.9.3. The empirical geometric near-field effect is calculated for each jet component (primary internal, primary external, mixed) in the prediction model.

Acoustic Near-Field

The acoustic near-field is also determined empirically. In this case, the wave length is used to measure the acoustic near-field distance of the observer from the source. The mean-square acoustic pressure is approximated by

$$\left\langle p^2 \right\rangle \propto \left(\lambda/r\right)^2 \left[1 + 1.3\left(\lambda/r\right)^2\right] \tag{137}$$

where $\lambda = c_a/f$ is the wave length in air at rest. When the mean-square acoustic pressure is converted to SPL, the term $20Log_{10}\left(\lambda/r\right)$ is the far-field spherical divergence. The near-field correction is $10Log_{10}\left[1 + 1.3\left(\gamma/r\right)^2\right]$.

Propagation Effects for the Primary Internal and External Jets

The following equation defines the propagation effects for the primary internal and external jets.

$$\Delta SPL_{pi} = 20Log_{10}\left(\frac{D_p}{r_p}\right) - 10Log_{10}\left(1+\frac{b}{r_p}\right) + 10Log_{10}\left[1+1.3\left(\frac{c_a}{r_p f}\right)^2\right] \qquad (138)$$
$$+ 20Log_{10}\left(\frac{P_a}{P_{std}}\right) + 20Log_{10}\left(\frac{\rho_{pi}+\rho_a}{2\rho_a}\right) + 10Log_{10}\left(N_{eng}\right)$$
$$- \left|A_{abs}(f, rh)\right| r_p + G - EGA$$

Table 3.9.2 defines the terms in the equation 138.

Table 3.9.2 – Definition of ΔSPL Adjustments for Primary Internal and External Jet Noise Components

Adjustment for:	Term
Spherical spreading	$20Log_{10}\left(\frac{D_p}{r_p}\right)$
Geometric near-field	$-10Log_{10}\left(1+\frac{b}{r_p}\right)$ where $b = 2D_p + \left(\frac{D_p c_a}{f}\right)^{1/2}$
Acoustic near-field	$10Log_{10}\left[1+1.3\left(\frac{c_a}{r_p f}\right)^2\right]$
Ambient pressure	$20Log_{10}\left(\frac{P_a}{P_{std}}\right)$
Density	$20Log_{10}\left(\frac{\rho_{pi}+\rho_a}{2\rho_a}\right)$
Number of sources	$10Log_{10}\left(N_{eng}\right)$
Atmospheric absorption	$-\left\|A_{abs}(f_{pi}, rh)\right\| r_p$ $f_p = \frac{f}{1 - M_a \cos\theta_p}$
Ground reflections	G
Extra Ground Attenuation	EGA

Propagation Effects for the Mixed Jet

The following equation defines the propagation effects for the mixed jet component

$$\Delta SPL_m = 20Log_{10}\left(\frac{D_m}{r_m}\right) - 10Log_{10}\left(1+\frac{b}{r_p}\right) + 10Log_{10}\left[1+1.3\left(\frac{c_a}{r_p f}\right)^2\right] \qquad (139)$$
$$+20Log_{10}\left(\frac{P_a}{P_{std}}\right) + 20Log_{10}\left(\frac{\rho_m+\rho_a}{2\rho_a}\right) + 10Log_{10}\left(N_{eng}\right)$$
$$-\left|A_{abs}(f,rh)\right| r_s + G - EGA$$

Table 3.9.3 defines the terms in the equation above.

Table 3.9.3 – Definition of ΔSPL Adjustments
for Mixed Jet Noise Components

Adjustment for:	Term
Spherical spreading	$20Log_{10}\left(\frac{D_m}{r_m}\right)$
Geometric near-field	$-10Log_{10}\left(1+\frac{b}{r_p}\right)$ where $b = 2D_m + \left(\frac{D_m c_a}{f}\right)^{1/2}$
Acoustic near-field	$10Log_{10}\left[1+1.3\left(\frac{c_a}{r_p f}\right)^2\right]$
Ambient pressure	$20Log_{10}\left(\frac{P_a}{P_{std}}\right)$
Density	$20Log_{10}\left(\frac{\rho_m+\rho_a}{2\rho_a}\right)$
Number of sources	$10Log_{10}\left(N_{eng}\right)$
Atmospheric absorption	$-\left\|A_{abs}(f_m,rh)\right\| r_m$ $f_m = \frac{f}{1-M_a\cos\theta_m}$
Ground reflections	G
Extra Ground Attenuation	EGA

Propagation Effects for the Broadband Shock Components

The following equation defines the propagation effects for the mixed jet component

$$\Delta SPL_{shock} = 10Log_{10}\left(N_{eng}\right) + 20Log_{10}\left(\frac{\rho_a(z_s)c_a^2(z_s)}{\rho_a(z_o)c_a^2(z_o)}\right) - \left|A_{abs}(f,rh)\right|r_s + G - EGA \qquad (140)$$

Table 3.9.4 defines the terms in equation 140.

Table 3.9.4 – Definition of ΔSPL Adjustments

Adjustment for:	Term
Number of sources	$10Log_{10}\left(N_{eng}\right)$
Ambient Pressure	$20Log_{10}\left(\frac{\rho_a(z_s)c_a^2(z_s)}{\rho_a(z_o)c_a^2(z_o)}\right)$
Atmospheric absorption	$-\left\|A_{abs}(f,rh)\right\|r_s$
Ground reflections	G
Extra Ground Attenuation	EGA

Total Jet Noise

The total jet noise is the logarithmic sum of the five jet noise components,

$$SPL_{total}(f,\theta,\phi,r_s) = 10Log_{10}\Sigma \tag{141}$$

where

$$\Sigma = 10^{SPL_{pi}/10} + 10^{SPL_{pe}/10} + 10^{SPL_{m}/10} + 10^{SPL_{shock,pi}/10} + 10^{SPL_{shock,m}/10} \tag{142}$$

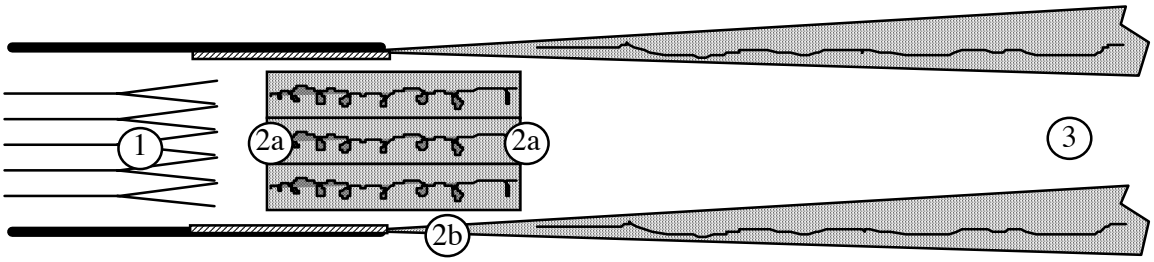

Component Separation of Extrapolated Data

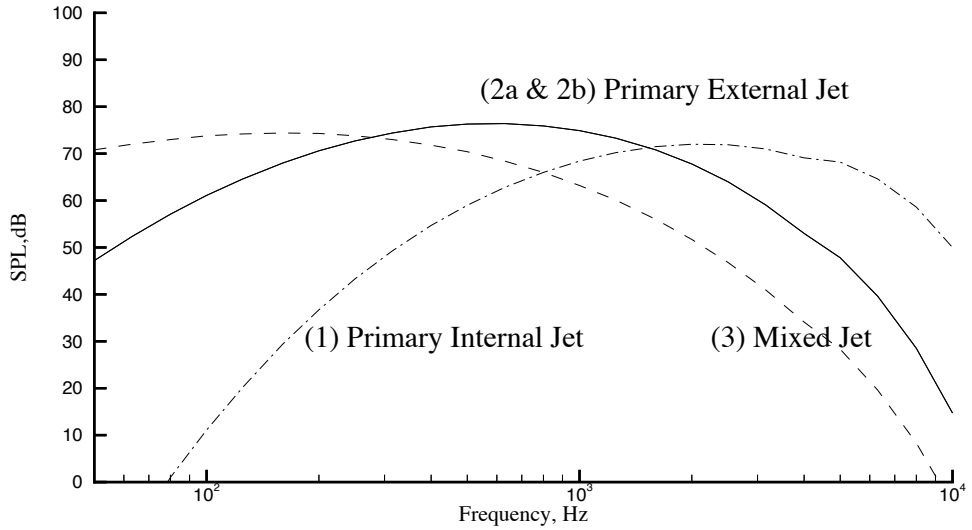

Figure 3.9.1 Mixer-Ejector noise concept

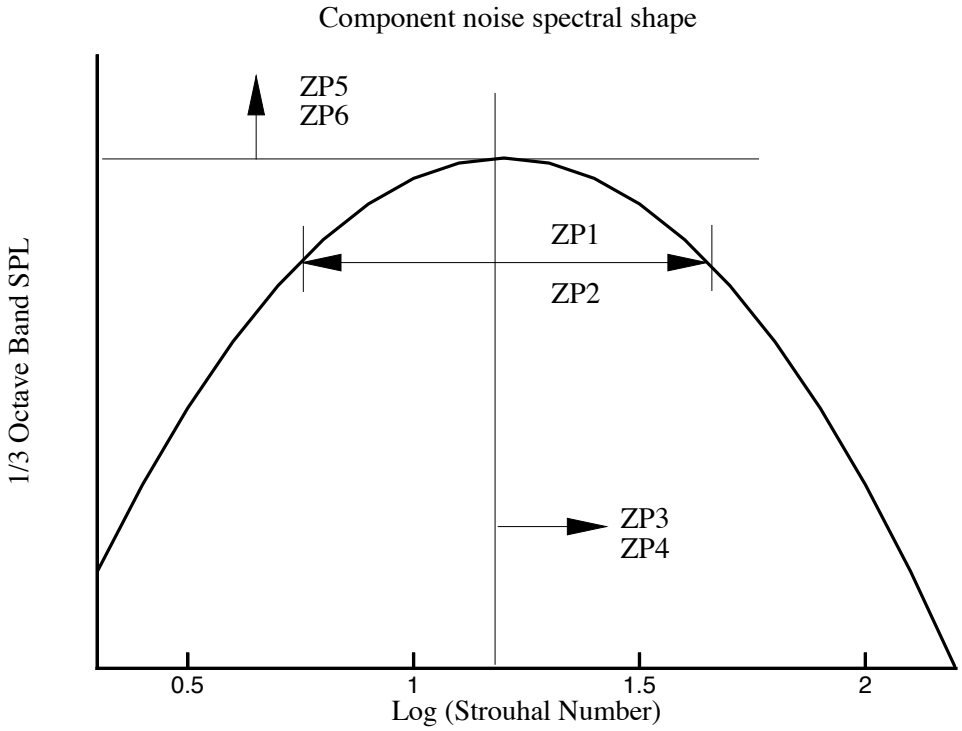

Figure 3.9.2 Effects of parametric variation on component spectra

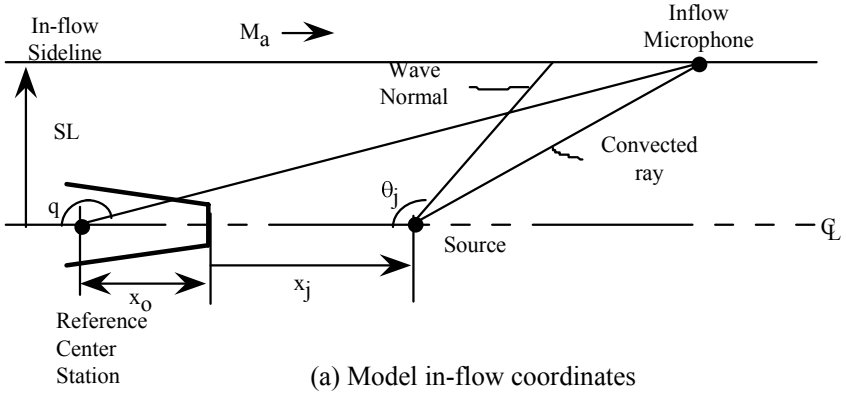

(a) Model in-flow coordinates

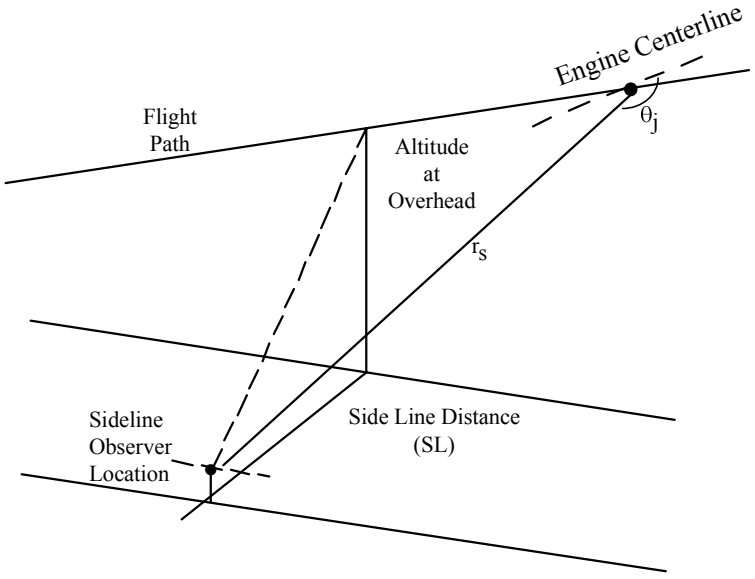

(b) Full-scale flyover coordinates

Figure 3.9.3 Schematic of jet noise propagation from a distributed source location

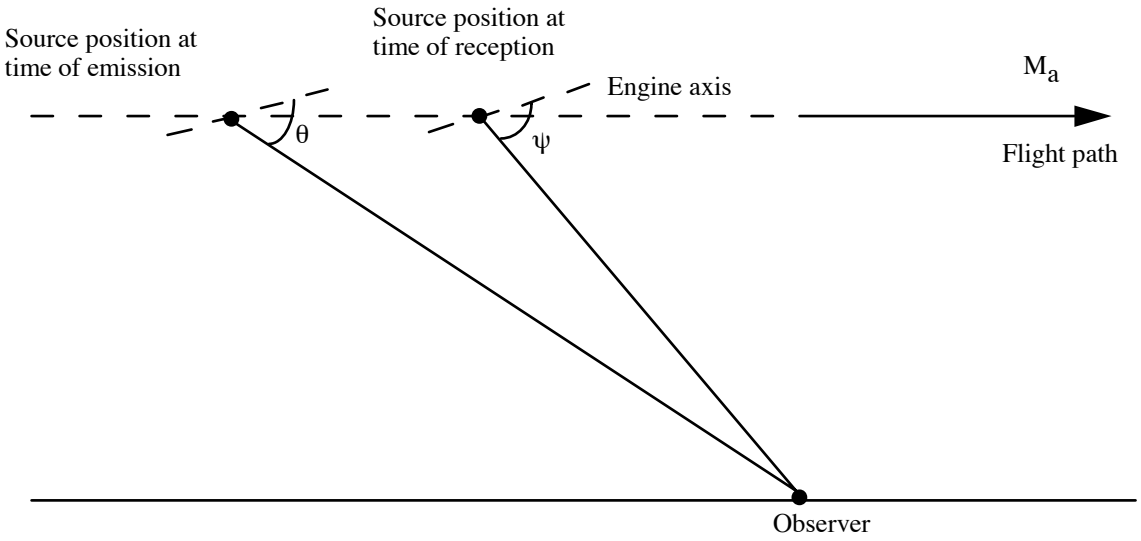

Figure 3.9.4 Schematic of emission and reception coordinates

3.10 Jet Noise (Stone Methodology)

The method described in this section was developed during the HSR program by Modern Technologies Corporation (MTC) for General Electric Aircraft Engines [14]. The method predicts jet mixing and broadband shock noise for a 2-D mixer ejector nozzle system. For purposes of analysis, the jet is conceptually divided into three regions: the internal region within the ejector, the premerged region immediately down stream of the ejector, and the merged region far enough down stream that primary and secondary regions of the flow can no longer be identified. Five noise sources may result from these regions: internal mixing noise, internal broadband shock noise, premerged mixing noise, external broadband shock noise, and merged mixing noise. The method consists of semi-empirical correlations of component noise characteristics in terms of geometric and aero/thermodynamic parameters. Each source is modeled by analogy to a round convergent nozzle, with different characteristic velocities and lengths along with appropriate physical properties. The model was developed from experimental data taken in GE's Cell 41 anechoic free-jet facility. The code was verified by comparisons with GEAE databases over a range of variables including simulated flight Mach numbers from 0 to 0.32 and primary jet velocities from 1100 to 2800 ft/sec. The source code provided by MTC has been incorporated into the HSRNOISE code with minor modifications to accommodate the HSRNOISE code design and coordinate system.

Symbols

A_{ej}	ejector exit area, ft^2
A_{pri}	primary nozzle flow area, ft^2
A_{sec}	secondary nozzle flow area, ft^2
A_{th}	primary nozzle throat area, ft^2 (***input parameter***– `APT`)
c	sound speed, ft/sec
c_{amb}	ambient sound speed, ft/sec
CER	core expansion ratio, (***input parameter*** – `CER`)
C_{source}	coefficient of component noise sources
$D_{eq,ej}$	ejector nozzle equivalent diameter, ft $\left(\sqrt{4A_{ej}/\pi}\right)$
$D_{h,pri}$	primary nozzle hydraulic diameter, ft (***input parameter*** – `DHP`)
DM	degree of mixing, (***input parameter*** – `DM`)
f	one-third-octave band center frequency
f_{pk}	peak frequency of broadband suppression, (***input parameter*** – `FPK`)
F	directivity function, dB
g	gravitational constant, 32.174 ft/sec^2
h_{ej}	ejector height, ft (***input parameter*** – `HEX`)
L_{ej}	ejector length, ft (***input parameter*** – `LE`)
$L_{bulk,end}$	length from primary exit to end of bulk treatment, ft (***input parameter*** – `LBE`)
$L_{bulk,start}$	length from primary exit to start of bulk treatment, ft (***input parameter*** – `LBS`)
$L_{perf,end}$	length from primary exit to end of perforate treatment, ft (***input parameter*** – `LPE`)

$L_{perf,start}$ length from primary exit to start of perforate treatment, ft (***input parameter*** – LPS)
M_a aircraft Mach number
M_j jet Mach number
M_d primary nozzle design Mach number
$\overline{M}$ molecular weight
$\overline{M}_{pri}$ molecular weight of primary jet, (***input parameter*** – MMC)
P_{amb} ambient pressure, lb/ft^2 (***input parameter*** – PAMB)
P_s static pressure, lb/ft^2
P_t total pressure, lb/ft^2
$P_{t,pri}$ total pressure of the primary jet upstream of the nozzle, lb/ft^2 (***input parameter*** – PC)
PEN mixer spoke penetration to nozzle full scale height ratio (***input parameter*** – PEN)
r_s distance from source to observer, ft
R gas constant, 53.35 ft-lbf / lbm ^oR
S spectrum directivity function
St Strouhal number
St_{pk} peak Strouhal number
SAR suppressor area ratio (***input parameter*** – SAR)
T_{amb} ambient temperature, ^oR
T_s static temperature, ^oR
T_t total temperature, ^oR
$T_{t,mix}$ total temperature of the mixed jets, ^oR (***input parameter*** – TEX)
$T_{t,pri}$ total temperature of the primary jet upstream of the nozzle, ^oR (***input parameter*** – TC)
V velocity, ft/sec
V_a flight velocity, ft/sec (***input parameter*** – VI)
V_{mix} exit velocity of mixed jets, ft/sec (***input parameter*** – VEX)
$\dot{w}^*$ pumping ratio $\left(\dot{w}^* = \dot{w}_{\sec} / \dot{w}_{pri}\right)$ (***input parameter*** – WSWP)
w_{ej} ejector width, ft (***input parameter*** – WEX)
α_I angle of misalignment between primary nozzle and ejector flow, degrees
α_J jet angle-of-attack, degrees
$\Delta dB_{bulk,pk}$ peak bulk suppression at FPK per foot of treatment (***input parameter*** – SUPPK)
$\Delta dB_{perf,pk}$ Peak perforate suppression, dB/wavelength (***input parameter*** – DL)
γ ratio of specific heat of ambient flow
γ_{pri} primary jet ratio of specific heat (***input parameter*** – GAMMAC)
ϕ azimuth angle, degrees
ρ density, lbm/ft^3
θ polar directivity angle, degrees
ω density exponent

Subscripts

amb ambient
bulk bulk

D	Doppler
e	effective
end	end
eq	equivalent
exit	exit
fe	fully expanded
guess	guess
IM	internal mixing noise
IS	internal shock noise
mix	mixed
MM	merged mixing noise
perf	perforate
pk	peak
pri	primary
PM	premerged mixed noise
PS	premerged shock noise
s	static
sec	secondary
start	start
sup	suppression
t	total
th	throat

Superscripts

*	nondimensional

Component Formulation

For purposes of this analysis, the jet is conceptually divided into three regions as depicted in figure 3.10.1. The regions are; the internal region within the ejector, the premerged region immediately downstream of the ejector, and the merged region far enough downstream that the primary and secondary regions of flow can no longer be identified. Five noise sources may result from these three regions; internal mixing noise, internal broadband shock noise, premerged mixing noise, premerged broadband shock noise, and merged mixing noise. The formulations described in this section represent free-field lossless sound pressure levels. Since propagation and flight effects for each source are different, they are also defined in this section.

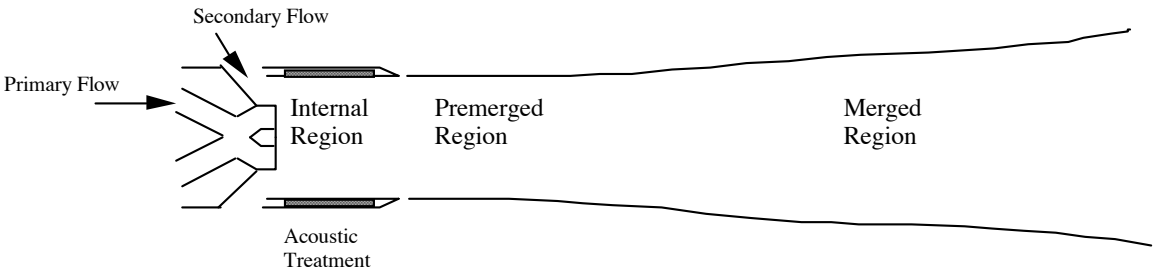

Figure 3.10.1 Two-dimensional mixer ejector noise generating regions

Iteration Procedure

Prior to computing the component acoustic pressures, thermodynamic properties of the primary and secondary flow regions are computed using an iterative procedure. The procedure is based on conservation of mass, momentum, and energy and begins with an initial guess of the total-to-static pressure ratio of the secondary flow. From this the mass flow rates of the primary and secondary flows are computed. The ratio of the computed mass flow rates is compared to the input pumping ratio. If the initial pass does not converge, the pressure ratio guess is revised, and the procedure is repeated, until the procedure converges. In some cases the procedure may not converge. Should this occur, it is an indication that a consistent set of parameters cannot be computed from the input parameters provided.

Step 1. Assume an initial guess for the total-to-static pressure ratio of the secondary stream.

$$P^*_{guess,\sec} \equiv \frac{P_{t,\sec}}{P_{amb}} = 1.108 \tag{1}$$

Assume an initial guess for the primary flow area is equal to the primary nozzle exit area.

$$A_{pri,exit} = A_{pri} \tag{2}$$

The primary nozzle area is obtained from the primary nozzle throat area A_{th} and the core expansion ratio CER.

$$A_{pri} = A_{th}(CER) \tag{3}$$

Step 2. Compute the secondary flow parameters.

Secondary flow static pressure:

$$P_{s,\sec} = P_{t,\sec} / P^*_{guess} \tag{4}$$

Secondary flow static temperature:

$$T_{s,\sec} = T_{t,\sec}\left(\frac{1}{P^*_{guess}}\right)^{(1-1/\gamma)} \tag{5}$$

$$\gamma = 1.4 \tag{6}$$

Secondary flow sound speed:

$$c_{\sec} = \sqrt{\gamma g R T_{s,\sec}} \tag{7}$$

Secondary flow Mach number:

$$M_{j,\sec} = \sqrt{\frac{2\left[\left(T_{t,\sec}/T_{s,\sec}\right)-1\right]}{\gamma - 1}} \tag{8}$$

Secondary flow velocity:

$$V_{\sec} = M_{j,\sec} c_{\sec} \tag{9}$$

Secondary flow density:

$$\rho_{\sec} = \frac{P_{s,\sec}}{R T_{s,\sec}} \tag{10}$$

Secondary flow area:

$$A_{\sec} = A_{\sec} + A_{pri} - A_{pri,exit} \tag{11}$$

Secondary flow mass flow rate:

$$\dot{m}_{\sec} = \rho_{\sec} A_{\sec} V_{\sec} \tag{12}$$

Step 3. Compute the primary flow parameters.

Primary flow static temperature:

$$T_{s,pri} = T_{t,pri}\left(\frac{1}{P^*_{pri}}\right)^{1-1/\gamma_{pri}} \tag{13}$$

Total to static pressure ratio:

$$P^*_{pri} = P_{t,pri} / P_{s,\sec} \tag{14}$$

Ratio of specific heat:

$$\begin{aligned}\gamma_{pri} &= 1.42427 - 1.07556x10^{-4}\Delta T + 2.67072x10^{-8}\Delta T^2 \\ &\quad - 2.960911x10^{-12}\Delta T^3 - 3.82470x10^{-17}\Delta T^4\end{aligned} \tag{15}$$

$$\Delta T = T_{t,pri} - T_{amb} \tag{16}$$

Sound speed:

$$c_{pri} = \sqrt{\gamma_{pri} g R_{pri} T_{s,pri}} \tag{17}$$

$$R_{pri} = \frac{1544}{\overline{M}_{pri}} \tag{18}$$

$$\overline{M}_{pri} = 28.9691 + 3.3221x10^{-12}\Delta T + 2.77821x10^{-10}\Delta T^2 \tag{19}$$

Primary jet Mach number:

$$M_{j,pri} = \sqrt{\frac{2\left[\left(T_{t,pri}/T_{s,pri}\right)-1\right]}{\gamma_{pri}-1}} \tag{20}$$

Primary flow velocity:

$$V_{pri} = M_{j,pri} c_{pri} \tag{21}$$

Primary flow density:

$$\rho_{pri} = \frac{P_{s,pri}}{R_{pri} T_{s,pri}} \tag{22}$$

Primary flow exit area:

$$A_{pri,exit} = A_{pri} \frac{M_d}{M_{j,pri}} \left[\frac{1 + \left(\gamma_{pri} - 1\right) M_{j,pri}^2 / 2}{1 + \left(\gamma_{pri} - 1\right) M_d^2 / 2} \right]^{\frac{1\left(\gamma_{pri}+1\right)}{2\left(\gamma_{pri}-1\right)}} \tag{23}$$

Primary weight flow rate:

$$\dot{w}_{pri} = \rho_{pri} A_{pri} V_{pri} \tag{24}$$

Step 4. Compute secondary mass flow rate from pumping ratio supplied as input.

$$\dot{w}_{\text{sec}}(calculated) = \dot{w}^* \dot{w}_{pri} \tag{25}$$

Step 5. Compare calculated secondary weight flow rate to secondary mass flow rate supplied as input. If $|\Gamma - 1| \geq 0.0001$ where

$$\Gamma = \frac{\dot{w}_{\text{sec}}(calculated)}{\dot{w}_{\text{sec}}(input)} \tag{26}$$

Set new guess for pressure ratio to

$$P^*_{guess}(new) = 0.8 P^*_{guess}(old) + 0.2\left(P^*_{guess}(old)\right)^{\Gamma} \tag{27}$$

and repeat steps 2 through 5. If $|\Gamma - 1| < 0.0001$ the procedure converged.

Mixed Jet Parameters

Two options are provided to determine the properties of the mixed jet. Option 1 allows the user to input the total temperature and jet velocity of the mixed jet from which other properties are computed. Option 2 computes the mixed jet properties on a mass average basis of the primary and secondary streams.

Option 1: When $T_{t,mix}$ and V_{mix} are provided as input

$$T_{s,mix} = T_{t,mix} - \left(1 - \frac{1}{\gamma_{mix}}\right) \frac{V_{mix}^2}{2gR_{mix}} \tag{28}$$

where the ratio of specific heat of the mixed flow γ_m is the mass average of the ratio of specific heats from the primary and secondary streams.

$$\gamma_{mix} = \frac{\gamma_{pri} + \dot{w}^* \gamma}{1 + \dot{w}^*} \tag{29}$$

$$R_{mix} = \frac{1544}{\overline{M}_{mix}} \tag{30}$$

$$\overline{M}_{mix} = \frac{\overline{M}_{pri} + \dot{w}^* \overline{M}_{\sec}}{1 + \dot{w}^*} \tag{31}$$

Option 2: When $T_{t,mix}$ and V_{mix} are not provided as input, the static temperature is computed as a mass average of the two streams. The static temperature at the ejector exit is given by

$$T_{s,mix} = \left(\frac{T_{s,pri} + \dot{w}^* T_{s,\sec}}{1 + \dot{w}^*} \right) \left(\frac{P_{amb}}{P_{\sec}} \right)^{1-1/\gamma_{mix}} \tag{32}$$

The mixed jet velocity and total temperature are computed internally by the following equations.

$$V_{mix} = \frac{\dot{w}_{pri} + \dot{w}_{\sec}}{\rho_{mix} A_{ej}} \tag{33}$$

$$T_{t,mix} = T_{s,mix} + \left(1 - \frac{1}{\gamma_{mix}} \right) \frac{V_{mix}^2}{2 g R_{mix}} \tag{34}$$

The mixed jet density, sound speed, and Mach number are computed by

$$\rho_{mix} = \frac{P_{amb}}{R_{mix} T_{s,mix}} \tag{35}$$

$$c_{mix} = \sqrt{g \gamma_{mix} R_{mix} T_{s,mix}} \tag{36}$$

$$M_{j,mix} = \frac{V_{mix}}{c_{mix}} \tag{37}$$

Mixer Ejector Correlation Parameters

In addition to the thermodynamic properties in the three noise generating regions, parameters such as the degree of mixing and the suppressor area ratio were established to correlate the noise characteristics of the mixer ejector nozzle system.

Degree of Mixing

The degree of mixing parameter enables noise characteristics to be empirically correlated to measured flow field characteristics. The characteristic velocity of the premerged region is bounded by the fully mixed jet velocity at the low end and by the fully mixed primary jet at the high end. The degree of mixing parameter is defined as the ratio of the difference between the fully expanded primary jet velocity and the characteristic secondary velocity of the premerged region, to the difference between the primary velocity and the fully mixed jet velocity. An empirical relation for *DM* was obtained as a function of the suppressor area ratio, the penetration, and the ratio of the ejector length to the hydraulic diameter of the primary nozzle and the primary nozzle pressure ratio. Algebraically, the degree of mixing is given by

$$DM = \frac{0.93Z}{2.3 + Z} \tag{38}$$

where

$$Z = \frac{SAR(PEN)^3\left(L_e / D_{h,pri}\right)}{\left(NPR\right)^{1.5}} \tag{39}$$

Suppressor Area Ratio

The suppressor area ratio *SAR* is defined as the ratio of the total mixing area (i.e. sum of the primary and secondary flow areas) to the throat area of the primary jet:

$$SAR = \frac{A_{pri} + A_{\sec}}{A_{th}} \tag{40}$$

Mixer Area Ratio

The mixer area ratio and the geometric factor are also used to correlate the noise of the mixer ejector. The mixer area ratio is defined as the ratio of the mixer ejector exit area to the total mixing area:

$$MAR = \frac{A_{ej}}{A_{pri} + A_{\sec}} \tag{41}$$

Geometric Factor

The geometric factor is used to define the azimuthal directivity effects of the mixer ejector nozzle. The geometric factor *GF* is a function of the aspect ratio and the azimuth angle and is defined as

$$GF = \begin{cases} \left[\left(h_{ej}/w_{ej}\right)\cos\phi\right]^{-1} & \phi \geq \phi_{cor} \\ \sin\phi & \phi < \phi_{cor} \end{cases} \tag{42}$$

where the corner angle is given by

$$\phi_{cor} = \tan^{-1}\left(h_{ej}/w_{ej}\right) \tag{43}$$

Figure 3.10.2 defines the mixer ejector coordinate system.

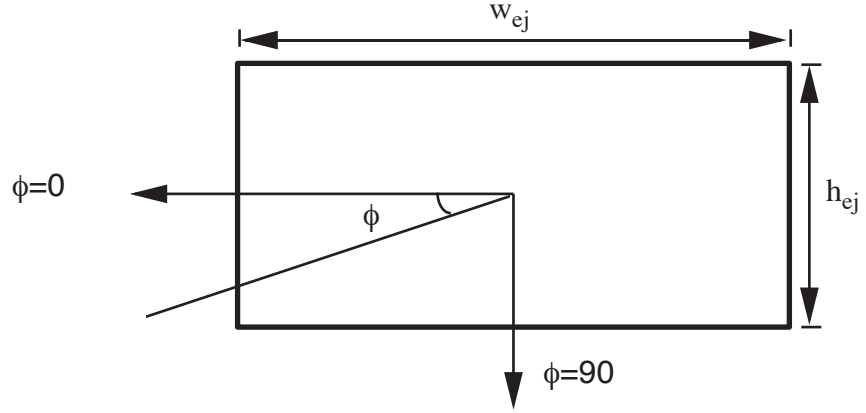

Figure 3.10.2 Two-dimensional mixer ejector nozzle coordinate system

Internal Mixing Noise

The free-field lossless sound pressure level for the primary internal mixing noise component is given by

$$\begin{aligned} SPL_{IM}\left(r_s, f, \theta, \phi\right) = {} & 147 + 10Log_{10}\left(A_{pri}/r_s^2\right) + 10\omega_{IM}Log_{10}\left(\rho_{pri}/\rho_{\sec}\right) \\ & + 60Log_{10}\left(V_{e,pri}/c_a\right) - \Delta_{HW} - 19F_{1,IS}(\theta)Log_{10}(GF) \\ & - F_{2,IS}(\theta') + 60Log_{10}\left[1 + M_a\left(\frac{\theta}{150}\right)^{10}\right] - 40Log_{10}\left(1 - M_a\cos\theta_D\right) \\ & - S_{IM}(f,\theta) - \Delta dB_{\sup} \end{aligned} \tag{44}$$

The amplitude of the internal mixing noise is determined by the primary flow area, the density and jet velocity of the primary and secondary streams, and the length and equivalent diameter of the ejector. By analogy to circular jets, temperature effects are determined by the density ratio and the density ratio exponent ω_{IM}. The density ratio exponent is given by

$$\omega_{IM} = \frac{3(V_{e,IM}/c_a)^{3.5}}{\left[0.6 + (V_{e,IM}/c_a)^{3.5}\right]} - 1 \tag{45}$$

where $V_{e,IM}$ is the internal mixing noise effective velocity defined as

$$V_{e,IM} = V_{pri}\left[1-\left(V_{\sec}/V_{pri}\right)\cos\alpha_I\right]^{2/3} \tag{46}$$

The angle α_I represents the angle of misalignment between the primary nozzle and the ejector flow.

The hardwall shielding term Δ_{HW} is defined as the ratio of the ejector length to the equivalent exit diameter of the ejector. The hardwall shielding term is given by

$$\Delta_{HW} = 0.5L_{ej}/D_{ej,eq} \tag{47}$$

where the equivalent exit diameter of the ejector is

$$D_{ej,eq} = \sqrt{\frac{4A_{ej}}{\pi}} \tag{48}$$

and the exit area of the mixer ejector is

$$A_{ej} = w_{ej}h_{ej} \tag{49}$$

Internal Mixing Noise Directivity

The internal mixing noise directivity in the absence of flight effects is defined by two terms. The term $19F_{1,IM}(\theta)Log_{10}(GF)$ (in equation 44) combines azimuthal and polar angle effects. The function $F_{1,IM}(\theta)$ is given by

$$F_{1,IM}(\theta) = \begin{cases} \dfrac{\theta'_{IM}}{125} & \theta'_{IM} \le 125 \\ 1-\dfrac{\left(\theta'_{IM}-125\right)}{90} & \theta'_{IM} > 125 \end{cases} \tag{50}$$

where the effective directivity angle θ'_{IM} is defined as

$$\theta'_{IM} = \theta\left(\frac{V_{e,IM}}{c_a}\right)^{0.1} \tag{51}$$

The function $F_{2,IM}(\theta')$ is obtained from table 3.10.1.

Table 3.10.1 Internal Mixing Noise Directivity Function

θ'_{IM}	$F_{2,IM}$	θ'_{IM}	$F_{2,IM}$
0	19.4	110	6.1
10	18.6	120	5.4
20	17.8	130	5.6
30	17.0	140	10.2
40	16.2	150	14.3
50	15.4	160	19.0
60	14.6	170	23.2
70	12.9	180	27.7
80	11.1	190	31.0
90	9.4	200	34.4
100	7.9	250	50.6

Internal Mixing Noise Flight Effects

Adjustments to the amplitude of the internal mixing noise level due to flight effects are determined by two terms. The term $60Log_{10}\left[1+M_a(\theta/150)^{10}\right]$ is very small except for angles greater than 120 degrees. The convective amplification term $-40Log_{10}\left[1-M_a\cos\theta_D\right]$ is also used to describe the change in noise levels due to the motion of the aircraft.

Internal Mixing Noise Spectrum Directivity Relations

The internal mixing noise spectrum is correlated as a function of a modified Strouhal number, which includes azimuthal and aspect ratio effects as well as temperature effects. The length scale for the Strouhal number is the hydraulic diameter of the primary jet. The characteristic velocity is the internal mixing noise effective velocity. The internal mixing noise Strouhal number is defined as

$$St_{IM} = \frac{fD_{h,pri}}{V_{e,IM}}\sqrt{GF}\left[\left(\frac{T_{t,pri}}{T_{s,pri}}\right)^{0.4\left(1+\cos\theta'_{IM}\right)}\left(1-M_a\cos\theta_D\right)\right] \tag{52}$$

and includes a Doppler shift. The internal mixing noise peak Strouhal number varies only slightly with the effective directivity angle as indicated by the values presented in table 3.10.2. The internal mixing noise spectrum function is obtained from table 3.10.3 as a function of the effective directivity angle and of $Log_{10}\left(St'_{IM}\right)$ given by

$$Log_{10}\left(St'_{IM}\right) = Log_{10}\left(St_{IM}\right) - Log_{10}\left(St_{pk,IM}\right) \tag{53}$$

Table 3.10.2 Internal Mixing Noise Peak Strouhal Number

θ'_{IM}	$Log_{10}\left(St_{pk,IM}\right)$	θ'_{IM}	$Log_{10}\left(St_{pk,IM}\right)$
0	0.6	110	0.5
10	0.6	120	0.5
20	0.6	130	0.5
30	0.6	140	0.5
40	0.6	150	0.5
50	0.6	160	0.5
60	0.6	170	0.5
70	0.6	180	0.5
80	0.5	190	0.5
90	0.5	200	0.5
100	0.5	250	0.5

Table 3.10.3 Internal Mixing Noise Spectrum Directivity Function, $S_{IM}(f,\theta)$

$Log_{10}(St'_{IM})$	Effective Directivity Angle, θ'_{IM}, degrees											
	0.0	70.0	80.0	90.0	100.0	110.0	120.0	130.0	140.0	150.0	160.0	250.0
-3.6	99.0	99.0	91.9	97.1	95.7	77.7	66.0	57.8	57.1	56.8	54.9	54.9
-2.3	43.7	43.7	45.1	47.7	47.0	38.7	34.2	30.2	32.4	32.7	31.5	31.5
-2.2	39.6	39.6	41.5	43.9	43.3	35.7	31.8	28.2	30.5	30.8	29.7	29.7
-2.1	36.2	36.2	38.1	40.3	39.7	32.8	29.4	26.3	28.6	29.0	28.0	28.0
-2.0	32.9	32.9	34.8	36.8	36.2	30.0	27.0	24.4	26.8	27.3	26.3	26.3
-1.9	29.7	29.7	31.6	33.5	32.9	27.3	24.8	22.5	25.1	25.6	24.6	24.6
-1.8	26.7	26.7	28.6	30.4	29.8	24.7	22.6	20.7	23.4	23.9	23.0	23.0
-1.7	23.9	23.9	25.8	27.4	26.8	22.3	20.5	19.0	21.7	22.3	21.5	21.5
-1.6	21.2	21.2	23.1	24.6	23.9	20.0	18.5	17.3	20.1	20.8	20.0	20.0
-1.5	18.6	18.6	20.5	21.9	21.2	17.8	16.6	16.6	18.6	19.2	18.5	18.5
-1.4	16.2	16.2	18.1	19.4	18.7	15.7	14.7	14.0	17.0	17.7	17.0	17.0
-1.3	14.0	14.0	15.9	16.9	16.3	13.7	13.0	12.5	15.5	16.1	15.5	15.5
-1.2	11.9	11.9	13.8	14.7	14.0	11.8	11.3	10.9	13.9	14.6	14.0	14.0
-1.1	9.9	9.9	11.8	12.6	11.9	10.0	9.6	9.4	12.4	13.0	12.5	12.5
-1.0	8.1	8.1	9.9	10.6	10.1	8.5	8.2	8.1	11.0	11.6	11.1	11.1
-0.9	6.6	6.6	8.1	8.8	8.4	7.1	7.0	6.9	9.7	10.3	9.9	9.9
-0.8	5.6	5.6	6.5	7.2	7.0	6.0	6.0	6.0	8.5	9.2	8.8	8.8
-0.7	4.8	4.8	5.3	5.9	5.9	5.2	5.2	5.2	7.5	8.1	7.8	7.8
-0.6	4.0	4.0	4.4	4.9	4.9	4.5	4.5	4.6	6.8	7.1	6.8	6.8
-0.5	3.4	3.4	3.8	4.1	4.1	3.9	4.0	4.1	6.2	6.0	5.8	5.8
-0.4	3.0	3.0	3.2	3.4	3.4	3.3	3.4	3.6	5.3	5.0	4.8	4.8
-0.3	2.4	2.4	2.5	2.7	2.7	2.7	2.8	2.8	4.0	3.7	3.5	3.5
-0.2	1.8	1.8	1.8	1.9	2.0	2.0	2.0	2.0	2.7	2.6	2.5	2.5
-0.1	0.9	0.9	0.9	1.0	1.0	1.0	1.0	1.0	1.4	1.3	1.3	1.3
0.0	0.0	0.0	0.0	0.0	0.0	0.0	0.0	0.0	0.0	0.0	0.0	0.0
0.4	4.0	4.0	4.0	4.0	4.0	4.0	4.0	4.0	4.0	4.0	4.0	4.0
0.5	5.0	5.0	5.0	5.0	5.0	5.5	5.5	5.5	5.5	5.5	5.5	5.5
0.6	6.0	6.0	6.0	6.0	6.0	7.2	7.2	7.2	7.2	7.2	7.2	7.2
0.7	7.0	7.0	7.0	7.0	7.0	9.2	9.2	9.2	9.2	9.2	9.2	9.2
0.8	8.0	8.0	8.0	8.0	8.0	11.5	11.5	11.5	11.5	11.5	11.5	11.5
0.9	9.0	9.0	9.0	9.0	9.0	14.0	14.0	14.0	14.0	14.0	14.0	14.0
1.0	10.0	10.0	10.0	10.0	10.0	16.5	16.5	16.5	16.5	16.5	16.5	16.5
3.6	36.0	36.0	36.0	36.0	36.0	81.5	81.5	81.5	81.5	81.5	81.5	81.5

Internal Mixing Acoustic Suppression

Acoustic suppression of the internal jet noise is provided by perforate and bulk absorber liners. The effectiveness of the liners depends on the source location and the peak attenuation frequency of the liner. Numerically, the effective length of the perforate liner is defined as

$$L_{perf} = L_{perf,end} - \max(x_s, L_{perf,start}) \tag{54}$$

where $L_{perf,start}$ is the length from the primary exit to the start of perforate treatment, and $L_{perf,end}$ is the length from the primary exit to the end of perforate treatment. The source location x_s is given by

$$x_s = D_{h,pri} x_d \tag{55}$$

where x_d is the source location per unit nozzle diameter and is defined in table 3.10.4 as a function of the Strouhal number given by

$$St = \frac{fD_{h,pri}}{V_{e,IM}} \tag{56}$$

The length scale is the hydraulic diameter of the primary jet and the characteristic velocity is the internal mixing noise effective velocity previously defined.

Similarly, the effective length of the perforate liner is

$$L_{bulk} = L_{bulk,end} - \max(x_s, L_{bulk,start}) \tag{57}$$

where $L_{bulk,start}$ is the length from the primary exit to the start of the bulk treatment, and $L_{bulk,end}$ is the length from the primary exit to the start of bulk treatment.

Table 3.10.4 Normalized Source Location for Internal Mixing Noise

St	x_d	St	x_d
0.007147	40.0	0.768205	3.5
0.011104	35.0	0.924181	3.0
0.017610	30.0	1.002430	2.8
0.021333	28.0	1.092880	2.6
0.025976	26.0	1.198580	2.4
0.031817	24.0	1.323700	2.2
0.039245	22.0	1.474060	2.0
0.048810	20.0	1.658080	1.8
0.061320	18.0	1.888390	1.6
0.077999	16.0	2.026690	1.5
0.088468	15.0	2.184830	1.4
0.100790	14.0	2.367380	1.3
0.115416	13.0	2.580460	1.2
0.132952	12.0	2.832390	1.1
0.154224	11.0	3.134820	1.0
0.180389	10.0	3.504580	0.9
0.213125	9.0	3.966940	0.8
0.254950	8.0	4.561570	0.7
0.309823	7.0	5.354600	0.6
0.344058	6.5	6.465100	0.5
0.384350	6.0	8.131150	0.4
0.432363	5.5	10.908300	0.3
0.490427	5.0	16.463200	0.2
0.561909	4.5	33.129299	0.1
0.651856	4.0		

Perforate and Bulk Liner Acoustic Suppression

Acoustic suppression is modeled as the sum of perforate wall effects and bulk absorber effects. The total acoustic suppression is

$$\Delta dB_{\text{sup}} = \Delta dB_{perf} + \Delta dB_{bulk} \tag{58}$$

Suppression provided by the perforate liner is given by

$$\Delta dB_{perf} = \begin{cases} 0 & L_{perf} < 0.001 \\ \Delta dB_{perf,pk}\, L_{perf}\, F(\theta)/\lambda & L_{perf} \geq 0.001 \end{cases} \tag{59}$$

where $\Delta dB_{perf,pk}$ is the peak attenuation per unit wave length, and L_{perf} is the effective length of the perforate liner for a given frequency. The function $F(\theta)$ is defined as

$$F(\theta) = \min\left(1.0, 0.9^{\left(\frac{130-\theta}{10}\right)}\right) \tag{60}$$

The wavelength $\lambda = c_{\text{sec}} / f$ is based on the static temperature and sonic velocity of the expanded secondary flow.

Suppression provided by the bulk liner is given by

$$\Delta dB_{bulk} = C_{bulk}\, \Delta dB_{bulk,pk}\, L_{bulk} /(1 + M_{mix}) \tag{61}$$

where C_{bulk} is obtained from table 3.10.5, and $\Delta dB_{bulk,pk}$ is the peak attenuation per unit length (default 1.6628).

Table 3.10.5 Bulk Absorber Treatment Suppression for Internal Noise, C_{bulk}

	θ, deg								
$Log_{10}(f / f_{pk})$	0	90	100	110	120	130	140	150	180
-3.6	1.00000	1.00000	0.89100	0.74100	0.64600	0.60300	0.57500	0.49000	0.49000
0.0	1.00000	1.00000	0.89100	0.74100	0.64600	0.60300	0.57500	0.49000	0.49000
0.1	0.79400	0.79400	0.70800	0.58900	0.51300	0.47900	0.45700	0.38900	0.38900
0.2	0.63100	0.63100	0.56200	0.46800	0.40700	0.38000	0.36300	0.30900	0.30900
0.3	0.50100	0.50100	0.44700	0.37200	0.32400	0.30200	0.28800	0.24500	0.24500
0.4	0.39800	0.39800	0.35500	0.29500	0.25700	0.24000	0.22900	0.19500	0.19500
0.5	0.31600	0.31600	0.28200	0.23400	0.20400	0.19100	0.18200	0.15500	0.15500
0.6	0.25100	0.25100	0.22400	0.18600	0.16200	0.15100	0.14500	0.12300	0.12300
0.7	0.20000	0.20000	0.17800	0.14800	0.12900	0.12000	0.11500	0.09770	0.09770
0.8	0.15800	0.15800	0.14100	0.11700	0.10230	0.09550	0.09120	0.07760	0.07760
0.9	0.12600	0.12600	0.11200	0.09330	0.08130	0.07590	0.07240	0.06170	0.06170
1.0	0.10000	0.10000	0.08910	0.07410	0.06460	0.06030	0.05750	0.04900	0.04900
1.1	0.07940	0.07940	0.07080	0.05890	0.05130	0.04790	0.04570	0.03980	0.03980
1.2	0.06310	0.06310	0.05620	0.04680	0.04070	0.03800	0.03630	0.03090	0.03090
1.3	0.05010	0.05010	0.04470	0.03720	0.03240	0.03020	0.02880	0.02450	0.02450
1.4	0.03980	0.03980	0.03550	0.02950	0.02570	0.02400	0.02290	0.01950	0.01950
1.5	0.03160	0.03160	0.02820	0.02340	0.02040	0.01910	0.01820	0.01550	0.01550
1.6	0.02510	0.02510	0.02240	0.01860	0.01620	0.01510	0.01450	0.01230	0.01230
1.7	0.02000	0.02000	0.01780	0.01480	0.01290	0.01200	0.01150	0.00977	0.00977
1.8	0.01580	0.01580	0.01410	0.01170	0.01023	0.00955	0.00912	0.00776	0.00776
3.6	0.00025	0.00025	0.00022	0.00019	0.00016	0.00015	0.00014	0.00012	0.00012

Internal Shock Noise

The free-field lossless sound pressure level for the internal shock noise component is given by

$$\begin{aligned} SPL_{IS} &= C_{IS} + 10Log_{10}\left(A_{pri}/r_s^2\right) + 10Log_{10}\left|\beta_{IS}^4/\left(1+4.0\beta_{IS}^4\right)\right| \\ &+ 10Log_{10}\left(1-D_{h,pri}/D_{eq,pri}\right) - \Delta_{HW} + F_{1,IS}(\theta,\phi) - F_{2,IS}(\theta) \\ &- F_{3,IS}(\theta) - 40Log_{10}\left(1-M_a\cos\theta_D\right) - S_{IS}(f,\theta,\phi) - \Delta dB_{\text{sup}} \end{aligned} \tag{62}$$

The internal shock noise coefficient C_{IS} was found to be 8.5 dB higher for under-expanded jets than for over-expanded jets. C_{IS} is given by

$$C_{IS} = \begin{cases} 154.5 & \text{for} M_{j,pri} \le M_d \quad (\text{Over}-\text{expanded}) \\ 163.0 & \text{for} M_{j,pri} > M_d \quad (\text{Under}-\text{expanded}) \end{cases} \tag{63}$$

The area correlation factor for the internal shock noise is the primary jet flow area A_{pri}.

The shock cell strength parameter β_{IS} is defined as the square root of the difference between the square of primary jet Mach number and the square of the design Mach number. If the jet is over-expanded the design Mach number is assumed to be one. The shock cell strength parameter is

$$\beta_{IS} = \begin{cases} \sqrt{M_{j,pri}^2 - 1} & \text{for } M_{j,pri} \le 1.10 M_d \\ \sqrt{M_{j,pri}^2 - M_d^2} & \text{for } M_{j,pri} > 1.10 M_d \end{cases} \tag{64}$$

For non-circular nozzles, the ratio of the hydraulic diameter to the equivalent circular nozzle diameter is used to account for geometric effects. The hydraulic diameter $D_{h,pri}$ is equal to four times the primary exit area divided by the perimeter. The equivalent diameter $D_{eq,pri}$ is equal to the square root of 4 times the primary exit area divided by π. For rectangular nozzles, $D_{h,pri}/D_{eq,pri}$ can be expressed as a function of aspect ratio as $\sqrt{\pi AR}/(1+AR)$. Here the aspect ratio is defined as the ratio of the nozzle width to the nozzle height. Figure 3.10.3 shows that increasing aspect ratio increases the internal shock noise.

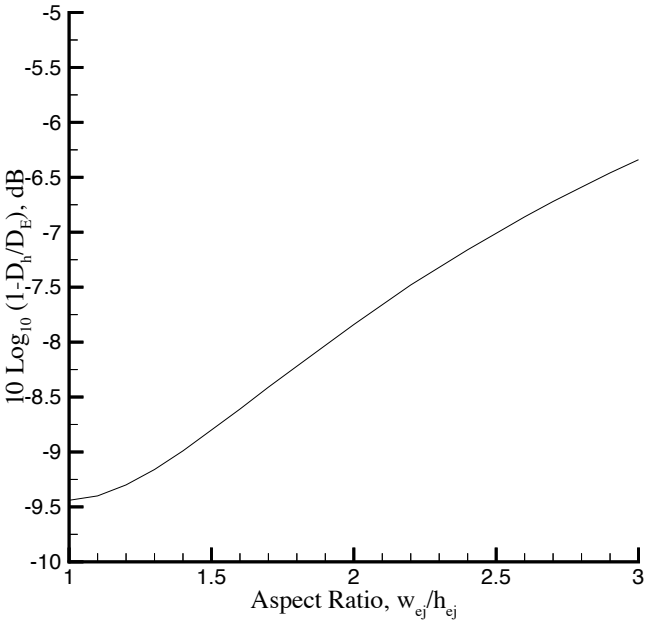

Figure 3.10.3 Effect of aspect ratio of rectangular nozzles on internal shock noise

Internal Shock Noise Directivity

The internal shock noise directivity (in the absence of flight effects) is defined by three functions. Function $F_{1,IS}$ combines polar and azimuthal effects and is given by

$$F_{1,IS}(\theta,\phi) = \begin{cases} 11(\theta/120)Log_{10}(GF) & \text{for } \theta < 120 \\ 11Log_{10}(GF) & \text{for } \theta \geq 120 \end{cases} \tag{65}$$

$F_{2,IS}$ and $F_{3,IS}$ are explicit functions of the Mach angle θ'_{IS} defined by

$$\theta'_{IS} = 180 - \sin^{-1}(1 - M_{pri}) \tag{66}$$

$F_{2,IS}$ is given by

$$F_{2,IS}(\theta) = \begin{cases} 0 & \text{for } \theta < \theta'_{IS} \\ 0.25(\theta - \theta'_{IS}) & \text{for } \theta \geq \theta'_{IS} \end{cases} \tag{67}$$

and $F_{3,IS}$ is defined by the values given in table 3.10.6.

Table 3.10.6 Internal Shock Noise Directivity Function

θ	$F_{3,IS}(\theta)$ $\left(M_{pri} > 1.1M_d\right)$	$F_{3,IS}(\theta)$ $\left(M_{pri} \le 1.1M_d\right)$
0	23.7	30.8
10	21.6	27.2
20	19.6	24.8
30	17.7	21.8
40	15.9	18.8
50	14.2	15.8
60	12.6	14.2
70	11.1	12.7
80	9.6	10.0
90	8.1	8.1
100	8.5	6.1
110	8.9	5.6
120	9.6	6.6
130	11.0	7.6
140	13.0	9.1
150	15.5	10.6
160	19.5	12.1
170	26.5	13.6
180	34.5	15.6

Internal Shock Noise Flight Effects

The effect of flight on the amplitude of the internal shock noise component is defined by the convective amplification term $-40Log_{10}\left(1 - M_a \cos\theta_D\right)$.

Internal Shock Noise Spectrum Directivity Relations

The internal shock noise spectrum is correlated as a function of a modified Strouhal number, which includes azimuthal and aspect ratio effects. The length scale for the Strouhal number is the hydraulic diameter of the primary jet. The characteristic velocity is the internal shock noise is the primary jet velocity. The internal shock noise Strouhal number is defined as

$$Log_{10}\left(St_{IS}\right) = \frac{fD_{h,pri}}{0.7V_{pri}}\sqrt{GF\left(M_{pri}^2 - 1\right)}\left(1 - M_a \cos\theta_D\right) \tag{68}$$

and includes a Doppler shift. The internal shock noise peak Strouhal number varies significantly as a function of the Mach angle and whether the jet is over-expanded or under-expanded. Table 3.10.7 provided a listing of the logarithm of the peak Strouhal number for over-expanded and under-expanded jets. The internal shock noise spectrum function is obtained from table 3.10.8 as a function of $Log_{10}\left(St'_{PS}\right)$ given by

$$Log_{10}\left(St'_{IS}\right) = Log_{10}\left(St_{IS}\right) - Log_{10}\left(St_{pk,IS}\right) \tag{69}$$

Table 3.10.7 Internal Shock Noise Peak Strouhal Number

θ'	$Log_{10}\left(St_{pk,IS}\right)$ $\left(M_{pri} \le 1.1M_d\right)$	$Log_{10}\left(St_{pk,IS}\right)$ $\left(M_{pri} > 1.1M_d\right)$
0	0.0	-0.3
10	0.0	-0.3
20	0.0	-0.3
30	0.0	-0.2
40	0.0	-0.2
50	0.0	-0.2
60	0.0	-0.2
70	0.0	-0.1
80	0.0	-0.1
90	0.1	0.0
100	0.1	0.0
110	0.1	0.1
120	0.2	0.2
130	0.3	0.3
140	0.4	0.3
150	0.5	0.3
160	0.6	0.3
170	0.7	0.3
180	0.8	0.3

Table 3.10.8 Internal Shock Noise Spectrum Function

$Log_{10}\left(St'_{IS}\right)$	S_{IS}
-3.6	176.0
-1.0	1.0
0.1	0.5
3.6	35.5

Internal Shock Noise Suppression

The effect of acoustic suppression on the internal shock noise is computed in the same manner as described for the internal mixing acoustic suppression. The source location x_s is replaced with

$$x_s = 3D_{h,pri}\sqrt{M_{j,pri}^2 - 1} \tag{70}$$

for the internal shock noise suppression analysis.

Premerged Mixing Noise

The free-field lossless sound pressure level for the premerged mixing noise component is given by

$$\begin{aligned} SPL_{PM}(r_s, f, \theta, \phi) &= C_{PM} + 10Log_{10}\left(A_{PM}/r_s^2\right) + 10\omega_{PM}Log_{10}\left(\rho_{PM}/\rho_a\right) \\ &+ 75Log_{10}\left(V_{e,PM}/c_a\right) + F_{1,PM}(\theta,\phi) - F_{2,PM}(\theta) \\ &- 15Log_{10}\left[(1 + M_{c.PM}\cos\theta)^2 + 0.04M_{c.PM}^2\right] \\ &- 10Log_{10}\left(1 - M_a\cos\theta_D\right) - S_{PM}(f,\theta) \end{aligned} \tag{71}$$

The premerged mixing noise coefficient C_{PM} has a minimum value of 137 and a maximum value of 142 depending on the primary nozzle pressure ratio, the suppressor area ratio, and the lobe penetration. C_{PM} is

$$C_{PM} = \min\left[142, \max\left(137, \quad 112.0 + 12.5\frac{P_{t,pri}/P_a}{\sqrt{SAR\sqrt{PEN}}}\right)\right] \tag{72}$$

The area correlation factor for the premerged mixing noise is the effective premerged area A_{PM}. A_{PM} is a function of the degree of mixing, the mixer area ratio, the primary flow area, and the ejector exit area. A_{PM} is given by

$$A_{PM} = (1 - DM)\frac{A_{pri}}{MAR} + (DM)A_{ej} \tag{73}$$

The density correction factor for the premerged mixing region is

$$\omega_{PM} = \frac{3(V_{e,PM}/c_a)^{3.5}}{\left[0.6 + (V_{e,PM}/c_a)^{3.5}\right]} - 1 \tag{74}$$

where $V_{e,PM}$ is the effective premerged velocity given by

$$V_{e,PM} = V_{PM}\sqrt{1 - (V_a/V_{PM})\cos\alpha_J} \tag{75}$$

and the premerged jet velocity V_{PM} is

$$V_{PM} = (1 - DM)V_{fe,pri} + (DM)V_{mix} \tag{76}$$

The fully expanded velocity of the primary jet $V_{fe,pri}$ is given by

$$V_{fe,pri} = M_{fe,pri}c_{fe} \tag{77}$$

The fully expanded velocity of the primary jet is obtained from the fully expanded Mach number

$$M_{fe,pri} = \left\{ 2 \frac{\left[\left(T_{t,pri} / T_{s,fe} \right) \right] - 1}{\left(\gamma_{pri} - 1 \right)} \right\}^{1/2} \tag{78}$$

and the sound speed at the exit of the mixer ejector

$$c_{fe} = \sqrt{\gamma_{pri} g R_{pri} T_{s,fe}} \tag{79}$$

The fully expanded static temperature is

$$T_{s,fe} = T_{t,pri} \left(\frac{P_{t,pri}}{P_{amb}} \right)^{\left(-1 + \frac{1}{\gamma pri} \right)} \tag{80}$$

The density of the premerged mixing region is determined by the degree of mixing, the primary jet density, and the mixed jet density. The density of the premerged mixing region is

$$\rho_{PM} = (1 - DM)\rho_{pri} + (DM)\rho_{mix} \tag{81}$$

Premerged Mixing Noise Directivity

Two functions define the shape of the premerged mixing noise directivity in the absence of flight effects. $F_{1,PM}(\theta, \phi)$ defines the relationship between the polar and azimuthal angle effects. $F_{1,PM}(\theta, \phi)$ is given by

$$F_{1,PM}(\theta,\phi) = \begin{cases} -4.5(\theta'_{PM}/90)^2 Log_{10}(GF) & \text{for } \theta \le 90 \\ -4.5\left[0.5\left(\frac{\theta'_{PM}}{90} \right) + 1.5\left(\frac{\theta'_{Pre}}{120} \right) \right] Log_{10}(GF) & \text{for } 90 < \theta < 100 \\ -13.5(\theta'_{PM}/120)^2 Log_{10}(GF) & \text{for } \theta \ge 100 \end{cases} \tag{82}$$

where

$$\theta'_{PM} = \theta \left(\frac{V_{PM}}{c_a} \right)^{0.1} \tag{83}$$

$F_{2,PM}(\theta)$ is a simple function of polar angle and is presented in table 3.10.9. It should be noted that the effects of source location have been removed from the function $F_{1,PM}$ and $F_{2,PM}$.

Table 3.10.9 Premerged Mixing Noise Directivity Function

θ	$F_{2,PM}(\theta)$	θ	$F_{2,PM}(\theta)$
0	8.7	110	7.2
10	8.7	120	6.7
20	8.7	130	9.6
30	8.7	140	11.5
40	8.7	150	15.7
50	8.7	160	18.4
60	8.7	170	19.4
70	8.7	180	20.4
80	8.7	190	21.4
90	8.7	200	22.4
100	7.7	250	27.4

Premerged Mixing Noise Flight Effects

The effects of source motion are defined by two functions. The first incorporates the effects of the source convection within the jet. The convection Mach number is defined as

$$M_{c,PM} = 0.62(V_{PM} - V_a \cos\alpha_J) / c_{amb} \tag{84}$$

The angle α_J is the angle-of-attack of the jet. In the HSRNOISE code, the aircraft angle-of-attack is used. The second effect of flight on the amplitude of the premerged mixing noise component is defined by the term $-10nLog_{10}(1 - M_a \cos\theta_D)$. Note that $n = 1$ for the premerged mixing noise as compared to 4 for the internal mixing noise component.

Premerged Mixing Noise Spectral Directivity

The premerged mixing noise spectrum is correlated as a function of a modified Strouhal number, which includes temperature effects. The length scale for the Strouhal number is the hydraulic diameter of the primary jet. The characteristic velocity is the premerged mixing noise effective velocity. The internal mixing noise Strouhal number is defined as

$$St_{PM} = \frac{fD_{h,pri}}{V_{e,PM}} \left[\left(\frac{T_{t,pri}}{T_{amb}} \right)^{0.4(1+\cos\theta)} (1 - M_a \cos\theta_D) \right] \tag{85}$$

and includes a Doppler shift. The peak Strouhal number is a function of the Mach angle. For angles less than 110 degrees the peak remains constant. As the Mach angle increases, the peak shifts to lower Strouhal numbers. The peak Strouhal number for the premerged mixing noise component is presented in table 3.10.10. The premerged mixing noise spectrum function is presented in table 3.10.11 as a function of $Log_{10}(St'_{PM})$ given by

$$Log_{10}(St'_{PM}) = Log_{10}(St_{PM}) - Log_{10}(St_{pk,PM}) \tag{86}$$

Table 3.10.10 Premerged Mixing Noise Peak Strouhal Number

θ	$Log_{10}\left(St_{pk,PM}\right)$	θ	$Log_{10}\left(St_{pk,PM}\right)$
0	0.1	110	0.1
10	0.1	120	0.0
20	0.1	130	-0.1
30	0.1	140	-0.2
40	0.1	150	-0.3
50	0.1	160	-0.4
60	0.1	170	-0.5
70	0.1	180	-0.5
80	0.1	190	-0.6
90	0.1	200	-0.6
100	0.1	250	-0.7

Table 3.10.11 Premerged Mixing Noise Spectrum Function

$Log_{10}\left(St'_{PM}\right)$	S_{PM}
-3.6	163.0
-0.9	22.5
-0.8	18.0
-0.7	14.0
-0.6	10.5
-0.5	7.5
-0.4	5.0
-0.3	3.0
-0.2	1.5
-0.1	0.5
0.0	0.0
0.1	0.4
0.2	1.0
0.3	2.5
3.6	52.0

Premerged Shock Noise

The free-field lossless sound pressure level for the premerged shock noise component is given by

$$\begin{aligned} SPL_{PS}\left(r_s, f, \theta\right) &= C_{PS} + 10Log_{10}\left(A_{PM}/r_s^2\right) + 10Log_{10}\left[\beta_{PS}^4/\left(1+\beta_{PS}^4\right)\right] \\ &- F_{1,PS}\left(\theta\right) - F_{2,PS}\left(\theta\right) - 40Log_{10}\left(1 - M_a\cos\theta_D\right) - S_{PS}\left(f\right) \end{aligned} \tag{87}$$

The coefficient C_{PS} is assigned a value of 157 for nozzle pressure ratios of 4 or greater. Nozzle pressure ratios less than 4 are computed by $C_{PS} = 77 + 20\left(P_{t,pri}/P_{amb}\right)$.

$$C_{PS} = \min\left[157, 77 + 20\left(P_{t,pri}/P_{amb}\right)\right] \tag{88}$$

The area correlation parameter is the effective premerged area A_{PM}.

The shock cell strength parameter β_{PS} is defined as

$$\beta_{PS} = \sqrt{M_{j,PS}^2 - 1} \tag{89}$$

where the Mach number $M_{j,PS}^2$ is defined as the product of the premerged effective Mach number and the mixed jet Mach number. $M_{j,PS}^2$ is given by

$$M_{j,PS}^2 = \left(\frac{V_{PM}}{c_{PM}}\right)\left(\frac{V_{mix}}{c_{mix}}\right) \tag{90}$$

where the premerged sound speed is

$$c_{PM} = \sqrt{g\gamma_{mix}R_{mix}T_{s,PM}} \tag{91}$$

The static temperature of the premerged jet is

$$T_{s,PM} = T_{t,PM} - \left(1 - \frac{1}{\gamma_{mix}}\right)\frac{V_{PM}^2}{2gR_{mix}} \tag{92}$$

where the total pressure of the premerged region is

$$T_{t,PM} = (1 - DM)T_{t,pri} + (DM)T_{t,mix} \tag{93}$$

Premerged Shock Noise Directivity

The directivity of the premerged shock noise is described by two functions. $F_{1,PS}$ is a function of the polar angle and the Mach angle θ'_{PS}. The premerged directivity function is given by

$$F_{1,PS}(\theta) = \begin{cases} 0 & \text{for } \theta < \theta'_{PS} \\ 0.75(\theta - \theta'_{PS}) & \text{for } \theta \geq \theta'_{PS} \end{cases} \tag{94}$$

where the Mach angle is defined in terms of the premerged jet Mach number as

$$\theta'_{PS} = 180 - \sin^{-1}(1 - M_{j,PS}) \tag{95}$$

The second directivity function is presented in table 3.10.12.

Table 3.10.12 Premerged Shock Noise Directivity Function

θ	$F_{2,PS}$	θ	$F_{2,PS}$
0	8.7	100	9.2
10	7.2	110	10.7
20	6.7	120	12.2
30	6.2	130	13.7
40	5.7	140	14.2
50	5.2	150	14.7
60	6.0	160	15.2
70	6.6	170	15.7
80	7.1	180	16.2
90	7.7		

No variations due to azimutal angle or aspect ratio are included in the prediction of the premerged shock noise.

Premerged Shock Noise Flight Effects

Correction to the premerged shock noise amplitude due to flight effects are given by the convection amplification term $40Log_{10}\left(1-M\cos\theta_D\right)$.

Premerged Shock Noise Spectrum Directivity Relations

The premerged shock noise spectrum is correlated as a function of a modified Strouhal number, which includes the strength of the shock cells and the premerged jet velocity. The length scale for the Strouhal number is the equivalent diameter of the primary jet. The characteristic velocity is the premerged jet velocity. The premerged shock noise Strouhal number is defined as

$$St_{PS} = \left(fD_{eq,pri}/0.7V_{PM}\right)\beta_{PS}\left(1-M_a\cos\theta_D\right)\times \frac{}{\sqrt{\left\{1+0.7\left(V_{PM}/c_a\right)\cos\theta\right\}^2+0.0196\left(V_{PM}/c_a\right)^2}} \quad (96)$$

and includes a Doppler shift. The premerged shock noise peak Strouhal number is given by

$$Log_{10}St_{pk,PS} = \begin{cases} -0.3 & \theta \le 50 \\ -0.2 & 50 < \theta \le 180 \end{cases} \quad (97)$$

The premerged shock noise spectrum function is presented in table 3.10.13 as a function of $Log_{10}\left(St'_{PS}\right)$ given by

$$Log_{10}\left(St'_{PS}\right) = Log_{10}\left(St_{PS}\right) - Log_{10}\left(St_{pk,PS}\right) \quad (98)$$

Table 3.10.13 Premerged Shock Noise Spectrum Function

$Log_{10}(St'_{PS})$	S_{PS}
-3.6	138.5
-0.2	5.9
-0.1	2.0
0.0	0.0
1.0	1.0
3.6	36.0

Merged Mixing Noise

The free-field lossless sound pressure level for the merged mixing noise component is

$$\begin{aligned} SPL_{MM}(r_s, f, \theta, \phi) = C_{MM} &+ 10Log_{10}\left(A_{ej}/r_s^2\right) + 10\omega_{MM}Log_{10}\left(\rho_{mix}/\rho_{amb}\right) \\ &+ 75Log_{10}\left(V_{MM}/c_a\right) - F_1(\theta,\phi) - F_2(\theta) \\ &- 15Log_{10}\left[(1 + M_{c.MM}\cos\theta)^2 + 0.04M_{c.MM}^2\right] \\ &- 10Log_{10}\left(1 - M_a\cos\theta_D\right) - S_{MM}(f,\theta) \end{aligned} \tag{99}$$

The merged mixing noise coefficient C_{MM} is given by

$$C_{MM} = \min\left[142.5,\ \max\left(138,\ 131.7 + 6.0\frac{P_{t,pri}/P_{amb}}{SAR\sqrt{PEN}}\right)\right] \tag{100}$$

C_{MM} has a minimum value of 138 and a maximum value of 142.5. The primary nozzle pressure ratio, the suppressor area ratio, and the lobe penetration determine the actual value of the coefficient.

The density correction for the merged mixing region is

$$\omega_{MM} = \frac{3(V_{e,MM}/c_a)^{3.5}}{\left[0.6 + (V_{e,MM}/c_a)^{3.5}\right]} - 1 \tag{101}$$

where $V_{e,MM}$ is the effective premerged velocity given by

$$V_{e,MM} = V_{mix}\sqrt{1 - (V_a/V_{mix})\cos\alpha_J} \tag{102}$$

The angle α_J is the angle-of-attack of the jet. In the HSRNOISE code, the aircraft angle-of-attack is used.

Merged Mixing Noise Directivity

Two functions define the shape of the merged mixing noise directivity in the absence of flight effects. $F_{1,MM}(\theta,\phi)$ defines the polar directivity and azimuthal directivity effects. $F_{1,MM}(\theta,\phi)$ is given by

$$F_{1,MM}(\theta,\phi) = \begin{cases} 0 & \text{for } \theta'_M \le 120 \\ \left[\dfrac{(\theta'_M - 120)}{8}\right] Log_{10}(GF) & \text{for } \theta'_M > 120 \end{cases} \tag{103}$$

where

$$\theta'_{\Pr e} = \theta\left(\frac{V_{PM}}{c_a}\right)^{0.1} \tag{104}$$

The function $F_{2,MM}(\theta)$ is obtained from table 3.10.14. The original formulation for the independent variable θ in reference 14 is a function of the source location and may obtain values greater than 180 degrees. Entries in table 3.10.14 greater than 180 degrees can be ignored.

Table 3.10.14 Merged Mixing Noise Directivity Function

θ	$F_{2,MM}$	θ	$F_{2,MM}$
0	10.9	110	4.4
10	10.5	120	3.2
20	10.1	130	2.0
30	9.7	140	3.2
40	9.3	150	3.9
50	8.9	160	10.9
60	8.5	170	17.9
70	8.1	180	24.9
80	7.9	190	31.9
90	7.7	200	38.9
100	4.9	250	73.9

Merged Mixing Noise Flight Effects

The effects of source motion on the merged mixing noise component is defined by two functions. The first incorporates the effects of the source convection within the jet. The convection Mach number is defined as

$$M_{c,MM} = 0.62(V_{e,MM} - V_a \cos\alpha_J)/c_{amb} \tag{105}$$

The second fight effect term is the convection amplification to the first power.

Merged Mixing Noise Spectrum Directivity Relations

The merged mixing noise spectrum is correlated as a function of a modified Strouhal number, which includes temperature effects. The length scale for the Strouhal number is the equivalent diameter of the primary jet. The characteristic velocity is the merged mixing noise effective velocity. The Strouhal number for the merged mixing region is given by

$$St_{MM} = \frac{fD_{ej,eq}}{V_{e,MM}}\left[\left(\frac{T_{t,mix}}{T_{amb}}\right)^{0.4\left(1+\cos\theta'\right)}\left(1 - M_a \cos\theta_D\right)\right] \tag{106}$$

The peak Strouhal number St_{pk} is obtained from table 3.10.15 as a function of the directivity angle. For angles less than 70 degrees the peak remains constant. As the Mach angle increases, the peak shifts to higher Strouhal numbers. The peak Strouhal number for the merged mixing noise component is presented in table 3.10.15. The merged mixing noise spectrum function is presented in table 3.10.16 as a function of $Log_{10}\left(St'_{MM}\right)$ given by

$$Log_{10}\left(St'_{MM}\right) = Log_{10}\left(St_{MM}\right) - Log_{10}\left(St_{pk,MM}\right) \tag{107}$$

Table 3.10.15 Merged Mixing Noise Peak Strouhal Number

θ	$Log_{10}\left(St_{pk.MM}\right)$	θ	$Log_{10}\left(St_{pk,MM}\right)$
0	0.3	110	0.5
10	0.3	120	0.5
20	0.3	130	0.5
30	0.3	140	0.5
40	0.3	150	0.6
50	0.3	160	0.6
60	0.3	170	0.7
70	0.3	180	0.7
80	0.4	190	0.8
90	0.4	200	0.8
100	0.4	250	1.0

Table 3.10.16 Merged Mixing Noise Spectrum Function $S_{MM}(f,\theta)$

$Log(St'_{MM})$	Directivity angle, θ degrees			
	0	120	130	250
-3.6	157.8	157.8	157.8	157.8
-1.0	25.2	25.2	25.2	25.2
-0.9	20.8	20.8	20.8	20.8
-0.8	16.8	16.8	16.8	16.8
-0.7	13.2	13.2	13.2	13.2
-0.6	10.0	10.0	10.0	10.0
-0.5	7.2	7.2	7.2	7.2
-0.4	4.8	4.8	4.8	4.8
-0.3	3.0	3.0	3.0	3.0
-0.2	1.6	1.6	1.6	1.6
-0.1	0.6	0.6	0.6	0.6
0.0	0.0	0.0	0.0	0.0
0.1	0.8	0.8	0.9	0.9
0.2	2.4	2.4	2.7	2.7
0.3	4.4	4.4	5.0	5.0
0.4	6.8	6.8	7.8	7.8
0.5	9.6	9.6	11.4	11.4
0.6	12.8	12.8	14.6	14.6
0.7	16.4	16.4	18.6	18.6
0.8	20.4	20.4	23.0	23.0
0.9	24.8	24.8	27.4	27.4
3.6	143.6	143.6	146.2	146.2

Mixer Ejector Propagation Effects

Propagation effects for the method described in this section include ambient pressure, atmospheric attenuation, ground reflection attenuation, and extra ground attenuation (EGA). For convenience, source modification for the number of sources is also included with the propagation effects. The free-field lossless spectra is modified for propagation effectes by

$$SPL = SPL_{free-field\ lossless} + \Delta SPL \tag{108}$$

where ΔSPL is given by

$$\Delta SPL = 20Log_{10}\left(\frac{\rho_a(z_s)c_a^2(z_s)}{\rho_a(z_o)c_a^2(z_o)}\right) - A_{abs}r_s + G - EGA + 10Log_{10}(N_{eng}) \tag{109}$$

Additional details concerning propagation effects can be found in section 3.13.

3.11 Airframe Noise

The airframe noise prediction method adopted for the HSR program is based on the method developed by Fink [15]. Airframe noise is produced by elements of the wing, fuselage, and landing gear. The noise generating mechanisms are divided into the following eight components:

1. Wing Noise
2. Leading Edge Noise
3. Horizontal Tail Noise
4. Vertical Tail Noise
5. Inboard Flap Noise
6. Outboard Flap Noise
7. Main Gear Noise
8. Nose Gear Noise

Fink developed empirical functions for each noise component based on flyover data from a wide variety of aircraft including a sail plane, general aviation aircraft, a business jet, a Boeing 747 commercial transport, and a delta wing Convair F106B. Since Fink's method was developed from primarily conventional subsonic airplane designs, a model scale airframe noise test was conducted in the Boeing Low-speed Aeroacoustic Facility. The objective was to provide estimates of the high-speed civil transport (HSCT) airframe noise levels. Noise data were collected on a full span 3% scale model of a double delta HSCT configuration. From this data, spectral corrections for the Fink method were developed.

Symbols

$A_{f,in}$	wing inboard trailing edge flap area, ft^2 (***input parameter*** **–** `AFIN`)
$A_{f,out}$	wing outboard trailing edge flap area, ft^2 (***input parameter*** **–** `AFOUT`)
A_h	horizontal tail area, ft^2 (***input parameter*** **–** `AH`)
A_v	vertical tail area, ft^2 (***input parameter*** **–** `AV`)
A_w	wing area, ft^2 (***input parameter*** **–** `AW`)
$b_{f,in}$	inboard flap span, ft (***input parameter*** **–** `BFIN`)
$b_{f.out}$	outboard flap span, ft (***input parameter*** **–** `BFOUT`)
b_h	horizontal tail span, ft (***input parameter*** **–** `BH`)
b_v	vertical tail span, ft (***input parameter*** **–** `BV`)
b_w	wing span, ft (***input parameter*** **–** `BW`)
c_a	ambient sound speed**,** ft/sec (***input parameter*** **–** `CA`)
d_{mg}	wheel diameter main gear, ft (***input parameter*** **–** `DMG`)
d_{ng}	wheel diameter nose gear, ft (***input parameter*** **–** `DNG`)
D	directivity function
f	one-third-octave band center frequencies, Hz
F	spectrum function

g_c	gravitational constant, 32.174 ft/sec^2
G	general function
k	constant coefficient
L_{mg}	length of main gear strut, ft (***input parameter*** **–** `RLMG`)
L_{ng}	length of nose gear strut, ft (***input parameter*** – `RLMG`)
M_a	aircraft Mach number (***input parameter*** – `MA`)
N_{mg}	number of main gear (***input parameter*** **–** `NMG`)
N_{ng}	number of nose gear (***input parameter*** – `NMG`)
$N_{w,mg}$	number of wheels per main gear (***input parameter*** **–** `NWMG`)
$N_{w,ng}$	number of wheels per nose gear (***input parameter*** – `NWMG`)
$N_{f,in}$	number of inboard training edge slots (***input parameter*** **–** `NFSIN`)
$N_{f,out}$	number of outboard training edge slots (***input parameter*** – `NFSOUT`)
p_{ref}	reference pressure, 4.177 x 10^{-7} (lb/ft^2)
$\left\langle p^2 \right\rangle^*$	nondimensional mean-square acoustic pressure
r_s	source radius, $r_s = 150$ ft
r_s^*	nondimensional source radius, $r_s^* = r_s / b_w$
R_e	Reynolds number
St	Strouhal number
T_a	ambient temperature, ^{o}F
$\beta_{f,in}$	inboard flap deflection angle, degrees (***input parameter*** – `FLAIN`)
$\beta_{f,out}$	outboard flap deflection angle, degrees (***input parameter*** – `FLAOUT`)
δ^*	nondimensional turbulent boundary thickness
ϕ	azimuthal angle, degrees
μ_a	ambient dynamic viscosity, lbm/ft-sec
Π^*	nondimensional acoustic power
θ_D	Doppler angle, degrees
ρ_a	ambient density (lbm/ft^3), (***input parameter*** **–** `RHOA`)

Method

The airframe prediction equations for each component are cast in the following general form. The nondimensional mean-square pressure $\left\langle p^2 \right\rangle^*$ is

$$\left\langle p^2 \right\rangle^* = \frac{\Pi^*}{4\pi r_s^{*2}} D(\theta_D, \phi) F(St) \qquad (1)$$

where Π^* is the nondimensional acoustic power, D is the directivity function, and F is the spectrum function. The general form of the nondimensional acoustic power is

$$\Pi^* = kM_a^n G \tag{2}$$

where k is constant, M_a^n is the aircraft Mach number raised to a power, and G is uniquely defined for each airframe source. G is a function of the boundary layer thickness for airfoil related noise sources such as wing and flap noise. For the landing gear sources, G is a function of the geometric properties of the landing gear.

The free-field lossless sound pressure level for a given component is obtained from

$$SPL = 10Log_{10}\left\langle p^2 \right\rangle^* + 20Log_{10}\frac{\rho_a c_a^2}{p_{ref}} \tag{3}$$

Each airframe noise component is predicted at a source radius of 150 feet. The total airframe noise is the sum o f the mean-square pressures of the individual components.

Wing Noise

The primary noise generating mechanism of the wing is the convection of the turbulent boundary layer past the trailing edge. The acoustic power is given by

$$\Pi^* = kM_a^5 \delta_w^* \tag{4}$$

$$k = \begin{cases} 4.464 \times 10^{-5} & \text{CleanWing} \\ 7.075 \times 10^{-6} & \text{SuperCleanWing} \end{cases} \tag{5}$$

For most commercial transports including the HSCT, $k = 7.075 \times 10^{-6}$.

The nondimensional turbulent boundary layer thickness is computed from the flat plate equation developed by Prandtl.

$$\delta_w^* = 0.37\frac{A_w}{b_w^2}\left(\frac{\rho_a M_a c_a A_w}{\mu_a b_w}\right)^{-0.2} \tag{6}$$

The ambient dynamic viscosity is given by

$$\mu_a = 2.279\frac{T_a^{1.5} \times 10^{-8}}{(T_a + 198.6)} \tag{7}$$

where the ambient temperature T_a is

$$T_a = \left(\frac{c_a}{49.01} \right)^2 \tag{8}$$

The directivity function is assumed to be aligned with the lift dipole and is given by

$$D(\theta_D, \phi) = 4\cos^2(\phi)\cos^2(\theta_D / 2) \tag{9}$$

The spectrum function is an empirical function of the Strouhal number. The spectrum function for a delta wing is given by

$$F(St_w) = 0.485(10St_w)^4 \left[(10St_w)^{1.5} + 0.5 \right]^{-4} \tag{10}$$

where the length scale for the Strouhal number is based on the wing span.

$$St_w = \frac{f\delta_w^* b_w}{M_a c_a} \left[1 - M_a \cos(\theta_D) \right] \tag{11}$$

Leading Edge Slat

Leading edge slat noise is caused by two mechanisms. First, the slat produces an increment of wing trailing edge noise due to the impact on the boundary layer of the wing. Second, the leading edge slat itself produces trailing edge noise. The equations for the acoustic power, boundary layer thickness, and directivity function are similar to the equations for wing noise. The constant k for the leading edge slat was derived for a rectangular wing.

$$\Pi^* = kM_a^5 \delta_w^* \tag{12}$$

$$k = 4.464 \times 10^{-5} \tag{13}$$

$$\delta_w^* = 0.37 \frac{A_w}{b_w^2} \left(\frac{\rho_a M_a c_a A_w}{\mu_a b_w} \right)^{-0.2} \tag{14}$$

$$D(\theta_D, \phi) = 4\cos^2(\phi)\cos^2(\theta_D / 2) \tag{15}$$

As a result of the two noise generating mechanisms, two spectrum functions F_1 and F_2 are required.

$$F_1(St_w) = 0.485(10St_w)^4 \left[(10St_w)^{1.35} + 0.5 \right]^{-4} \tag{16}$$

$$F_2(St_w) = 0.613(2.19St_w)^4 \left[(2.19St_w)^{1.5} + 0.5 \right]^{-4} \tag{17}$$

These spectrum functions were empirically derived based on the wing Strouhal number

$$St_w = \frac{f\delta_w^* b_w}{M_a c_a}\left[1 - M_a \cos(\theta_D)\right] \tag{18}$$

Total leading edge slat noise is the sum of the mean-square pressures from the two noise generating mechanisms

$$\left\langle p^2 \right\rangle^* = \left\langle p^2 \right\rangle_1^* + \left\langle p^2 \right\rangle_2^* = \frac{\Pi^*}{4\pi r_s^{*2}} D(\theta_D, \phi)\left[F_1(S_w) + F_2(S_w)\right] \tag{19}$$

Horizontal and Vertical Tail

The noise generated by the horizontal and vertical tails is also similar to the noise generated by the wing. The noise generating mechanism is the same, e.g. the convection of the turbulent boundary layer past the trailing edge. Since the equations for the horizontal and vertical tails are identical except for the directivity functions, only the formulation for the horizontal tail is presented. To obtain the formulation for the vertical tail, replace the subscript *h* with *v* in the following equations.

$$\Pi^* = kM_a^5 \delta_h^* \tag{20}$$

$$k = 4.464 \times 10^{-5} \tag{21}$$

$$\delta_h^* = 0.37 \frac{A_h}{b_h^2}\left(\frac{\rho_a M_a c_a A_h}{\mu_a b_h}\right)^{-0.2} \tag{22}$$

$$D(\theta_D, \phi) = \begin{cases} 4\cos^2(\phi)\cos^2(\theta_D/2) & \text{Horizontal Tail} \\ 4\sin^2(\phi)\cos^2(\theta_D/2) & \text{Vertical Tail} \end{cases} \tag{23}$$

$$F(St_h) = 0.613(10St_h)^4\left[(10St_h)^{1.5} + 0.5\right]^{-4} \tag{24}$$

$$St_h = \frac{f\delta_h^* b_h}{M_a c_a}\left[1 - M_a \cos(\theta_D)\right] \tag{25}$$

Inboard and Outboard Flap Noise

The noise generated by the inboard and outboard flaps is also the result of the convection of the turbulent boundary layer past the trailing edge. Since the equations for the inboard and outboard flaps are identical, only the formulation for the inboard flap is presented.

To obtain the formulation for the outboard flap, replace the subscript *f,in* with *f,out* in the following equations.

$$\Pi^* = kM_a^6 G \tag{26}$$

$$k = \begin{cases} 2.787 \times 10^{-4} & \text{Single or Double Slotted Flaps} \\ 3.509 \times 10^{-4} & \text{Triple Slotted Flaps} \end{cases} \tag{27}$$

$$G = \frac{A_{f,in}}{b_w^2} \sin^2\left(\beta_{f,in}\right) \tag{28}$$

$$D\left(\theta_D, \phi\right) = 3\left(\sin\delta_{f,in}\cos\theta_D + \cos\delta_{f,in}\sin\theta_D\cos\phi\right)^2 \tag{29}$$

The spectrum function for single or double slotted flaps is given by

$$F\left(St_{f,in}\right) = \begin{cases} 0.0480St_{f,in} & St_{f,in} < 2 \\ 0.1406St_{f,in}^{-0.55} & 2 \le St_{f,in} \le 20 \\ 216.49St_{f,in}^{-3} & St_{f,in} > 20 \end{cases} \tag{30}$$

where the Strouhal number is

$$St_{f,in} = \frac{fA_{f,in}}{M_a c_a b_{f,in}}\left[1 - M_a\cos\left(\theta_D\right)\right] \tag{31}$$

The spectrum function for triple slotted flaps is given by

$$F\left(St_{f,in}\right) = \begin{cases} 0.0257St_{f,in} & St_{f,in} < 2 \\ 0.0536St_{f,in}^{-0.0625} & 2 \le St_{f,in} \le 75 \\ 17078St_{f,in}^{-3} & St_{f,in} > 75 \end{cases} \tag{32}$$

The slot configuration for the HSCT was single slotted flaps.

Main Gear and Nose Gear Noise

The noise generating mechanism from the gear is complex and highly dependent on the landing gear design. Gear noise is dominated by two mechanisms; noise generated by the wheels and noise generated by the strut. Separate formulations for wheel and strut noise are provided.

Since the equations for the main gear and the nose gear are identical, only the formulation for the main gear is presented. To obtain the formulation for the nose gear, replace the subscript *mg* with *ng* in the following equations.

Wheel Noise

The acoustic power, directivity, and spectrum functions for wheel noise are given by

$$\Pi^* = kM_a^6 G \tag{33}$$

$$k = 4.349 \times 10^{-4} \tag{34}$$

$$G = N_{mg}\left(\frac{d_{mg}}{b_w}\right)^2 \tag{35}$$

$$D(\theta_D, \phi) = \frac{3}{2}\sin^2(\theta_D) \tag{36}$$

$$F(St_{mg}) = 13.59 St_{mg}^2 \left(12.5 + St_{mg}^2\right)^{-2.25} \tag{37}$$

$$St_{mg} = \frac{f d_{mg}}{M_a c_a}\left[1 - M_a \cos(\theta_D)\right] \tag{38}$$

Strut Noise

The acoustic power, directivity, and spectrum functions for strut noise are given by

$$\Pi^* = kM_a^6 G \tag{39}$$

$$k = 2.753 \times 10^{-4} \tag{40}$$

$$G = \left(\frac{d_{mg}}{b_w}\right)^2 \frac{L_{mg}}{d_{mg}} \tag{41}$$

$$D(\theta_D, \phi) = 3\sin^2(\theta_D)\sin^2(\phi) \tag{42}$$

$$F(St_{mg}) = 1.280 St_{mg}^2 \left(1.06 + St_{mg}^2\right)^{-3} \tag{43}$$

Total gear noise is the sum of the mean-square pressures from the wheels and the strut

$$\text{e.g. } \left\langle p^2 \right\rangle^* = \left\langle p^2 \right\rangle^*_{wheel} + \left\langle p^2 \right\rangle^*_{strut} \tag{44}$$

or

$$\left\langle \mathrm{p}^2 \right\rangle^* = \frac{\Pi^*}{4\pi r_s^{*2}} \left[D_{wheels}(\theta_D, \phi) F_{wheels}\left(St_{mg}\right) + D_{strut}(\theta_D, \phi) F_{strut}\left(St_{mg}\right) \right] \tag{45}$$

Spectral Adjustment for HSCT Configuration

Acoustic data were collected in the Boeing Low-Speed Aeroacoustic Facility (LSAF) on a 3% full span model of a double delta HSCT wing configuration. The model measured approximately 106 inches long with a wing span of approximately 45 inches. The inboard wing leading edges were swept approximately 68 degrees and the outboard leading edges were swept approximately 48 degrees. The adjustable leading edge flaps were deflected 30 degrees, and the adjustable trailing edges were deflected 20 degrees. Removable landing gear were used on the model. The main gear was modeled as a triple-post strut with six wheels per truck. The nose gear was modeled as a single-post with two-wheels. There were no gear cavities or doors, and the model had flow-through nacelles.

Boeing made noise predictions using the Fink method. At the 90 degree angle a set of spectral deltas were derived to improve the agreement between prediction and measurement. A set of directivity deltas were derived based on the PNLT directivity shape. The spectral deltas are computed by

$$\Delta = A(\theta) B(f) \tag{46}$$

The deltas are then added to the sound pressure level

$$SPL_{Corrected} = SPL_{Fink} + \Delta \tag{47}$$

Table 3.11.1 provides the decibel corrections that are applied to wing, leading edge flaps, horizontal tail, vertical tail, inboard flap, and outboard flap. Corrections were not derived for the main gear or the nose gear.

Total Noise

The free-field lossless total airframe noise is the sum of the mean-square pressures of the eight airframe subcomponents. Propagation effects are defined in section 3.13.

Table 3.11.1 Airframe Noise Adjustment Functions for the HSCT Configuration, (dB)

	Emission Angle, degrees																	
		10	20	30	40	50	60	70	80	90	100	110	120	130	140	150	160	170
Freq.	A(θ)	1.4	1.4	1.4	1.4	1.4	1.4	1.4	1.4	1.0	0.7	0.5	0.3	0.0	-0.2	-0.5	-0.8	-1.0
Hz.	B(f)																	
50	-12.0	-16.8	-16.8	-16.8	-16.8	-16.8	-16.8	-16.8	-16.8	-12.0	-8.4	-6.0	-3.6	0.0	2.4	6.0	9.6	12.0
63	-11.0	-15.4	-15.4	-15.4	-15.4	-15.4	-15.4	-15.4	-15.4	-11.0	-7.7	-5.5	-3.3	0.0	2.2	5.5	8.8	11.0
80	-10.0	-14.0	-14.0	-14.0	-14.0	-14.0	-14.0	-14.0	-14.0	-10.0	-7.0	-5.0	-3.0	0.0	2.0	5.0	8.0	10.0
100	-9.0	-12.6	-12.6	-12.6	-12.6	-12.6	-12.6	-12.6	-12.6	-9.0	-6.3	-4.5	-2.7	0.0	1.8	4.5	7.2	9.0
125	-8.0	-11.2	-11.2	-11.2	-11.2	-11.2	-11.2	-11.2	-11.2	-8.0	-5.6	-4.0	-2.4	0.0	1.6	4.0	6.4	8.0
160	-8.0	-11.2	-11.2	-11.2	-11.2	-11.2	-11.2	-11.2	-11.2	-8.0	-5.6	-4.0	-2.4	0.0	1.6	4.0	6.4	8.0
200	-9.0	-12.6	-12.6	-12.6	-12.6	-12.6	-12.6	-12.6	-12.6	-9.0	-6.3	-4.5	-2.7	0.0	1.8	4.5	7.2	9.0
250	-9.5	-13.3	-13.3	-13.3	-13.3	-13.3	-13.3	-13.3	-13.3	-9.5	-6.7	-4.8	-2.9	0.0	1.9	4.8	7.6	9.5
315	-9.0	-12.6	-12.6	-12.6	-12.6	-12.6	-12.6	-12.6	-12.6	-9.0	-6.3	-4.5	-2.7	0.0	1.8	4.5	7.2	9.0
400	-9.0	-12.6	-12.6	-12.6	-12.6	-12.6	-12.6	-12.6	-12.6	-9.0	-6.3	-4.5	-2.7	0.0	1.8	4.5	7.2	9.0
500	-9.0	-12.6	-12.6	-12.6	-12.6	-12.6	-12.6	-12.6	-12.6	-9.0	-6.3	-4.5	-2.7	0.0	1.8	4.5	7.2	9.0
630	-10.0	-14.0	-14.0	-14.0	-14.0	-14.0	-14.0	-14.0	-14.0	-10.0	-7.0	-5.0	-3.0	0.0	2.0	5.0	8.0	10.0
800	-10.0	-14.0	-14.0	-14.0	-14.0	-14.0	-14.0	-14.0	-14.0	-10.0	-7.0	-5.0	-3.0	0.0	2.0	5.0	8.0	10.0
1000	-10.0	-14.0	-14.0	-14.0	-14.0	-14.0	-14.0	-14.0	-14.0	-10.0	-7.0	-5.0	-3.0	0.0	2.0	5.0	8.0	10.0
1250	-9.0	-12.6	-12.6	-12.6	-12.6	-12.6	-12.6	-12.6	-12.6	-9.0	-6.3	-4.5	-2.7	0.0	1.8	4.5	7.2	9.0
1600	-9.0	-12.6	-12.6	-12.6	-12.6	-12.6	-12.6	-12.6	-12.6	-9.0	-6.3	-4.5	-2.7	0.0	1.8	4.5	7.2	9.0
2000	-9.0	-12.6	-12.6	-12.6	-12.6	-12.6	-12.6	-12.6	-12.6	-9.0	-6.3	-4.5	-2.7	0.0	1.8	4.5	7.2	9.0
2500	-9.0	-12.6	-12.6	-12.6	-12.6	-12.6	-12.6	-12.6	-12.6	-9.0	-6.3	-4.5	-2.7	0.0	1.8	4.5	7.2	9.0
3150	-9.0	-12.6	-12.6	-12.6	-12.6	-12.6	-12.6	-12.6	-12.6	-9.0	-6.3	-4.5	-2.7	0.0	1.8	4.5	7.2	9.0
4000	-9.0	-12.6	-12.6	-12.6	-12.6	-12.6	-12.6	-12.6	-12.6	-9.0	-6.3	-4.5	-2.7	0.0	1.8	4.5	7.2	9.0
5000	-9.0	-12.6	-12.6	-12.6	-12.6	-12.6	-12.6	-12.6	-12.6	-9.0	-6.3	-4.5	-2.7	0.0	1.8	4.5	7.2	9.0
6300	-9.0	-12.6	-12.6	-12.6	-12.6	-12.6	-12.6	-12.6	-12.6	-9.0	-6.3	-4.5	-2.7	0.0	1.8	4.5	7.2	9.0
8000	-9.0	-12.6	-12.6	-12.6	-12.6	-12.6	-12.6	-12.6	-12.6	-9.0	-6.3	-4.5	-2.7	0.0	1.8	4.5	7.2	9.0
10K	-8.0	-11.2	-11.2	-11.2	-11.2	-11.2	-11.2	-11.2	-11.2	-8.0	-5.6	-4.0	-2.4	0.0	1.6	4.0	6.4	8.0

3.12 Jet Shielding

A change in the received noise spectra caused by the presence of adjacent jets is known as jet shielding. The method described in the section is a simplified method that was adopted for the HSR system studies. The method requires only geometric input and does not require input concerning the exhaust parameters of the adjacent jets or the spacing between the jets. Jet shielding can be applied to all aft radiated noise source.

Symbols

h	aircraft altitude at visual overhead, ft (***input parameter*** – `ALTEVO`)
N_{eng}	number of engines (***input parameter*** – `NENG`)
Sl	sideline distance, ft (***input parameter*** – `SL`)
x_a	aircraft position along the flight path, ft
y_a	aircraft position perpendicular to flight path, ft $(y_a = 0)$
z_a	aircraft position above ground level, ft (***input parameter*** – `ZA`)
β	angle between the flight path vector and the vector for the aircraft to the origin
ϕ	flight path angle, degrees (***input parameter*** – `FPA`)
ΔSPL	jet shielding suppression level, dB

The empirical equation which models jet shielding is given by

$$\Delta SPL = 10 Log_{10}\left[1 - \frac{\left(1 - e^{-\left(Sl/h\right)^2}\right)\left(N_{eng} - 1\right)\cos^2\beta}{N_{eng}}\right] \tag{1}$$

where

$$\cos^2\beta = \frac{\left(x_a\cos\phi + z_a\sin\phi\right)^2}{x_a^2 + z_a^2} \tag{2}$$

and the aircraft position along the flight path is

$$x_a = \frac{z_a - h}{\tan\phi} \tag{3}$$

Equation 1 is only valid for values of β between 0° and 90°. No shielding effect is applied for angles greater than 90°. Note that ΔSPL = 0 for the case of a single engine aircraft ($N_{eng} = 1$) and for an observer directly under the flight path ($Sl = 0$).

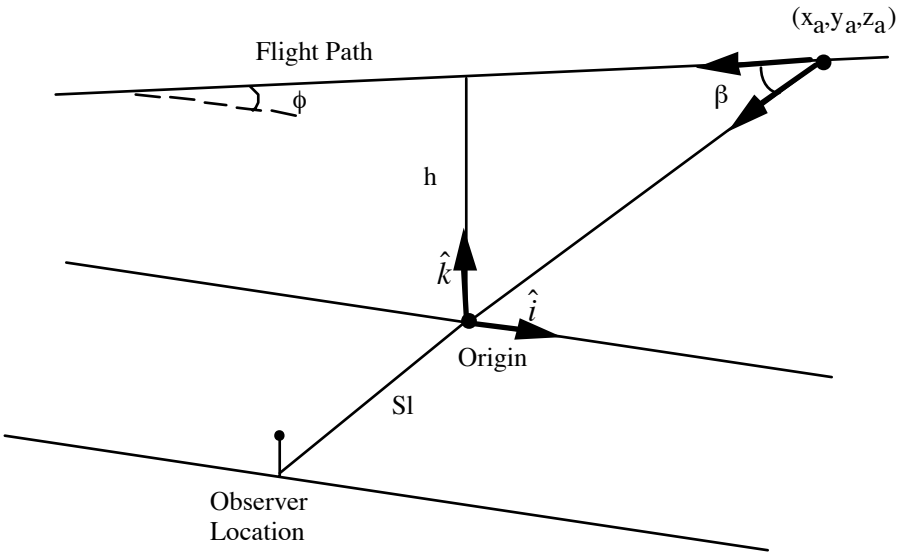

Figure 3.11.1 Jet shielding vector diagram

3.13 Propagation Effects

The fan, core, turbine, and airframe noise sources are modeled as point sources. The free-field spectra for each is computed at a reference distance of 150 feet and then propagated to the observer assuming straight line propagation. Propagation effects include spherical spreading, convective amplification, ambient pressure, atmospheric attenuation, ground reflection attenuation, and extra ground attenuation (EGA). For convenience, source modification for the number of sources is also included with the propagation effects. The free-field lossless spectra is modified for propagation effectes by

$$SPL = SPL_{free-field\ lossless} + \Delta SPL \tag{1}$$

where ΔSPL is given by

$$\Delta SPL = 20Log_{10}\left(\frac{150}{r_s}\right) - 40Log_{10}\left(1 - M_a \cos\theta_D\right) + 10Log_{10}\left(N_{eng}\right) + 20Log_{10}\left(\frac{\rho_a(z_s)c_a^2(z_s)}{\rho_a(z_o)c_a^2(z_o)}\right) - A_{abs}r_s + G - EGA \tag{2}$$

and where each adjustment term is defined in table 3.13.1.

Table 3.13.1 – Definition of ΔSPL Adjustments

Adjustment for:	Term
Spherical spreading	$20Log_{10}\left(\frac{150}{r_s}\right)$
Convective amplification	$40Log_{10}\left(1 - M_a \cos\theta_D\right)$
Number of sources	$10Log_{10}\left(N_{eng}\right)$
Ambient pressure	$20Log_{10}\left(\frac{\rho_a(z_s)c_a^2(z_s)}{\rho_a(z_o)c_a^2(z_o)}\right)$
Atmospheric absorption	$\left\|A_{abs}(f_{pi}, rh)\right\| r_s$ $f_p = \frac{f}{1 - M_a \cos\theta_p}$
Ground reflections	G
Extra Ground Attenuation	EGA

Atmospheric absorption is computed by either the SAE ARP866A method or the Shields and Bass method [16]. Ground effects include attenuation of the spectra due to

reflections from the surface and extra ground attenuation due to temperature and wind gradients. Ground reflection is predicted by the method developed by Chien and Soroka [17]. EGA is predicted by SAE AIR 923 [18].

The jet noise source is modeled as a distributed source. Special propagation effects are applied to the jet noise source to account for acoustic and geometric near field effects. These effects are described in detail in the sections 3.9 and 3.10.

3.14 Noise Metrics

One-third-octave band noise levels are predicted at a user defined location, typically one of the FAA certification points. Output from each noise source is provided for the range of frequencies and emission angles requested by the user. HSRNOISE computes the following noise metrics; OASPL, PNL, PNLT, and EPNL.

4.0 Code Verification

The HSRNOISE code was compared with noise levels predicted by the MCP code for the Technology Concept (TC) aircraft. The TC aircraft is a Mach 2.4 supersonic transport with a takeoff gross weight of 650,000 pounds and a range of 5000 nautical miles. The propulsion system is a mixed flow turbofan with a two-dimensional bifurcated inlet and a mixer ejector suppressor nozzle. The input parameters for this analysis are from the 3870.47 engine cycle.

One-third-octave band spectra, OASPL, PNL, PNLT, and EPNL noise predictions were made at the FAA approach, sideline, and centerline observer locations. Section 4.1 describes the analysis of the EPNL comparisons as well as comparisons of the OASPL, PNL, and PNLT noise metrics. Differences between the MCP and HSRNOISE predictions are explained. Section 4.2 describes the analysis of the one-third-octave band spectra. Free-field lossless and full system spectra are presented. The free-field lossless spectra identify differences in the implementation of the noise source methodologies. The full system predictions, which include atmospheric attenuation, ground reflections, extra ground attenuation, and jet shielding, identify differences in propagation effects. The input files used for the free-field lossless and full system predictions are provided in section 5.0.

4.1 EPNL Comparisons

This section presents comparisons of the EPNL levels predicted by the HSRNOISE and MCP codes. The EPNL noise metric was instrumental in determining the weight and range of the TC aircraft. Columns A, B, and C of table 4.1.1 show the results of the initial EPNL comparisons between the HSRNOISE and MCP codes. Differences in total aircraft EPNL of 2.1 at approach, 2.6 on the sideline and 1.0 on the centerline were not anticipated. Causes for the differences included different numerical techniques for integrating the PNLT time history, different procedures for computing the PNLT time history, different ground reflection models, and differences in source levels.

EPNL Numerical Integration

The EPNL noise metric is calculated by integrating the PNLT time history between the limits of the 10 dB down points. FAA FAR 36 Appendix B dictates that the EPNL should be calculated using half-second time intervals. Both the HSRNOISE and MCP codes predict the PNLT time history at fixed emission angles, which do not correspond to half-second time intervals. Since half-second PNLT data is not available, the question becomes what numerical integration technique is appropriate. Numerical integration was initially performed in the HSRNOISE code using the FAA procedure or equivalently the rectangular rule. Half-second PNLT data was obtained by interpolating the PNLT time history. The interpolation procedure was designed to ensure that the maximum PNLT was included in the interpolated time history. Numerical integration is performed in the MCP code using the trapezoidal rule.

To determine if the integration technique caused differences in EPNL levels, both the trapezoidal rule and the rectangular rule were implemented in the HSRNOISE EPNL algorithm. Column B of table 4.1.1 lists the EPNL levels predicted by the rectangular rule. These predictions are identified as method 1. Column D lists the EPNL levels predicted using the trapezoidal rule. These predictions are identified as method 2. Column F lists the difference between methods 1 and 2. Except for the sources with tones, both integration methods predict essentially the same levels. The trapezoidal rule was adopted as the EPNL integration technique for the HSRNOISE code because it does not require interpolation of the spectra. Interpolating spectra with tones may introduce errors in the half second interval data required for the rectangular rule integration.

Table 4.1.1 EPNL Comparisons between MCP and HSRNOISE Codes

	(A) MCP (Boeing)	**(B)** HSRNOISE (Method 1)	**(C)** Δ1	**(D)** HSRNOISE (Method 2)	**(E)** Δ2	**(F)** Δ3
Approach						
Fan	91.8	92.2	0.4	92.7	0.9	-0.5
Core	84.4	84.3	-0.1	84.1	-0.3	0.2
Turbine	94.5	97.6	3.1	97.1	2.6	0.5
Jet	92.6	95.0	2.4	95.0	2.4	0.0
Airframe	89.4	90.8	1.4	90.8	1.4	0.0
Total	99.7	101.8	2.1	101.8	2.1	0.0
Sideline						
Fan	89.1	89.0	-0.1	89.2	-0.1	-0.2
Core	74.3	76.7	2.4	76.8	2.5	-0.1
Turbine	81.3	85.4	4.1	85.3	4.0	0.1
Jet	100.6	103.6	3.0	103.5	2.9	0.1
Total	101.3	103.9	2.6	103.8	2.5	0.1
Centerline						
Fan	87.4	87.2	-0.2	87.6	0.2	-0.4
Core	79.0	78.3	-0.7	78.3	-0.7	0.0
Turbine	85.6	88.9	3.3	88.7	3.1	0.2
Jet	99.4	100.4	1.0	100.2	0.8	0.2
Total	100.2	101.2	1.0	101.0	0.8	0.2

Δ1 = B-A **Δ2 = D-A** **Δ3 = B-D**

Method 1: EPNL calculated using rectangular rule Method 2: EPNL calculated using trapezoidal rule

PNLT Calculations

OASPL, PNL, and PNLT time history comparisons are provided in figures 4.1.1 through 4.1.9. The PNLT comparisons identified a second difference between HSRNOISE and MCP. After discussing the PNLT comparisons with Boeing, it was learned that tone corrections below 1250 Hertz and SPL levels below 30 dB were not included the MCP predictions. This modification to the PNLT calculations was not incorporated into the HSRNOISE code.

Ground Reflection Model

The HSRNOISE and MCP codes use different methods to model the effects of ground reflections. The HSRNOISE code uses the Chien and Soroka model and the MCP code uses the Shivashankara model. All input parameter to the ground reflection models were explicitly defined with the exception of the ground flow resistance. Modeling the ground as a soft surface as opposed to a hard reflecting surface has a major impact on the shape of the received spectra and the EPNL level. A range of ground flow resistances were tested in the HSRNOISE code to determine the impact on the EPNL level. The EPNL levels listed in table 4.1.1 were calculated using a ground flow resistance of $1.1x10^6$ lbm/sec-ft^3, which is representative of an asphalt surface. The EPNL levels listed in table 4.1.2 were calculated using a ground flow resistance of $9.4x10^3$ lbm/sec-ft^3, which is representative of a grassy field. Interestingly, the value of the ground flow resistance, which gave the best EPNL comparison, did not yield the best spectral comparison. Figures 4.1.10 and 4.1.11 show the total aircraft spectra at the sideline location with a ground flow resistance of $1.1x10^6$ lbm/sec-ft^3 and $9.4x10^3$ lbm/sec-ft^3 respectively. The spectral shapes predicted by HSRNOISE and MCP are significantly different in figure 4.1.10, especially at the approach angle of 30 degrees. For this reason the ground flow resistance was set to $1.1x10^6$ lbm/sec-ft^3 for the spectral analysis.

Table 4.1.2 EPNL Comparisons between MCP and HSRNOISE Codes
Using Ground Flow Resistance Typical of a Grassy Field

	(A) MCP (Boeing)	**(B)** HSRNOISE (Method 2)	**(C)** Δ
Approach			
Fan	91.8	90.1	1.7
Core	84.4	82.9	1.5
Turbine	94.5	95.8	-1.3
Jet	92.6	93.1	-0.5
Airframe	89.4	89.9	-0.5
Total	99.7	100.0	-0.3
Sideline			
Fan	89.1	87.0	2.1
Core	74.3	74.9	-0.6
Turbine	81.3	82.7	-1.4
Jet	100.6	101.6	-1.0
Total	101.3	102.0	-0.7
Centerline			
Fan	87.4	85.7	1.7
Core	79.0	77.2	1.8
Turbine	85.6	87.0	-1.4
Jet	99.4	99.0	0.4
Total	100.2	99.6	0.6

Δ = A-B
Method 2: EPNL calculated using trapezoidal rule

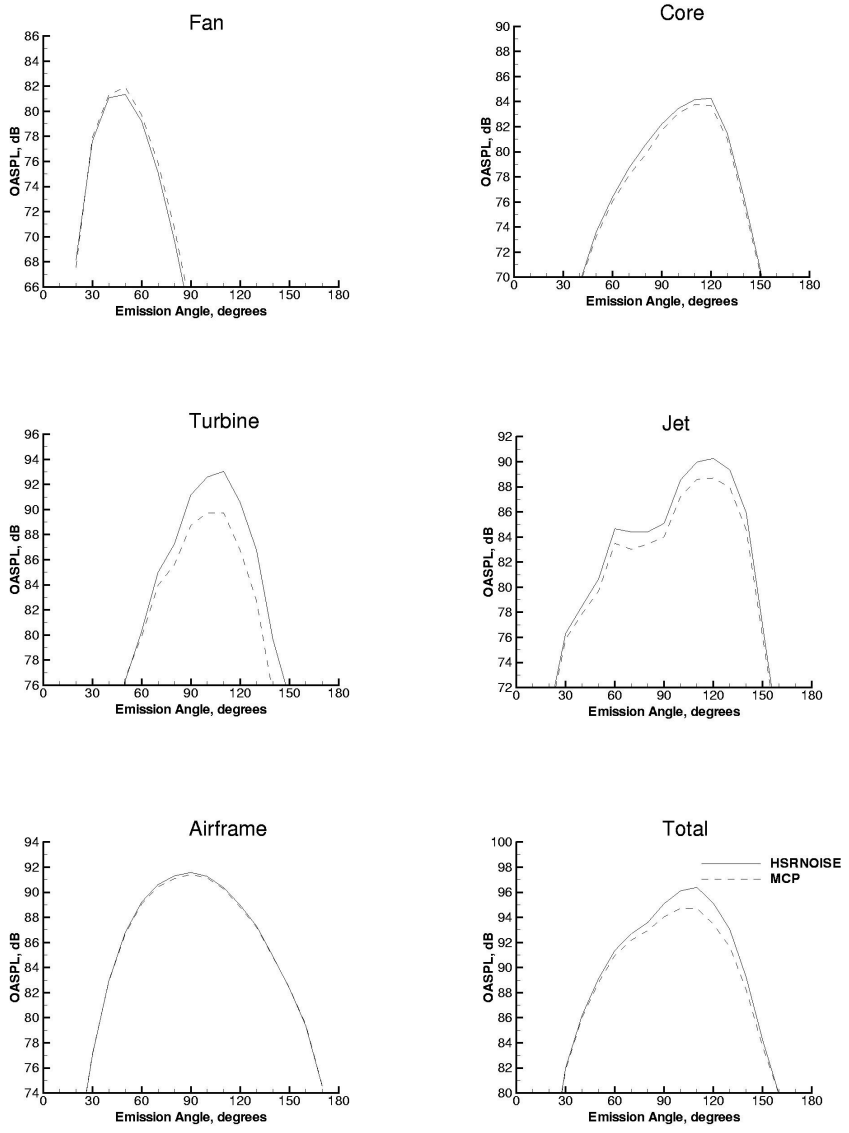

Figure 4.1.1 Approach OASPL comparisons for the TC aircraft

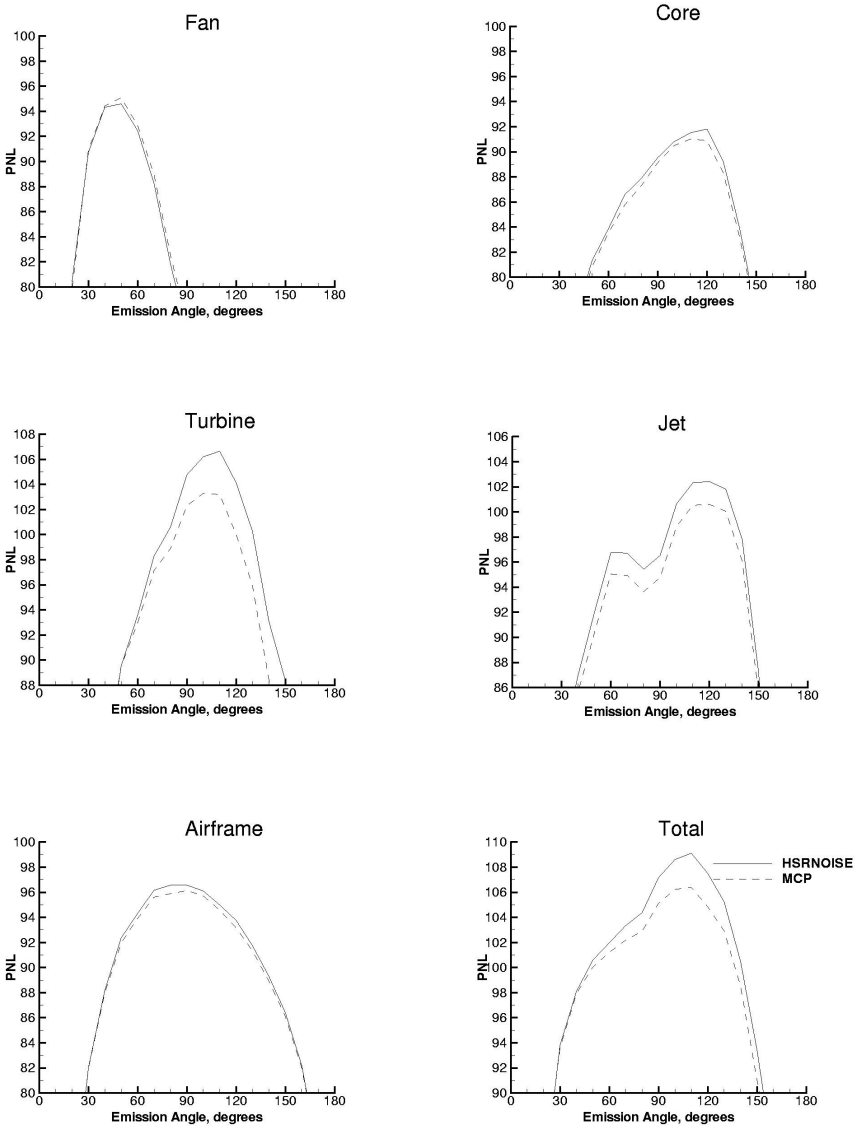

Figure 4.1.2 Approach PNL comparisons for the TC aircraft

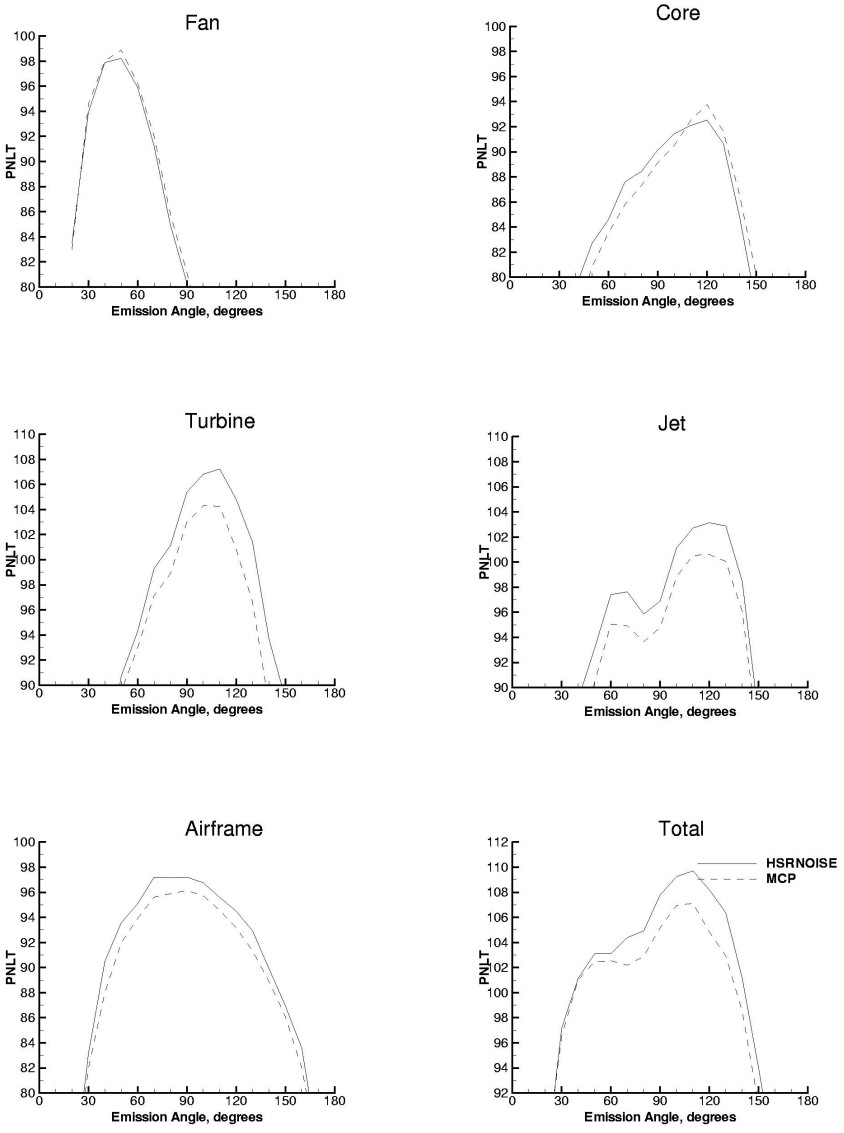

Figure 4.1.3 Approach PNLT comparisons for the TC aircraft

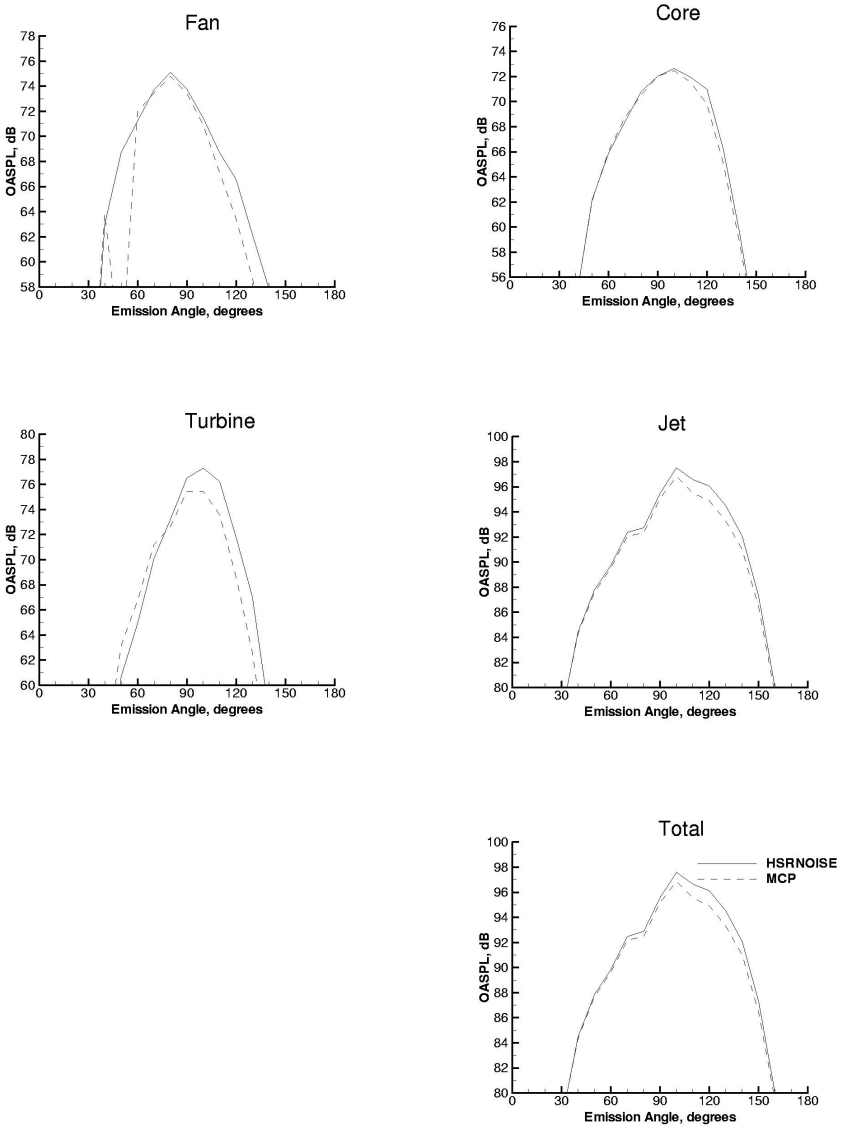

Figure 4.1.4 Sideline OASPL comparisons for the TC aircraft

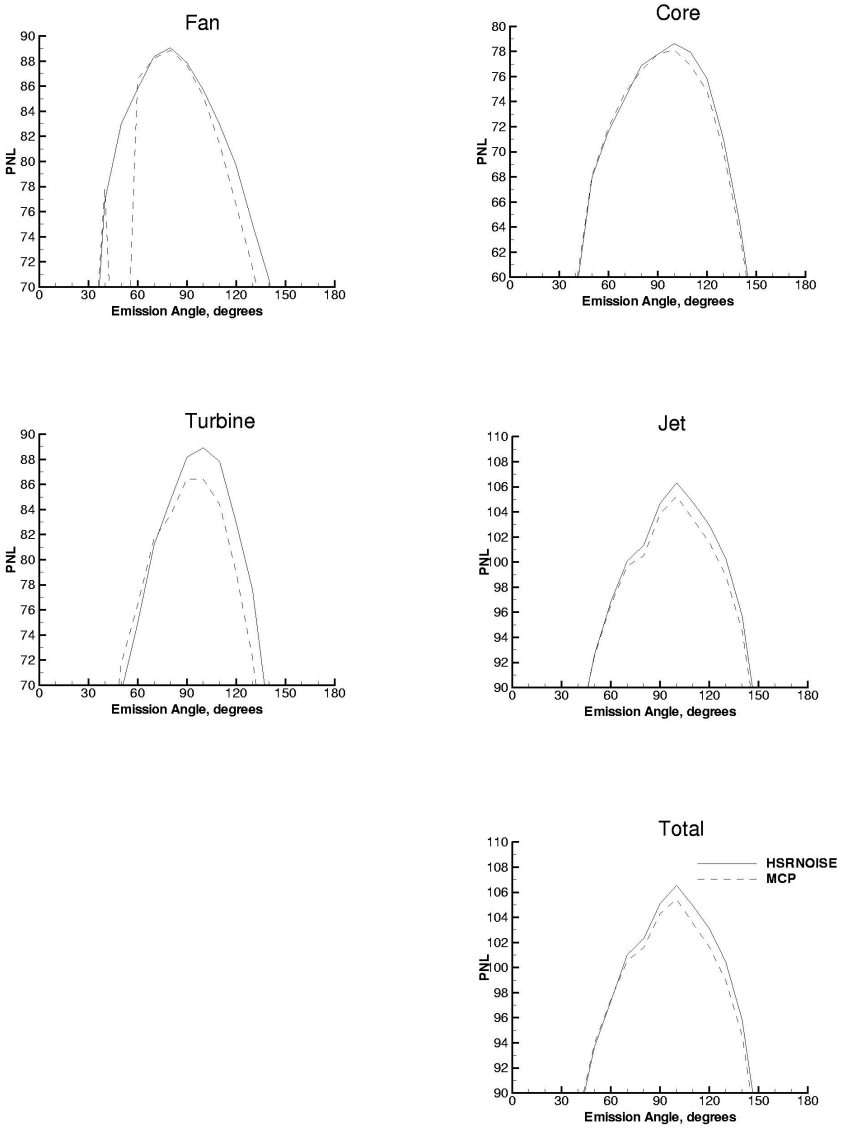

Figure 4.1.5 Sideline PNL comparisons for the TC aircraft

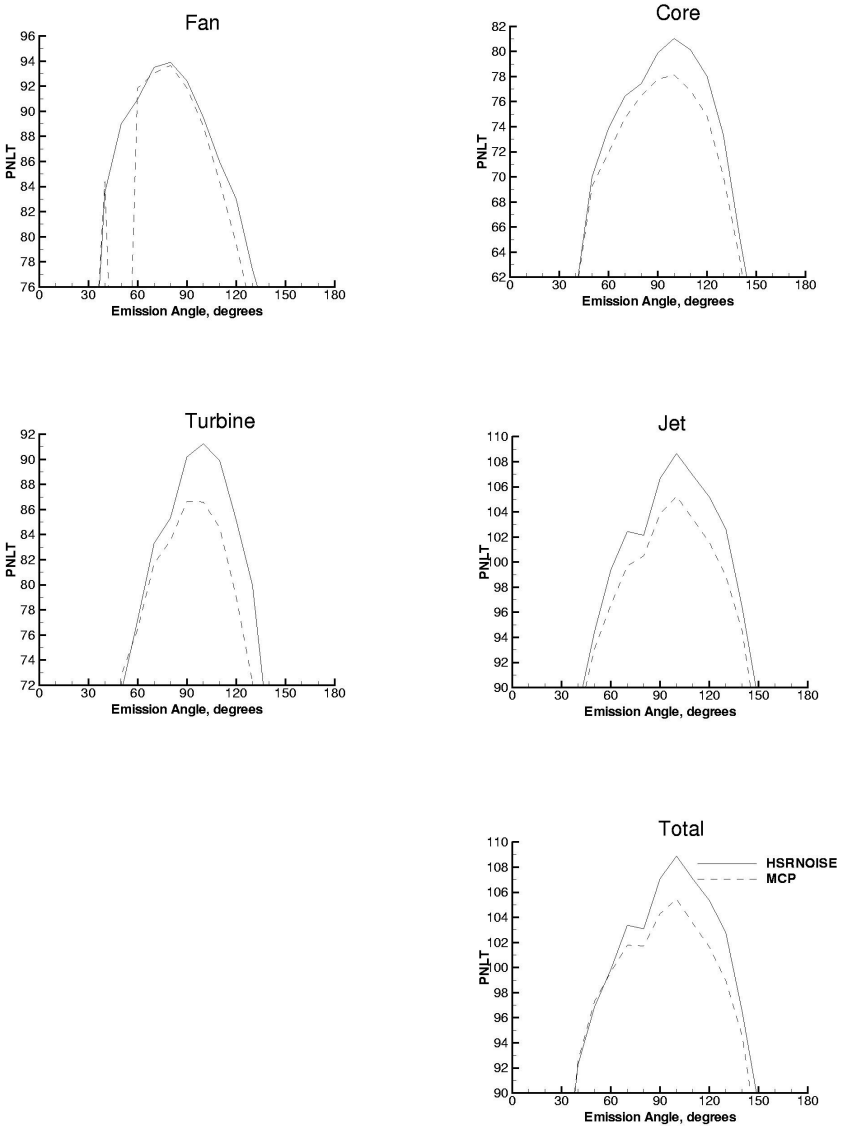

Figure 4.1.6 Sideline PNLT comparisons for the TC aircraft

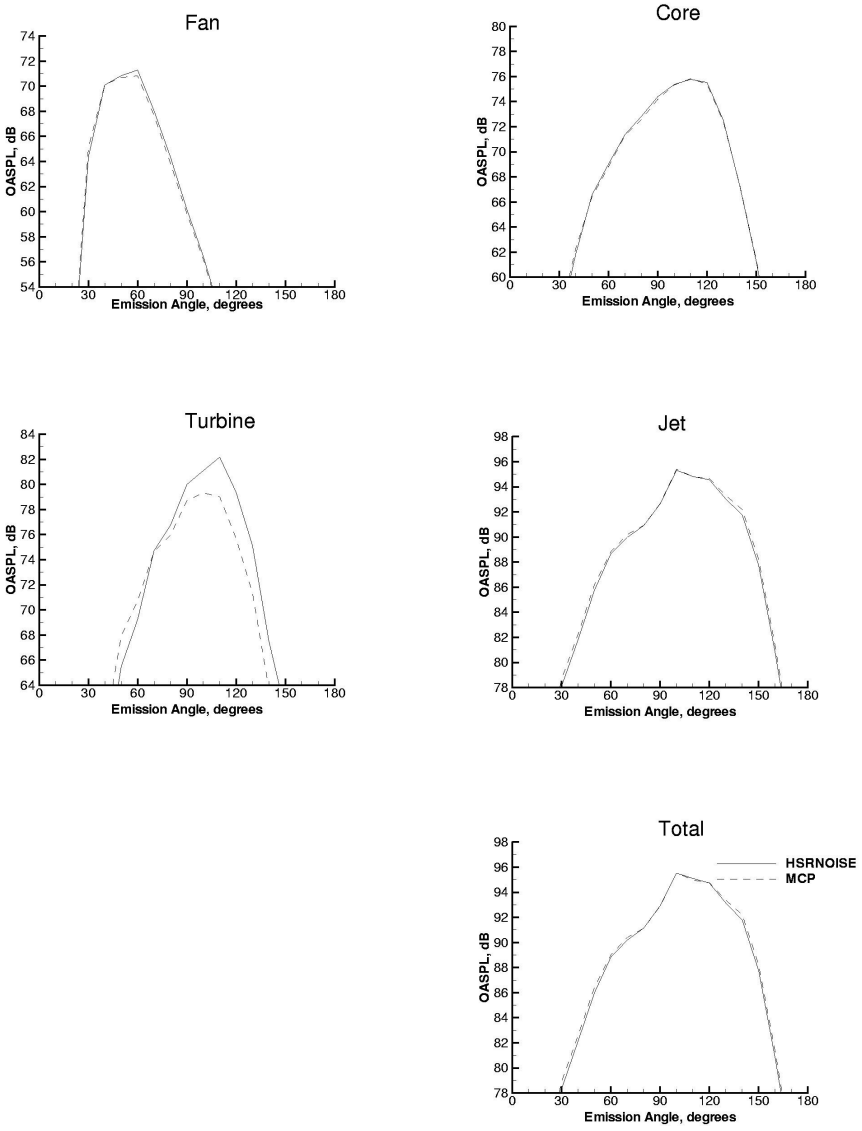

Figure 4.1.7 Centerline OASPL comparisons for the TC aircraft

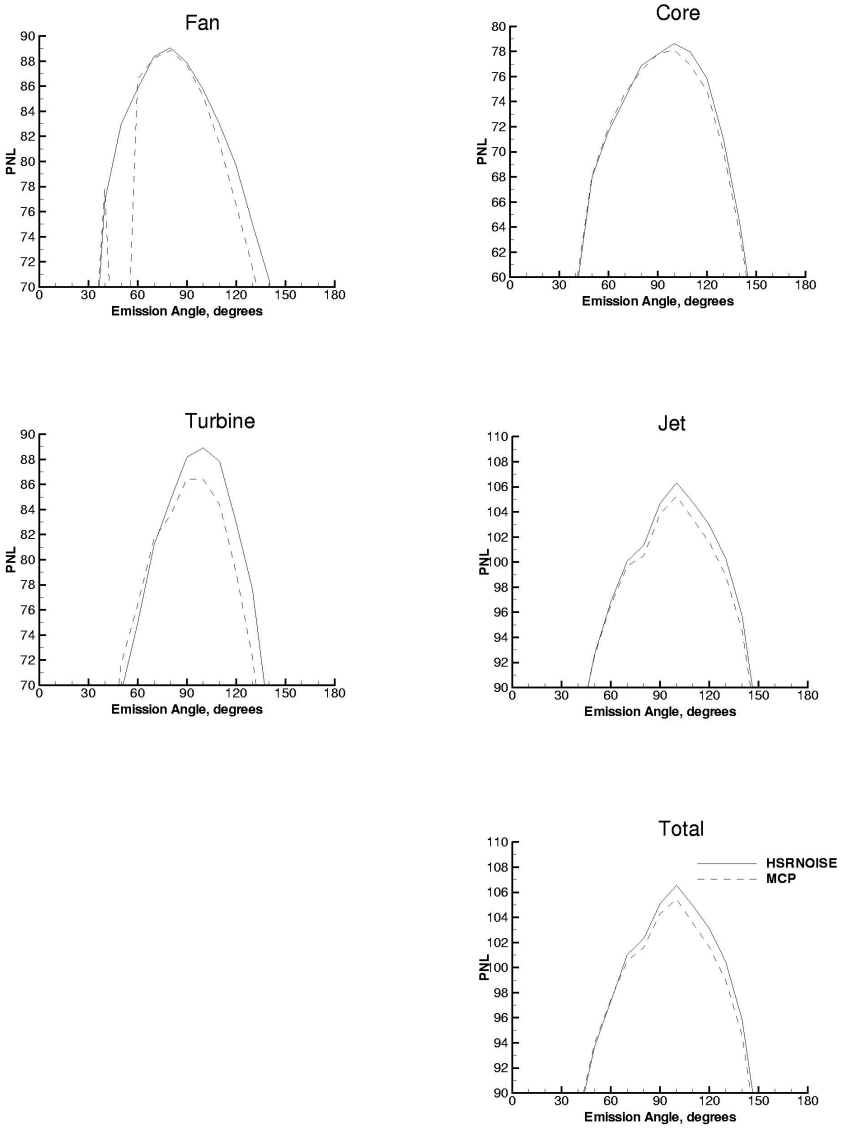

Figure 4.1.8 Centerline PNL comparisons for the TC aircraft

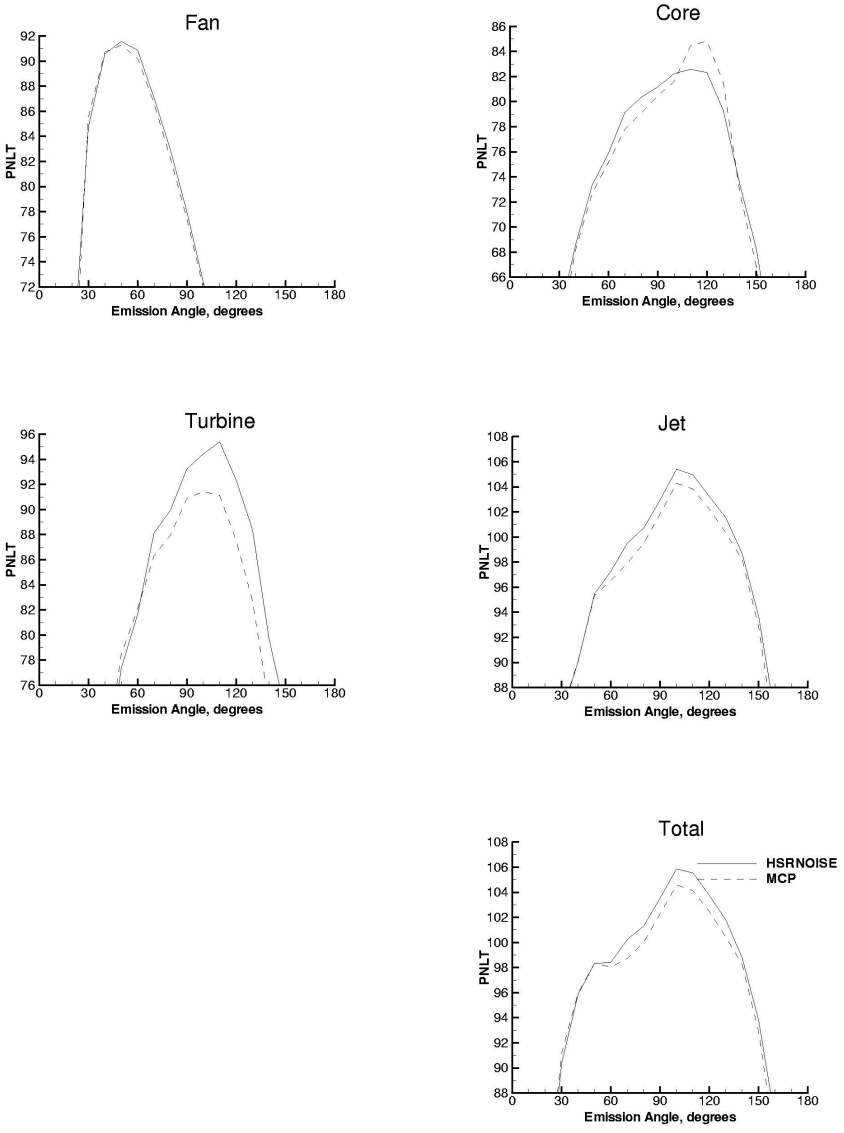

Figure 4.1.9 Centerline PNLT comparisons for the TC aircraft

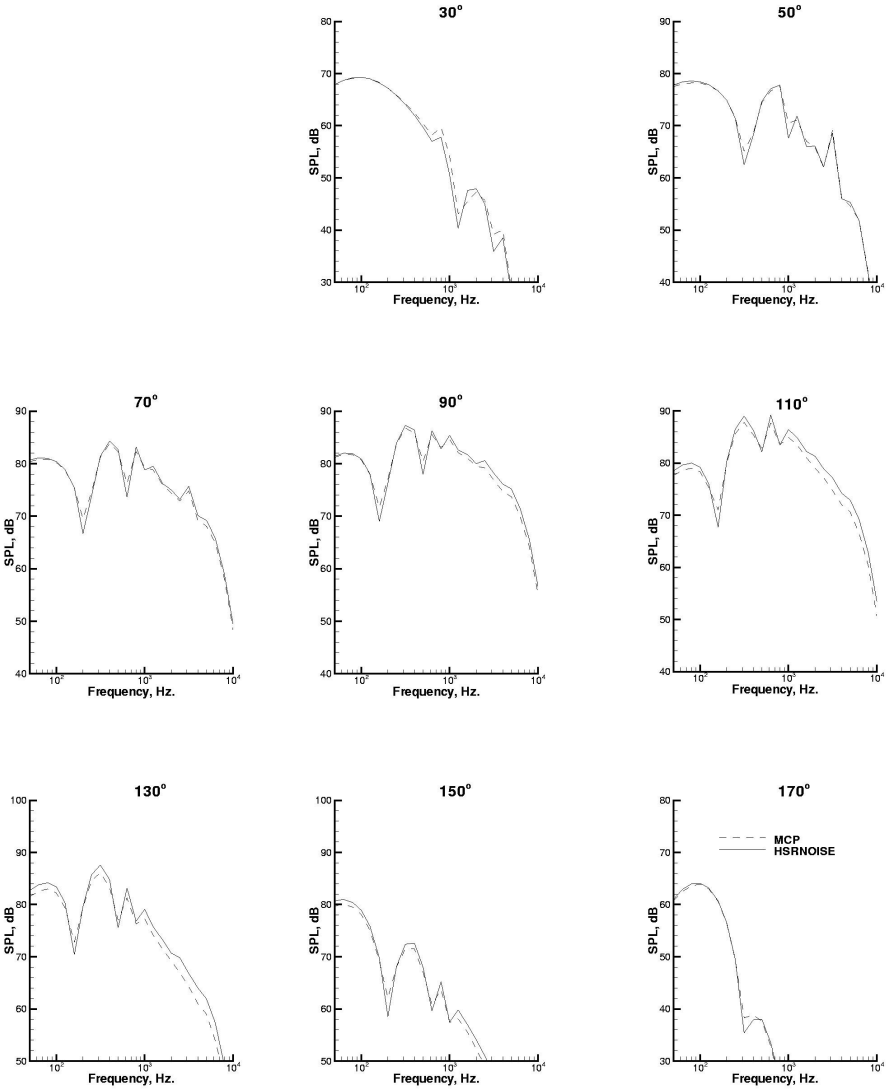

Figure 4.1.10 Total sideline noise prediction for the TC aircraft
Ground flow resistance 1.1 x 10^6 lbm/sec-ft^3

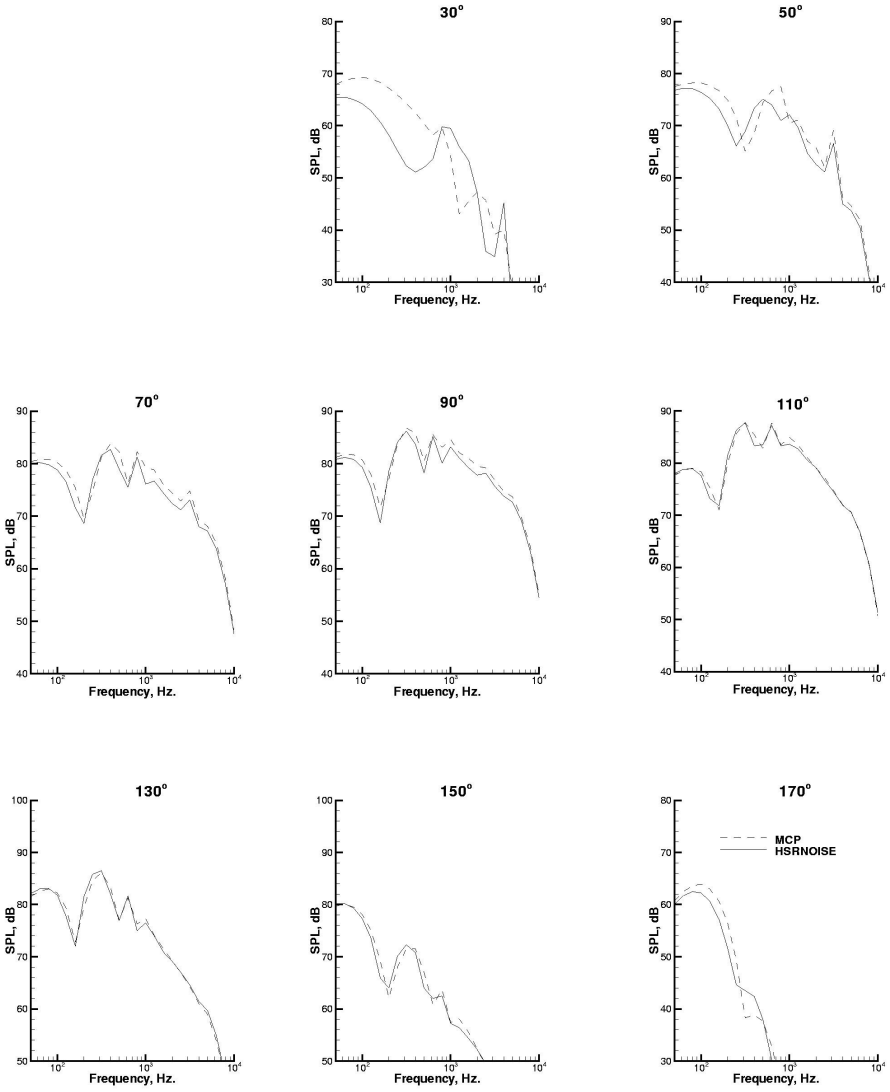

Figure 4.1.11 Total sideline noise prediction for the TC aircraft
Ground flow resistance 9.4 x 10^3 lbm/sec-ft^3

4.2 Spectral Analysis

The previous section provided a comparison of the EPNL noise levels for each noise source. However, as was demonstrated in the previous section, good EPNL comparisons do not necessarily imply good spectral comparisons. This section provides comparisons of the component spectra. Free-field predictions were made to remove the effects of ground reflection, EGA, and jet shielding. Corrections to the source spectra or "Deltas" were also removed from the free-field predictions. After the HSRNOISE code was verified with the free-field comparison, full system predictions were made. Free-field and full system predictions were made for the approach, sideline, and centerline conditions. Input files to the HSRNOISE code used in the spectral analysis are listed in Section 5.

One-third-octave band spectra were plotted at emission angles from 30 to 170 degrees in 20 degree increments. Each spectrum was divided into three regions as defined below.

Low Frequencies	50 - 250 Hertz
Mid Frequencies	315 - 1600 Hertz
High Frequencies	2000 - 10000 Hertz

Each region of the spectra was evaluated according to the following criteria

Excellent	$0.0 < \lvert\Delta\rvert \leq 0.3$
Good	$0.3 < \lvert\Delta\rvert \leq 0.7$
Fair	$0.7 < \lvert\Delta\rvert \leq 1.0$
Poor	$\lvert\Delta\rvert > 1.0$

where Δ is the RMS error for a given frequency range given by

$$\Delta = \sqrt{\frac{1}{N}\sum_{i=1}^{N}\left[SPL_{MCP,i} - SPL_{HSRNOISE,i}\right]^2} \qquad (1)$$

In equation 1, N is the frequency index. N equals 8 for the low, mid, and high frequency evaluations. N equals 24 when all frequencies are evaluated.

4.2.1 Total Aircraft Noise

Figures 4.2.1.1, 4.2.1.3, and 4.2.1.5 show the total aircraft free-field spectra for the approach, sideline, and centerline observer locations. Figures 4.2.1.2, 4.2.1.4, and 4.2.1.6 show comparisons of the full system predictions. RMS error values are provided in tables 4.2.1.1 through 4.2.1.6. Discrepancies between MCP and HSRNOISE predictions are apparent in both the free-field and full system spectra.

Table 4.1.1 (page 123) listed a difference of 2.1 EPNdB in the total aircraft noise for the approach case. The free-field spectra for this case is shown in figure 4.2.1.1. From the component analysis it was determined that fan tones dominate the high frequency spectra at emission angles of 30 and 50 degrees and turbine noise dominates the high frequency spectra for emission angles greater than 90 degrees. While the MCP and HSRNOISE codes use the same theoretical models to predict fan and turbine noise, the implementation of the methods are different. Refer to Sections 4.2.3 and 4.2.4 for details. Differences on the order of 1 to 1.5 dB were detected in the fan tone levels. Differences on the order of 1 to 5 dB were detected in the high frequency region of the free-field turbine spectra. Figure 4.2.1.2 shows the full system spectra for the approach case. In addition to the discrepancies observed in the free-field spectra, discrepancies are also noted in the full system spectra at the frequencies associated with ground dips.

Better EPNL comparisons were achieved for the sideline and centerline cases where fan and turbine noise are less important. Comparisons of the free-field spectra were excellent in the low frequency range and mostly excellent to good in the mid frequency range. As in the approach case, comparison of the high frequency spectra was poor. Discrepancies in the high frequency range are associated with the ground reflection model which will be explained in greater detail in the jet noise comparisons.

Table 4.2.1.1 Free-field Total Aircraft Approach Noise RMS Error Table, dB

Emission Angle / Frequencies	30°	50°	70°	90°	110°	130°	150°	170°
Low	0.3	0.3	0.3	0.1	0.1	0.1	0.3	0.3
Mid	0.5	0.6	0.6	0.3	0.8	0.9	0.6	0.6
High	0.7	0.8	1.4	2.0	3.4	4.1	0.8	1.4
All	0.5	0.6	0.9	1.1	2.0	2.4	0.6	0.9

Table 4.2.1.2 Full System Total Aircraft Approach Noise RMS Error Table, dB

Emission Angle / Frequencies	30°	50°	70°	90°	110°	130°	150°	170°
Low	0.9	1.4	1.8	0.9	0.9	1.6	1.4	1.8
Mid	0.5	1.2	0.9	1.2	1.6	1.4	1.2	0.9
High	0.9	0.9	2.2	3.2	4.2	3.7	0.9	2.2
All	0.8	1.2	1.7	2.1	2.6	2.4	1.2	1.7

Table 4.2.1.3 Free-field Total Aircraft Sideline Noise RMS Error Table, dB

Emission Angle Frequencies	30°	50°	70°	90°	110°	130°	150°	170°
Low	0.0	0.1	0.1	0.0	0.1	0.0	0.1	0.1
Mid	0.1	0.1	0.1	0.0	0.0	0.1	0.1	0.1
High	1.9	1.0	0.8	0.9	1.5	1.4	1.0	0.8
All	1.1	0.6	0.5	0.5	0.9	0.8	0.6	0.5

Table 4.2.1.4 Full System Total Aircraft Sideline Noise RMS Error Table, dB

Emission Angle Frequencies	30°	50°	70°	90°	110°	130°	150°	170°
Low	0.1	0.3	0.9	0.9	1.5	1.3	0.3	0.9
Mid	1.7	1.1	0.9	0.9	1.2	1.6	1.1	0.9
High	5.7	0.3	0.9	1.3	2.4	2.8	0.3	0.9
All	3.4	0.7	0.9	1.1	1.8	2.0	0.7	0.9

Table 4.2.1.5 Free-field Total Aircraft Centerline Noise RMS Error Table, dB

Emission Angle Frequencies	30°	50°	70°	90°	110°	130°	150°	170°
Low	0.1	0.1	0.1	0.1	0.3	0.0	0.1	0.1
Mid	0.5	0.8	0.4	0.1	0.3	0.3	0.8	0.4
High	1.7	1.8	1.6	2.5	3.0	3.1	1.8	1.6
All	1.0	1.1	1.0	1.5	1.8	1.8	1.1	1.0

Table 4.2.1.6 Full System Total Aircraft Centerline Noise RMS Error Table. dB

Emission Angle Frequencies	30°	50°	70°	90°	110°	130°	150°	170°
Low	1.2	1.3	2.1	1.3	1.3	2.2	1.3	2.1
Mid	1.0	0.8	0.6	0.6	0.6	0.7	0.8	0.6
High	0.9	0.8	1.3	1.8	2.0	1.8	0.8	1.3
All	1.0	1.0	1.5	1.3	1.4	1.7	1.0	1.5

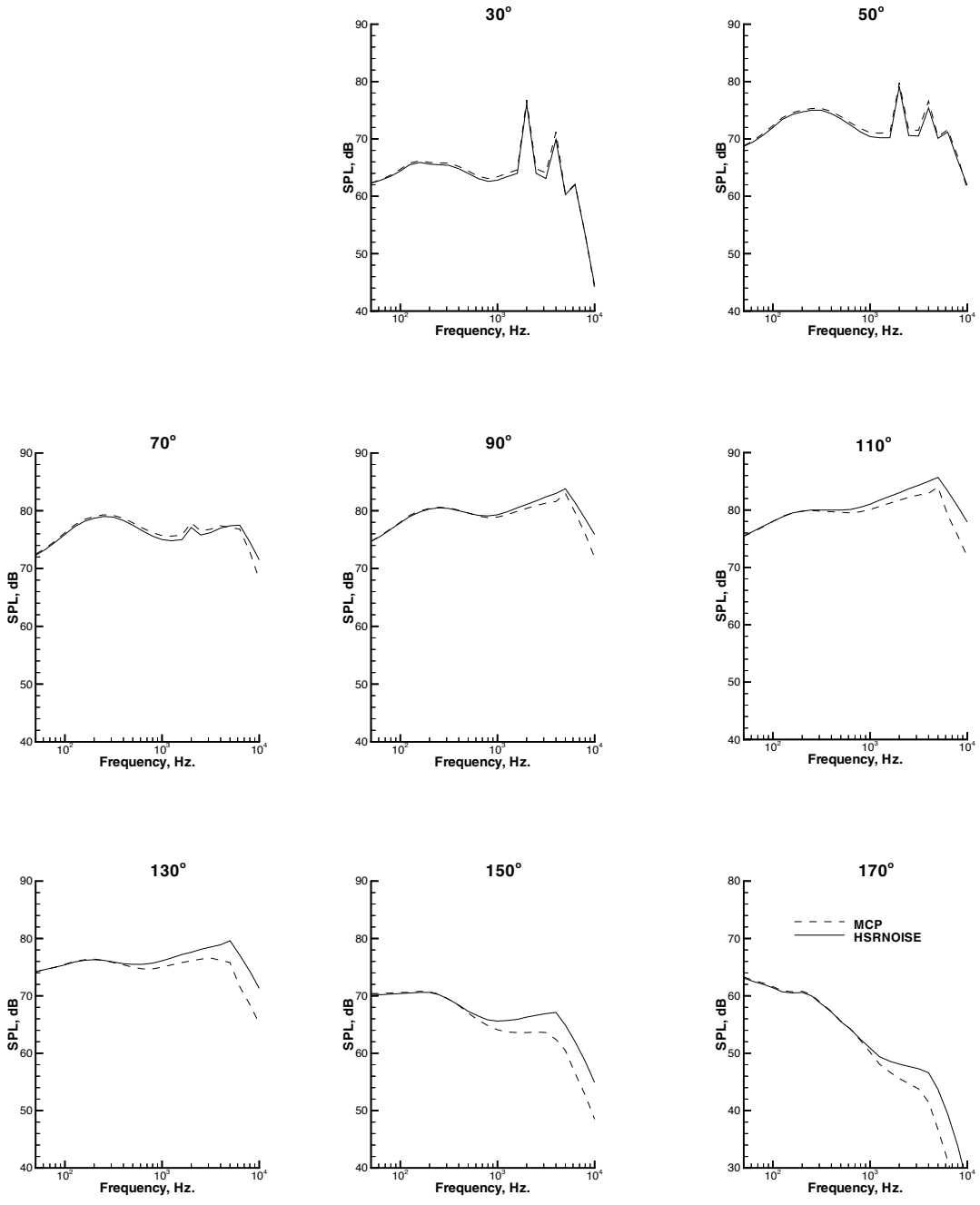

Figure 4.2.1.1 Approach total aircraft noise spectra for the TC aircraft (Free-field - Single Engine - No Deltas)

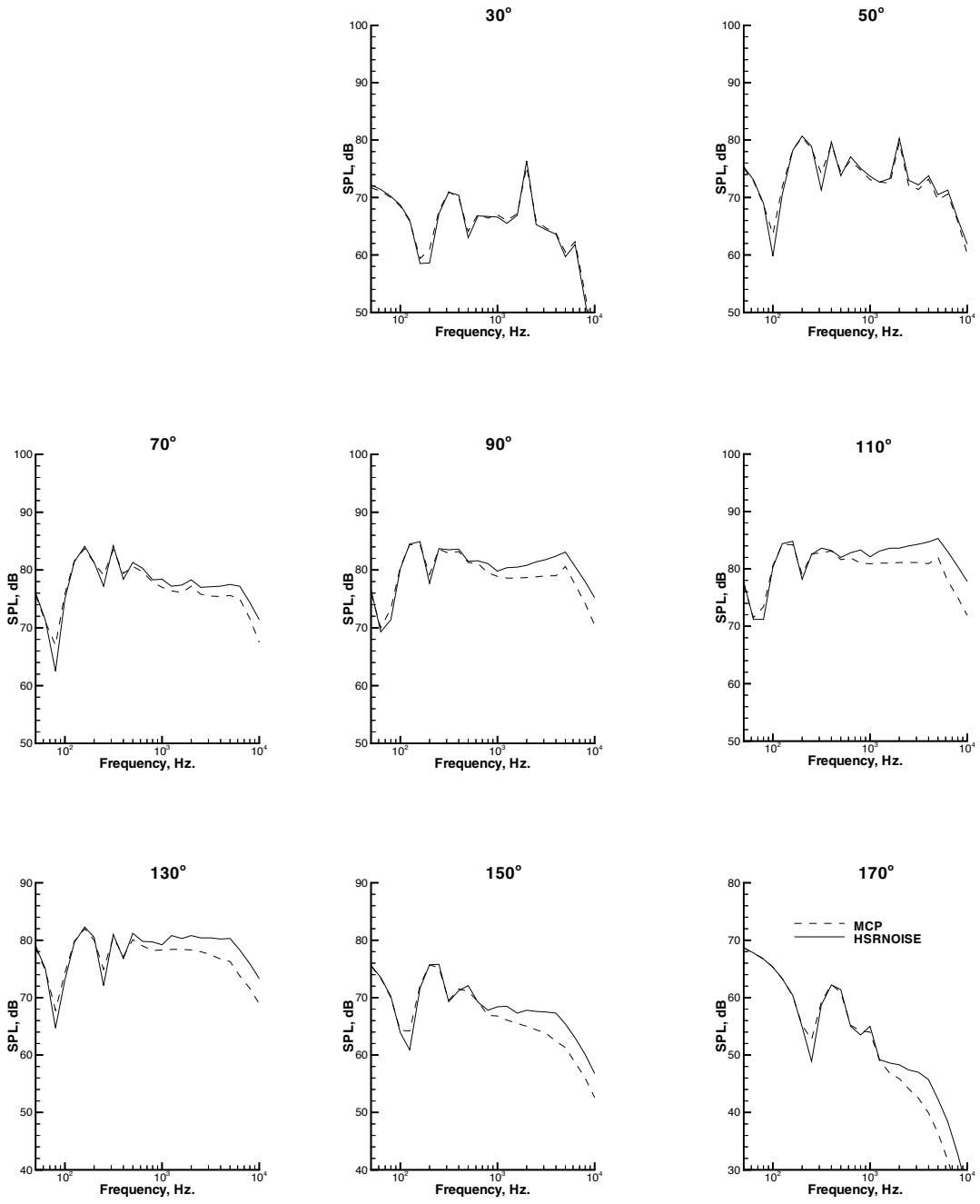

Figure 4.2.1.2 Approach total aircraft noise spectra for the TC aircraft (Full System)

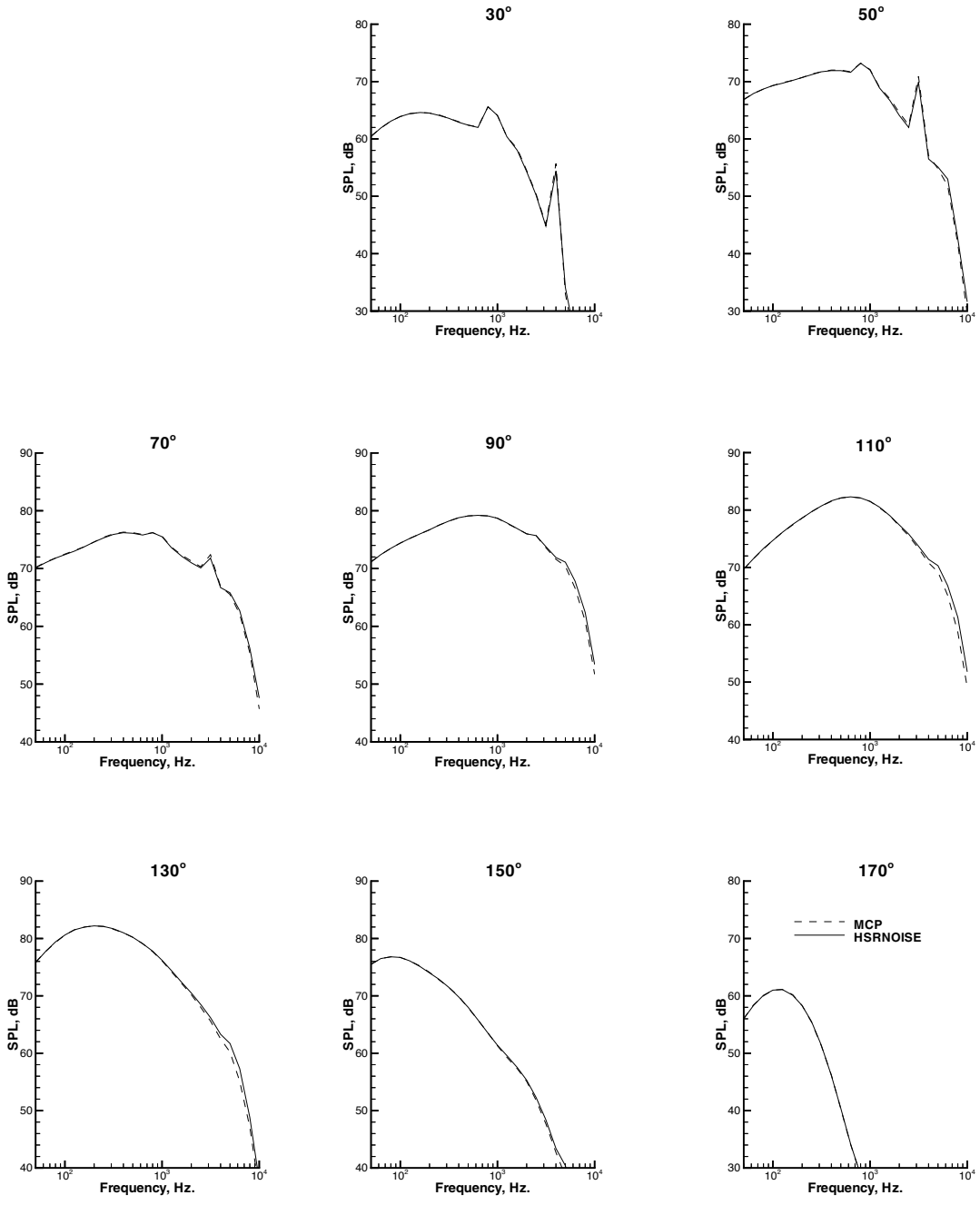

Figure 4.2.1.3 Sideline total aircraft noise spectra for the TC aircraft
(Free-field - Single Engine - No Deltas)

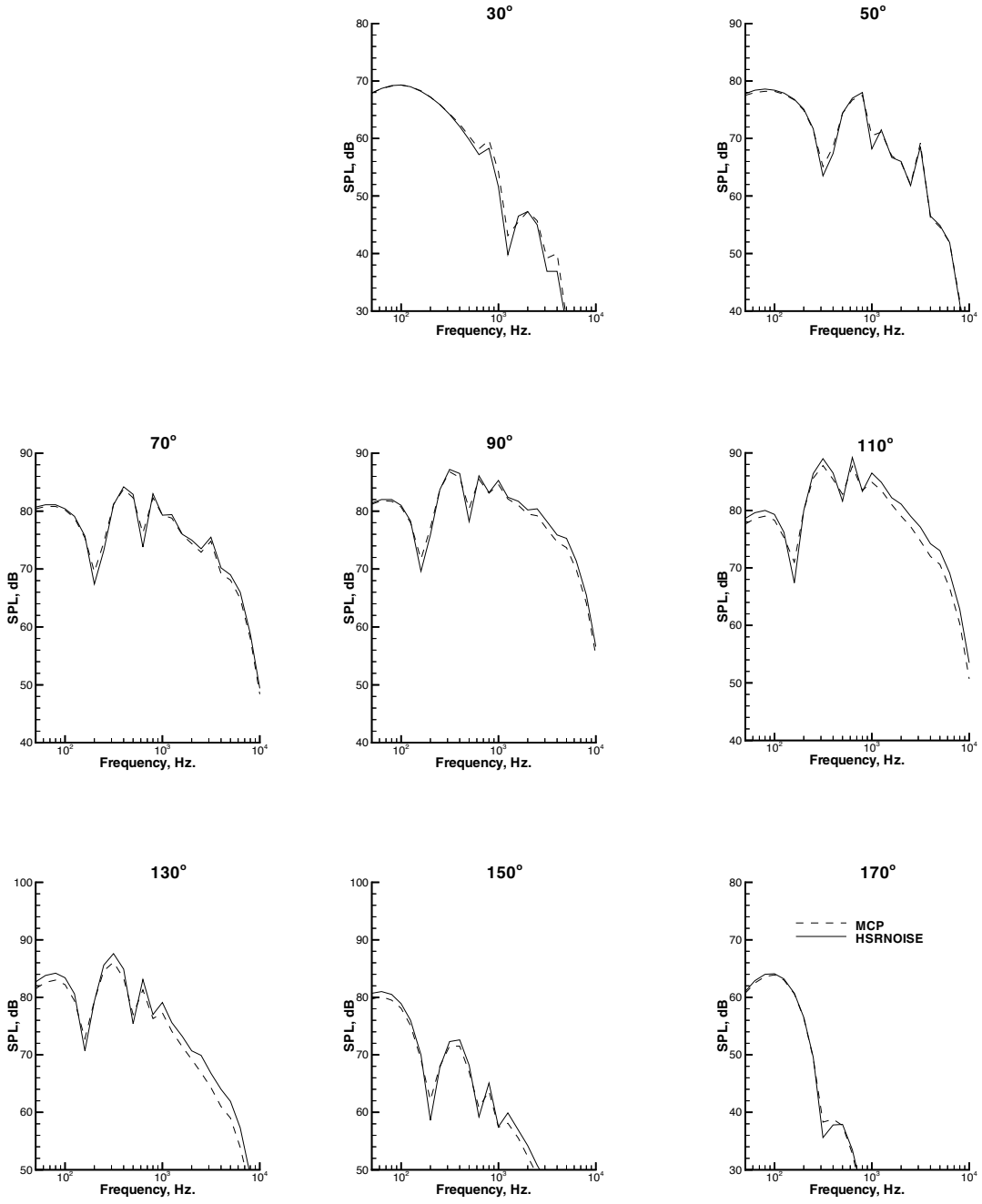

Figure 4.2.1.4 Sideline total aircraft noise spectra for the TC aircraft (Full System)

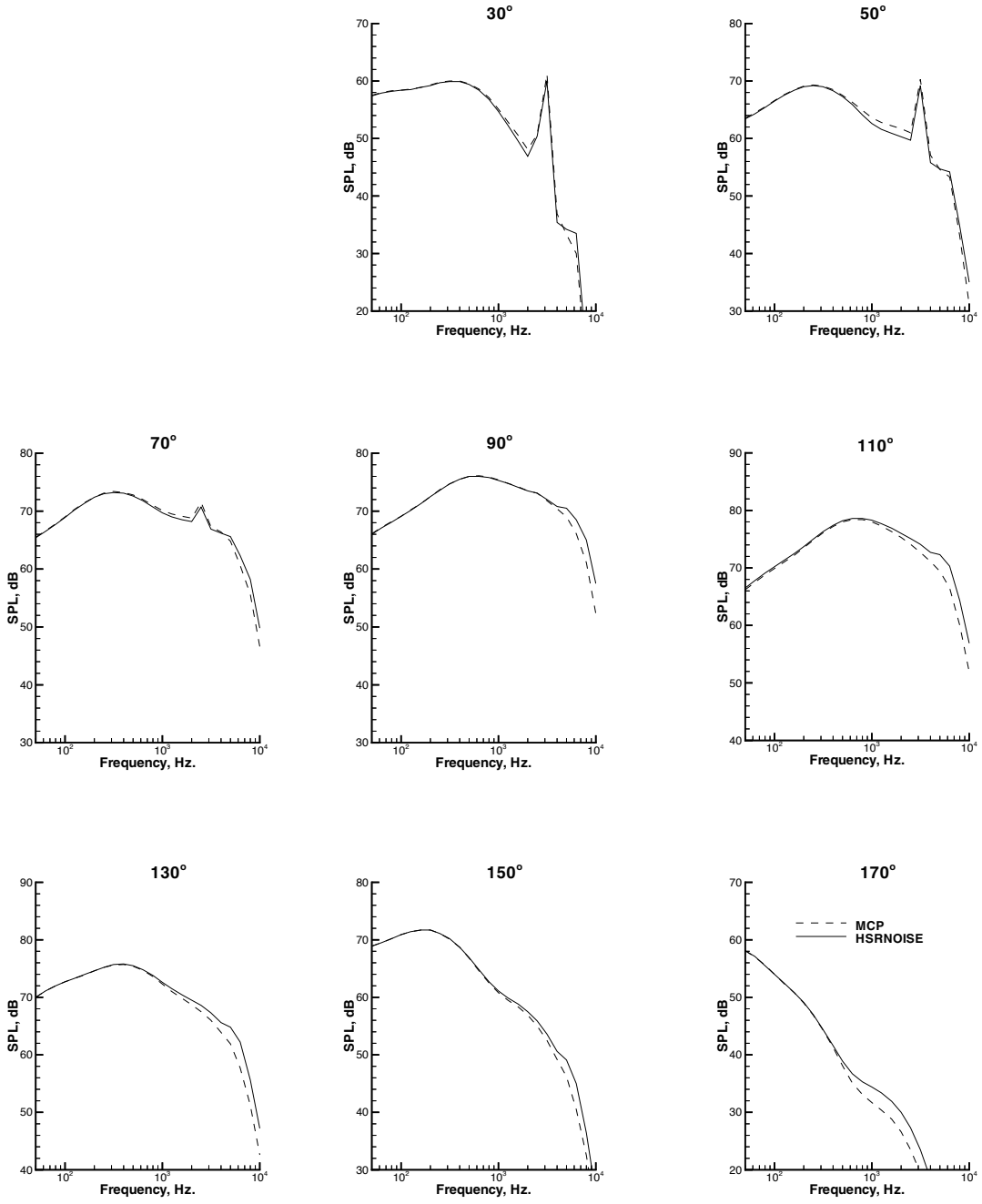

Figure 4.2.1.5 Centerline total aircraft noise spectra for the TC aircraft
(Free-field - Single Engine - No Deltas)

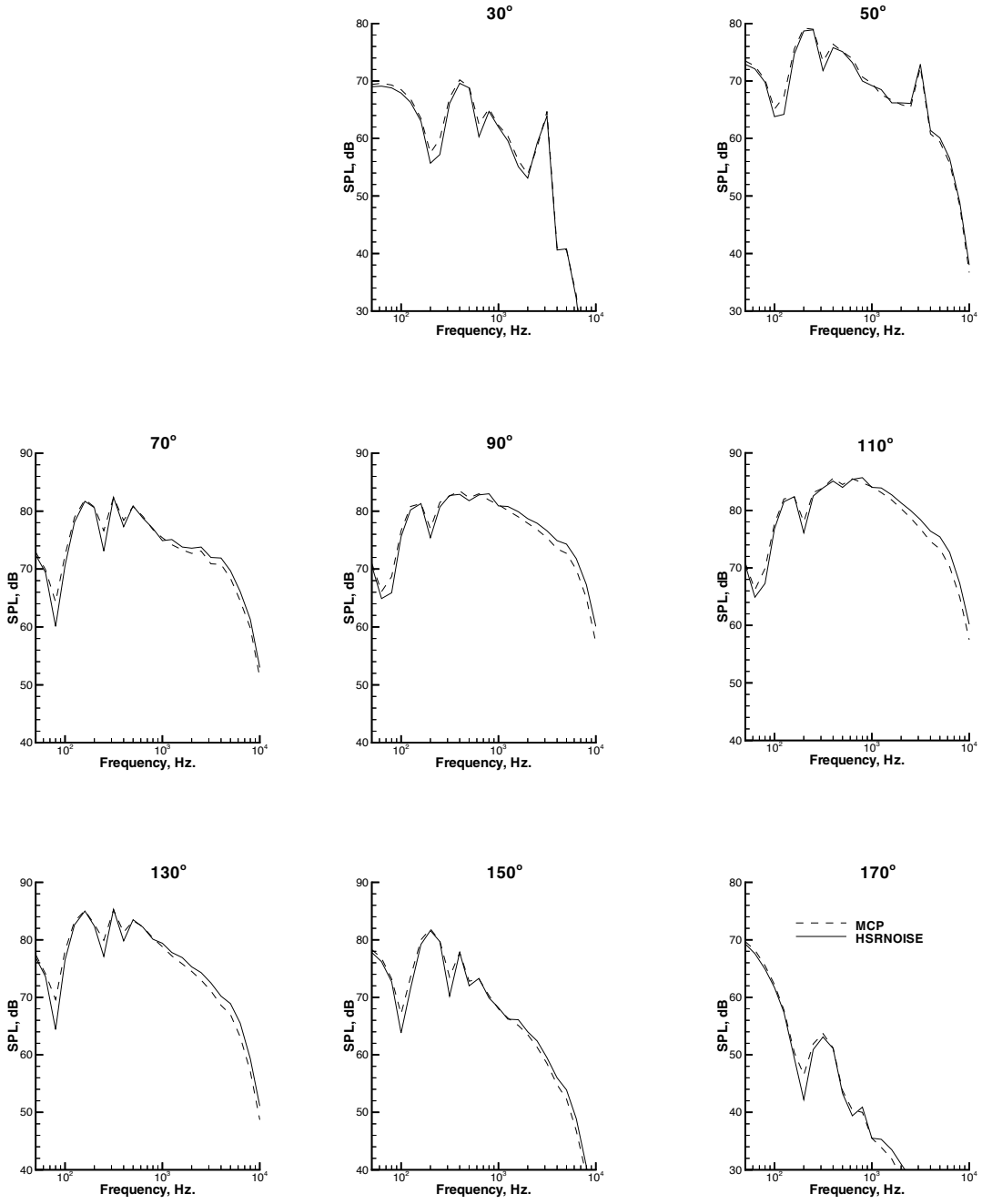

Figure 4.2.1.6 Centerline total aircraft noise spectra for the TC aircraft (Full System)

4.2.2 Jet Noise

Jet noise dominated the spectra for the sideline and centerline cases. Figures 4.2.2.1, 4.2.2.3, and 4.2.2.5 show the free-field one-third-octave band spectra for the approach, sideline, and centerline cases. Figures 4.2.2.2, 4.2.2.4, and 4.2.2.6 show the full system predictions. RMS error values are provided in tables 4.2.2.1 through 4.2.2.6. Comparisons of the free-field spectra were excellent for all frequency ranges. Comparisons of the full system spectra were good to fair in the low frequency range, fair to poor in the mid frequency range, and generally poor in the high frequency range.

The approach and centerline predictions provide insight into the cause of the discrepancies between the HSRNOISE and MCP predictions. The free-field and full system predictions differ only by the execution of the ground reflection model. HSRNOISE uses the Chien and Soroka ground reflection model while MCP uses the Shivashankara model. Although the locations of the ground dips between the two methods match very well, SPL differences as large as 4 dB were noted at frequencies corresponding to the ground dips. The ground flow resistance parameter was adjusted in an attempt to reduce the discrepancies. The default of SIGMA= 1.1×10^6 lbm/sec-ft^3 provided the best comparison.

In addition to differences in SPL levels at the ground dips, the Shivashankara model attenuates high frequencies more than the Chien and Soroka model. In general, differences on the order of 2 dB were noted at all directivity angles for frequencies greater than 1000 Hertz. Since the PNLT noise metric weights the high frequency spectra, the HSRNOISE code would be expected to predict higher EPNL levels than the MCP code.

The full system sideline predictions include extra ground attenuation (EGA) and jet shielding in addition to ground reflections. The methods used to predict EGA and jet shielding are identical to those used in MCP. Differences in the SPL are consistent with those for the approach and sideline cases.

It should be noted that the jet noise was predicted using the Boeing JN8C4 methodology. Comparisons were not made using Stone's jet noise methodology because it was a last minute addition to the HSRNOISE code.

Table 4.2.2.1 Free-field Approach Jet Noise RMS Error Table, dB

Emission Angle Frequencies	30°	50°	70°	90°	110°	130°	150°	170°
Low	0.1	0.1	0.2	0.2	0.2	0.2	0.1	0.2
Mid	0.2	0.3	0.3	0.3	0.3	0.3	0.3	0.3
High	0.3	0.3	0.3	0.3	0.3	0.3	0.3	0.3
All	0.2	0.2	0.2	0.2	0.3	0.3	0.2	0.2

Table 4.2.2.2 Full System Approach Jet Noise RMS Error Table, dB

Emission Angle Frequencies	30°	50°	70°	90°	110°	130°	150°	170°
Low	0.8	1.3	1.6	0.9	0.8	1.5	1.3	1.6
Mid	0.6	1.3	1.4	1.3	1.4	1.2	1.3	1.4
High	1.7	2.1	2.2	2.3	2.3	2.2	2.1	2.2
All	1.1	1.6	1.8	1.6	1.6	1.7	1.6	1.8

Table 4.2.2.3 Free-field Sideline Jet Noise RMS Error Table, dB

Emission Angle Frequencies	30°	50°	70°	90°	110°	130°	150°	170°
Low	0.0	0.0	0.0	0.0	0.1	0.0	0.0	0.0
Mid	0.1	0.0	0.0	0.1	0.0	0.1	0.0	0.0
High	0.2	0.1	0.1	0.1	0.1	0.1	0.1	0.1
All	0.1	0.1	0.1	0.1	0.1	0.1	0.1	0.1

Table 4.2.2.4 Full System Sideline Jet Noise RMS Error Table, dB

Emission Angle Frequencies	30°	50°	70°	90°	110°	130°	150°	170°
Low	0.1	0.3	0.9	0.9	1.5	1.3	0.3	0.9
Mid	1.7	1.1	1.0	0.9	1.2	1.5	1.1	1.0
High	1.9	0.5	1.0	1.3	2.1	2.3	0.5	1.0
All	1.5	0.7	1.0	1.1	1.7	1.7	0.7	1.0

Table 4.2.2.5 Free-field Centerline Jet Noise RMS Error Table, dB

Emission Angle Frequencies	30°	50°	70°	90°	110°	130°	150°	170°
Low	0.0	0.0	0.0	0.0	0.1	0.0	0.0	0.0
Mid	0.1	0.0	0.0	0.1	0.0	0.0	0.0	0.0
High	0.3	0.1	0.1	0.1	0.1	0.1	0.1	0.1
All	0.2	0.1	0.1	0.1	0.1	0.1	0.1	0.1

Table 4.2.2.6 Full System Centerline Jet Noise RMS Error Table, dB

Emission Angle Frequencies	30°	50°	70°	90°	110°	130°	150°	170°
Low	0.1	0.3	0.9	0.9	1.5	1.3	0.3	0.9
Mid	1.7	1.1	1.0	0.9	1.2	1.5	1.1	1.0
High	1.9	0.5	1.0	1.3	2.1	2.3	0.5	1.0
All	1.5	0.7	1.0	1.1	1.7	1.7	0.7	1.0

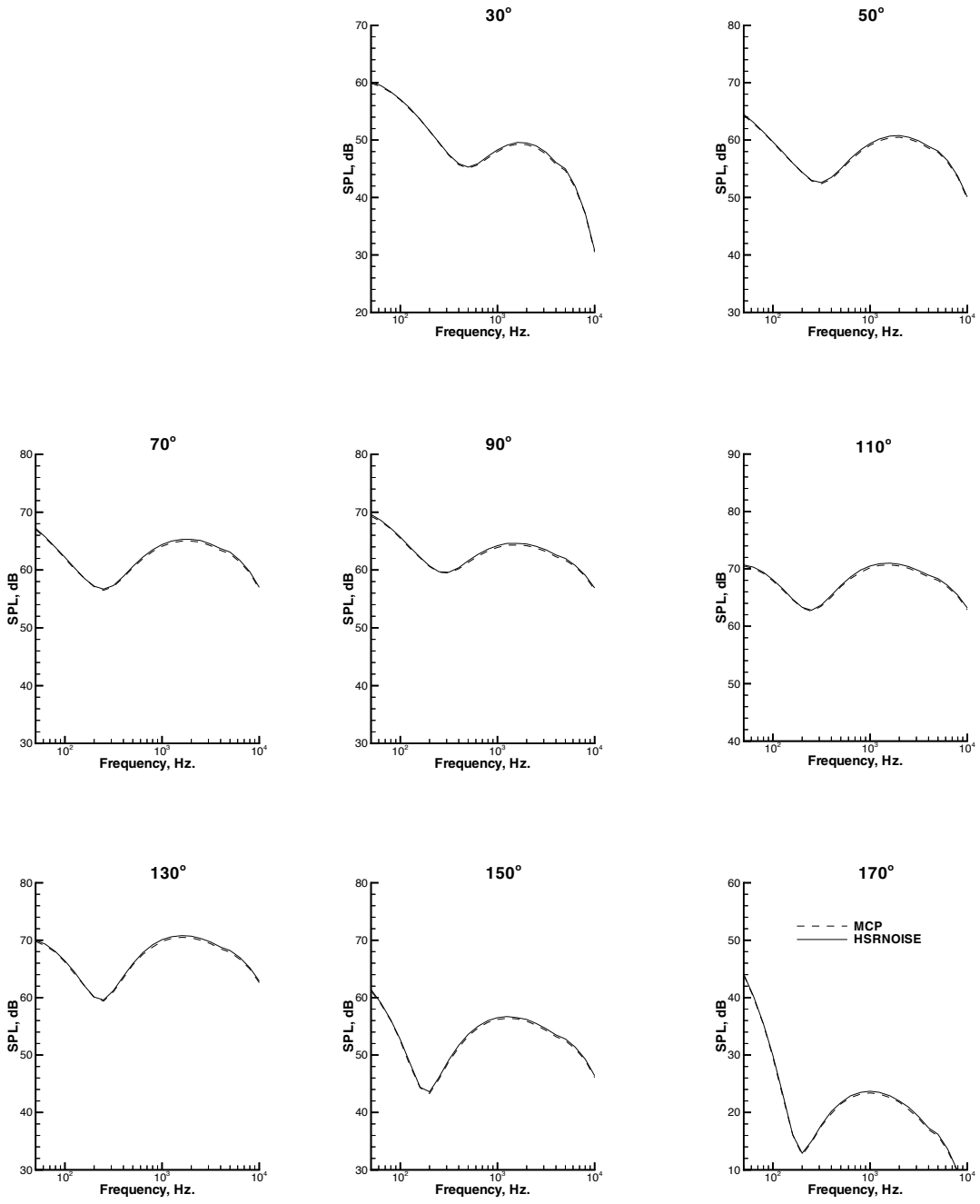

Figure 4.2.2.1 Approach jet noise spectra for the TC aircraft
(Free-field - Single Engine - No Deltas)

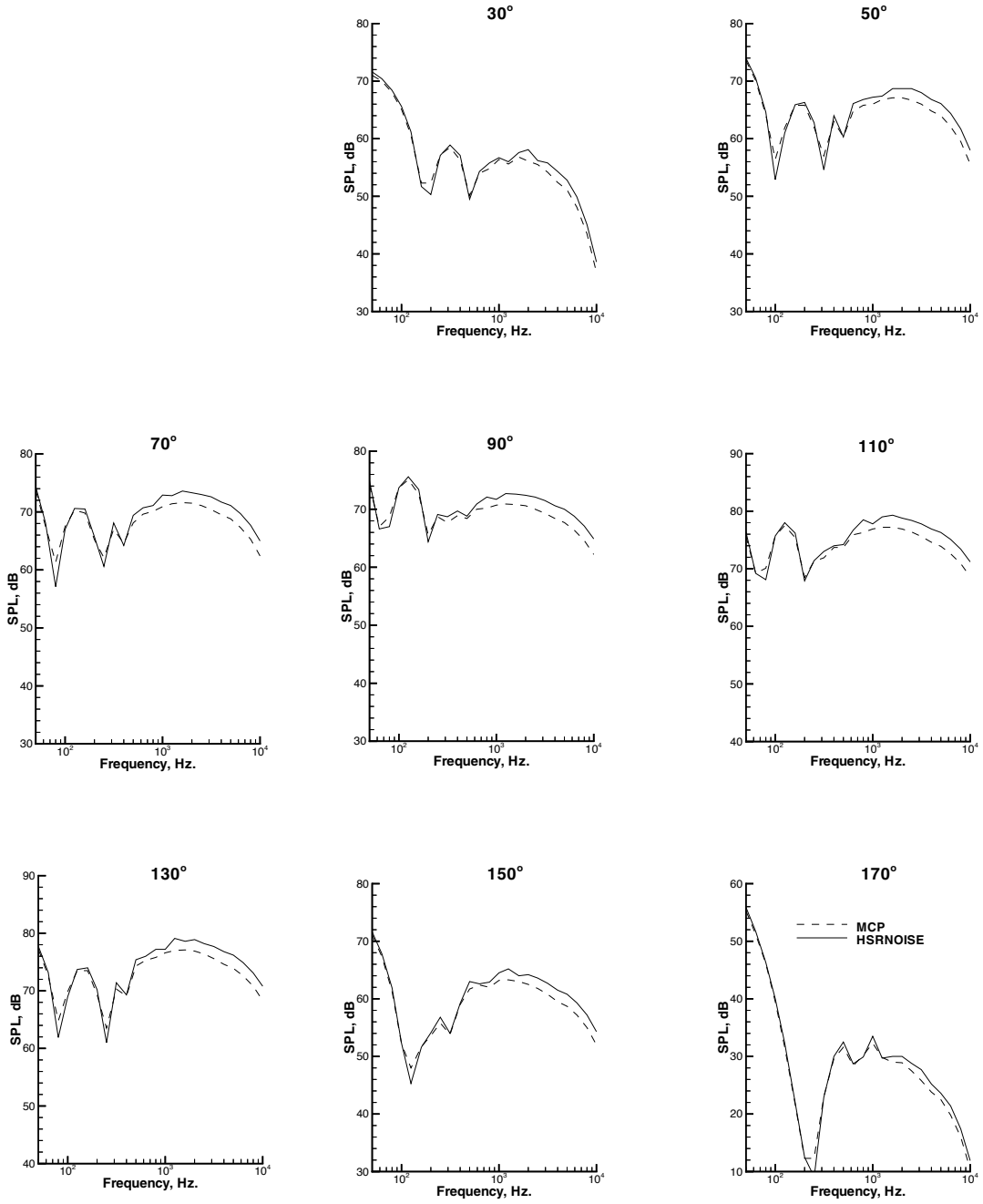

Figure 4.2.2.2 Approach jet noise spectra for the TC aircraft (Full System)

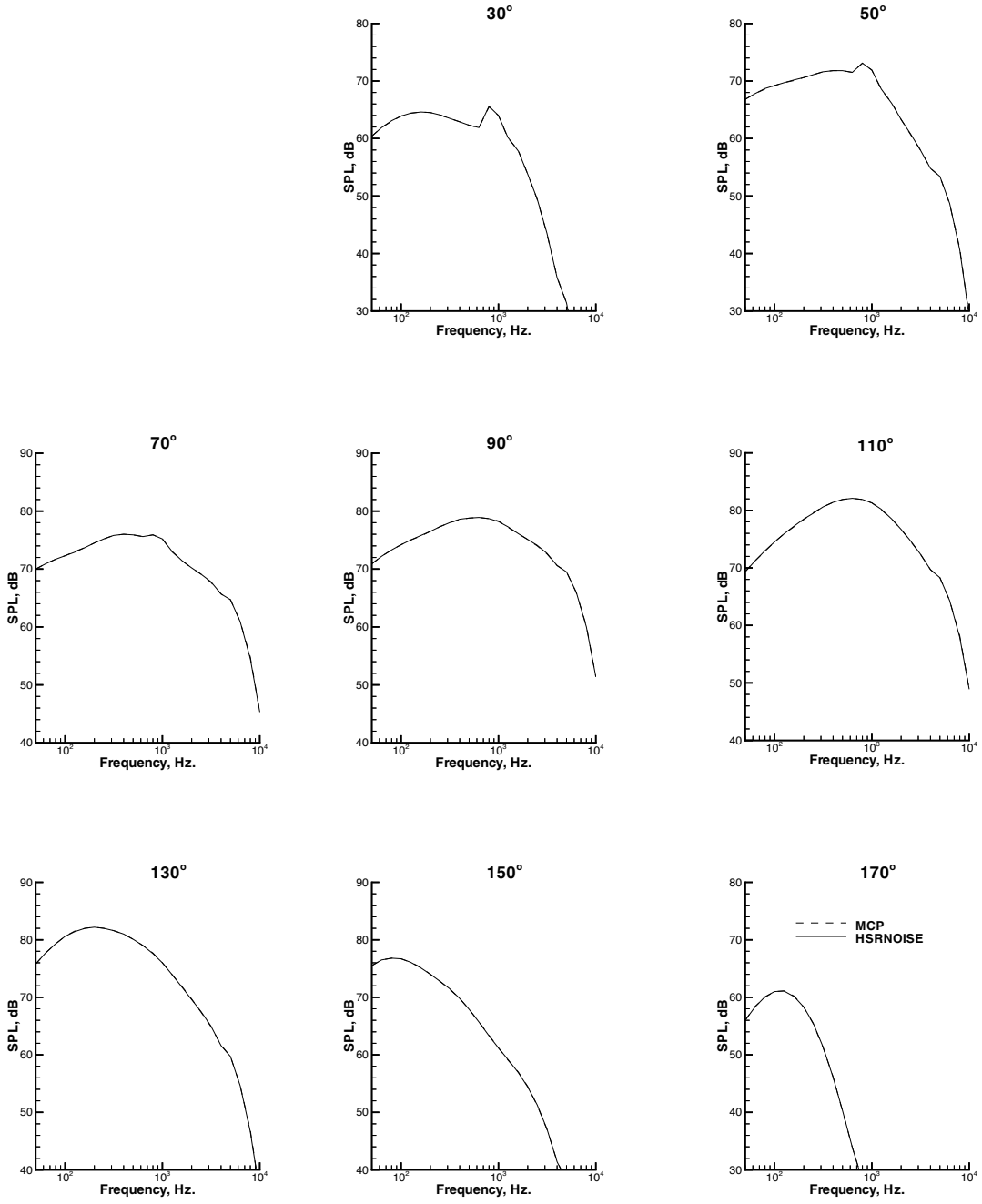

Figure 4.2.2.3 Sideline jet noise spectra for the TC aircraft
(Free-field - Single Engine - No Deltas)

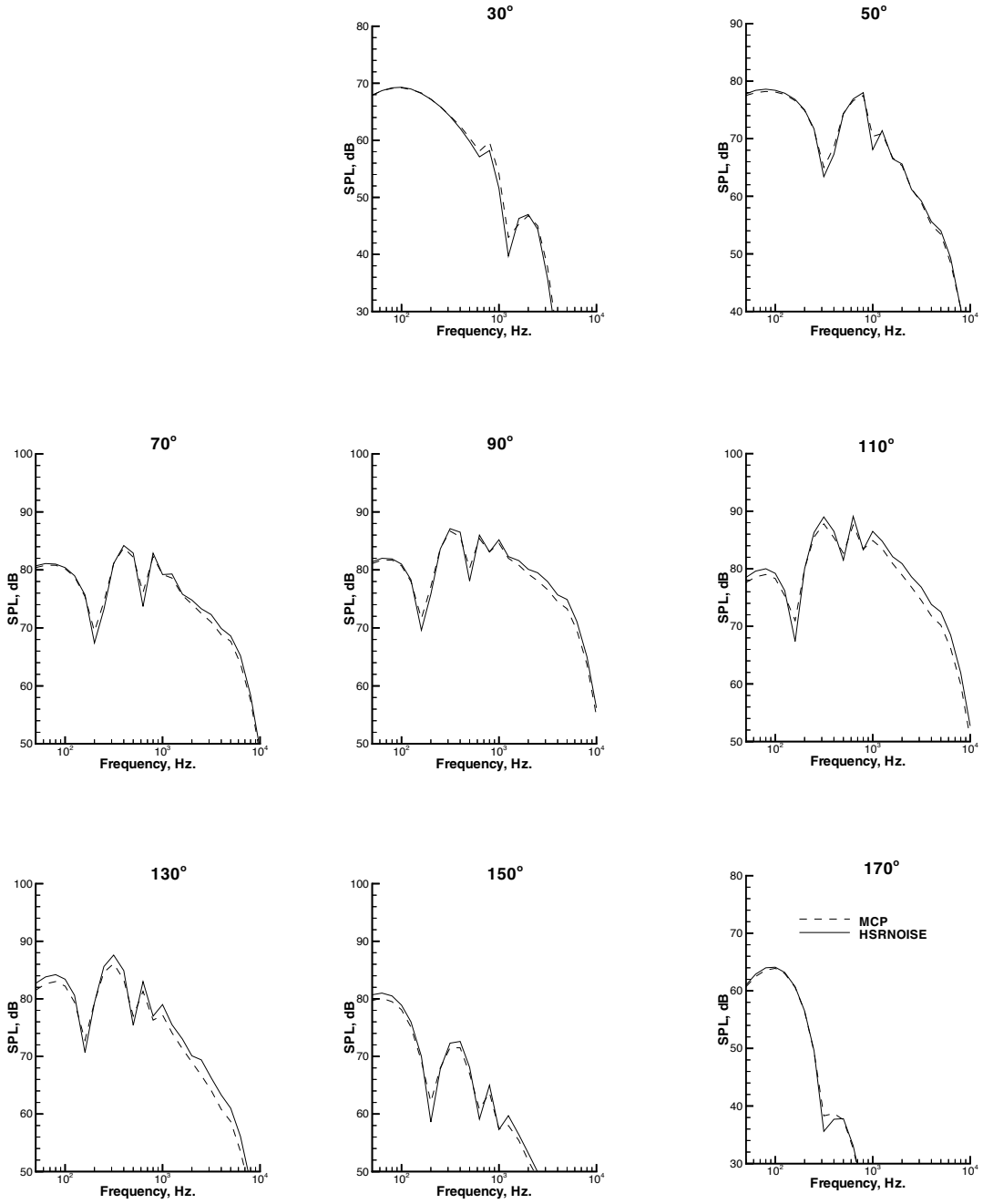

Figure 4.2.2.4 Sideline jet noise spectra for the TC aircraft
(Full System)

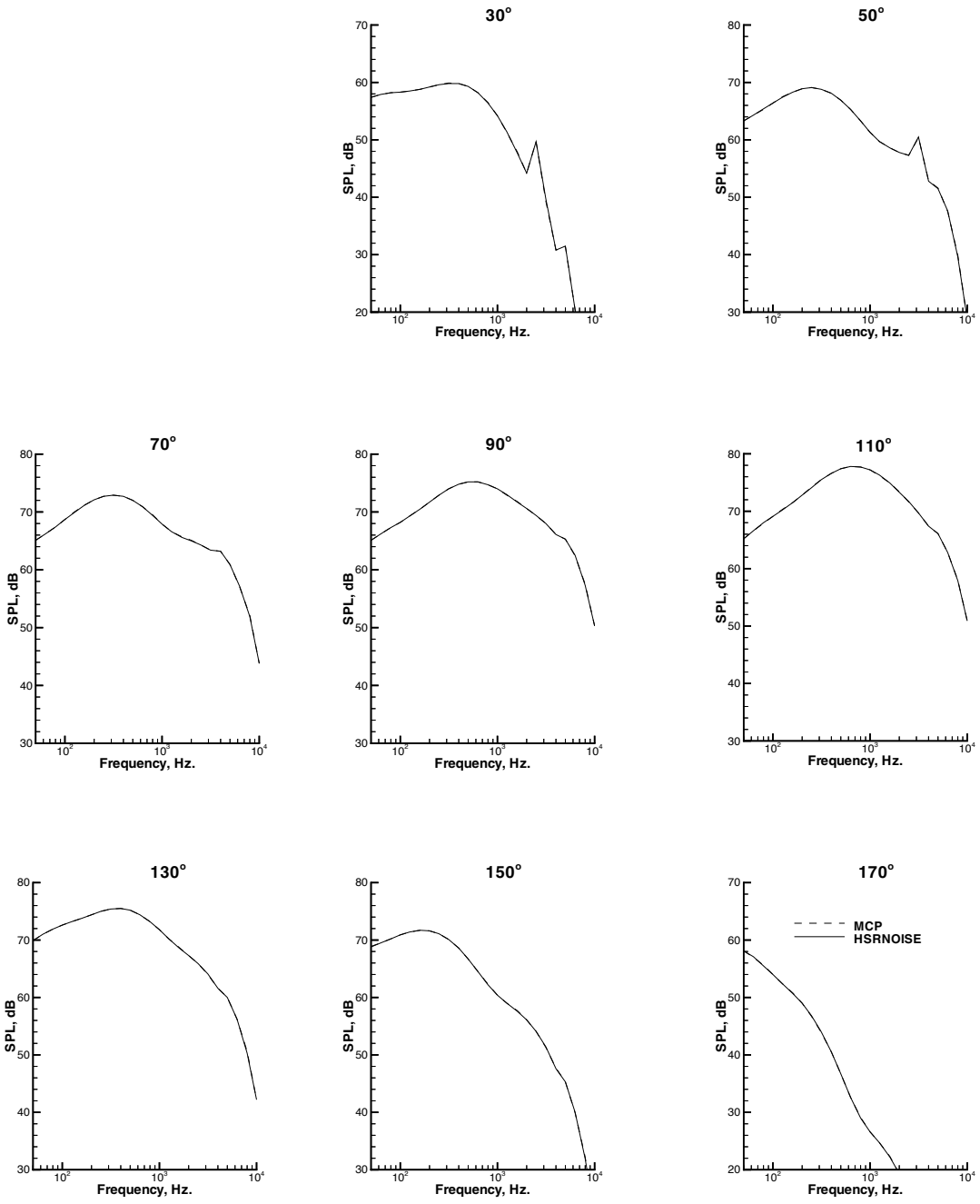

Figure 4.2.2.5 Centerline jet noise spectra for the TC aircraft
(Free-field - Single Engine - No Deltas)

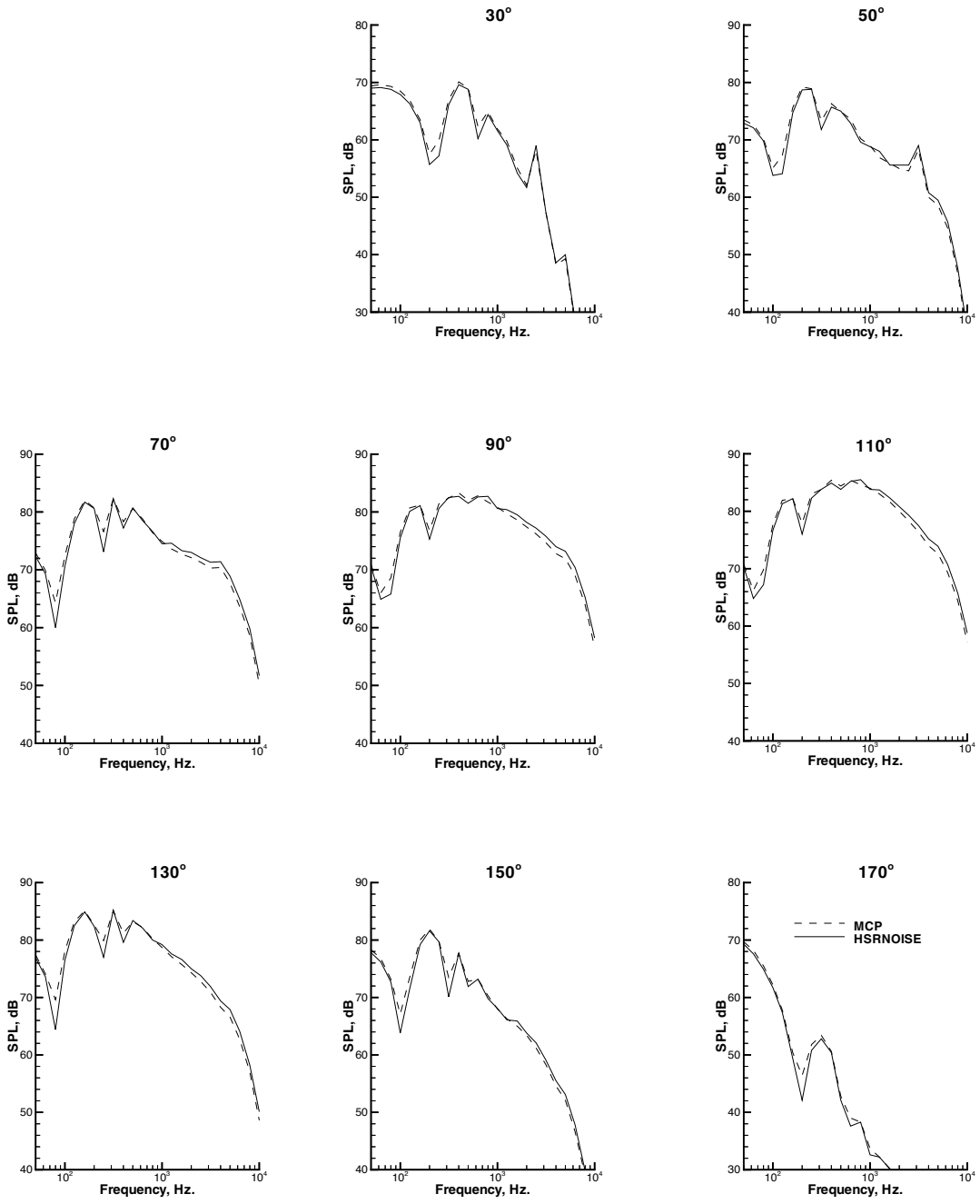

Figure 4.2.2.6 Centerline jet noise spectra for the TC aircraft (Full System)

4.2.3 Turbine Noise

Turbine noise dominated the high frequency spectra during approach for emission angles greater than 90 degrees. Figures 4.2.3.1, 4.2.3.3, and 4.2.3.5 show the free-field one-third-octave band spectra for the approach, sideline, and centerline cases. Figures 4.2.3.2, 4.2.3.4, and 4.2.3.6 show the full system predictions. RMS error values are provided in tables 4.2.3.1 through 4.2.3.6. These spectra (both free-field and full system) were rated as poor for all frequency ranges.

Following discussions with engineers at Boeing, three causes for the discrepancies in the turbine predictions were identified. First, convective amplification was accounted for twice in the MCP turbine module. This causes the MCP spectra to be high for angles less than 90 degrees and low for angles greater than 90 degrees. Second, the emission angle rather than the Doppler angle was used to Doppler shift the MCP turbine spectra. Finally, the algorithm used to predict the turbine noise required a correction to remove atmospheric attenuation built into the method. This correction was discovered too late in the HSR program to be incorporated into the MCP predictions.

Spectral differences between 3 and 9 dB were noted in the high frequency range of the full system turbine spectra. Implementation differences identified in the free-field predictions combined with the differences noted in the ground reflection model discussed in the section 4.2.2 caused the EPNL levels predicted by HSRNOISE to be 3 EPNdB higher than the levels predicted by MCP.

Table 4.2.3.1 Free-field Approach Turbine Noise RMS Error Table, dB

Emission Angle / Frequencies	30°	50°	70°	90°	110°	130°	150°	170°
Low	1.6	1.3	0.8	1.0	0.3	0.4	1.3	0.8
Mid	1.8	1.5	0.9	1.2	0.5	0.3	1.5	0.9
High	3.7	3.1	3.1	2.6	3.0	3.7	3.1	3.1
All	2.6	2.1	1.9	1.8	1.8	2.2	2.1	1.9

Table 4.2.3.2 Full System Approach Turbine Noise RMS Error Table, dB

Emission Angle / Frequencies	30°	50°	70°	90°	110°	130°	150°	170°
Low	3.0	2.8	2.6	0.9	1.1	1.7	2.8	2.6
Mid	2.5	2.1	0.9	1.5	2.2	2.5	2.1	0.9
High	1.0	0.8	2.3	3.4	4.9	6.5	0.8	2.3
All	2.4	2.1	2.1	2.2	3.2	4.1	2.1	2.1

Table 4.2.3.3 Free-field Sideline Turbine Noise RMS Error Table, dB

Emission Angle / Frequencies	30°	50°	70°	90°	110°	130°	150°	170°
Low	3.6	2.8	1.8	0.1	1.0	2.8	2.8	1.8
Mid	3.5	2.7	1.7	0.3	1.2	2.9	2.7	1.7
High	5.8	4.1	3.8	4.5	6.4	8.1	4.1	3.8
All	4.4	3.3	2.6	2.6	3.8	5.2	3.3	2.6

Table 4.2.3.4 Full System Sideline Turbine Noise RMS Error Table, dB

Emission Angle / Frequencies	30°	50°	70°	90°	110°	130°	150°	170°
Low	3.6	2.6	2.2	0.8	1.9	3.5	2.6	2.2
Mid	4.7	3.4	1.9	1.1	2.2	4.1	3.4	1.9
High	12.6	1.5	1.5	3.1	5.6	7.2	1.5	1.5
All	8.0	2.6	1.9	1.9	3.6	5.2	2.6	1.9

Table 4.2.3.5 Free-field Centerline Turbine Noise RMS Error Table, dB

Emission Angle / Frequencies	30°	50°	70°	90°	110°	130°	150°	170°
Low	4.4	3.5	1.5	0.4	1.5	2.2	3.5	1.5
Mid	4.3	3.4	1.3	0.3	1.6	2.4	3.4	1.3
High	5.1	3.5	2.7	4.0	5.4	7.6	3.5	2.7
All	4.6	3.4	1.9	2.3	3.4	4.8	3.4	1.9

Table 4.2.3.6 Full System Centerline Turbine Noise RMS Error Table, dB

Emission Angle / Frequencies	30°	50°	70°	90°	110°	130°	150°	170°
Low	4.6	3.8	2.6	1.1	1.4	2.2	3.8	2.6
Mid	4.2	3.0	0.8	1.0	2.6	3.3	3.0	0.8
High	5.0	1.2	1.9	3.7	5.4	7.2	1.2	1.9
All	4.6	2.9	1.9	2.3	3.6	4.8	2.9	1.9

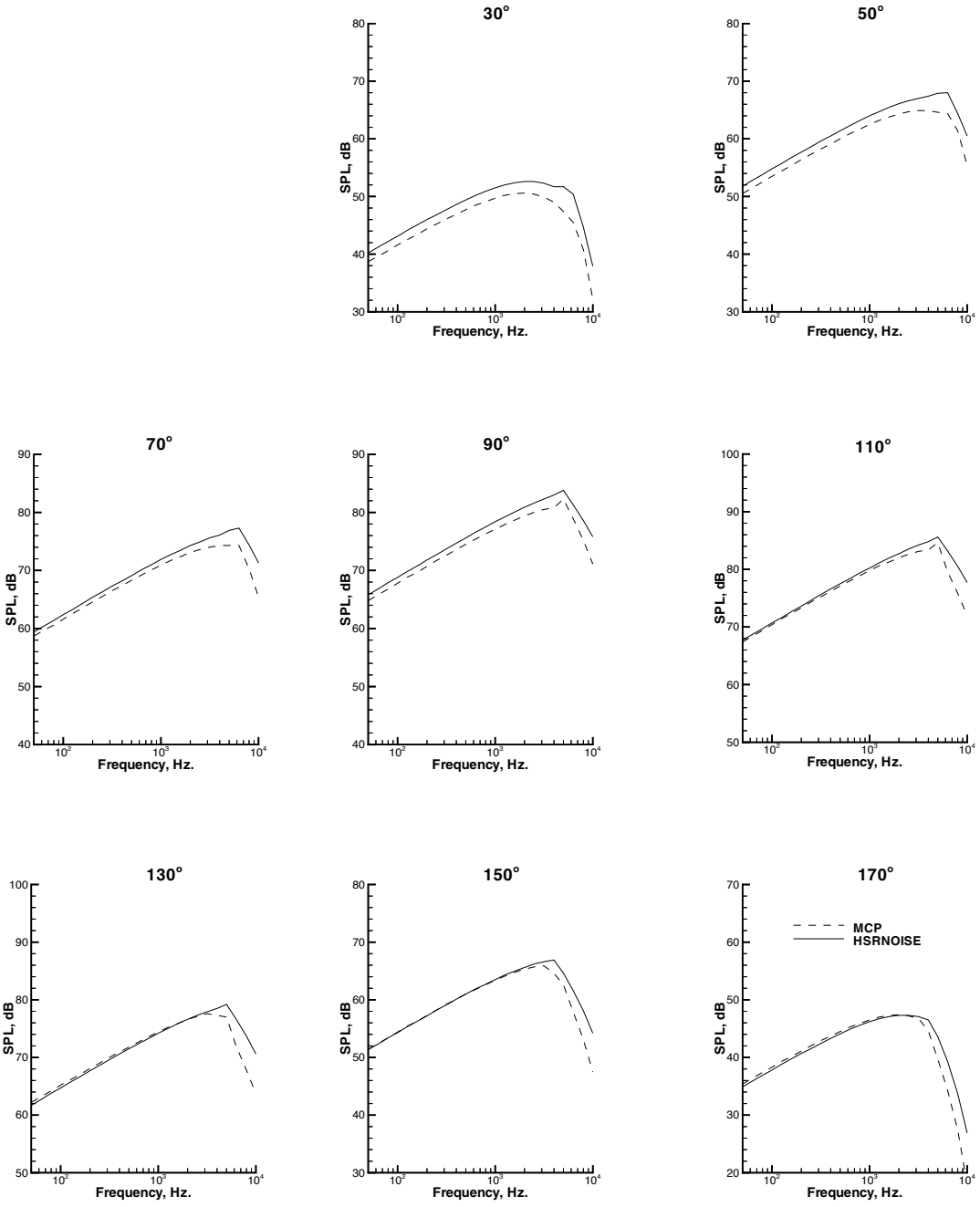

Figure 4.2.3.1 Approach turbine noise spectra for the TC aircraft
(Free-field - Single Engine - No Deltas)

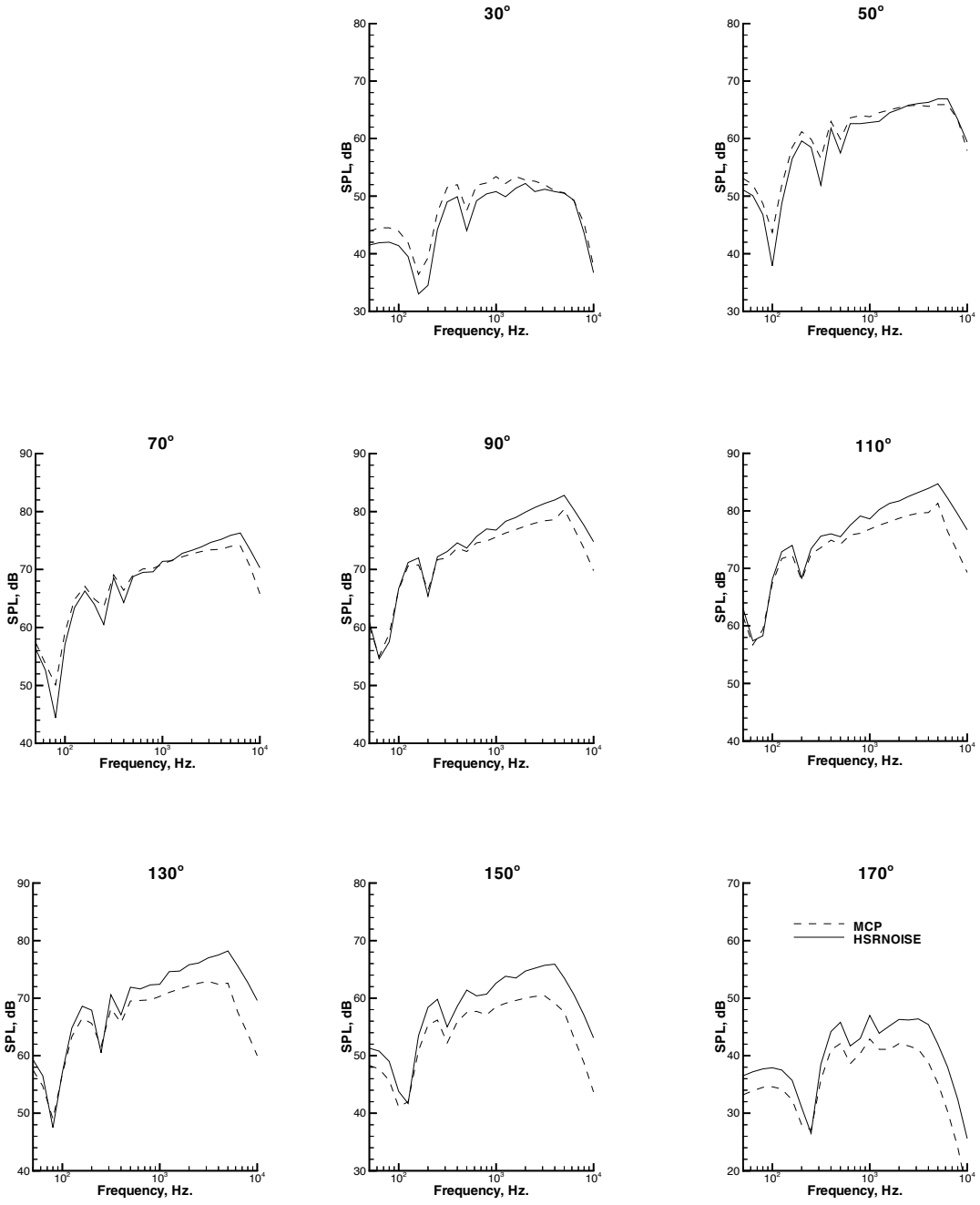

Figure 4.2.3.2 Approach turbine noise spectra for the TC aircraft (Full System)

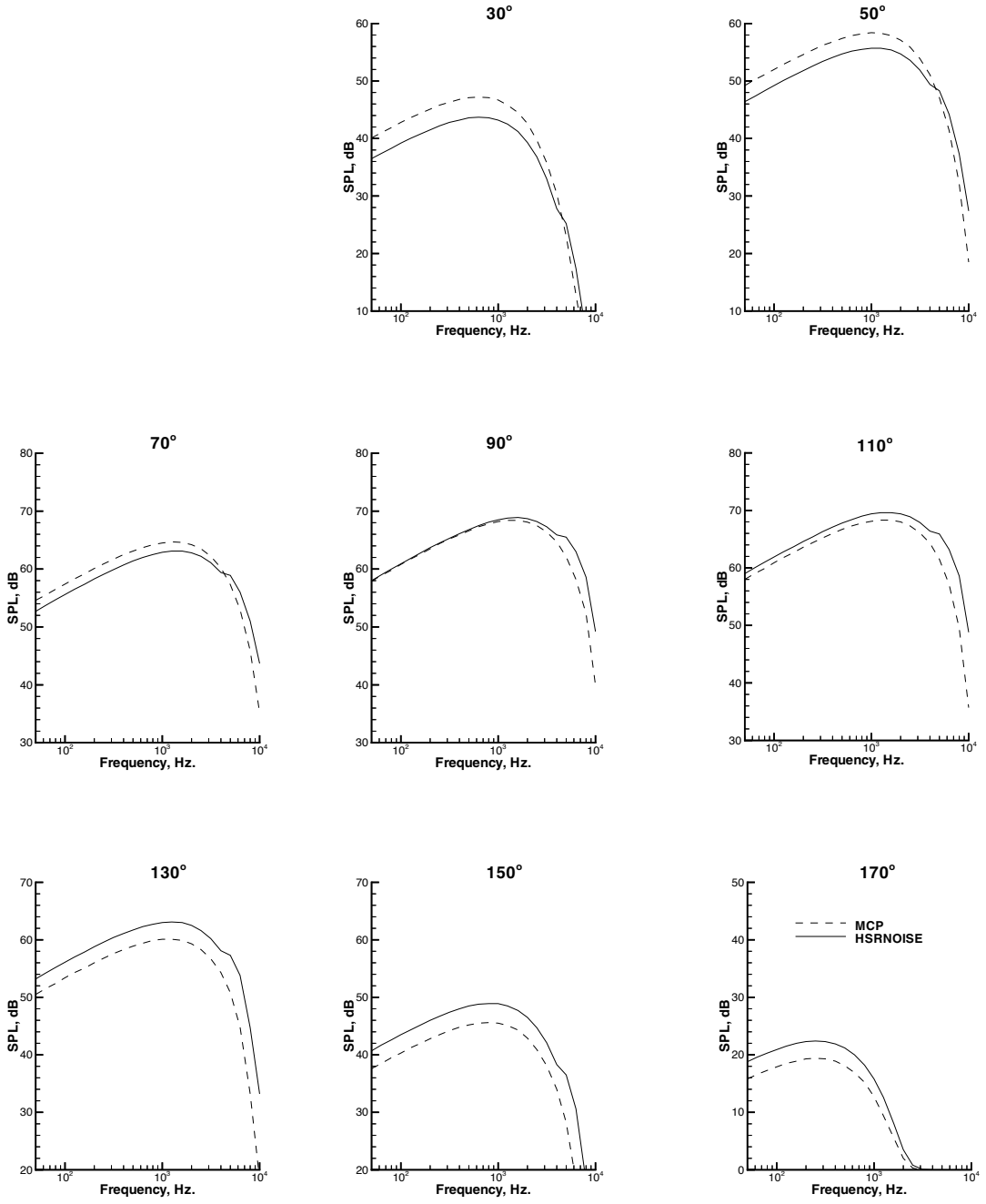

Figure 4.2.3.3 Sideline turbine noise spectra for the TC aircraft
(Free-field - Single Engine - No Deltas)

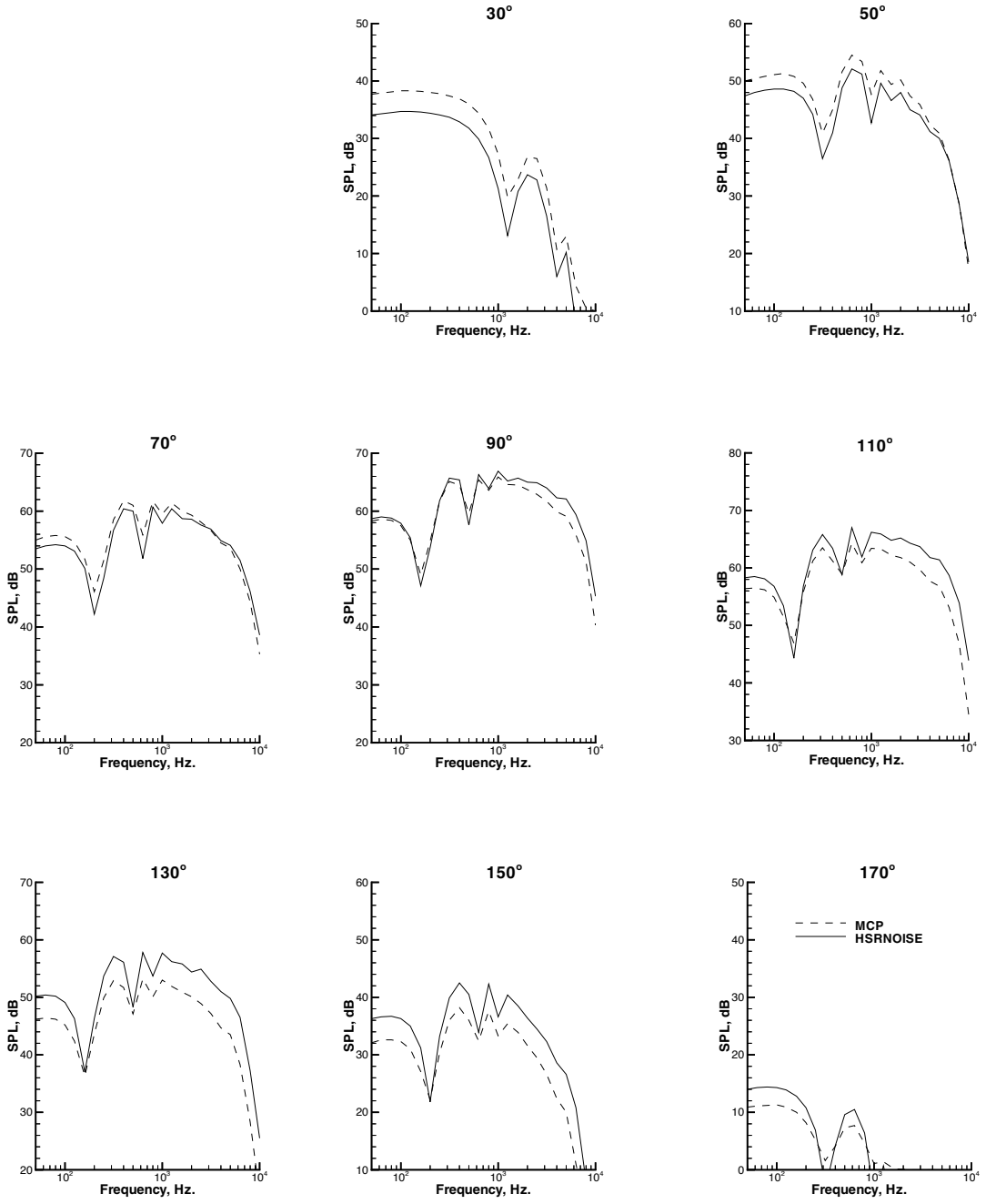

Figure 4.2.3.4 Sideline turbine noise spectra for the TC aircraft (Full System)

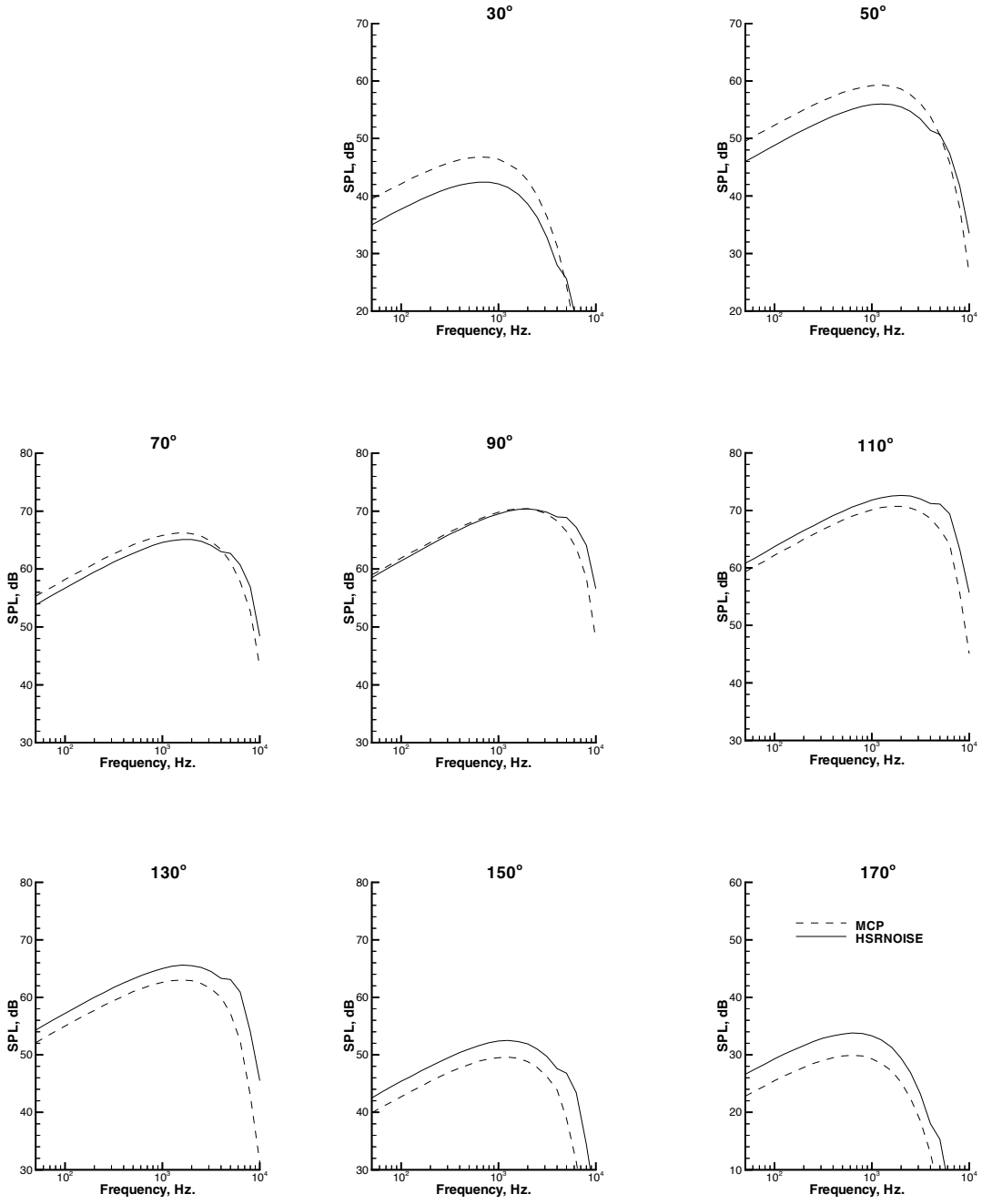

Figure 4.2.3.5 Centerline turbine noise spectra for the TC aircraft
(Free-field - Single Engine - No Deltas)

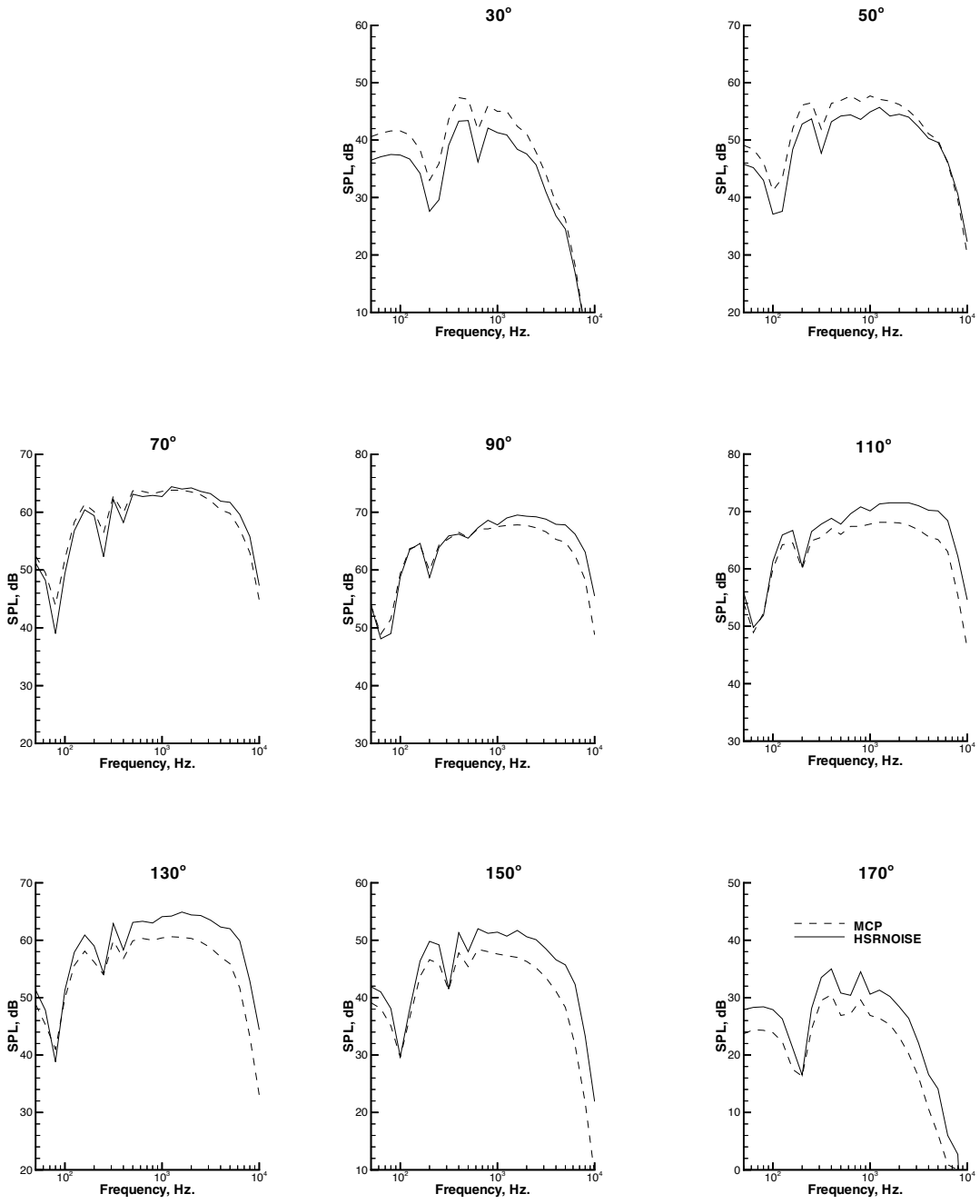

Figure 4.2.3.6 Centerline turbine noise spectra for the TC aircraft (Full System)

4.2.4 Fan Noise

The high frequency spectrum of the fan noise component was a dominant source during approach for emission angles less than 90 degrees. Figures 4.2.4.1, 4.2.4.3, and 4.2.4.5 show the free-field one-third-octave band spectra for the approach, sideline, and centerline cases. Figures 4.2.4.2, 4.2.4.4, and 4.2.4.6 show comparisons of the full system predictions. RMS error values are provided in tables 4.2.4.1 through 4.2.4.6.

Discrepancies on the order of 0.5 to 3 dB were noted in the free-field spectra. The largest discrepancies occurred in the low and high frequency ranges. Discrepancies on the order of 0.3 to 0.5 dB were noted in the mid frequency range. One implementation difference between HSRNOISE and MCP was identified. The broadband spectrum index is a function of the peak frequency. HSRNOISE uses the peak frequency as defined by equation 6 on section 3.6. MCP uses the center frequency of the one-third-octave band in which the peak frequency occurs. This implementation difference only affects the broadband component.

Discrepancies were also noted in the free-field tone levels. This discrepancy is most evident in the free-field centerline spectra (figure 4.2.4.5). At 30 degrees, the fundamental tone occurs at 4000 Hertz, and is approximately 20 dB above the broadband component. A difference of 1.5 dB was noted between the HSRNOISE and MCP predicted levels. Unfortunately, the cause of this discrepancy was not resolved.

Table 4.2.4.1 Free-field Approach Fan Noise RMS Error Table, dB

Emission Angle Frequencies	30°	50°	70°	90°	110°	130°	150°	170°
Low	0.9	0.5	0.9	1.0	1.0	1.1	0.5	0.9
Mid	0.4	0.3	0.3	0.3	0.3	0.3	0.3	0.3
High	0.7	1.1	1.3	1.3	1.3	1.3	1.1	1.3
All	0.7	0.7	0.9	0.9	1.0	1.0	0.7	0.9

Table 4.2.4.2 Full System Approach Fan Noise RMS Error Table, dB

Emission Angle Frequencies	30°	50°	70°	90°	110°	130°	150°	170°
Low	0.9	1.5	2.1	3.5	3.9	5.5	1.5	2.1
Mid	0.6	1.1	0.8	0.8	1.0	0.9	1.1	0.8
High	2.3	1.8	1.3	0.9	1.0	1.4	1.8	1.3
All	1.5	1.5	1.5	2.1	2.4	3.3	1.5	1.5

Table 4.2.4.3 Free-field Sideline Fan Noise RMS Error Table, dB

Emission Angle Frequencies	30°	50°	70°	90°	110°	130°	150°	170°
Low	1.0	0.9	1.0	0.9	0.9	1.0	0.9	1.0
Mid	0.3	0.4	0.4	0.4	0.5	0.5	0.4	0.4
High	2.9	2.0	1.3	1.2	1.1	1.5	2.0	1.3
All	1.8	1.3	0.9	0.9	0.9	1.1	1.3	0.9

Table 4.2.4.4 Full System Sideline Fan Noise RMS Error Table, dB

Emission Angle Frequencies	30°	50°	70°	90°	110°	130°	150°	170°
Low	1.3	2.0	2.0	1.8	1.9	2.7	2.0	2.0
Mid	2.1	1.5	1.1	1.2	1.3	3.5	1.5	1.1
High	6.1	2.1	1.4	1.0	1.2	3.0	2.1	1.4
All	3.8	1.9	1.5	1.4	1.5	3.1	1.9	1.5

Table 4.2.4.5 Free-field Centerline Fan Noise RMS Error Table, dB

Emission Angle Frequencies	30°	50°	70°	90°	110°	130°	150°	170°
Low	1.0	0.9	1.0	0.9	0.9	1.0	0.9	1.0
Mid	0.3	0.4	0.4	0.4	0.5	0.5	0.4	0.4
High	2.9	2.0	1.3	1.2	1.1	1.5	2.0	1.3
All	1.8	1.3	0.9	0.9	0.9	1.1	1.3	0.9

Table 4.2.4.6 Full System Centerline Fan Noise RMS Error Table, dB

Emission Angle Frequencies	30°	50°	70°	90°	110°	130°	150°	170°
Low	3.1	3.6	5.2	4.1	4.0	5.2	3.6	5.2
Mid	1.4	1.1	0.8	0.7	0.6	0.7	1.1	0.8
High	1.6	1.1	1.0	0.9	0.7	0.8	1.1	1.0
All	2.2	2.3	3.1	2.5	2.4	3.1	2.3	3.1

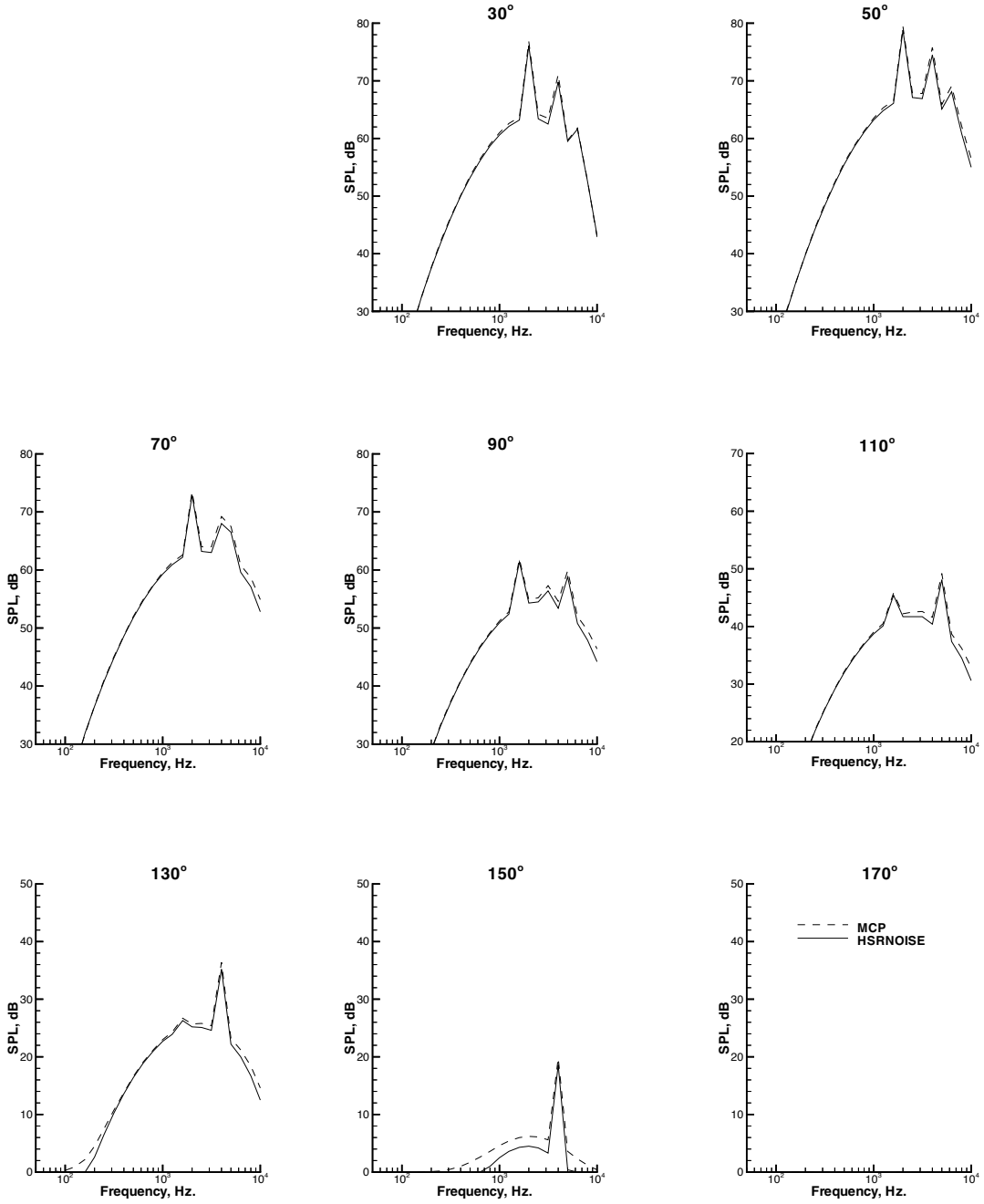

Figure 4.2.4.1 Approach fan noise spectra for the TC aircraft
(Free-field - Single Engine - No Deltas)

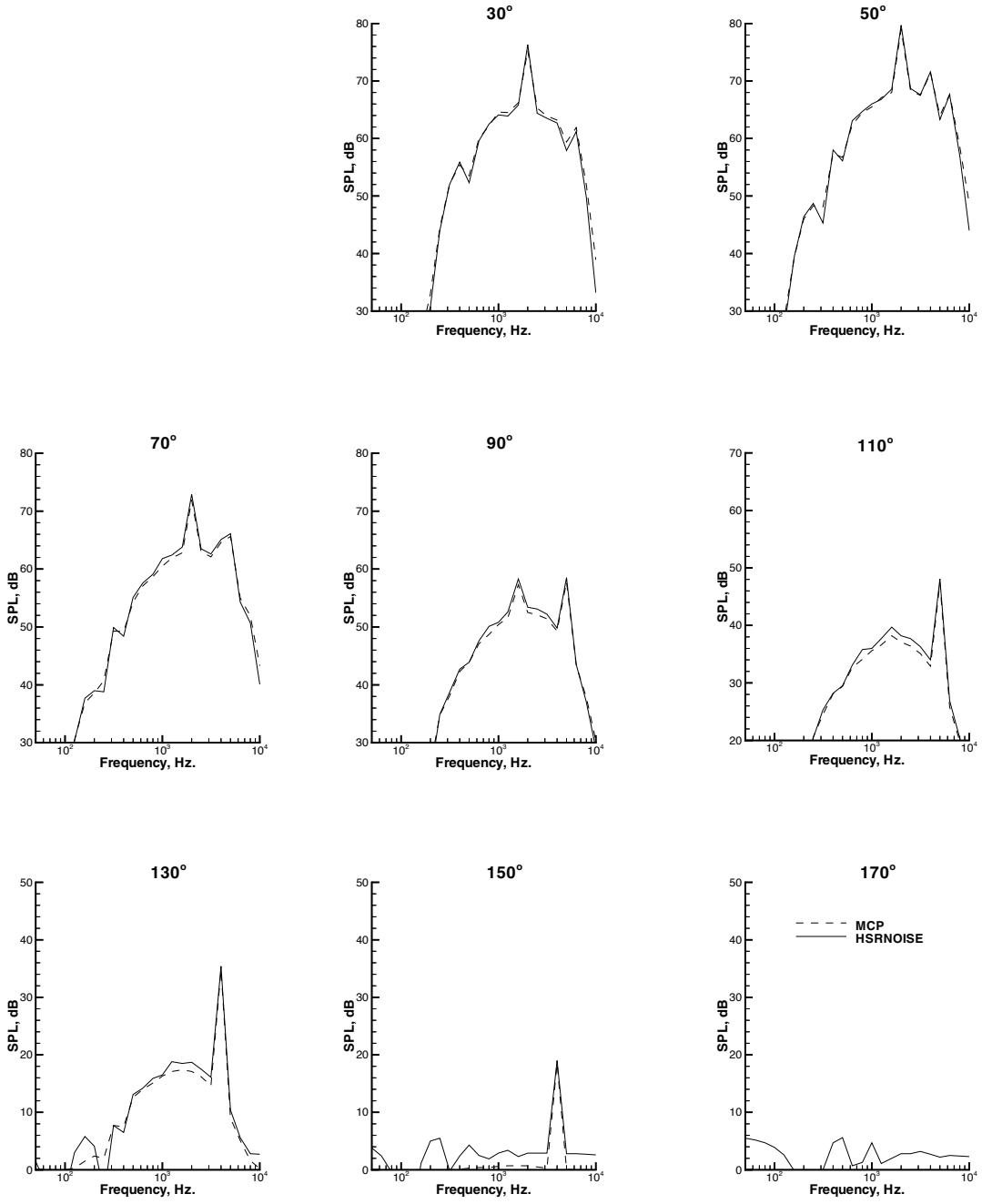

Figure 4.2.4.2 Approach fan noise spectra for the TC aircraft (Full System)

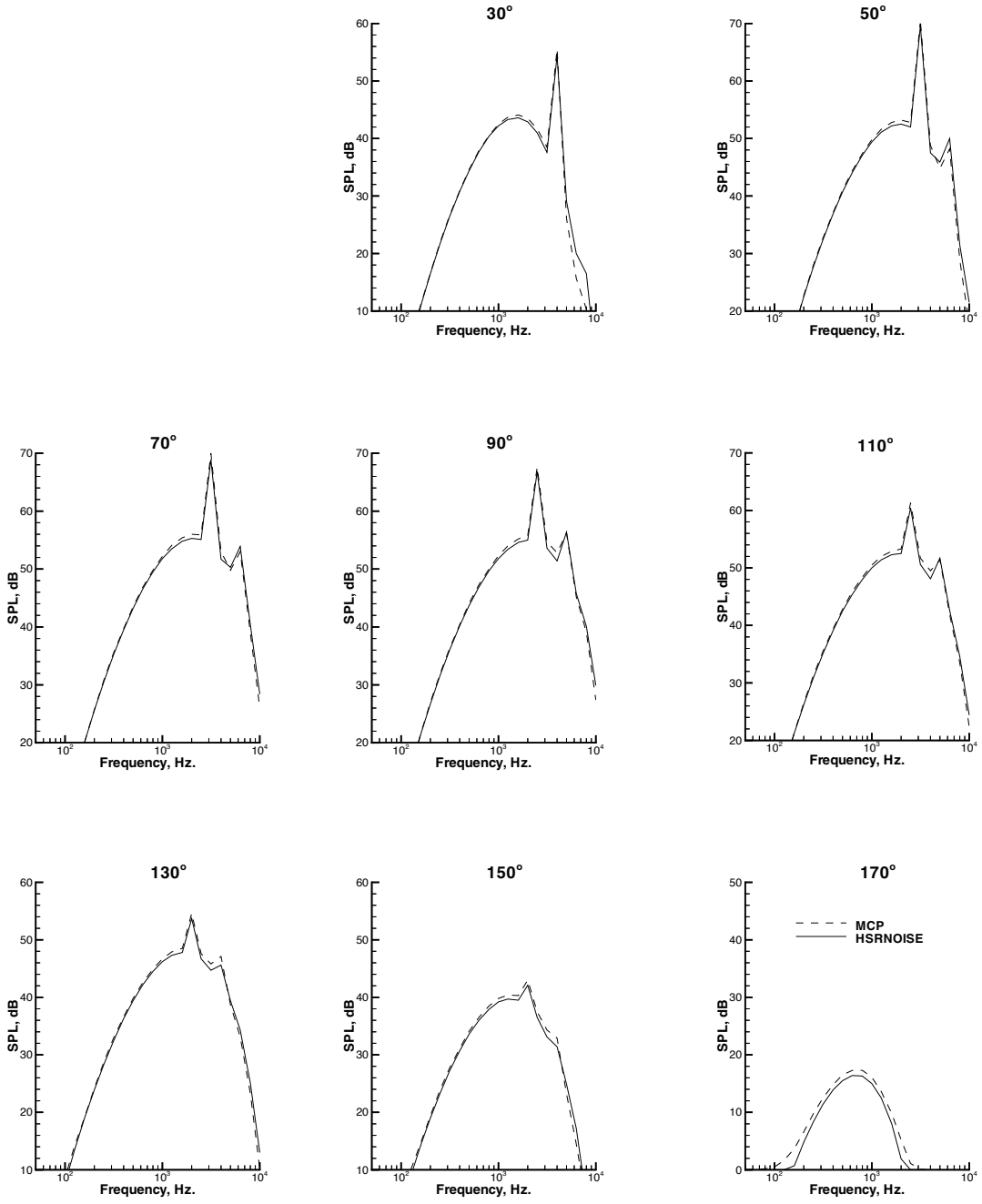

Figure 4.2.4.3 Sideline fan noise spectra for the TC aircraft
(Free-field - Single Engine - No Deltas)

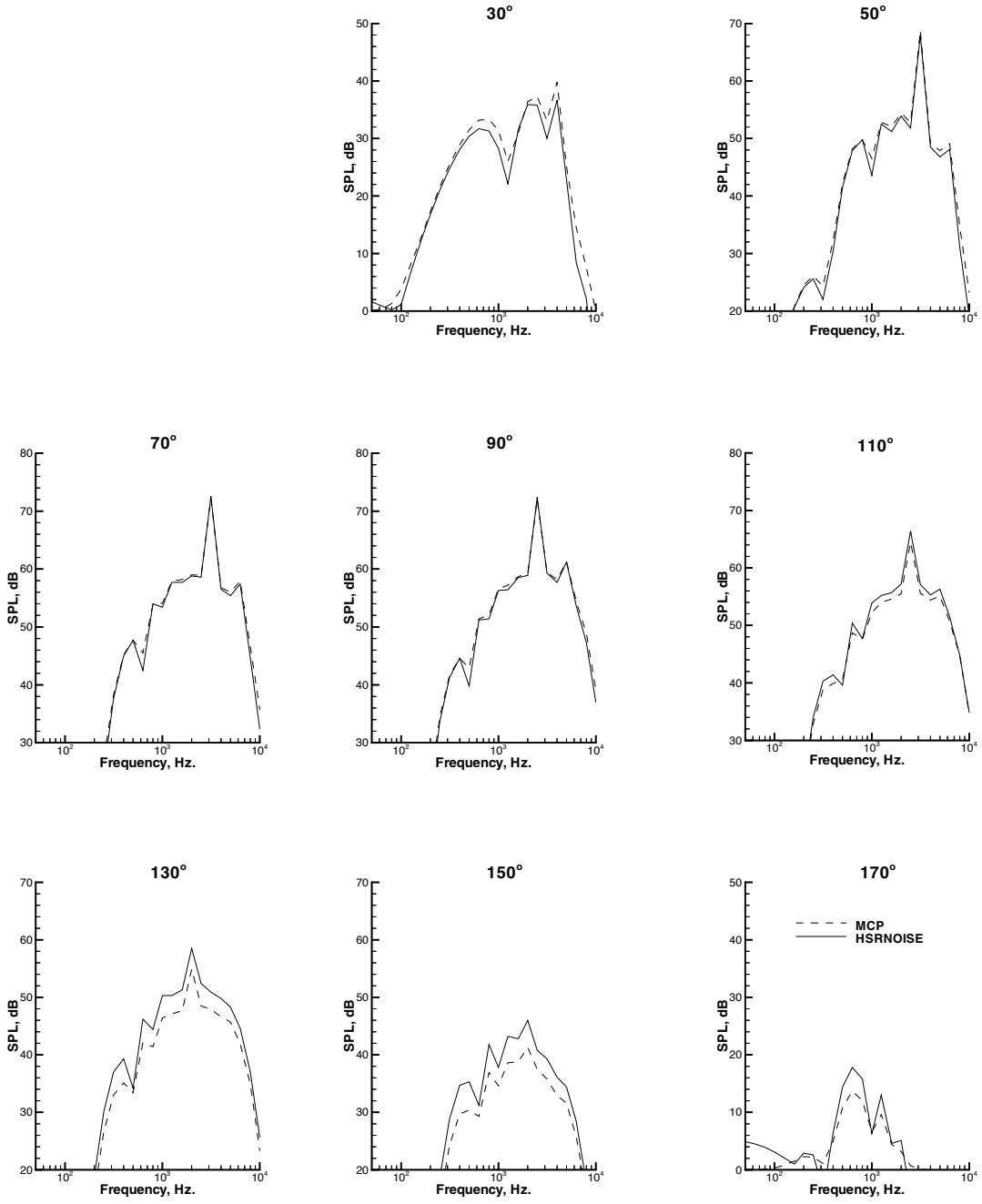

Figure 4.2.4.4 Sideline fan noise spectra for the TC aircraft
(Full System)

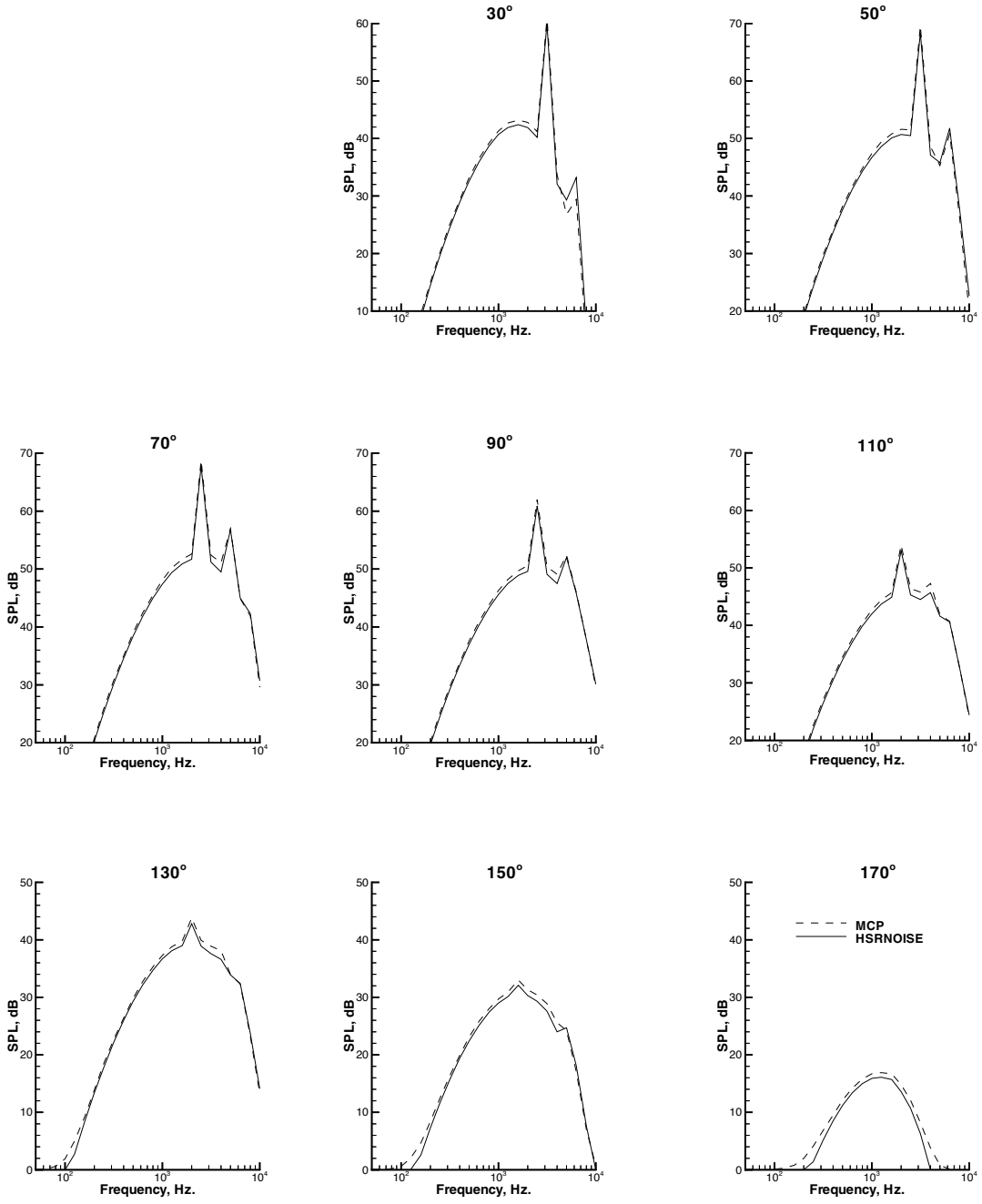

Figure 4.2.4.5 Centerline fan noise spectra for the TC aircraft
(Free-field - Single Engine - No Deltas)

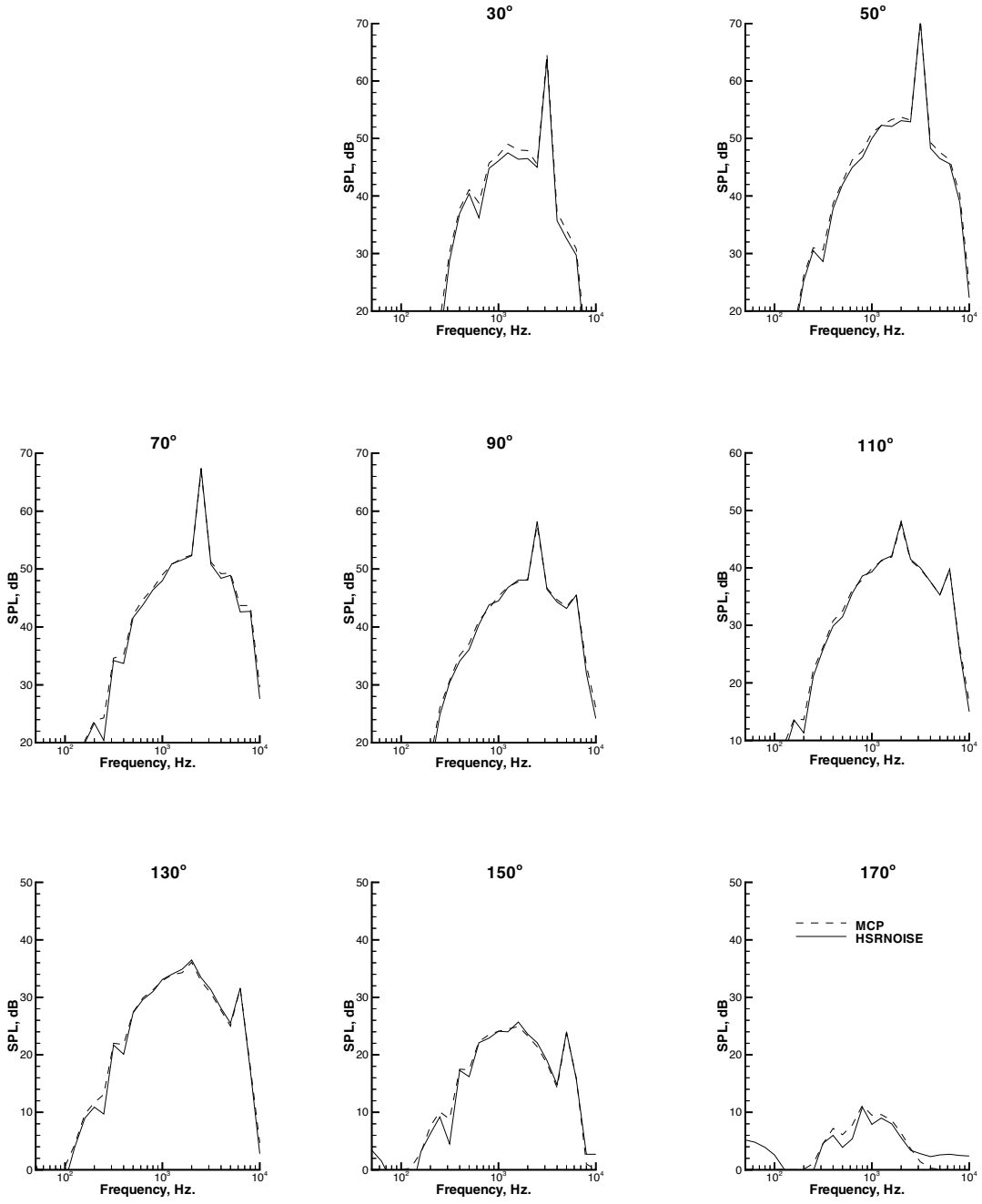

Figure 4.2.4.6 Centerline fan noise spectra for the TC aircraft (Full System)

4.2.5 Airframe Noise

Airframe noise was only predicted for the approach case. Figure 4.2.5 shows the free-field one-third-octave band spectra for the approach, sideline, and centerline cases. Figure 4.2.5.2 shows the full system prediction. RMS error values are provided in tables 4.2.5.1 and 4.2.5.2.

Comparisons of the free-field spectrum were excellent. Comparisons of the full system spectrum were excellent in the low frequency region except for frequencies corresponding to the ground dips. Comparisons of the mid-frequency region were good to fair. The spectral match was poor in the high frequency region. The discrepancy in the high frequency spectra is a result of the ground reflection model. As discussed in the section on jet noise, the Shivashankara model attenuates the high frequencies more than the Chien and Soroka model.

Table 4.2.5.1 Free-field Approach Airframe Noise RMS Error Table, dB

Emission Angle / Frequencies	30°	50°	70°	90°	110°	130°	150°	170°
Low	0.3	0.3	0.3	0.3	0.2	0.2	0.3	0.3
Mid	0.3	0.2	0.3	0.3	0.3	0.2	0.2	0.3
High	1.5	0.8	0.6	0.5	0.5	0.6	0.8	0.6
All	0.9	0.5	0.4	0.4	0.4	0.4	0.5	0.4

Table 4.2.5.2 Full System Approach Airframe Noise RMS Error Table, dB

Emission Angle / Frequencies	30°	50°	70°	90°	110°	130°	150°	170°
Low	0.9	1.5	1.8	1.0	1.0	1.7	1.5	1.8
Mid	0.5	1.1	1.0	0.8	0.9	0.8	1.1	1.0
High	1.1	1.6	1.7	1.8	1.8	1.7	1.6	1.7
All	0.9	1.4	1.5	1.3	1.3	1.5	1.4	1.5

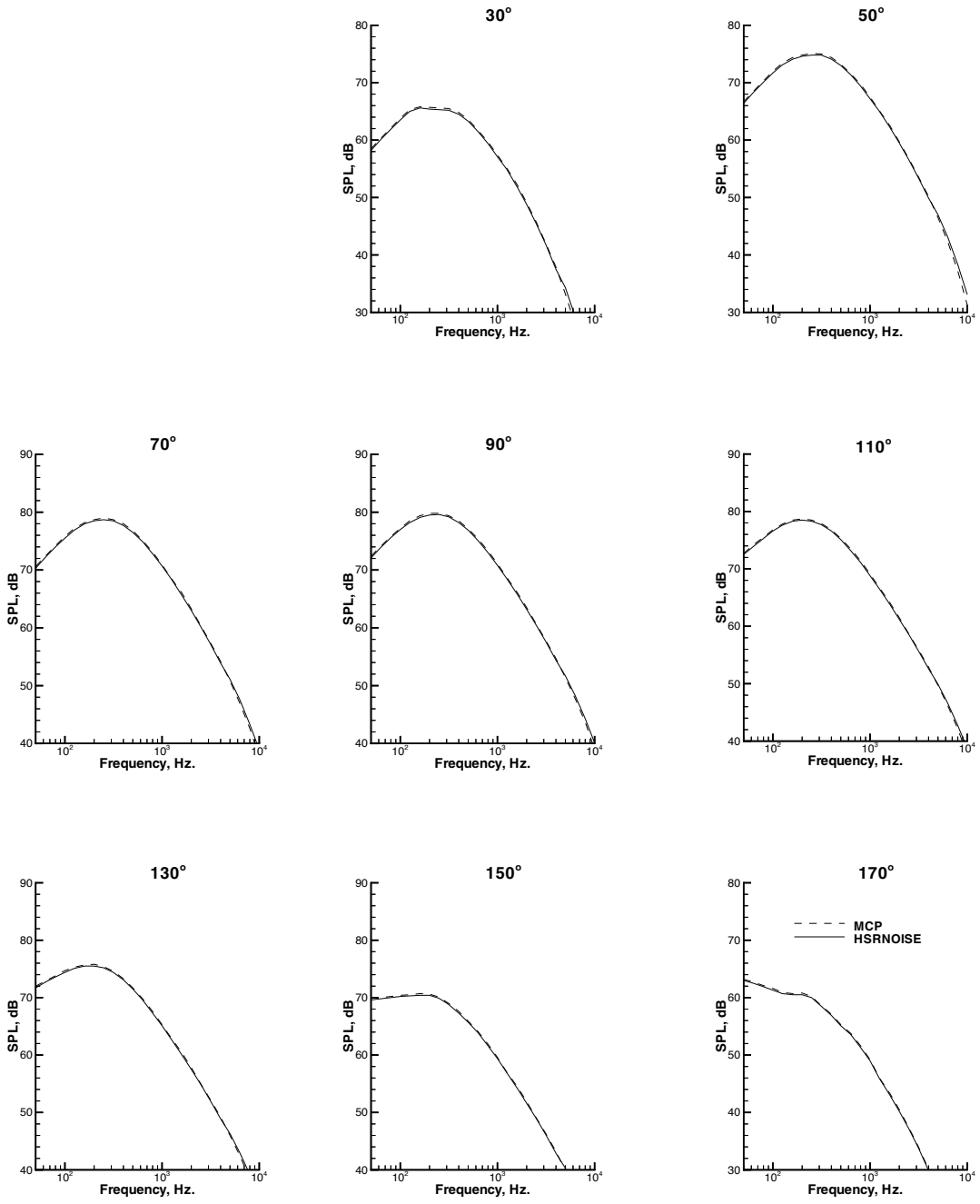

Figure 4.2.5.1 Approach airframe noise spectra for the TC aircraft
(Free-field - Single Engine - No Deltas)

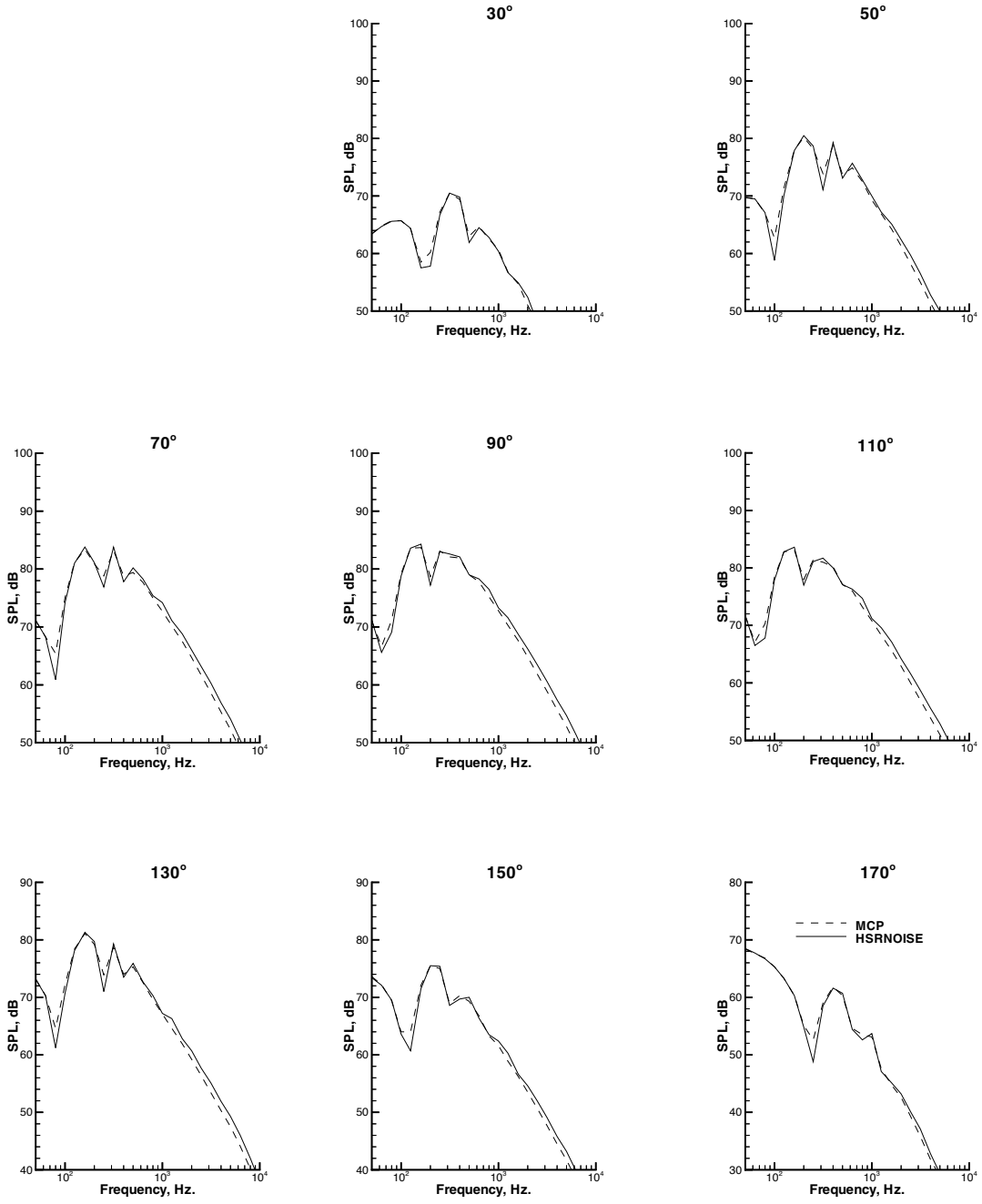

Figure 4.2.5.2 Approach airframe noise spectra for the TC aircraft (Full System)

4.2.6 Core Noise

Core noise did not contribute to the total noise of the TC aircraft for the approach, sideline, or centerline cases. Figures 4.2.6.1, 4.2.6.3, and 4.2.6.5 show the free-field one–third octave band spectra for the approach, sideline, and centerline cases. Figures 4.2.6.2, 4.2.6.4, and 4.2.6.6 show the full system predictions. RMS error values are provided in tables 4.2.6.1 through 4.2.6.6.

An examination of figures 4.2.6.1 through 4.2.6.6 shows a shift in the spectrum predicted by the MCP and HSRNOISE programs. This shift is not due to the Doppler effect. In fact, the core noise spectrum is not Doppler shifted in either the MCP or the HSRNOISE codes. This shift is caused by different implementations of the spectrum function. The core noise spectrum function is tabulated as a function of the nondimensional parameter η defined as

$$\eta = 10 Log_{10}\left(\frac{f}{f_{peak}}\right) \qquad \text{(Eq. 6 Section 3.7)}$$

In the MCP code η is converted to an integer before determining the spectrum level. Since the spectrum function is tabulated for integer values, interpolation is not required. In the HSRNOISE code, η is treated as a real variable and consequently, interpolation of the spectrum function is required. This relatively minor implementation difference caused the low and high frequency ranges to differ by more than one dB.

In some cases, the MCP core spectra did not contain SPL levels for the 24 one–third octave bands as can be seen in the figure 4.2.6.1. This caused very large RMS errors to be tabulated in the low and high frequency ranges. Because core noise was not a significant noise source, this discrepancy was not resolved.

As with the other noise sources, differences in level were noted at frequencies corresponding to the ground dips. The poor match in the high frequency range observed in the other sources was not as prevalent in the core comparisons because the shift noted in the free-field comparisons tended to mask the increased attenuation of the ground reflection model.

Table 4.2.6.1 Free-field Approach Core Noise RMS Error Table, dB

Emission Angle Frequencies	30°	50°	70°	90°	110°	130°	150°	170°
Low	43.1	42.4	27.1	9.6	0.6	1.4	42.4	27.1
Mid	0.5	0.4	0.9	0.6	0.3	0.8	0.4	0.9
High	0.9	0.8	0.6	1.8	8.6	25.5	0.8	0.6
All	24.9	24.5	15.7	5.6	5.0	14.7	24.5	15.7

Table 4.2.6.2 Full System Approach Core Noise RMS Error Table, dB

Emission Angle Frequencies	30°	50°	70°	90°	110°	130°	150°	170°
Low	47.1	42.5	27.3	9.8	1.2	2.5	42.5	27.3
Mid	0.5	1.3	1.4	0.7	1.0	1.4	1.3	1.4
High	0.9	0.8	1.4	0.6	9.2	25.9	0.8	1.4
All	27.2	24.5	15.8	5.7	5.4	15.0	24.5	15.8

Table 4.2.6.3 Free-field Sideline Core Noise RMS Error Table, dB

Emission Angle Frequencies	30°	50°	70°	90°	110°	130°	150°	170°
Low	48.8	44.7	32.4	5.2	1.3	0.2	44.7	32.4
Mid	1.0	0.5	0.8	0.5	0.6	0.8	0.5	0.8
High	5.1	1.9	1.5	1.1	22.6	31.7	1.9	1.5
All	28.3	25.9	18.7	3.1	13.1	18.3	25.9	18.7

Table 4.2.6.4 Full System Sideline Core Noise RMS Error Table, dB

Emission Angle Frequencies	30°	50°	70°	90°	110°	130°	150°	170°
Low	51.1	48.6	32.5	5.3	1.9	1.4	48.6	32.5
Mid	2.0	1.3	1.1	0.9	1.2	1.2	1.3	1.1
High	2.8	1.7	0.8	0.9	21.5	32.5	1.7	0.8
All	29.6	28.1	18.8	3.2	12.5	18.8	28.1	18.8

Table 4.2.6.5 Free-field Centerline Core Noise RMS Error Table, dB

Emission Angle Frequencies	30°	50°	70°	90°	110°	130°	150°	170°
Low	50.4	46.1	39.7	12.9	1.2	0.3	46.1	39.7
Mid	1.0	0.9	0.7	0.9	0.6	1.1	0.9	0.7
High	4.4	1.5	0.9	1.3	14.5	36.0	1.5	0.9
All	29.2	26.6	22.9	7.5	8.4	20.8	26.6	22.9

Table 4.2.6.6 Full System Centerline Core Noise RMS Error Table, dB

Emission Angle Frequencies	30°	50°	70°	90°	110°	130°	150°	170°
Low	53.8	49.4	39.8	13.1	1.7	1.7	49.4	39.8
Mid	1.2	0.7	0.8	0.5	0.9	0.5	0.7	0.8
High	0.8	1.0	0.8	0.7	14.0	36.6	1.0	0.8
All	31.1	28.5	23.0	7.6	8.1	21.2	28.5	23.0

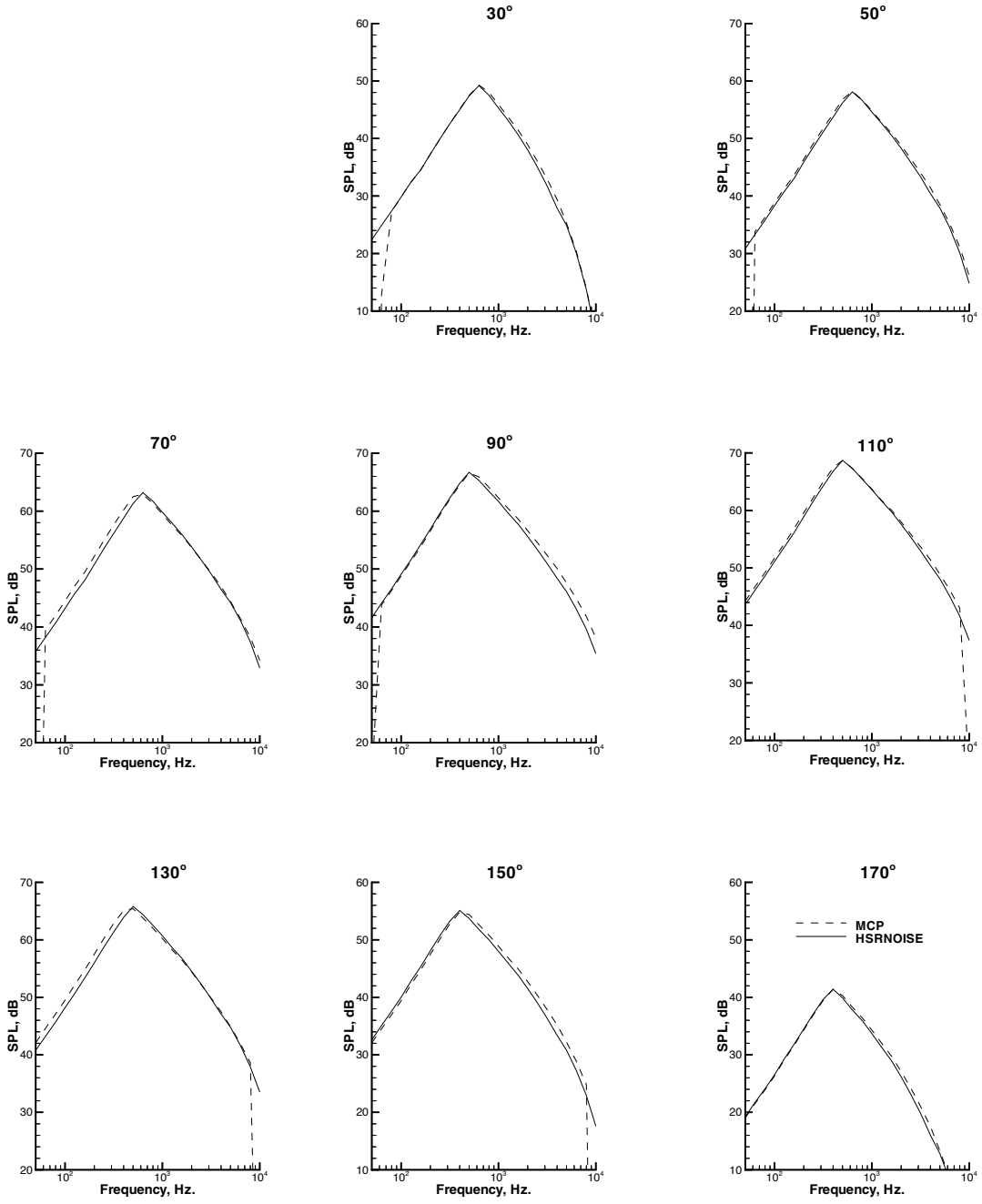

Figure 4.2.6.1 Approach core noise spectra for the TC aircraft
(Free-field - Single Engine - No Deltas)

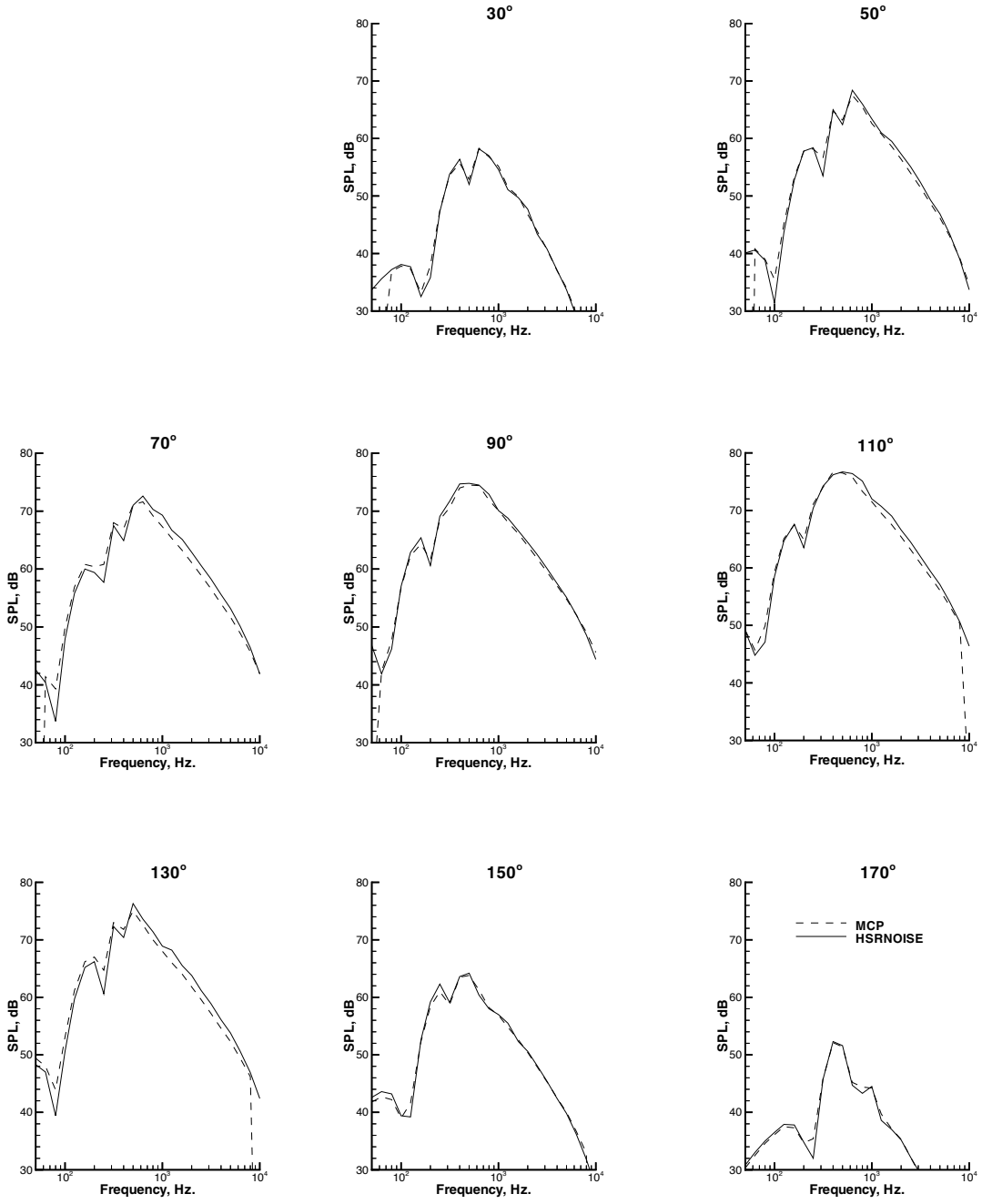

Figure 4.2.6.2 Approach core noise spectra for the TC aircraft (Full System)

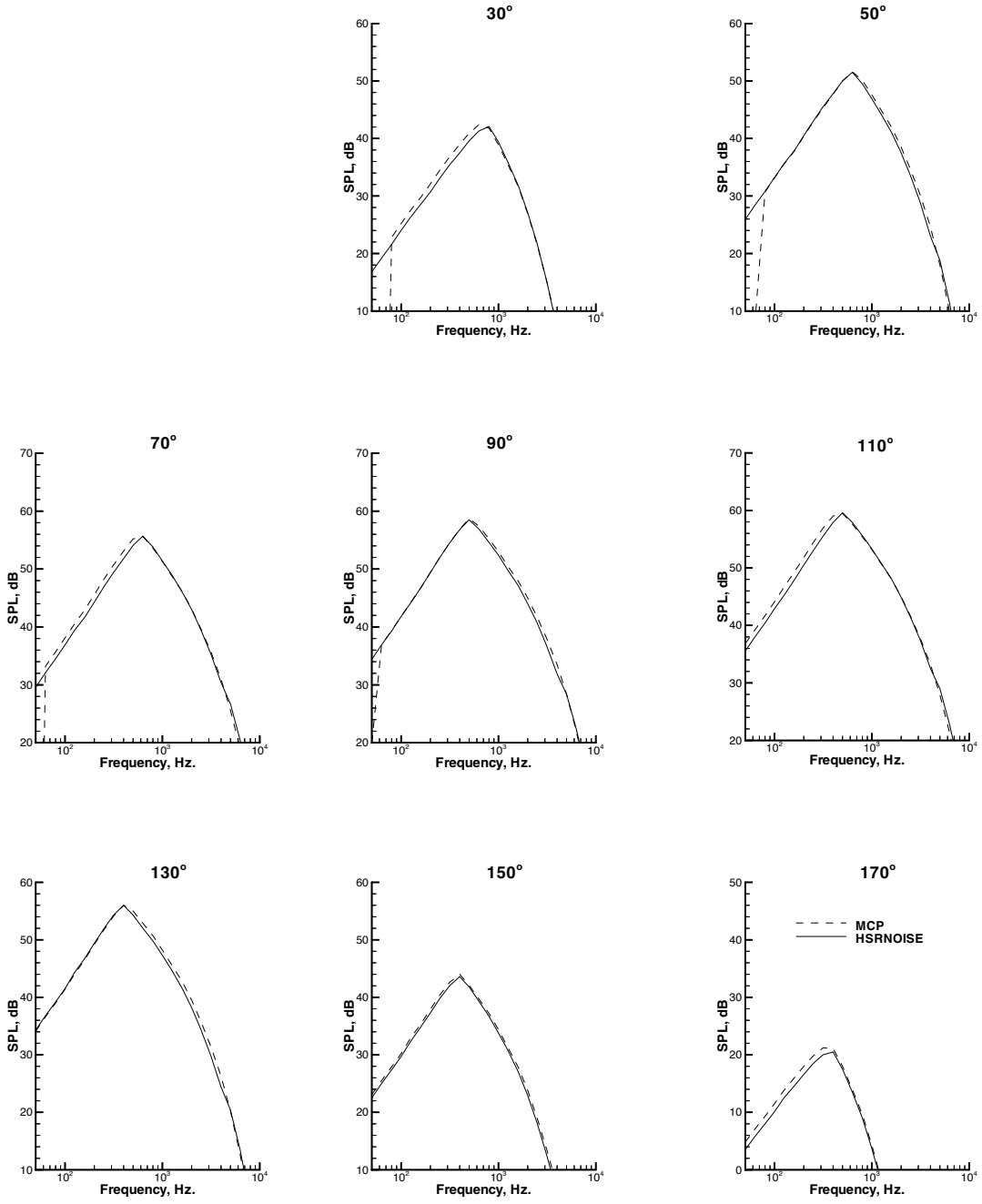

Figure 4.2.6.3 Sideline core noise spectra for the TC aircraft
(Free-field - Single Engine - No Deltas)

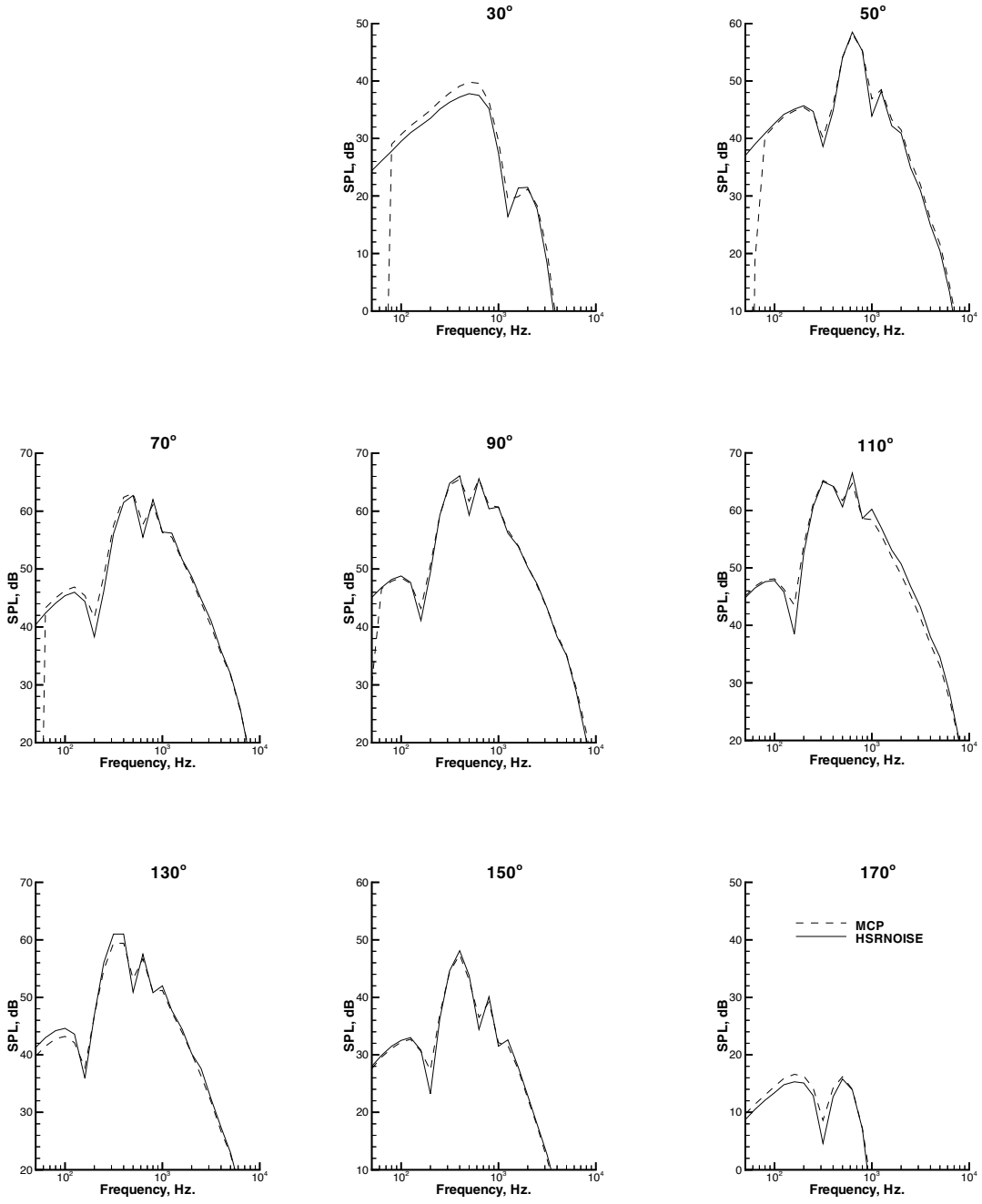

Figure 4.2.6.4 Sideline core noise spectra for the TC aircraft (Full System)

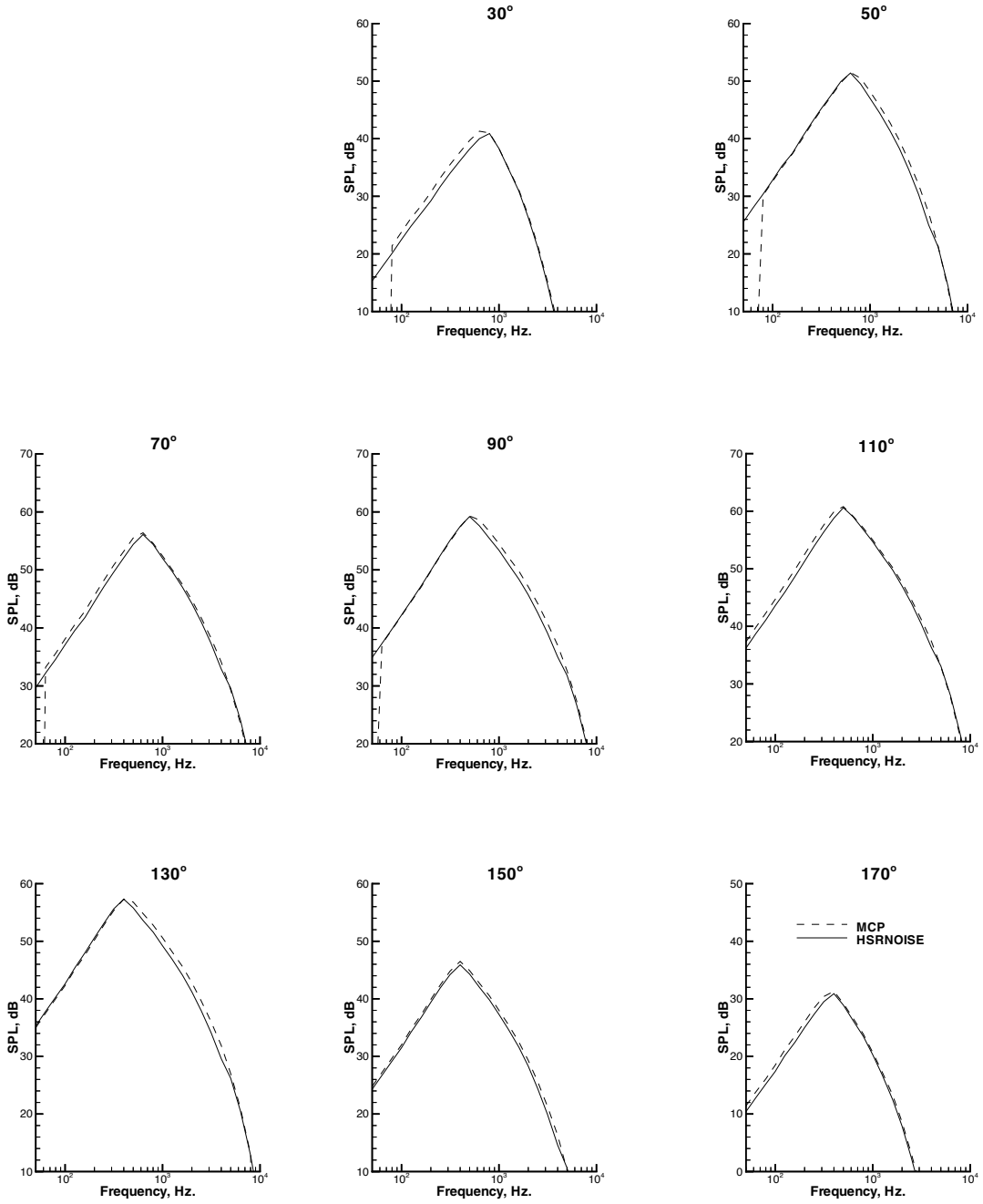

Figure 4.2.6.5 Centerline core noise spectra for the TC aircraft
(Free-field - Single Engine - No Deltas)

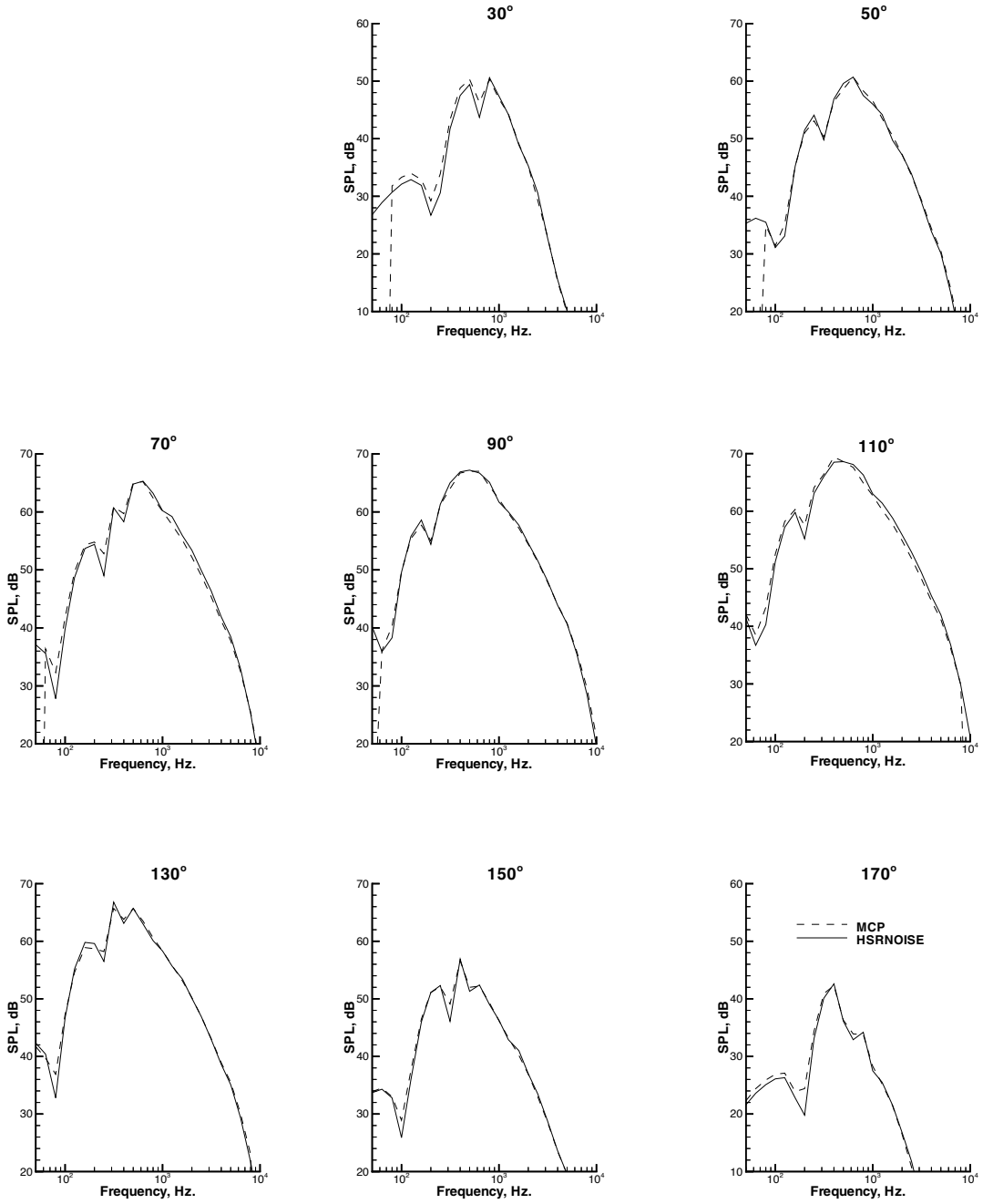

Figure 4.2.6.6 Centerline core noise spectra for the TC aircraft (Full System)

4.3 Conclusions

Comparisons have been presented for the SPL, OASPL, PNL, PNLT, and EPNL noise levels predicted by the HSRNOISE and MCP codes for the Technology Concept (TC) aircraft. It was anticipated that the HSRNOISE would match the EPNLs predicted by the MCP within a range of +/- 0.25. Unfortunately, this criterion was not met. Several philosophical design differences between the two codes were identified which explain the differences in EPNL levels.

One very significant difference between the two codes is the way in which the PNLT noise metric is calculated. In the MCP predictions, tone corrections are not made for frequencies below 1250 Hertz and for SPL levels below 30 dB. This modification to the PNLT time history resulted in MCP predicting lower EPNL levels than HSRNOISE.

HSRNOISE and MCP use different ground reflection models. HSRNOISE uses the Chien and Soroka ground reflection model; MCP uses the Shivashankara model. The Chien and Soroka model predicts deeper ground dips and attenuates the high frequency region less than the Shivashankara model. The deeper ground dips caused the PNLT correction to be higher in the HSRNOISE code, which also contributed to the higher EPNL levels. Of course, modifying the PNLT algorithm to the one used in the MCP code would reduce some of this discrepancy.

Differences were also identified in the implementation of the fan, core, and turbine source models. In the case of the fan and core modules, the differences were related to spectrum index function. MCP relates the spectrum index to the center frequency before calculation of the SPL. HSRNOISE relates the spectrum index to the center frequency after calculating the SPL. This causes differences in the magnitude of the predicted SPL. The MCP core module did not always predict SPL levels for the 24 one-third-octave bands. This causes the PNLT correction to be higher than expected when the spectrum is truncated in the high frequency range. An error was identified in the MCP turbine module, which had the effect of lowering the EPNL level during approach. It should be noted that very good agreement was obtained for the free-field predictions of the jet and airframe components.

The HSRNOISE code was developed to provide members of the HSR program with a code to continue research on the HSCT. This report provides a User's Manual, fully documents the noise prediction algorithms, and provides comparisons of predicted noise levels for the TC aircraft. While the HSRNOISE and MCP codes did not predict identical EPNL levels as was anticipated, the main causes for the discrepancies have been identified. Because of the termination of the HSR program discrepancies between the two codes were not fully resolved.

5.0 Input Files

This section presents the input files used in the verification of the HSRNOISE code. Free-field and full system files are listed for the approach, sideline, and centerline cases. Free-field input files are included in section 5.1. Full system input files are included in section 5.2.

5.1 Free-field

The free-field input files include atmospheric absorption but do not include ground reflections, EGA or jet shielding. Note that the airframe and jet noise source include spectral correction. Spectral corrections were removed from the fan, core, and turbine noise sources.

5.1.1 Free-field Approach

```
#
#  Approach test case for the HSRNOISE code
#
#  Free-field predictions
 $GEOM
   HMIC    =  0.0       ,
   SL      =  0.0
 $END
 $WEATHER
   PSIAMB  =   14.7     ,
   RH      =   70.0     ,
   TFAMB   =   77.0
 $END
 $FLIPATH
   ALTEVO  =   394.0    ,
   FPA     =    -3.0    ,
   PAE     =     7.1    ,
   VAIR    =   267.7168
 $END
 $SOURCE
   IAFRAM  = T,
   IATM    = 1,
   IEGA    = F,
   IGRND   = F,
   IFAN    = T,
   ICORE   = T,
   IJET    = T,
   ITUR    = T,
   NENG    = 1
 $END
 $DELTAS
   FANDIBB = 17*0.0  ,
   FANSPBB = 24*0.0  ,
   FANBPF  =    0.0  ,
   FAN2BPF =    0.0  ,
   FAN3BPF =    0.0  ,
   FAN4BPF =    0.0  ,
   CORDIBB = 17*0.0 ,
```

```
   CORSPBB = 24*0.0  ,
   TURDIBB = 17*0.0 ,
   TURSPBB = 24*0.0  ,
   TURDITN = 17*0.0 ,
   TURSPTN = 24*0.0 ,
   AIRFDICW   =  8*1.4, 1.0, 0.7, 0.5, 0.3, 0.0, -0.2, -0.5, -0.8, -
1.0,
   AIRFSPCW   =  -12., -11., -10., -9., 2*-8., -9.,
                 -9.5, 3*-9., 3*-10., 9*-9.0, -8.0,
   AIRFDILE   =  8*1.4, 1.0, 0.7, 0.5, 0.3, 0.0, -0.2, -0.5, -0.8, -
1.0,
   AIRFSPLE   =  -12., -11., -10., -9., 2*-8., -9.,
                 -9.5, 3*-9., 3*-10., 9*-9.0, -8.0,
   AIRFDITEI  =  8*1.4, 1.0, 0.7, 0.5, 0.3, 0.0, -0.2, -0.5, -0.8, -
1.0,
   AIRFSPTEI  =  -12., -11., -10., -9., 2*-8., -9.,
                 -9.5, 3*-9., 3*-10., 9*-9.0, -8.0,
   AIRFDITEO  =  8*1.4, 1.0, 0.7, 0.5, 0.3, 0.0, -0.2, -0.5, -0.8, -
1.0,
   AIRFSPTEO  =  -12., -11., -10., -9., 2*-8., -9.,
                 -9.5, 3*-9., 3*-10., 9*-9.0, -8.0,
   AIRFDIHT   =  8*1.4, 1.0, 0.7, 0.5, 0.3, 0.0, -0.2, -0.5, -0.8, -
1.0,
   AIRFSPHT   =  -12., -11., -10., -9., 2*-8., -9.,
                 -9.5, 3*-9., 3*-10., 9*-9.0, -8.0,
   AIRFDIVT   =  8*1.4, 1.0, 0.7, 0.5, 0.3, 0.0, -0.2, -0.5, -0.8, -
1.0,
   AIRFSPVT   =  -12., -11., -10., -9., 2*-8., -9.,
                 -9.5, 3*-9., 3*-10., 9*-9.0, -8.0,
   AIRFDIMG   =  17*0.0,
   AIRFSPMG   =  24*0.0,
   AIRFDING   =  17*0.0,
   AIRFSPNG   =  24*0.0
 $END
 $FANIN
   AFAN    =   16.98436  ,
   FANRPM  =   3609.0    ,
   NB1     =   27        ,
   UT      =   923.13    ,
   ISHAPE  =   0         ,
   IDOOR   =   0
 $END
 $COREIN
   AB      =   1111.27  ,
   BL      =   0.75     ,
   ICR     =   2        ,
   NFN     =   90       ,
   PLD     =    0.15    ,
   P3      =   92.0     ,
   P4      =   85.2     ,
   P7      =   20.28    ,
   T3      =   940.7    ,
   T4      =   1880.5   ,
   T7      =   1201.5   ,
   W3      =   141.2    ,
   WFP4    =  3.9999999E-02
 $END
```

```
$TURIN
  CSS     =   151.42    ,
  MDOT    =   200.20    ,
  NBLADE  =   88        ,
  TS      =   1172.34   ,
  TURCAL  =      0.0    ,
  TURRPM  =   3609.0    ,
  VTR     =   937.8076
$END
$JN8C4IN
  APRI    =   8.476     ,
  TPRI    =   989.84    ,
  VPRI    =   1048.88   ,
  WPRI    =   327.87    ,
  ATHP    =   7.474     ,
  PLUGD   =   0.0       ,
  VSEC    =   369.42    ,
  WSEC    =   316.23    ,
  ASEC    =   12.352    ,
  TSEC    =   514.51    ,
  SPOKE   =   20. ,
  PEN     =   0.925  ,
  DIVANG  =   0.0    ,
  EJL     =   11.0   ,
  EJD     =   5.15   ,
  XMAR    =   0.98   ,
  EJLIN   =   7.09   ,
  FLIN    =   2500.0 ,
  EJASP   =   1.42   ,
  CFG     =   0.95   ,
  PSI0    =   0.0    ,
  DELPE   =   0.0 ,
  DELPI   =   0.0 ,
  DELMIX  =   0.0
$END
$AIRFIN
  ICWING = 2,
  IVTAIL = 1,
  IHTAIL = 1,
  ILEDGE = 1,
  ITEIN  = 1,
  ITEOUT = 1,
  INGEAR = 1,
  IMGEAR = 1,
  AW = 8878.0,
  BW = 154.3,
  AV = 435.0,
  BV = 16.8,
  AH = 726.0,
  BH = 71.0,
  AFIN = 100.0,
  BFIN = 10.0,
  FLAIN = 10.0,
  NFSIN = 1,
  AFOUT = 200.0,
  BFOUT = 20.0,
  FLAOUT = 10.0,
```

```
  NFSOUT = 1,
  NNG = 1,
  NWNG = 2,
  DNG = 3.3,
  RLNG = 13.7,
  NMG = 2,
  NWMG = 8,
  DMG = 3.7,
  RLMG = 16.0,
$END
```

5.1.2 Sideline

```
#
#  Sideline test case for the HSRNOISE code
#
#  Free-field predictions without Deltas
#
 $GEOM
   HMIC    =      0.0,
   SL      =   1476.0
 $END
 $WEATHER
   PSIAMB  =   14.7    ,
   RH      =   70.0    ,
   TFAMB   =   77.0
 $END
 $FLIPATH
   ALTEVO  =   700.0000    ,
   FPA     =   8.100000    ,
   PAE     =   17.00000    ,
   VAIR    =   374.5672
 $END
 $SOURCE
   IAFRAM  = F,
   IATM    = 1,
   IEGA    = F,
   IGRND   = F,
   IFAN    = T,
   ICORE   = T,
   IJET    = T,
   ITUR    = T,
   NENG    = 1
 $END
 $DELTAS
   FANDIBB = 17*0.0  ,
   FANSPBB = 24*0.0  ,
   FANBPF  =    0.0  ,
   FAN2BPF =    0.0  ,
   FAN3BPF =    0.0  ,
   FAN4BPF =    0.0  ,
   CORDIBB = 17*0.0,
   CORSPBB = 24*0.0 ,
   TURDIBB = 17*0.0,
   TURSPBB = 24*0.0 ,
   TURDITN = 17*0.0  ,
   TURSPTN = 24*0.0
 $END
 $FANIN
   AFAN    =   16.98436  ,
   FANRPM  =   5618.0    ,
   NB1     =   27        ,
   UT      =   1431.22   ,
   ISHAPE  =   0         ,
   IDOOR   =   0
 $END
 $COREIN
   AB      =   1111.27  ,
```

```
  BL      =   0.75     ,
  ICR     =   2        ,
  NFN     =   330      ,
  PLD     =  0.15      ,
  P3      =   294.5    ,
  P4      =   274.6    ,
  P7      =   50.15    ,
  T3      =   1362.1   ,
  T4      =   3239.4   ,
  T7      =   1992.8   ,
  W3      =   340.8    ,
  WFP4    =  3.9999999E-02
$END
$TURIN
  CSS     =   151.42    ,
  MDOT    =   487.50    ,
  NBLADE  =   88        ,
  TS      =   1919.03   ,
  TURCAL  =      0.0    ,
  TURRPM  =   5618.0    ,
  VTR     =   1508.941
$END
$JN8C4IN
  APRI    =   8.48      ,
  TPRI    =   1668.84   ,
  VPRI    =   2467.14   ,
  WPRI    =   698.95    ,
  ATHP    =   7.47      ,
  PLUGD   =   0.0       ,
  VSEC    =   564.42    ,
  WSEC    =   440.94    ,
  ASEC    =   11.95     ,
  TSEC    =   546.03    ,
  SPOKE   =   20.    ,
  PEN     =   0.925  ,
  DIVANG  =   0.0    ,
  EJL     =   11.0   ,
  EJD     =   5.15   ,
  XMAR    =   0.919  ,
  EJLIN   =   7.09   ,
  FLIN    =   2500.0 ,
  EJASP   =   1.42   ,
  CFG     =   0.95   ,
  PSI0    =   0.0    ,
  DELPE   =   0.0 ,
  DELPI   =   0.0 ,
  DELMIX  =   0.0
$END
```

5.1.3 Free-field Centerline

```
#
#  Centerline test case for the HSRNOISE code
#
#  Free-field predictions without Deltas
#
 $GEOM
   HMIC    =  0.0       ,
   SL      =  0.0
 $END
 $WEATHER
   PSIAMB  =   14.7     ,
   RH      =   70.0     ,
   TFAMB   =   77.0
 $END
 $FLIPATH
 ALTEVO  =   1273.0  ,
 FPA     =   2.30    ,
 PAE     =   11.7    ,
 VAIR    =   377.7744
 $END
 $SOURCE
 IAFRAM  = F,
 IATM    = 1,
 IEGA    = F,
 IGRND   = F,
 IFAN    = T,
 ICORE   = T,
 IJET    = T,
 ITUR    = T,
 NENG    = 1
 $END
 $DELTAS
   FANDIBB = 17*0.0  ,
   FANSPBB = 24*0.0  ,
   FANBPF  =    0.0  ,
   FAN2BPF =    0.0  ,
   FAN3BPF =    0.0  ,
   FAN4BPF =    0.0
   CORDIBB = 17*0.0 ,
   CORSPBB = 24*0.0  ,
   TURDIBB = 17*0.0 ,
   TURSPBB = 24*0.0  ,
   TURDITN = 17*0.0 ,
   TURSPTN = 24*0.0
 $END
 $FANIN
   AFAN    =   16.98436    ,
   FANRPM  =   4898.000    ,
   NB1     =          27,
   UT      =   1249.580,
   ISHAPE  = 0 ,
   IDOOR   = 0
 $END
 $COREIN
```

```
  AB      =   1111.27 ,
  BL      =   0.75    ,
  ICR     =   2       ,
  NFN     =   210     ,
  PLD     =   0.15    ,
  P3      =   193.9   ,
  P4      =   180.4   ,
  P7      =   34.41   ,
  T3      =   1189.8  ,
  T4      =   2672.5  ,
  T7      =   1638.1  ,
  W3      =   249.1   ,
  WFP4    =  3.9999999E-02
$END
$TURIN
  CSS     =   151.42   ,
  MDOT    =   354.8    ,
  NBLADE  =   88       ,
  TS      =   1580.61  ,
  TURCAL  =    0.0     ,
  TURRPM  =   4898.0   ,
  VTR     =   1311.559
$END
$JN8C4IN
  APRI    =   8.476    ,
  TPRI    =   1350.24   ,
  VPRI    =   1921.09   ,
  WPRI    =   541.20    ,
  ATHP    =   7.47      ,
  PLUGD   =   0.0       ,
  VSEC    =   643.98    ,
  WSEC    =   475.90    ,
  ASEC    =   12.084    ,
  TSEC    =   544.19    ,
  SPOKE   =   20. ,
  PEN     =   0.925  ,
  DIVANG  =   0.0    ,
  EJL     =   11.0   ,
  EJD     =   5.15   ,
  XMAR    =   0.979  ,
  EJLIN   =   7.09   ,
  FLIN    =   2500.0 ,
  EJASP   =   1.42   ,
  CFG     =   0.95   ,
  PSI0    =   0.0    ,
  DELPE   =   0.0 ,
  DELPI   =   0.0 ,
  DELMIX  =   0.0
$END
```

5.2 Full System Input Files

The full system input files include ground reflections, EGA and jet shielding. Spectral corrections for all noise sources are included.

5.2.1 Full System Approach

```
#
#  Approach test case for the HSRNOISE code
#
#  Full system predictions with Deltas
#
 $GEOM
   HMIC    =  4.0       ,
   SL      =  0.0
 $END
 $WEATHER
   PSIAMB  =   14.7     ,
   RH      =   70.0     ,
   TFAMB   =   77.0     ,
   SIGMA   =  1.1E6
 $END
 $FLIPATH
   ALTEVO  =   394.0    ,
   FPA     =    -3.0    ,
   PAE     =     7.1    ,
   VAIR    =   267.7168
 $END
 $SOURCE
   IAFRAM  = T,
   IATM    = 1,
   IEGA    = F,
   IGRND   = T,
   IFAN    = T,
   ICORE   = T,
   IJET    = T,
   ITUR    = T,
   NENG    = 4
 $END
 $DELTAS
   FANDIBB = 17*-8.5 ,
   FANSPBB = 24*1.0  ,
   FANBPF  =   -8.5  ,
   FAN2BPF =   -8.5  ,
   FAN3BPF =   -8.5  ,
   FAN4BPF =   -8.5  ,
   CORDIBB = 17*0.0 ,
   CORSPBB = 24*0.0 ,
   TURDIBB = 17*0.0 ,
   TURSPBB = 24*0.0  ,
   TURDITN = 17*0.0 ,
   TURSPTN = 24*0.0 ,
   AIRFDICW   =  8*1.4, 1.0, 0.7, 0.5, 0.3, 0.0, -0.2, -0.5, -0.8, -
1.0,
```

```
   AIRFSPCW   =  -12., -11., -10., -9., 2*-8., -9.,
                 -9.5, 3*-9., 3*-10., 9*-9.0, -8.0,
   AIRFDILE   =  8*1.4, 1.0, 0.7, 0.5, 0.3, 0.0, -0.2, -0.5, -0.8, -
1.0,
   AIRFSPLE   =  -12., -11., -10., -9., 2*-8., -9.,
                 -9.5, 3*-9., 3*-10., 9*-9.0, -8.0,
   AIRFDITEI  =  8*1.4, 1.0, 0.7, 0.5, 0.3, 0.0, -0.2, -0.5, -0.8, -
1.0,
   AIRFSPTEI  =  -12., -11., -10., -9., 2*-8., -9.,
                 -9.5, 3*-9., 3*-10., 9*-9.0, -8.0,
   AIRFDITEO  =  8*1.4, 1.0, 0.7, 0.5, 0.3, 0.0, -0.2, -0.5, -0.8, -
1.0,
   AIRFSPTEO  =  -12., -11., -10., -9., 2*-8., -9.,
                 -9.5, 3*-9., 3*-10., 9*-9.0, -8.0,
   AIRFDIHT   =  8*1.4, 1.0, 0.7, 0.5, 0.3, 0.0, -0.2, -0.5, -0.8, -
1.0,
   AIRFSPHT   =  -12., -11., -10., -9., 2*-8., -9.,
                 -9.5, 3*-9., 3*-10., 9*-9.0, -8.0,
   AIRFDIVT   =  8*1.4, 1.0, 0.7, 0.5, 0.3, 0.0, -0.2, -0.5, -0.8, -
1.0,
   AIRFSPVT   =  -12., -11., -10., -9., 2*-8., -9.,
                 -9.5, 3*-9., 3*-10., 9*-9.0, -8.0,
   AIRFDIMG   =  17*0.0,
   AIRFSPMG   =  24*0.0,
   AIRFDING   =  17*0.0,
   AIRFSPNG   =  24*0.0
 $END
 $FANIN
   AFAN    =   16.98436  ,
   FANRPM  =   3609.0    ,
   NB1     =   27        ,
   UT      =   923.13    ,
   ISHAPE  =   1         ,
   IDOOR   =   0
 $END
 $COREIN
   AB      =   1111.27  ,
   BL      =   0.75     ,
   ICR     =   2        ,
   NFN     =   90       ,
   PLD     =    0.15    ,
   P3      =   92.0     ,
   P4      =   85.2     ,
   P7      =   20.28    ,
   T3      =   940.7    ,
   T4      =   1880.5   ,
   T7      =   1201.5   ,
   W3      =   141.2    ,
   WFP4    =  3.9999999E-02
 $END
 $TURIN
   CSS     =   151.42    ,
   MDOT    =   200.20    ,
   NBLADE  =   88        ,
   TS      =   1172.34   ,
   TURCAL  =     10.0    ,
   TURRPM  =   3609.0    ,
```

```
  VTR     =   937.8076
$END
$JN8C4IN
  APRI    =   8.476     ,
  TPRI    =   989.84    ,
  VPRI    =   1048.88   ,
  WPRI    =   327.87    ,
  ATHP    =   7.474     ,
  PLUGD   =   0.0       ,
  VSEC    =   369.42    ,
  WSEC    =   316.23    ,
  ASEC    =   12.352    ,
  TSEC    =   514.51    ,
  SPOKE   =   20. ,
  PEN     =   0.925  ,
  DIVANG  =   0.0    ,
  EJL     =   11.0   ,
  EJD     =   5.15   ,
  XMAR    =   0.98   ,
  EJLIN   =   7.09   ,
  FLIN    =   2500.0 ,
  EJASP   =   1.42   ,
  CFG     =   0.95   ,
  PSI0    =   0.0    ,
  DELPE   =   0.2 ,
  DELPI   =  -1.0 ,
  DELMIX  =   0.1
$END
$AIRFIN
  ICWING = 2,
  IVTAIL = 1,
  IHTAIL = 1,
  ILEDGE = 1,
  ITEIN  = 1,
  ITEOUT = 1,
  INGEAR = 1,
  IMGEAR = 1,
  AW = 8878.0,
  BW = 154.3,
  AV = 435.0,
  BV = 16.8,
  AH = 726.0,
  BH = 71.0,
  AFIN = 100.0,
  BFIN = 10.0,
  FLAIN = 10.0,
  NFSIN = 1,
  AFOUT = 200.0,
  BFOUT = 20.0,
  FLAOUT = 10.0,
  NFSOUT = 1,
  NNG = 1,
  NWNG = 2,
  DNG = 3.3,
  RLNG = 13.7,
  NMG = 2,
  NWMG = 8,
```

```
  DMG = 3.7,
  RLMG = 16.0,
$END
```

5.2.2 Full System Sideline

```
#
#  Sideline test case for the HSRNOISE code
#
#  Full system predictions with Deltas
#
 $GEOM
   HMIC    =      4.0,
   SL      =   1476.0
 $END
 $WEATHER
   PSIAMB  =   14.7    ,
   RH      =   70.0    ,
   TFAMB   =   77.0    ,
   SIGMA   = 1.1E6
 $END
 $FLIPATH
   ALTEVO  =   700.0000    ,
   FPA     =   8.100000    ,
   PAE     =   17.00000    ,
   VAIR    =   374.5672
 $END
 $SOURCE
   IAFRAM   = F,
   IATM     = 1,
   IEGA     = T,
   IGRND    = T,
   IFAN     = T,
   ICORE    = T,
   IJET     = T,
   IJETSHLD = T,
   ITUR     = T,
   NENG     = 4
 $END
 $DELTAS
   FANDIBB = 17*-4.5  ,
   FANSPBB = 24*1.1   ,
   FANBPF  =  -4.5,
   FAN2BPF =  -4.5,
   FAN3BPF =  -4.5,
   FAN4BPF =  -4.5,
   CORDIBB = 4*-0.1,-0.4,-0.7,-1.0,4*-1.1,-1.0,
             -0.9,-0.8,-0.6,-0.5,-0.3,
   CORSPBB = 24*0.0 ,
   TURDIBB = 4*-0.1,-0.4,-0.7,-1.0,4*-1.1,-1.0,
             -0.9,-0.8,-0.6,-0.5,-0.3,
   TURSPBB = 24*0.0 ,
   TURDITN = 4*-0.1,-0.4,-0.7,-1.0,4*-1.1,-1.0,
             -0.9,-0.8,-0.6,-0.5,-0.3,
   TURSPTN = 24*0.0
 $END
 $FANIN
   AFAN    =   16.98436  ,
   FANRPM  =   5618.0    ,
   NB1     =   27        ,
```

```
  UT      =   1431.22   ,
  ISHAPE  =   1         ,
  IDOOR   =   1
$END
$COREIN
  AB      =   1111.27  ,
  BL      =   0.75     ,
  ICR     =   2        ,
  NFN     =   330      ,
  PLD     =  0.15      ,
  P3      =   294.5    ,
  P4      =   274.6    ,
  P7      =   50.15    ,
  T3      =   1362.1   ,
  T4      =   3239.4   ,
  T7      =   1992.8   ,
  W3      =   340.8    ,
  WFP4    =  3.9999999E-02
$END
$TURIN
  CSS     =   151.42    ,
  MDOT    =   487.50    ,
  NBLADE  =   88        ,
  TS      =   1919.03   ,
  TURCAL  =     10.0    ,
  TURRPM  =   5618.0    ,
  VTR     =   1508.941
$END
$JN8C4IN
  APRI    =   8.48      ,
  TPRI    =   1668.84   ,
  VPRI    =   2467.14   ,
  WPRI    =   698.95    ,
  ATHP    =   7.47      ,
  PLUGD   =   0.0       ,
  VSEC    =   564.42    ,
  WSEC    =   440.94    ,
  ASEC    =   11.95     ,
  TSEC    =   546.03    ,
  SPOKE   =   20.    ,
  PEN     =   0.925  ,
  DIVANG  =   0.0    ,
  EJL     =   11.0   ,
  EJD     =   5.15   ,
  XMAR    =   0.919  ,
  EJLIN   =   7.09   ,
  FLIN    =   2500.0 ,
  EJASP   =   1.42   ,
  CFG     =   0.95   ,
  PSI0    =   0.0    ,
  DELPE   =  -1.8 ,
  DELPI   =  -1.3 ,
  DELMIX  =  -0.1
$END
```

5.2.3 Full System Centerline

```
#
#  Centerline test case for the HSRNOISE code
#
#  Full system predictions with Deltas
#
 $GEOM
   HMIC    =  4.0       ,
   SL      =  0.0
 $END
 $WEATHER
   PSIAMB  =   14.7     ,
   RH      =   70.0     ,
   TFAMB   =   77.0     ,
   SIGMA   =   1.1E6
 $END
 $FLIPATH
   ALTEVO  =   1273.0  ,
   FPA     =   2.30    ,
   PAE     =   11.7    ,
   VAIR    =   377.7744
 $END
 $SOURCE
   IAFRAM  = F,
   IATM    = 1,
   IEGA    = F,
   IGRND   = T,
   IFAN    = T,
   ICORE   = T,
   IJET    = T,
   ITUR    = T,
   NENG    = 4
 $END
 $DELTAS
   FANDIBB = 17*-6.7 ,
   FANSPBB = 24*1.1  ,
   FANBPF  =  -6.7,
   FAN2BPF =  -6.7,
   FAN3BPF =  -6.7,
   FAN4BPF =  -6.7,
   CORDIBB = 4*-0.1,-0.4,-0.7,-1.0,4*-1.1,-1.0,
             -0.9,-0.8,-0.6,-0.5,-0.3,
   CORSPBB = 24*0.0  ,
   TURDIBB = 4*-0.1,-0.4,-0.7,-1.0,4*-1.1,-1.0,
             -0.9,-0.8,-0.6,-0.5,-0.3,
   TURSPBB = 24*0.0  ,
   TURDITN = 4*-0.1,-0.4,-0.7,-1.0,4*-1.1,-1.0,
             -0.9,-0.8,-0.6,-0.5,-0.3,
   TURSPTN = 24*0.0
 $END
 $FANIN
   AFAN    =   16.98436    ,
   FANRPM  =   4898.000    ,
   NB1     =          27,
   UT      =   1249.580,
```

```
  ISHAPE  = 1 ,
  IDOOR   = 0
$END
$COREIN
  AB      =   1111.27 ,
  BL      =   0.75    ,
  ICR     =   2       ,
  NFN     =   210     ,
  PLD     =   0.15    ,
  P3      =   193.9   ,
  P4      =   180.4   ,
  P7      =   34.41   ,
  T3      =   1189.8  ,
  T4      =   2672.5  ,
  T7      =   1638.1  ,
  W3      =   249.1   ,
  WFP4    =  3.9999999E-02
$END
$TURIN
  CSS     =   151.42   ,
  MDOT    =   354.8    ,
  NBLADE  =   88       ,
  TS      =   1580.61  ,
  TURCAL  =   10.0     ,
  TURRPM  =   4898.0   ,
  VTR     =   1311.559
$END
$JN8C4IN
  APRI    =   8.476    ,
  TPRI    =   1350.24   ,
  VPRI    =   1921.09   ,
  WPRI    =   541.20    ,
  ATHP    =   7.47      ,
  PLUGD   =   0.0       ,
  VSEC    =   643.98    ,
  WSEC    =   475.90    ,
  ASEC    =   12.084    ,
  TSEC    =   544.19    ,
  SPOKE   =   20. ,
  PEN     =   0.925  ,
  DIVANG  =   0.0    ,
  EJL     =   11.0   ,
  EJD     =   5.15   ,
  XMAR    =   0.979  ,
  EJLIN   =   7.09   ,
  FLIN    =   2500.0 ,
  EJASP   =   1.42   ,
  CFG     =   0.95   ,
  PSI0    =   0.0    ,
  DELPE   =  -1.8 ,
  DELPI   =  -1.1 ,
  DELMIX  =   0.1
$END
```

6.0 References

1. Gliebe, P.; "XF-120 Fan Noise Correlation", Memorandum C1-1L5-FP-96-149, GE Aircraft Engines, Cincinnati, Ohio, October 1996.

2. Heidmann, M. F.: "Interim Prediction Method for Fan Compressor Source Noise", NASA TM X-71763, 1979.

3. Mathews, D. C.; and Rekos, N. F., Jr.: "Prediction and Measurement of Direct Combustion Noise in Turbopropulsion Systems", Journal of Aircraft, vol. 14, no. 9, 1977, pp. 850-859.

4. Krejsa, Eugene A. and Valerino, Michael F.: "Interim Prediction Method for Turbine Noise", NASA TM X-73566, November, 1976.

5. Gliebe, P.; Coordination Memorandum GE-98-075-N, GE Aircraft Engines, Cincinnati, Ohio, June 1998.

6. Standard Values of Atmospheric Absorption as a Function of Temperature and Humidity, Aerospace Recommended Practice 866A, 1975, SAE.

7. Viswanathan, K.; and Lu, H. Y.: "An empirical Jet Noise Prediction Procedure for Rectangular Mixer-Ejector Nozzles", Boeing Document No. D6-82061, The Boeing Commercial Airplane Group, Seattle, Washington, August 1997.

8. Viswanathan, K.; and Lu, H. Y.: "JN8C4: Sample Input and Validation", CPC Coordination Memorandum BO98-046, The Boeing Commercial Airplane Group, Seattle, Washington, July 27,1998.

9. Viswanathan, K.; and Lu, H. Y. : "Jet Noise Testing and JN8 Updates", presented at the Airframe Annual Review, Los Angeles, CA, February 9-12, 1999.

10. Tam, C. K. W.: "Broadband Shock-Associated Noise from Supersonic Jets in Flight", Journal of Sound and Vibration, Vol. 151(1), 1991, pp. 131-147.

11. Tam, C. K. W.: "Broadband Shock Associated Noise from Supersonic Jets Measured by a Ground Observer", AIAA Journal, Vol. 30, No. 10, October 1992.

12. Tam, C. K. W.: “Prediction Method for Broadband Shock-Associated Noise from Supersonic Rectangular Jets”, Journal of Aircraft, Vol. 33, No. 2, March-April 1996.

13. Ponton, M. K., Manning, J.C. and Seiner, J.M.: “Far-Field Acoustics of Rectangular Nozzles with Various Throat Aspect Ratios”, NASA TM 89002, 1986

14. Stone, J. R.; and Clark, B. J.: “2-D Mixer Ejector Nozzle Noise Analysis and Prediction Code Development”, HSR/CPC Program Coordination Memorandum GE99-034-N, Modern Technologies Corporation, December 22, 1999.

15. Fink, Martin R.: “Airframe Noise Prediction Method”, FAA-RD-77-29, March 1977.

16. Bass, H. E.; and Shields, F. D.: “Atmospheric Attenuation of High Frequency Noise and Application to Fractional Octave Bands”, NASA CR-2760, 1977.

17. Chien, C. F.; and Soroka, W. W.: “Sound Propagation Along an Impedance Plane”, Journal of Sound and Vibration, vol. 43, no. 1, Nov. 8, 1975, pp. 9-20.

18. “Method for Calculating the Attenuation of Aircraft Ground to Ground Noise Propagation During Takeoff and Landing”; SAE Aerospace Informational Report 923, August 15, 1966.

REPORT DOCUMENTATION PAGE

Form Approved
OMB No. 0704-0188

1. REPORT DATE *(DD-MM-YYYY)*	2. REPORT TYPE	3. DATES COVERED *(From - To)*
01- 11 - 2004	Contractor Report	

4. TITLE AND SUBTITLE

High Speed Research Noise Prediction Code (HSRNOISE) User's and Theoretical Manual

5a. CONTRACT NUMBER

NAS1-00135

5b. GRANT NUMBER

5c. PROGRAM ELEMENT NUMBER

6. AUTHOR(S)

Rawls, John W., Jr., and Yeager, Jessie C.

5d. PROJECT NUMBER

5e. TASK NUMBER

5f. WORK UNIT NUMBER

23-781-20-12

7. PERFORMING ORGANIZATION NAME(S) AND ADDRESS(ES)

NASA Langley Research Center
Hampton, VA 23681-2199

Lockheed Martin Engineering
Hampton, VA 23666

8. PERFORMING ORGANIZATION REPORT NUMBER

02-DF28-01

9. SPONSORING/MONITORING AGENCY NAME(S) AND ADDRESS(ES)

National Aeronautics and Space Administration
Washington, DC 20546-0001

10. SPONSOR/MONITOR'S ACRONYM(S)

NASA

11. SPONSOR/MONITOR'S REPORT NUMBER(S)

NASA/CR-2004-213014

12. DISTRIBUTION/AVAILABILITY STATEMENT

Unclassified - Unlimited
Subject Category 71
Availability: NASA CASI (301) 621-0390 Distribution: Nonstandard

13. SUPPLEMENTARY NOTES

Langley Technical Monitor: Robert Golub
An electronic version can be found at http://techreports.larc.nasa.gov/ltrs/ or http://ntrs.nasa.gov

14. ABSTRACT

This report describes a computer program, HSRNOISE, that predicts noise levels for a supersonic aircraft powered by mixed flow turbofan engines with rectangular mixer-ejector nozzles. It fully documents the noise prediction algorithms, provides instructions for executing the HSRNOISE code, and provides predicted noise levels for the High Speed Research (HSR) program Technology Concept (TC) aircraft. The component source noise prediction algorithms were developed jointly by Boeing, General Electric Aircraft Engines (GEAE), NASA and Pratt & Whitney during the course of the NASA HSR program. Modern Technologies Corporation developed an alternative mixer ejector jet noise prediction method under contract to GEAE that has also been incorporated into the HSRNOISE prediction code. Algorithms for determining propagation effects and calculating noise metrics were taken from the NASA Aircraft Noise Prediction Program.

15. SUBJECT TERMS

Noise prediction; Supersonic noise prediction; High Speed Research noise; Mixer-ejector noise prediction

16. SECURITY CLASSIFICATION OF:			17. LIMITATION OF ABSTRACT	18. NUMBER OF PAGES	19a. NAME OF RESPONSIBLE PERSON
a. REPORT	b. ABSTRACT	c. THIS PAGE			STI Help Desk (email: help@sti.nasa.gov)
					19b. TELEPHONE NUMBER *(Include area code)*
U	U	U	UU	206	(301) 621-0390